

**DETERMINATION OF EARTHQUAKE PERFORMANCE OF
SULEYMANIYE MOSQUE**

SAMIYE MİRCAN KAYA

Bogazici University Library



39001101519802

14

**BOĞAZIÇI UNIVERSITY
1999**

**DETERMINATION OF EARTHQUAKE PERFORMANCE OF
SULEYMANIYE MOSQUE**

**By Samiye Kaya
B.Sc in Civil Engineering, Yıldız University, 1986**

**Submitted to Boğaziçi University,
Kandilli Earthquake Observatory and
Earthquake Research Institute
Department of Earthquake Engineering in
Partial Fulfillment of the Requirements for the degree of
Master of Science
In
EARTHQUAKE ENGINEERING**

**Boğaziçi University
1999**

**BOĞAZIÇI
ÜNİVERSİTESİ
KÜTÜPHANESİ**



TABLE OF CONTENTS

ACKNOWLEDGEMENT	I
ABSTRACT	II
ÖNSÖZ	III
LIST OF FIGURES	IV
LIST OF TABLES	XV
LIST OF SYMBOLS	XVI
1.INTRODUCTION	
1.1 HISTORICAL BACKGROUND	1
2.DESCRPTION OF THE STRUCTURAL SYSTEM	
2.1.1 MATERIAL PROPERTIES	4
2.2 STRUCTURAL SYSTEM	11
2.2.2 SUBSTRUCTURE	12
3.STRUCTURAL ANALYSIS BY FINITE ELEMENT MODEL	
3.1 STRUCTURAL MODEL PROPERTIES	13
3.2 STRUCTURAL IDEALIZATION	15
3.3 ANALYSIS UNDER DEAD LOAD	23
3.4 ANALYSIS UNDER DYNAMIC LOADS	52
3.5 ANALYSIS UNDER DIFFERENT COMBINATIONS OF MATERIAL PROPERTIES AND BOUNDARY CONDITIONS	63
4.SPECTRAL RESPONSE ANALYSIS OF THE IMPROVED MODEL UNDER A SCENARIO EARTHQUAKE FOR ISTANBUL	66
5.CONCLUSIONS	114
6.REFERENCES	115
APPENDIX 1-HISTORICAL EARTHQUAKES OF ISTANBUL	118
APPENDIX 2-DESTRUCTIVE EARTHQUAKES IN ISTANBUL	120
APPENDIX 3-A CLASSIFICATION OF THE ANATOLIAN MOSQUE ACCORDING TO SUPPORT	121

ACKNOWLEDGEMENT

I would like to express my deepest gratitude to my thesis supervisor Professor Dr.Özal Yüzügüllü who proposed the subject and guided and encouraged throughout the study with his vast engineering knowledge.

I would like to express my sincere thanks to Professor Mustafa Erdik and Professor Nuray Aydınoglu for their supports in the study.

I am grateful to Hafez Keypour for his great efforts for improving the finite element model,to Kemal Beyen and Aydın Mert for their helps during the material tests in Süleymaniye,to Muzaffer Gül for providing the necessary earthquake records for the”time history analysis” and to all other members of Earthquake Engineering Department for their companions during the study.

My special gratitude is for my dearest friend Hülya Dışkaya for her inspiration and support during the compilation of the report.

Finally,I wish to thank to my husband Erhan Kemal Kaya and to my lovely children Setenay and Oğuz for their patience.They have always been understanding to their busy mom who never got tired of finding new directions in life.

ABSTRACT

Built between 1549-1557 by the great Turkish architect Mimar Sinan and named after the legendary Ottoman Emperor Süleyman the Magnificent, the Süleymaniye Mosque is considered to be the masterpiece of the Ottoman architecture.

It is a fact that the research studies carried out up today towards the determination of the earthquake performance of this masterpiece of Ottoman-Turkish Engineering is very limited. Within the framework of research activities being carried out at the Earthquake Engineering Department of Kandilli Earthquake Observatory and Earthquake Research Institute for the important historic edifices which was initiated with the Hagia Sophia, the present study on Süleymaniye Mosque is aimed at the exploration of the earthquake performance and dynamic characteristics of the structure. The three dimensional finite element model of the structure previously prepared by A. Selahiye was refined. Non-destructive material tests were carried out in the mosque in order to determine the material characteristics. The data obtained from the tests were used in the study and as a further step, the effects of different materials were investigated. At this stage the effects of different boundary conditions were also combined in the study. The earthquake records obtained from the strong ground motion accelerometers previously installed on Süleymaniye Mosque were also analysed to obtain the natural vibration frequencies and to compare the resulting values with those obtained by other methods. As a last stage of the study, the analysis of the improved model under a scenario earthquake for İstanbul was carried out.

ÖNSÖZ

1549-1557 yılları arasında büyük Türk mimar Mimar Sinan tarafından inşa edilen ve Osmanlı İmparatoru Muhteşem Süleyman'ın adını alan Süleymaniye Camii, Osmanlı mimarisinin başyapıtı olarak düşünülür.

Bu Osmanlı-Türk başyapıtının deprem performansının belirlenmesi yönünde bugüne kadar yapılmış olan araştırma çalışmalarının çok kısıtlı olduğu bir gerçektir. Aya Sofya ile başlayan ve önemli tarihi eserler için Kandilli Rasathanesi ve Deprem Araştırma Enstitüsü Deprem Mühendisliği Bölümü tarafından yürütülmekte olan araştırma faaliyetleri kapsamında yapılmış olan bu çalışma, yapının deprem performansı ve dinamik özelliklerinin belirlenmesini hedeflemiştir. Daha önce A. Selahiye tarafından sonlu elemanlar yöntemi ile hazırlanmış olan yapının üç boyutlu modeli geliştirilmiş ve yenilenmiştir. Yapı malzeme özelliklerinin belirlenmesi amacıyla camide tahribatsız malzeme testleri yapılmıştır. Testlerden elde edilen veriler bu çalışmada kullanılmış ve daha ileri bir aşama olarak da farklı malzeme özelliklerinin yapı modeline etkileri araştırılmıştır. Bu aşamada farklı sınır koşulları da çalışmaya dahil edilmiştir. Doğal titreşim frekanslarını elde etmek ve sonuçları diğer yöntemlerle elde edilenlerle karşılaştırmak üzere, daha önce Süleymaniye Camii'ne yerleştirilmiş olan kuvvetli yer hareketi ivme ölçerleri vasıtasıyla elde edilmiş olan deprem kayıtları analiz edilmiştir. Çalışmanın son aşamasında ise geliştirilmiş model üzerinde İstanbul için olası bir senaryo depreminin etkisi analiz edilmiştir.

LIST OF FIGURES

FIGURE 2.2.1.1 3 Dimensional View of the Accelerometer Positions on the Mosque

FIGURE 2.3.1.1 A Classification of the Anatolian Mosque According to Support System

FIGURE 3.2.1 Cross Section of the Main Pier

FIGURE 3.2.2 Cross Section of the Simplified Piers

FIGURE 3.2.3 General 3-Dimensional View From South-East

FIGURE 3.2.4 General 3-Dimensional View from South-East

FIGURE 3.2.5 View from East, North, top and 3D view from South-West

FIGURE 3.2.6 General Names for Each Part

FIGURE 3.2.7 General View of the Piers upto the Middle

FIGURE 3.2.8 General View of the Whole Piers

FIGURE 3.2.9 General View of the Whole Piers

FIGURE 3.2.10 Position of Supports shown with (-)

FIGURE 3.2.11 Position of Supports shown with (+)

FIGURE 3.3.1 General Deformed Configuration (3-D View from South-East)
Simple Static Analysis Under Self Weight

FIGURE 3.3.2 General Deformed Configuration (View from Top)

FIGURE 3.3.3 Deformed Configuration in the Half of the Model
Simple Static Analysis Under Self Weight

FIGURE 3.3.3 Deformed configuration in the half of the Model
Simple Static Analysis Under Self Weight

FIGURE 3.3.4 Displacement Contours in the Half of the Model
Simple Static Analysis Under Self Weight

FIGURE 3.3.5 Deformed Configuration in the Half of Piers
Simple Static Anlysis Under Self Weight

FIGURE 3.3.6 Stress Contours in the Half of Piers
Simple Static Analysis Under Self Weight

FIGURE 3.3.7 Deformed Configuration in the Main Arches
Simple Static Analysis Under Self Weight

FIGURE 3.3.8 Displacement Contours in the Main Arches
Simple Static Analysis Under Self Weight

FIGURE 3.3.9 Vectors Showing Compression in the Main Arches
Simple Static Analysis Under Self Weight

FIGURE 3.3.10 General Deformed Configuration of Main Arches
Simple Static Analysis Under Self Weight

FIGURE 3.3.11 Semidomes&Side Windows (Half of the Model) Displacement Contours in the Shells,Simple Static Analysis Under Self Weight

FIGURE 3.3.12 Semidomes&Side Windows (Half of the Model).In Plane Normal Force Contours in Shells-Simple Static Analysis Under Self Weight.

FIGURE 3.3.13 Displacement Contours in the Half of Top Dome
Simple Static Analysis Under Self Weight

FIGURE 3.3.14 Stress Contours in the Half of Top Dome
Simple Static Analysis Under Self Weight

FIGURE 3.3.15 Displacement Contours in the Bottom of Dome
Simple Static Analysis Under Self Weight

FIGURE 3.3.16 Stress Contours in the Bottom of the Dome
Simple Static Analysis Under Self Weight

FIGURE 3.3.17 Semidomes&Side Windows Only.Displacement Contours in the Shells
Simple Static Analysis Under Self Weight

FIGURE 3.3.18 Stress Contours in the Half of Model
Simple Static Analysis Under Self Weight. Stress in Global X Direction.

FIGURE 3.3.19 Stress Contours in the Half of Model
Simple Static Analysis Under Self Weight.Stress in Global Y Direction.

FIGURE 3.3.20 Stress Contours in the Half of Model
Simple Static Analysis Under Self Weight.Stress in Global Z Direction.

FIGURE 3.3.21 Stress Contours in the Half of Model
Simple Static Analysis Under Self Weight.Maximum Principal Stress (Tension+).

FIGURE 3.3.22 Stress Contours in the Half of Model
Simple Static Analysis Under Self Weight. Minimum Principal Stress (Compression-).

FIGURE 3.3.23 Stress Contours in the Half of Piers
Simple Static Analysis Under Self Weight. Stress Contours in Global Y Direction.

FIGURE 3.3.24 Stress Contours in the Half of Piers
Simple Static Analysis Under Self Weight. Stress Contours in Global Z Direction.

FIGURE 3.3.25 Stress Contours in the Half of Piers
Simple Static Analysis Under Self Weight. Minimum Principal Stress (Compression -)

FIGURE 3.3.26 Stress Contours in the Half of Piers
Simple Static Analysis Under Self Weight. Stress in Global X Direction

FIGURE 3.3.27 Stress Contours in the Main Arches
Simple Static Analysis Under Self Weight. Stress in Global X Direction

FIGURE 3.3.28 Stress Contours in the Main Arches
Simple Static Analysis Under Self Weight. Stress in Global Y Direction

FIGURE 3.3.29 Stress Contours in the Main Arches
Simple Static Analysis Under Self Weight. Stress in Global Z Direction

FIGURE 3.3.30 Stress Contours in the Main Arches
Simple Static Analysis Under Self Weight. Directions of Maximum Principal Stresses

FIGURE 3.3.31 Stress Contours in the Main Arches
Simple Static Analysis Under Self Weight. Maximum Principal Stress (Tensions+)

FIGURE 3.3.32 Stress Contours in the Main Arches
Simple Static Analysis Under Self Weight. Minimum Principal Stress (Compressions-)

FIGURE 3.3.33 Stress Contours in the Bottom of the Dome
Simple Static Analysis Under Self Weight. Stress in Global Y Direction

FIGURE 3.3.34 Stress Contours in the Bottom of the Dome
Simple Static Analysis Under Self Weight. Stress in Global Z Direction

FIGURE 3.3.35 Stress Contours in the Bottom of the Dome
Simple Static Analysis Under Self Weight. Minimum Principal Stress

FIGURE 3.3.36 Stress Contours in the Bottom of the Dome
Simple Static Analysis Under Self Weight. Stress in Global X Direction

FIGURE 3.3.37 Stress Contours in the Bottom of the Dome
Simple Static Analysis Under Self Weight. Stress in Global Y Direction

FIGURE 3.3.38 Stress Contours in the Bottom of the Dome
Simple Static Analysis Under Self Weight. Stress in Global Z Direction

FIGURE 3.3.39 Stress Contours in the Half of Top Dome
Simple Static Analysis Under Self Weight. Minimum Principal Stress

FIGURE 3.3.40 Stress Contours in the Half of Top Dome
Simple Static Analysis Under Self Weight. Stress in Global X Direction

FIGURE 3.3.41 Semidomes&Side Windows Only. In Plane Normal Force Contours in Shells
Simple Static Analysis Under Self Weight. Minimum Normal Force in Radial Direction

FIGURE 3.3.42 Semidomes&Side Windows Only. In Plane Normal Force Contours in Shells
Simple Static Analysis Under Self Weight. Minimum Normal Force in Transverse Direction

FIGURE 3.3.43 Semidomes&Side Windows in the Half of the Model. In Plane Normal Force
Contours in Shells. Simple Static Analysis Under Self Weight. Minimum Normal Force in
radial Direction

FIGURE 3.3.44 Semidomes&Side Windows in the Half of the Model. In Plane Normal Force
Contours in Shells. Simple Static Analysis Under Self Weight. Minimum Normal Force in
radial Direction

FIGURE 3.3.45 Semidomes&Side Windows Only. In Plane Normal Force Contours in
Shells. Simple Static Analysis Under Self Weight. Minimum Normal Force in radial Direction

FIGURE 3.3.46 Semidomes&Side Windows Only. In Plane Normal Force Contours in
Shells. Simple Static Analysis Under Self Weight. Minimum Normal Force in Local
Transverse Direction

FIGURE 3.3.47 Bending Moment Contours in the East Semidome. Simple Static Analysis
Under Self Weight. Bending Moment Force in Local Transverse Direction

FIGURE 3.3.48 Bending Moment Contours in the East Semidome. Simple Static Analysis
Under Self Weight. Bending Moment Force in Local Radial Direction

FIGURE 3.3.49 In Plane Normal Force Contours in the East Semidome. Simple Static
Analysis Under Self Weight. Normal Force in Local Transverse Direction

FIGURE 3.3.50 In Plane Normal Force Contours in the East Semidome. Simple Static
Analysis Under Self Weight. Normal Force in Local Radial Direction

FIGURE 3.3.51 In Plane Normal Force Contours in the East Semidome. Simple Static
Analysis Under Self Weight. Maximum Principal Force

FIGURE 3.3.52 In Plane Normal Force Contours in the East Semidome.Simple Static Analysis Under Self Weight.Minimum Principal Force

FIGURE 3.4.3.1 Modal Analysis 3-D View from South-East Mode1

FIGURE 3.4.3.2 Modal Analysis 3-D View from South-East Mode2

FIGURE 3.4.3.3 Modal Analysis 3-D View from South-East Mode3

FIGURE 3.4.3.4 Modal Analysis 3-D View from South-East Mode4

FIGURE 3.4.3.5 Modal Analysis Shaded 3-D View from South -East Mode1

FIGURE 3.4.3.6 Modal Analysis Shaded 3-D View from South -East Mode2

FIGURE 3.4.3.7 Modal Analysis Shaded 3-D View from South -East Mode3

FIGURE 3.4.3.8 Modal Analysis Shaded 3-D View from South -East Mode4

FIGURE 3.4.3.9 Modal Analysis Mode 1-2-3-4

FIGURE 3.4.3.10 Modal Analysis Mode 1-2-3-4 ,shaded

FIGURE 3.4.3.11 Modal Analysis 3-D View from South-East,South-West ,Top and Front Mode1

FIGURE 3.4.3.12 Modal Analysis 3-D View from South-East,South-West ,Top and Front Mode2

FIGURE 3.4.3.13 Modal Analysis 3-D View from South-East,South-West ,Top and Front Mode3

FIGURE 3.4.3.14 Modal Analysis 3-D View from South-East,South-West ,Top and Front Mode4

FIGURE 4.1 General Deformed Configuration (3-D View from South-East) Spectral Response Analysis (Positive X Direction+)

FIGURE 4.2 General Deformed Configuration (3-D View from South-East) Spectral Response Analysis (Negative X Direction-)

FIGURE 4.3 General Deformed Configuration (View from Top) Spectral Response Analysis (Positive X Direction-)

FIGURE 4.4 General Deformed Configuration (View from Top) Spectral Response Analysis (Negative X Direction-)

FIGURE 4.5 Deformed Configuration in the Half of Piers Spectral Response Analysis (Positive Y Direction+)

FIGURE 4.6 Deformed Configuration in the Half of Piers Spectral Response Analysis (Negative Y Direction-)

FIGURE 4.7 Displacement Contours in the Half of Model Spectral Response Analysis (Positive Y Direction+)

FIGURE 4.8 Displacement Contours in the Half of Model Spectral Response Analysis (Negative Y Direction-)

FIGURE 4.9 Stress Contours in the Half of Model Spectral Response Analysis (Positive Y Direction+)

FIGURE 4.10 Stress Contours in the Half of Model Spectral Response Analysis (Negative Y Direction-)

FIGURE 4.11 Stress Contours in the Half of Model Spectral Response Analysis (Positive Y Direction+)

FIGURE 4.12 Stress Contours in the Half of Model Spectral Response Analysis (Negative Y Direction-)

FIGURE 4.13 Stress Contours in the Half of Model Spectral Response Analysis (Positive Y Direction+)

FIGURE 4.14 Stress Contours in the Half of Model Spectral Response Analysis (Negative Y Direction-)

FIGURE 4.15 Stress Contours in the Half of Model Spectral Response Analysis (Positive Y Direction+).Maximum Principal Stress (Tensions+)

FIGURE 4.16 Stress Contours in the Half of Model Spectral Response Analysis (Negative Y Direction-).Maximum Principal Stress (Tensions+)

FIGURE 4.17 Stress Contours in the Half of Model.Spectral Response Analysis (Positive Y Direction+).Maximum Principal Stress Compression

FIGURE 4.18 Stress Contours in the Half of Model.Spectral Response Analysis (Negative Y Direction-).Minimum Principal Stress Compression

FIGURE 4.19 Stress Contours in the Half of Piers.Spectral Response Analysis (Positive X Direction+).Stress in Global X Direction

FIGURE 4.20 Stress Contours in the Half of Piers.Spectral Response Analysis (Negative X Direction-).Stress in Global X Direction

FIGURE 4.21 Stress Contours in the Half of Piers.Spectral Response Analysis (Positive X Direction+).Stress in Global Y Direction

FIGURE 4.22 Stress Contours in the Half of Piers.Spectral Response Analysis (Negative X Direction-).Stress in Global Y Direction

FIGURE 4.23 Stress Contours in the Half of Piers.Spectral Response Analysis (Positive X Direction+).Maximum Principal Stress in (Tensions+)

FIGURE 4.24 Stress Contours in the Half of Piers.Spectral Response Analysis (Negative X Direction-).Maximum Principal Stress in (Tensions+)

FIGURE 4.25 Stress Contours in the Half of Piers.Spectral Response Analysis (Positive X Direction+).Minimum Principal Stress (Compressions+)

FIGURE 4.26 Stress Contours in the Half of Piers.Spectral Response Analysis (Negative X Direction-).Minimum Principal Stress (Compressions-)

FIGURE 4.27 Stress Contours in the Half of Piers.Spectral Response Analysis (Positive Y Direction+).Stress in Global X Direction

FIGURE 4.28 Stress Contours in the Half of Piers.Spectral Response Analysis (Negative Y Direction-).Stress in Global X Direction

FIGURE 4.29 Stress Contours in the Half of Piers.Spectral Response Analysis (Positive Y Direction+).Stress in Global Y Direction

FIGURE 4.30 Stress Contours in the Half of Piers.Spectral Response Analysis (Negative Y Direction-).Stress in Global Y Direction

FIGURE 4.31 Stress Contours in the Half of Piers.Spectral Response Analysis (Positive Y Direction+).Stress in Global Z Direction

FIGURE 4.32 Stress Contours in the Half of Piers.Spectral Response Analysis (Negative Y Direction-).Stress in Global Z Direction

FIGURE 4.33 Stress Contours in the Half of Piers.Spectral Response Analysis (Positive Y Direction+). Maximum Principal Stress (Tensions+)

FIGURE 4.34 Stress Contours in the Half of Piers.Spectral Response Analysis (Negative Y Direction-).Maximum Principal Stress (Tensions+)

FIGURE 4.35 Stress Contours in the Half of Piers.Spectral Response Analysis (Positive Y Direction+).Minimum Principal Stress (Compressions-)

FIGURE 4.36 Stress Contours in the Half of Piers.Spectral Response Analysis

(Negative Y Direction-).Minimum Principal Stress (Compressions-)

FIGURE 4.37 Stress Contours in the Half of Piers.Spectral Response Analysis (Positive X Direction+).

FIGURE 4.38 General Deformed Configuration of main Arches.Spectral Response Analysis (Negative X Direction-)

FIGURE 4.39 General Deformed Configuration of main Arches.Spectral Response Analysis (Positive X Direction+)

FIGURE 4.40 General Deformed Configuration of main Arches.Spectral Response Analysis (Negative X Direction-)

FIGURE 4.41 Vectors Showing Compression in the Main Arches.Spectral Response Analysis (Positive X Direction+)Directions of minimum Principal Stresses

FIGURE 4.42 Vectors Showing Compression in the Main Arches.Spectral Response Analysis (Negative X Direction-)Directions of minimum Principal Stresses

FIGURE 4.43 Displacement Contours in the Half of Top Model.Spectral Response Analysis (Positive X Direction+)Total Movements

FIGURE 4.44 Displacement Contours in the Half of Top Model.Spectral Response Analysis (Negative X Direction-)Total Movements

FIGURE 4.45 Stress Contours in the Bottom of the Dome.Spectral Response Analysis (Positive X Direction+)Stress in Global X Direction

FIGURE 4.46 Stress Contours in the Bottom of the Dome.Spectral Response Analysis (Negative X Direction-)Stress in Global X Direction

FIGURE 4.47 Stress Contours in the Bottom of the Dome.Spectral Response Analysis (Positive X Direction+)Stress in Global Y Direction

FIGURE 4.48 Stress Contours in the Bottom of the Dome.Spectral Response Analysis (Negative X Direction-)Stress in Global Y Direction

FIGURE 4.49 Stress Contours in the Bottom of the Dome.Spectral Response Analysis (Positive X Direction+)Stress in Global Z Direction

FIGURE 4.50 Stress Contours in the Bottom of the Dome.Spectral Response Analysis (Negative X Direction-) Stress in Global Z Direction

FIGURE 4.51 Stress Contours in the Bottom of the Dome.Spectral Response Analysis (Positive X Direction+) Maximum Principal Stress (Mostly Tension)

FIGURE 4.52 Stress Contours in the Bottom of the Dome.Spectral Response Analysis (Negative X Direction-) Maximum Principal Stress (Mostly Tension)

FIGURE 4.53 Stress Contours in the Bottom of the Dome.Spectral Response Analysis (Positive X Direction+) Minimum Principal Stress (Mostly Compression)

FIGURE 4.54 Stress Contours in the Bottom of the Dome.Spectral Response Analysis (Negative X Direction-) Minimum Principal Stress (Mostly Compression)

FIGURE 4.55 Displacement Contours in the Half of Top Dome.Spectral Response Analysis (Positive X Direction+) Minimum Principal Stress.Total Movements

FIGURE 4.56 Displacement Contours in the Half of Top Dome.Spectral Response Analysis (Negative X Direction-) Minimum Principal Stress.Total Movements

FIGURE 4.57 Displacement Contours in the Half of Top Dome.Spectral Response Analysis (Positive X Direction+) Minimum Principal Stress.Total Movements

FIGURE 4.58 Stress Contours in the Half of Top Dome.Spectral Response Analysis (Negative X Direction-) Stress in Global X Direction

FIGURE 4.59 Stress Contours in the Half of Top Dome.Spectral Response Analysis (Positive X Direction+) Stress in Global X Direction

FIGURE 4.60 Stress Contours in the Half of Top Dome.Spectral Response Analysis (Negative X Direction-) Stress in Global Y Direction

FIGURE 4.61 Stress Contours in the Half of Top Dome.Spectral Response Analysis (Positive X Direction+) Stress in Global Z Direction

FIGURE 4.62 Stress Contours in the Half of Top Dome.Spectral Response Analysis (Negative X Direction-) Stress in Global Z Direction

FIGURE 4.63 Stress Contours in the Half of Top Dome.Spectral Response Analysis (Positive X Direction+) Maximum Principal Stress (Mostly Tension)

FIGURE 4.64 Stress Contours in the Half of Top Dome.Spectral Response Analysis (Negative X Direction-) Maximum Principal Stress (Mostly Tension)

FIGURE 4.65 Stress Contours in the Half of Top Dome.Spectral Response Analysis (Positive X Direction+) Maximum Principal Stress (Mostly Compression)

FIGURE 4.66 Stress Contours in the Half of Top Dome.Spectral Response Analysis (Negative X Direction-) Maximum Principal Stress (Mostly Compression)

FIGURE 4.67 In-Plane Normal Force Contours in the East Semidome.Spectral Response Analysis (Positive X Direction+) Maximum Normal Force in Radial Direction

FIGURE 4.68 In-Plane Normal Force Contours in the East Semidome.Spectral Response Analysis (Negative X Direction-) Maximum Normal Force in Radial Direction

FIGURE 4.69 In-Plane Normal Force Contours in the East Semidome.Spectral Response Analysis (Positive X Direction+) Minimum Normal Force in Radial Direction

FIGURE 4.70 In-Plane Normal Force Contours in the East Semidome.Spectral Response Analysis (Negative X Direction-) Minimum Normal Force in Radial Direction

FIGURE 4.71 In-Plane Normal Force Contours in the East Semidome.Spectral Response Analysis (Positive X Direction+) Normal Force in Local Transverse Direction

FIGURE 4.72 In-Plane Normal Force Contours in the East Semidome.Spectral Response Analysis (Negative X Direction-) Normal Force in Local Transverse Direction

FIGURE 4.73 In-Plane Normal Force Contours in the East Semidome.Spectral Response Analysis (Positive X Direction+) Normal Force in Local Transverse Direction

FIGURE 4.74 In-Plane Normal Force Contours in the East Semidome.Spectral Response Analysis (Negative X Direction-) Normal Force in Local Transverse Direction

FIGURE 4.75 Displacement Contours in the Shells.Spectral Response Analysis (Positive Y Direction+) Total Movements

FIGURE 4.76 Displacement Contours in the Shells.Spectral Response Analysis (Negative Y Direction-) Total Movements

FIGURE 4.77 Displacement Contours in the Shells.Spectral Response Analysis (Positive Y Direction+) Total Movements

FIGURE 4.78 Displacement Contours in the Shells.Spectral Response Analysis (Negative Y Direction-) Total Movements

FIGURE 4.79 In-Plane Normal Force Contours in the East Semidome.Spectral Response Analysis (Positive Y Direction+) Normal Force in Local Radial Direction

FIGURE 4.80 In-Plane Normal Force Contours in the East Semidome.Spectral Response Analysis (Negative Y Direction-) Normal Force in Local Radial Direction

FIGURE 4.81 In-Plane Normal Force Contours in the East Semidome.Spectral Response Analysis (Positive Y Direction+) Normal Force in Local Radial Direction

FIGURE 4.82 In-Plane Normal Force Contours in the East Semidome.Spectral Response Analysis (Negative Y Direction-) Normal Force in Local Radial Direction

FIGURE 4.83 In-Plane Normal Force Contours in the Shells.Spectral Response Analysis (Positive Y Direction+) Minimum Normal Force in Local Radial Direction

FIGURE 4.84 In-Plane Normal Force Contours in the Shells.Spectral Response Analysis (Negative Y Direction+) Minimum Normal Force in Radial Direction

FIGURE 4.85 In-Plane Normal Force Contours in the Shells.Spectral Response Analysis (Positive Y Direction+) Normal Force in Local Transverse Direction

FIGURE 4.86 In-Plane Normal Force Contours in the Shells.Spectral Response Analysis (Negative Y Direction-) Normal Force in Local Transverse Direction

FIGURE 4.87 In-Plane Normal Force Contours in the Shells.Spectral Response Analysis (Positive Y Direction+) Normal Force in Local Radial Direction

FIGURE 4.88 In-Plane Normal Force Contours in the Shells.Spectral Response Analysis (Negative Y Direction-) Normal Force in Local Radial Direction

FIGURE 4.89 In-Plane Normal Force Contours in the Shells.Spectral Response Analysis (Positive Y Direction+) Maximum Normal Force in Local Radial Direction

FIGURE 4.90 In-Plane Normal Force Contours in the Shells.Spectral Response Analysis (Negative Y Direction-) Maximum Normal Force in Local Radial Direction

LIST OF TABLES

Table 2.1.1 Main Characteristics of Küfeki Stone

Table 2.1.1.2 Compressive Strength Values Obtained by Schmidt Hammer Test

Table 2.1.1.3 Ultrasonic Test Measurements

Table 2.1.1.4 Average Modulus of Elasticity

Table 3.1.2.1 Calculated and Measured Dynamic Properties

Table 3.3.1 Maximum and Minimum Stresses

Table 3.5.1 Material Properties Used in the Analysis

Table 3.5.2 Table of Dynamic Runs

Table 3.5.3 Description of the Boundary Conditions

Table 4.1 Spectral Acceleration Value

Table 4.2 Spectral Amplitude Ratios

Table 4.3 Comparison of Modal Frequencies

LIST OF SYMBOLS

E_m	: Modulus of Elasticity of Mortar
E_b	: Modulus of elasticity of the bricks
E_c	: Modulus of Elasticity of Concrete
D	: Density of material
V	: Velocity
ν	: Poisson's ratio
N_x, N_y, N_{xy}	: Membrane stress resultants/unit width in the local cartesian system,
M_x, M_y, M_{xy}	: Moments/unit width in the local cartesian system,
S_x, S_y	: Shear stress resultants/unit width in the local cartesian system.
K	: Stiffness matrix
U	: Vector of resulting displacements,
R	: Vector of applied loads
M	: Diagonal mass matrix,
Ω	: Diagonal matrix of eigenvalues,
Φ	: Matrix of corresponding eigenvectors (mode shapes)
$[M]$: Mass
$[C]$: Damping
$[K]$: Rigidity
$\{ü_g\}$: Ground vector respectively.

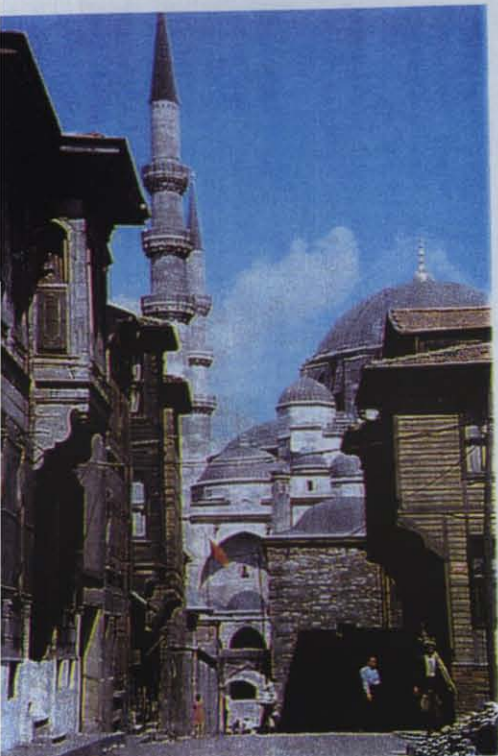


Bird's Eye View of Süleymaniye

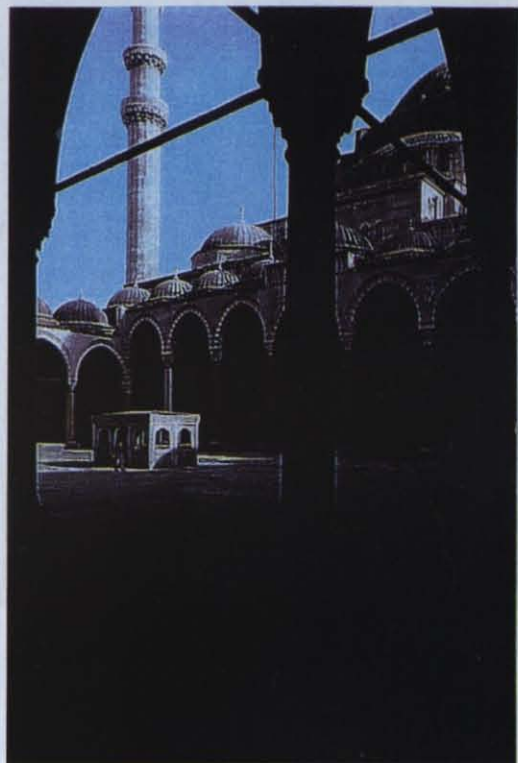
Close-up View of Süleymaniye



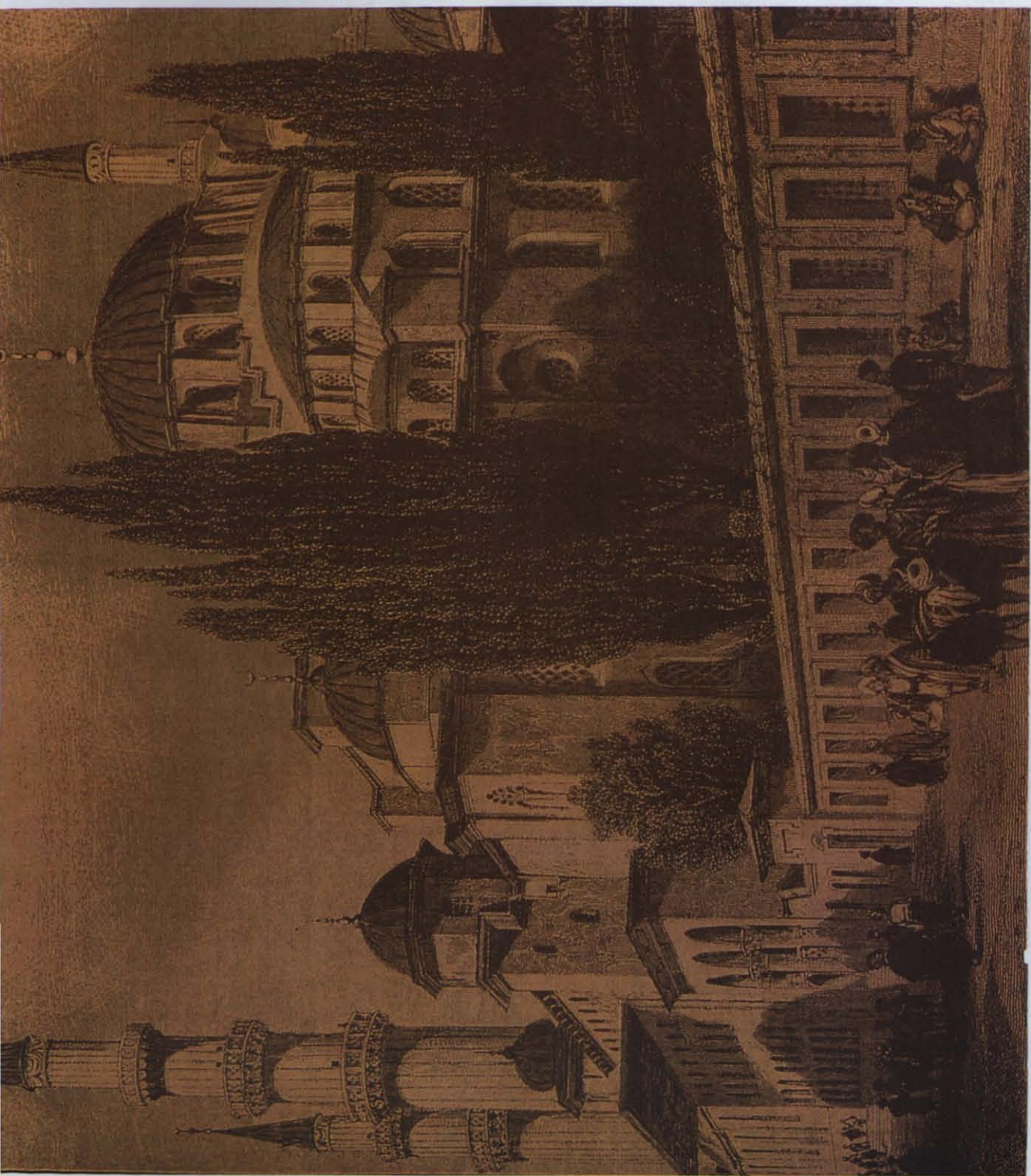
Bird's Eye View of Süleymaniye



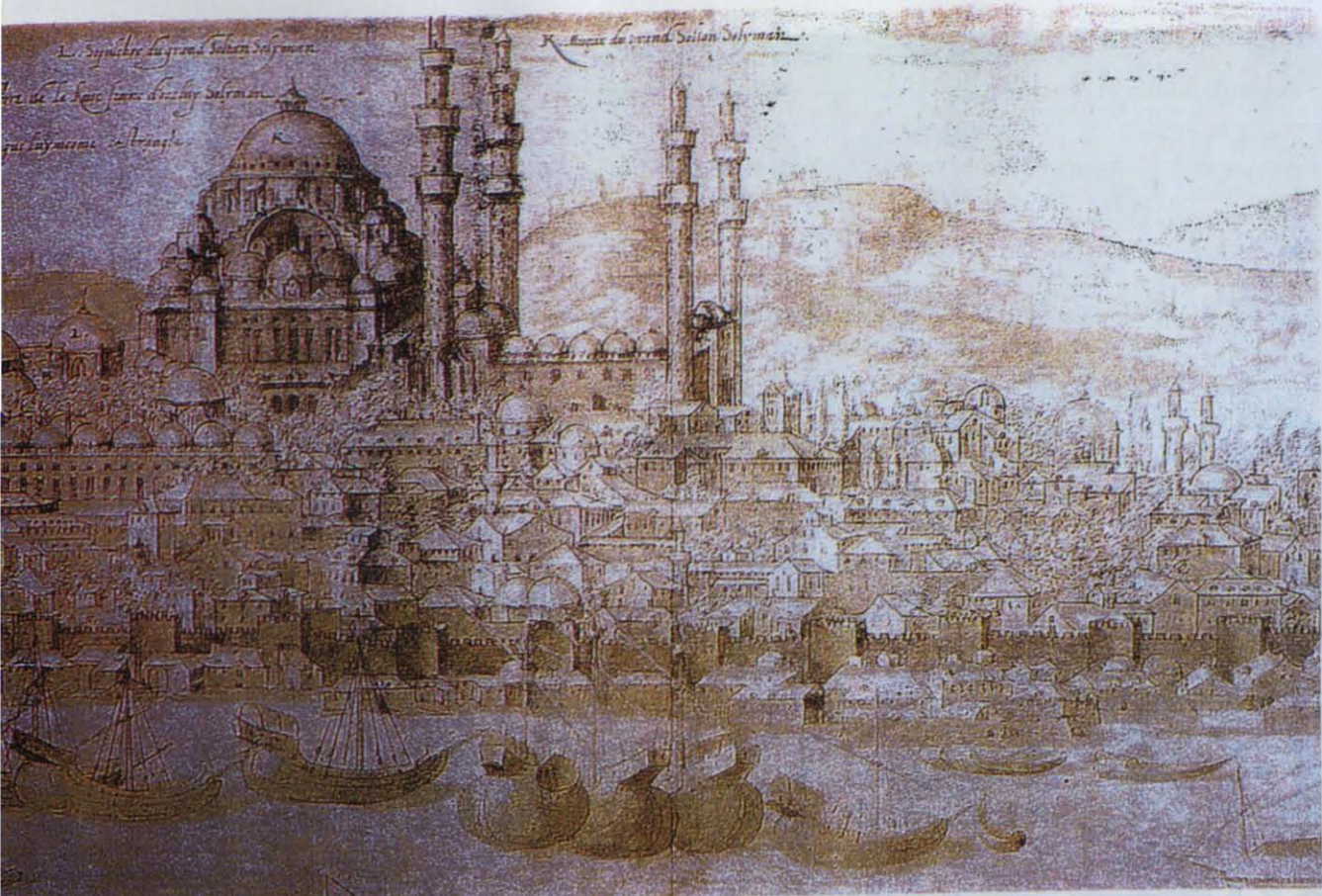
Close-up View of Süleymaniye



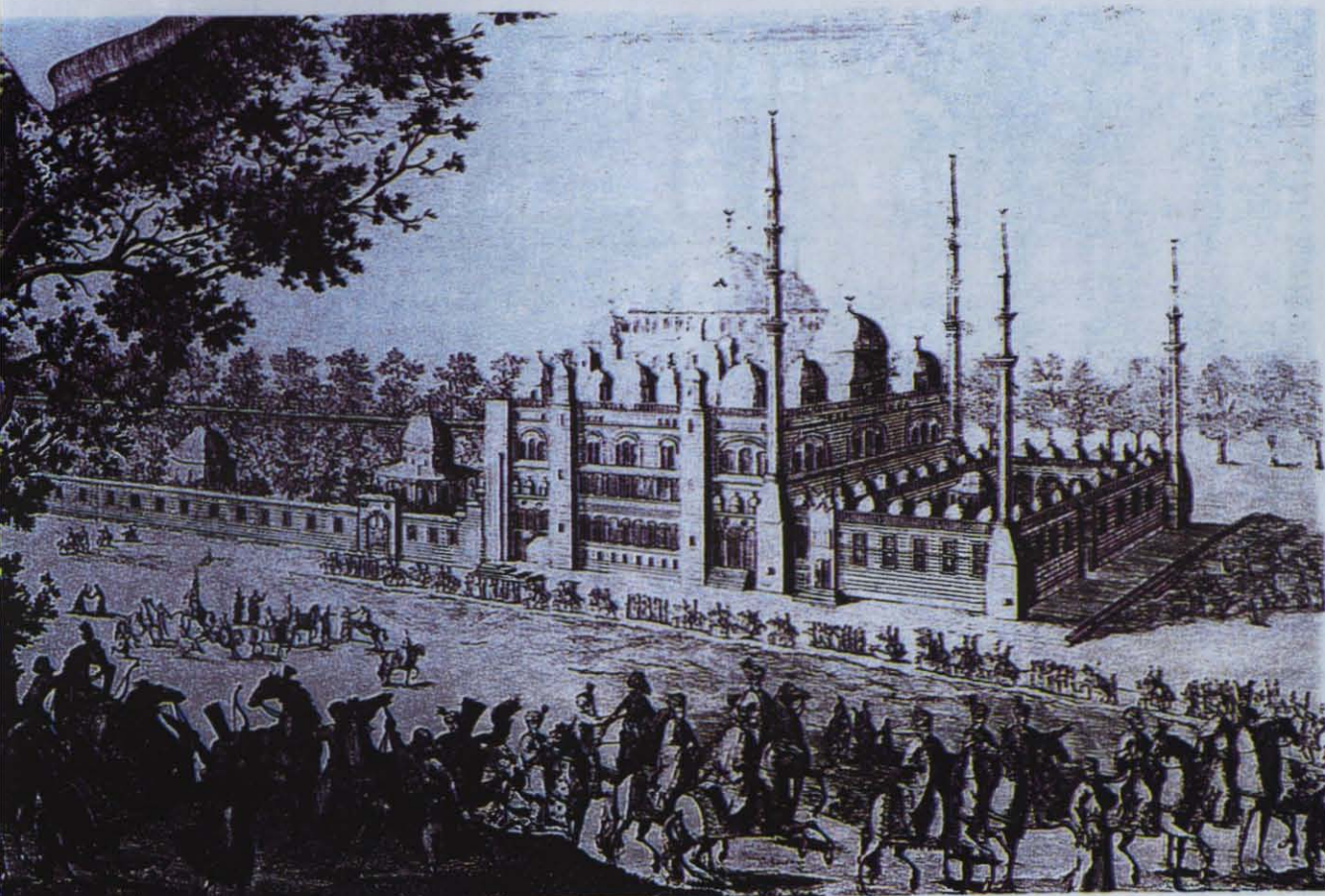
Close-up View of Süleymaniye



Süleymaniye in Painting



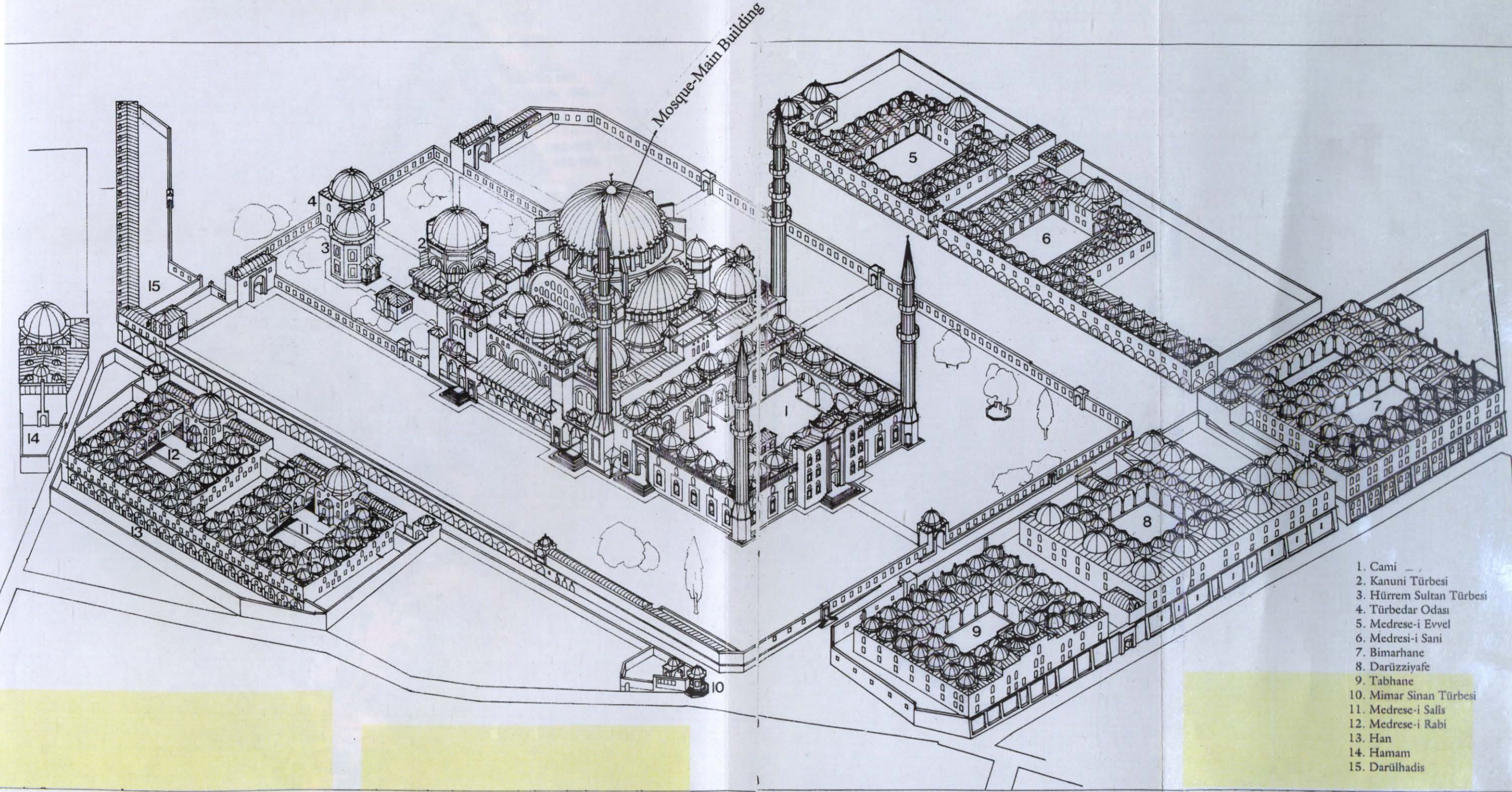
Süleymaniye in Painting (Lorisch)



Süleymaniye in Engraving (Fischer Von Erlach)



Interior View of Süleymaniye



Mosque-Main Building

1. Cami
2. Kanuni Türbesi
3. Hürrem Sultan Türbesi
4. Türbedar Odası
5. Medrese-i Evvel
6. Medrese-i Sani
7. Bimarhane
8. Darüzziyafe
9. Tabhane
10. Mimar Sinan Türbesi
11. Medrese-i Salis
12. Medrese-i Rabi
13. Han
14. Hamam
15. Darülhadis

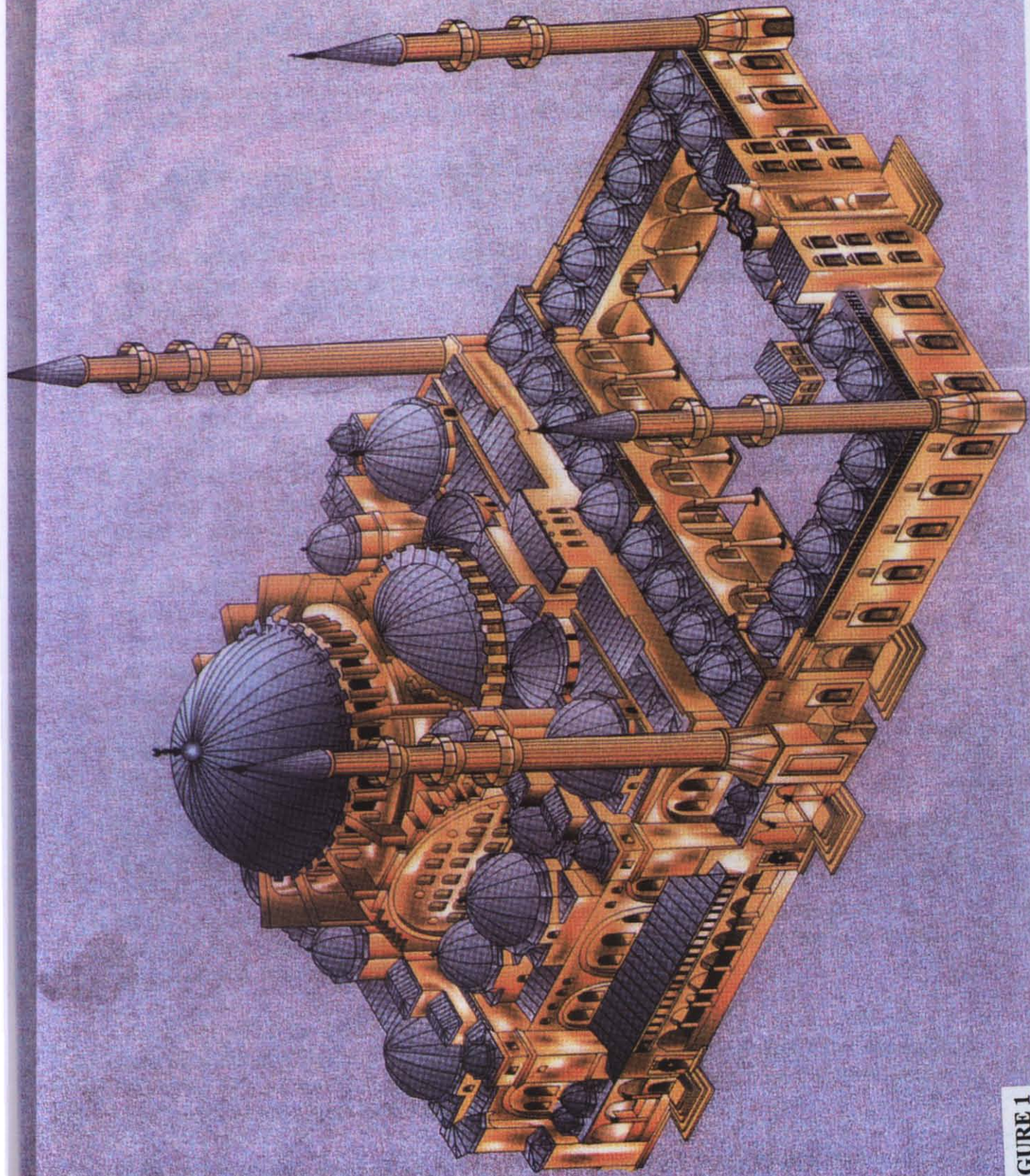


FIGURE 1

*Number in the parenthesis show the reference figure number cited.

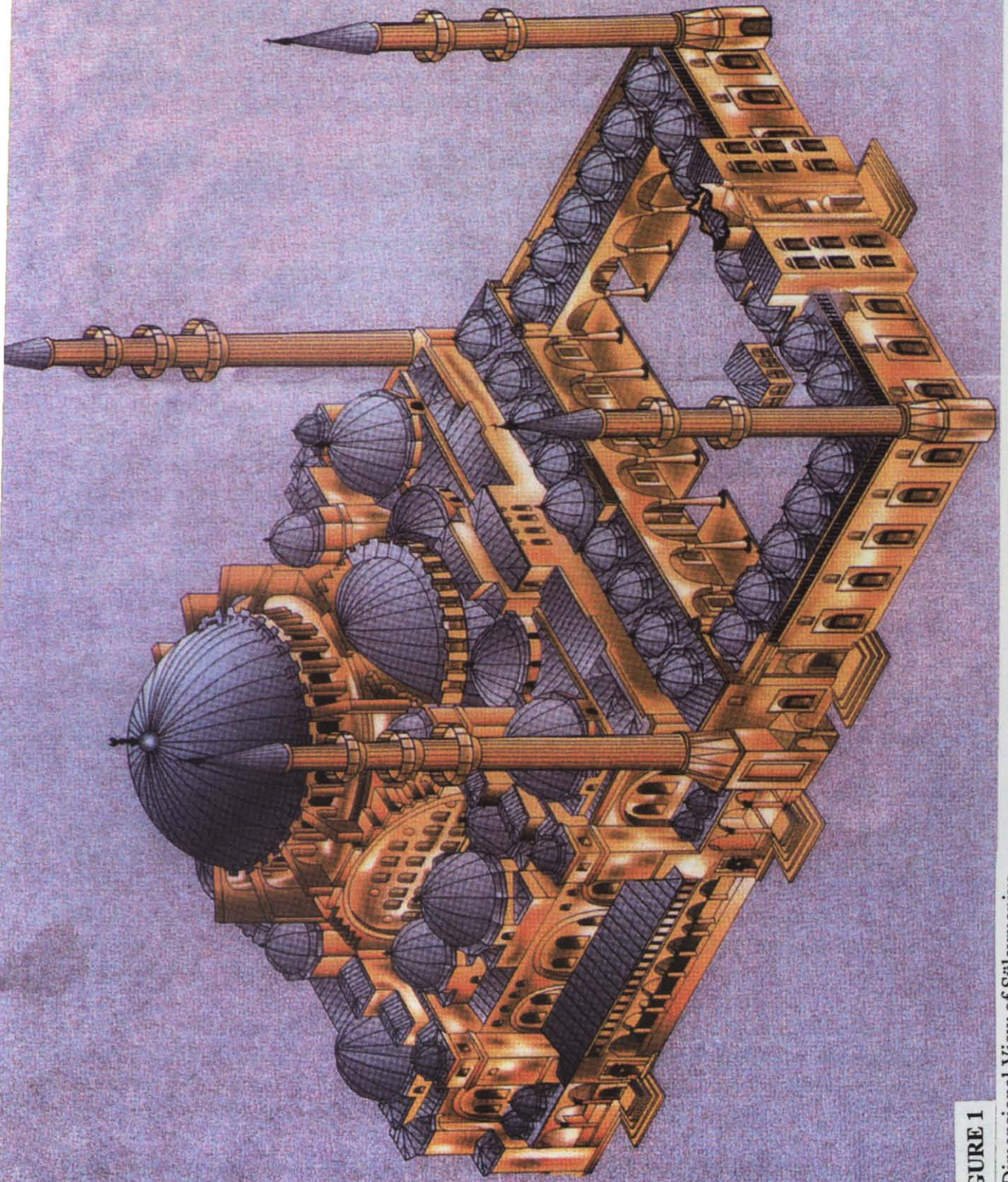
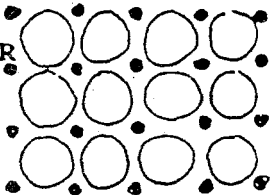
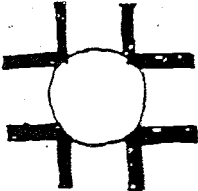
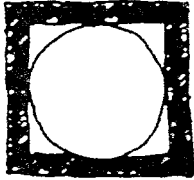
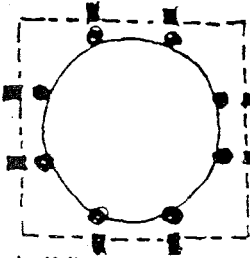


FIGURE 1

3-Dimensional View of Süleymaniye

*Nispetiye to the parallelepiped from the reference square, another chief.

A classification of the Anatolian Mosque According to Support

<u>support system</u>	<u>structural parti</u>	<u>examples before Sinan</u>	<u>dome diam.</u>	<u>Sinan's mosques</u>	<u>dome diam.</u>
COLUMNAR GRID		Great Mosque, Bursa (1399)	10.6 m	Pivale Pasa Mosque, Istanbul (1574)	8.5 m
ABUTTING WALLS		Yildirim Mosque, Bursa (1395) Yesil Mosque, Bursa (1424)	11.5 m 12 m	Haseki Hurrem Sultan Hamami, * Ist. (1557) Nisanci Mosque, Istanbul (1589)	8 m 13 m
PERIMETER WALLS or DOME ON CUBE		Yesil Mosque, Iznik (1378) Yildirim Mosque, Mudurnu (1382) Sultan Bayezid M., Edirne (1488)	11 m 19.5 m 21 m	Coban Mustafa Pasa M., Gebze (1523) Hadim Ibrahim Pasa M., Istanbul (1551) Mihrimah Sultan M., Istanbul (1565 ?)	14 m 12 m 18 m
POLYGONAL PIERS		Uc Serefeli M., Edirne (1447) Fatih Mosque, Istanbul (1470) Atik Ali Pasa M., Istanbul (1497) S. Bayezid M., Istanbul (1506) Fatih Pasa M., Diyarbakir (1520)	24.1 m 25 m 12.5 m 18 m 10 m	Schzade Mehmed M., Istanbul (1548) Sinan Pasa Mosque, Istanbul (1555) Suleymaniye Mosque, Istanbul (1557) Kara Ahmed Pasa M., Istanbul (1558) Selimiye Mosque, Edirne (1574)	19 m 12.5 m 25 m 12.5 m 31.2 m

* This is the only building on this list that is not a mosque; it is a bath house.

1. INTRODUCTION

1.1 HISTORICAL BACKGROUND

The historic studies provide informations about the original construction, the architects, engineers, artists succeeded in the production of the structure, social, political and artistic events. These elements are the memory of the past life of the monument and show the importance and the necessity of its preservation.

After an appropriate survey of the structural pathology, before any numerical or physical analysis, it is essential to make a deep historical survey.

Detailed information on restorations, replacements of structural elements, and strengthening works of the past are essential to get a complete scenario of the pathology and proceed to new interventions.

Unfortunately, very seldom precise documents of the works are found in the archives, and the structural aspects and details are not enough. The cronical usually reports the payment of works, but not their location and technical details which would be very useful for the analysis. This is because, for the ancient interventions, the structural and mechanical characteristics of the monumental buildings were not considered as fundamental. It is essential to provide as-built drawings and full description of the works which will be very useful for those who will work in the future on the same monument.

The masterpiece of the Ottoman architecture which was built between 1549-1557 is rather a social consideration and an image which has assimilated the whole Ottoman History. The Süleymaniye Mosque is unified with the image of the city of İstanbul. It is the most symbolist monument of the Empire standing as a master unit of the stunning silhouette of the city with its location. The biggest complex of the Ottoman Empire was on of the focus of the city life with its facilities like education center public kitchen, hospital, guest house; important building like old palace, its nearness to the shopping area and with its extraordinary location dominating the Golden-Horn.

The complex was realized with the biggest site organization throughout the architectural history. According to Barkan [1]*, 5 months before the inauguration date of 15 September 1557, the operational issues of the complex were fully coordinated. Before the completion of the construction, hundreds of employees with their salaries, duties; all the materials required for the operation of the foundation were defined, and necessary funds to sustain this operation were supplied.

It was written on the inscription on the entrance door of the Harem that the construction was initiated between 7th-17th June 1550 and completed on 16th August 1556. According to Barkan [1], the completion date is 15th October 1557. Melchior Loric writes that the inauguration ceremony was held on 4th October 1557.

The most important event of the inauguration ceremony was that, Süleyman the Magnificent had given the honour of inaugurating this masterpiece to Architect Sinan.

*Number in the paranthesis show the reference sequence number cited.

Architect Sinan Who was the Chief Court Architect to three Sultans produced over 400 works throughout his life. Born during the reign of Beyazıt II, he entered imperial service under Selim I, Selim II and Murat III. He is known to have been responsible for either planning or the constant involvement in and completion of over four hundred works over a vast geographical area, working with a variety of artisans.

Sinan worked as imperial architect at a time when the Court Architects' Guild, of which he was the head, was responsible for the entire body of public works throughout the Ottoman Empire in Asia, Europe and Africa, and was itself an organisation of highly skilled and talented artisans who originated from all parts of the Empire. It was a body which monitored all constructional activity ranging from training architects to the completion of the works on the site. Under the authoritative administration of Sinan, the guild expanded considerably and became firmly established within the imperial state system. It became an organisation encouraging constant innovation and ensured a formidable architectural programme which existed throughout the reigns from Süleyman the Magnificent, up to that of Murat III.

2.DESCRPTION OF THE STRUCTURAL SYSTEM

The structure is mainly constructed by stone and brick. The major part of it such as main piers, arches, internal secondary arches, buttress piers, and walls are made of stone. The domes are made of brick and covered by lead.

2.1.CONSTRUCTION MATERIALS AND THEIR MATERIAL PROPERTIES

2.1.1.MATERIAL PROPERTIES

STONE&BRICK

During the construction of the mosque, required materials were brought from various areas of the Ottoman Empire. Big stones, columns and cover marbles are the important materials among them. From time to time, it is known that, decorated elements were also requested. In the letter written to Egypt regarding the four pieces pier of 17 yards to 2 yards, decorated window frame same as the sample were requested. As it is understood from the decrees of the council of state, the most important materials were big columns, special ships were constructed. One of the big marble columns of the tripped dome separating the middle and the side yards of the mosque is known to be a Roman column brought from "Kıztaşı".

It is observed that the marbles and the valuable coloured stones were delivered, even from the structures founded by the previous Sultans. For example, the circular porphyry marble of slab in the Orhan Bey Medrese in İznik was dismantled and delivered to Süleymaniye. For supplying such materials, it can be said that many historical buildings in various locations of the Empire were plundered.

In general, the source of marble was Marmara Island and the structures previously built in İstanbul. Sand stone and other stones were brought from İzmit and Yalova; Timber from the Black Sea shores close to İstanbul, and Biga; Plaster and lime from İstanbul-İznik-Bursa region; brick from Hasköy and Galipoli; raw and processed iron from Bulgaria, and ropes from Samsun.

Among the various types of stones Architect Sinan used, the most widely used one is küfeki stone the results of the tests of which is reported [2]. The stone is used at different locations of the structures for various purposes such as structural material on piers walls, arches or decorative material for cooring walls and slabs. The art of using this material can be observed on the several historical edifices built by Sinan.

The results of the tests indicate that the mechanical characteristics like compressive, tensile and shear strength of the stone increase while the pores decrease leading resistance to external effects.

Table 2.1.1.1.gives the main characteristics of Küfeki stone [2].

Table 2.1.1.1. Main Characteristics of Küfeki Stone

Definition: Limestone with high level of porosity and fossilation	
Sources around İstanbul: Bakırköy, Sefaköy, Halkalı, Hadımköy, Sazlı Bosna	
Physical Characteristics	: -Unit weight : 2.19 g/cm ³ -Porosity : %12.6 -Water absorbtion (by weighth) : %5.70 -Water absorbtion (by volume): %11.08 -Capillarity : 4.93.10 ⁻⁶ (sample of 3 months) -Average weight loss during freezing and thawing : %0.28
Chemical Composition	: %54.37 CaO, %0.22 fe ₂ O ₃ Al ₂ O ₃ , %0.39MgO, %0.34SiO ₂ , %0.11 H ₂ O, %43.44 CO ₂ +H ₂ O (Arıç, Sayar, 1957)
Mechanical Characteristics	: -Single axis compressive strength : f _{b,1} =332 kgf/cm ² (15 cm ³) f _{b,30} =455 kgf/cm ² (15 cm ³) -Tensile strength : f _{c30} =36 kgf/cm ² -Modulus of elasticity : E=240 000 kgf/cm ² -Surface hardness readings: R ₍₁₎ =47.7 R ₍₃₀₎ =50.1 -Ultrasonic velocity : V ₍₁₎ =3.88 km/sec V ₍₃₀₎ =5.01 km/sec

Non-destructive Tests

In order to determine the parameters suitable for the definition of the static behaviour of the edifice, diagnostic investigations are conducted using only simple and rapid non-destructive tests testing techniques. It must be emphasised, however, that the use of only a preliminary evaluation of the mechanical characteristics of the masonry by defining their mechanical 'quality indices'. Even though these tests are unable to supply th equantitative mechanical parameters, their use is very important as they provide information on the homogeneity of the characteristics of the material and on the presence of the structural anomalies.

The only reliable means for the determination of the parameters that influence the mechanical behaviour of the material is that of utilising a slightly destructive method that require some interventions (coring and cutting). These actions must be studied in such a

way that the disturbance to the member is temporary. At the end of the tests, there should be no visible signs of the work remain on the structure.

For an historically significant monument like Süleymaniye, slightly destructive testing techniques cannot be used as even slight alterations of the elements are not permitted. Similar non-destructive testing methods were utilised on the exposed surfaces of Hagia Sophia with the above mentioned considerations.

Characteristics which may be specified and are capable of assessment by non-destructive techniques are:

- Structural integrity
- Durability
- Appearance and tolerance

In Süleymaniye, for the determination of the dynamic moduli and the average compressive strength, ultrasonic testing method and Schmidt Hammer testing method are used respectively.

Schmidt Hammer Test

Schmidt Hammer tests are aimed at a quantitative evaluation of the compressive strength of mortar and superficial strength of stones or brick materials. They can also provide information on local damage of the material. The results obtained with the test can be considered a 'quality index' which must be correlated with results obtained through mechanical tests on samples.

Testing with the Schmidt Hammer has had rather a chequered history, mainly because too much was expected of it initially and user disappointment led to rejection, even for purposes for which the instrument is suited.

Various structural elements were tested in Süleymaniye including main piers, Marble columns, infill walls, floors, exterior stone walls. Among them the most reliable measurements are those taken from exposed (uncovered) surfaces like stones of the main piers. Therefore, only the measurements belong to the main piers shall be given in this study.

Table 2.1.1.2. Compressive Strength Values Obtained by Schmidt Hammer Test

Name of the Element	Compressive Strength		Number of Measurements
	Average Measured Strength (N/mm ²)	Indicated from Hammer Curve (N/mm ²)	
Main pier 1	32	226	36
Main Pier 2	35	310	36
Main Pier 3	40	350	36
Main Pier 4	39	339	36

Ultrasonic Pulse Velocity Measurement

Among the non-destructive investigation methods, the sonic methods are the most widely spread tests used. The testing technique is based, in general, on the generation of sonic or ultrasonic impulses at a point in the structure. A signal is generated by a percussion system or by an electrodynamic or pneumatic transducers, and collected through a receiver, which can be placed in various positions. Elaboration of the data consists in measuring the time, the impulse takes to cover the section of material between the generator and the receiver, and in analysing the signal wave.

Ultrasonic waves are preferably used for the study of continuous structures, adopting measurements already coded for non-destructive tests on concrete. For masonry structures, that are typically homogeneous, it is necessary to use sonic impulses because the joints present in the masonry would constitute impenetrable barriers to the ultrasonic waves. By using sonic test methods, the following information can be obtained:

- Mechanical quality index
- Homogeneity of the characteristics of the masonries which a building is composed of
- The effect of grouting reinforcements
- The presence of cracks in continuous materials

The great advantage of this method over all other non-destructive tests is that the pulse passes through the complete thickness of the concrete which means that significant defects within the body of the member will be detected.

Four series of ultrasonic tests were conducted on the main piers of the mosque. The selected test locations had exposed surface (without plaster) The test results are summarized in Table 2.1.1.3 below.

Table 2.1.1.3.Ultrasonic Test Measurements

Test Location	Length	T i m e		Velocity m/sec		Modulus Of Elasticity N/m ² .10 ⁹	
		Reading1	Reading2	Reading1	Reading2	Reading1	Reading2
Pier 1	70,0	589,2		1188,05		2,54	
Pier 1	77,5	632,8		1224,72		2,70	
Pier 1	93,0	742,2		1253,03		2,83	
Pier 1	113,0	838,5		1347,64		3,27	
Pier 1	120,0	1209,0		992,56		1,77	
Pier 1	150,0	2038,4		735,87		9,75	
Pier 2	70,0	556,6	586,6	1257,64	1193,32	2,85	2,56
Pier 2	100,0	765,0	834,6	1307,19	1198,18	3,08	2,58
Pier 2	130,0	984,4	1121,1	1320,60	1159,58	3,14	2,42
Pier 3	70,0	540,4	613,9	1295,34	1140,25	3,02	2,34
Pier 3	100,0	806,0	830,0	1240,70	1204,82	2,77	2,61
Pier 3	130,0	1040,0	1056,0	1250,0	1231,06	2,81	2,73
Pier 4	70,0	509,0	699,0	1375,25	1001,43	3,40	1,81
Pier 4	100,0	1161,0	977,2	1112,35	1023,33	2,23	1,88
Pier 4	130,0	1384,0	1333,0	1119,72	1147,40	2,26	2,37

MORTAR

Historic mortars are complex systems formed of a binder material (aerial or hydraulic lime,gypsum) ,a variety of passive and active aggregates and some inorganic or organic additives to improve the mechanical strength of the mortar (fibers,milk,pozzolan,white of eggs as in the case of Süleymaniye,extracts and others)

The historic mortars, in general, do not fit modern standards as their aggregates very often contain a considerable amount of fine components and also relatively high proportions of the mortar and bricks used in their masonry [3].

Previous structural studies to determine the earthquake worthiness of monumental buildings in İstanbul like Hagia Sophia have shown that the monuments' static and dynamic behaviour depends strongly on the mechanical and chemical properties of the mortar and bricks used in their masonry [3].

Modulus of elasticity which has been estimated using in-situ,ultrasonic test at various brick and mortar locations in Hagia Sophia are:Brick:Eb=3.10 Gpa;Em=0.66 Gpa;
Composite:Ebm=1.83 Gpa

Ioanni Papayianni (Aristotle University of Thessaloniki, Department of Civil Engineering) In her research study on the suitability of materials for irreversible interventions [4], carried out within the framework of the Nato Science for Stability Programme (1993-1997) gives the following table:

Period/Monument Type of mortar	Binders L=lime P=pozzolana S=soil B=brick dust	Content in Ca(OH) ₂ %	Compressive strength kg/cm ²	Aggregates fines/coarse
Roman/Galerius Palace/Structural	L/S=1:1 or 1:0.5	30-35	30-40	1:1 2:1
Middle Byzantine/Hagia Sophia/Structural	L/P/B=1:1:1 or 1.5:1:1	25-30	45-50	2:1 3:1
Ottoman 15th cent.AD/Yahundi Hamam/Structural coating	L/S=1:1 L/S=1:2	40-45 30	20-30 30-40	5:1 5:1
18th cent.AD Mansion of Tzotza/ Structural Coating	L/S=1:1 L/S=1:2	35 30-35	10-15	10:1 15:1

By using the above given values, compressive strength of the mortar of the Süleymaniye Mosque in the model is assumed to be: 30 kg/cm²

The following equation was used to calculate the modulus of elasticity of the mortar:

$$E_m = 21\,000 \text{ kg/cm}^2 \text{ (Turkish Standards)}$$

$$E_m = 12\,000 \text{ kg/cm}^2$$

From a previous study on non-destructive testing technics of structural materials in historical structures (Eser Durukal, Özal Yüzügüllü and Kemal Beyen) [3], the modulus of elasticity of the brick is computed for the Hagia Sophia and the same value is used in this study.

$$E_b = 31\,000 \text{ kg/cm}^2$$

The modulus of elasticity of the composite material E_c (brick+mortar) was computed using.

$$E_c = 2E_b E_m / (E_b + E_m)$$

Where

E_b = Modulus of elasticity of the bricks; E_m = Modulus of elasticity of the mortar.

Therefore,

$$E_c = 50\,000 \text{ kg/cm}^2$$

Dynamic Modulus of Elasticity

The following equation was used to calculate the dynamic modulus of elasticity:

$$E = d \cdot v^2 (1 - \nu) / (1 - 2\nu)$$

Where

D=density of material (kg/m³)

V=velocity (m/sec);and

V=Poisson's ratio

The density of the stone is accepted to be 2000 kg/m³

Accordingly, average modulus of elasticity were computed by Matlab computer program and summarized in Table 2.1.1.4

Table 2.1.1.4. Average Modulus of Elasticity

Test Location	Modulus of Elasticity (N/m ²).10 ⁹
Main Pier 1	2,35
Main Pier 2	2,77
Main Pier 3	2,71
Main Pier 4	2,30

Table 2.1.2 Material Properties Used in Previous Studies[6]

Material Properties	Modulus of Elasticity (N/m ²).10 ⁹	Poisson Ratio	Mass	Thickness
Arches	3,5	0,20		
Piers	10,0	0,18		
Domes	3,5	0,18		0,50
Pendantives	3,5	0,20	2,0	
Semi-Domes	3,5	0,18		0,70

2.2.STRUCTURAL SYSTEM

2.2.1.SUPERSTRUCTURE

The Süleymaniye Mosque is a masterpiece exhibiting the classical Ottoman style and art techniques which have been applied in the most splendid manner. The space design of the Süleymaniye is in fact the renewal of the Hagia Sophia's middle dome figure with two semi-domes in the middle yard. Although it seems that the same figures were used, these two monuments are the products of two totally different traditions.

Early Ottoman domed buildings (14th-15th centuries) were based either on the concept of a single dome of medium size covering the whole inner space or, on the series of small domes one neighbouring the other at the same level. In both solutions, thrusts and seismic actions would thus be laterally transmitted to the massive exterior walls or piers.

The domed structures with vaults or pendentives and arches were widely used in Ottoman Architecture before the conquest of İstanbul, and this tradition goes back to the age before Seljuks. Therefore, it can be said that the domed systems are distinguished with respect to their construction, supporting systems and static behaviour.

Towards the middle of XVIth century, as a consequence of solving the domes of big dimensions, substantial improvements were achieved towards realising a huge space. During this period, Ottoman Architecture gave birth to its gifted master-Architect. Sinan who has realised numerous splendid masterpieces including the most simplified to the most complicated ones.

For supporting the domes, Sinan has used three different supporting systems. The loads and the stresses of the domes are transmitted to the foundations by means of supporting systems and secondary supporting elements at different levels. These supporting systems are: square, hexagonal and octagonal supporting systems.

The structural system of Süleymaniye is composed of domes, transition elements, arches, counter weight tower, piers, walls, buttresses and foundations. The Süleymaniye Mosque is the main building of the Süleymaniye complex (Fig. 2.2.1.1).

Its plan dimensions are 61 m in south direction and 73 m in the perpendicular direction. The mosque has one axis of symmetry in the north-south direction. The main dome is 26.2 m in diameter and the height reaches 49.5 m from the ground.

The circular base of the dome is transferred to the square geometry via the four decorative pendentives. The main arches are connected to the main piers at an elevation of 32m from the ground.

Semi-domes which exist on the north and south part of the structure connect to the main arches and rest upon the two exterior buttress piers. On either side of the semi-domes an exedra semi-dome stays which actually enlarges the internal volume of the mosque. There are also five smaller domes both on the west and on the east of the structure.

The huge dimensions of the main four piers are hidden by means of the detailing provided in the circumference of the piers. Those piers are connected to exterior buttresses via the double arches, at an elevation of 10 m from the ground. The counter weight towers sitting on the top of the main piers have intended to provide lateral supports.

The west and east walls, laying under the main arches, sit on the top of the small arching system which is springing to main piers and the internal columns at an elevation of 10 m from the ground level.

2.2.2 SUBSTRUCTURE

In the area inside the city walls of İstanbul, wooden grillage could be found under the foundations of old masonry buildings constructed on greywackes. Hagia Sophia, Byzantine churches and Ottoman mosques are situated in this area; the important one among which is the Süleymaniye Mosque with footings getting larger with depth and adapting to the rock layer via wooden grillage filled with mortar.

Evliya Çelebi, in his Book of Travels-Seyahatname(1898-1939) [6], has written that excavation and foundation phases of the mosque took a very long time: three years for excavation and crushing the stones and another three years for raising the foundations to the ground level.

However it is estimated that a deep excavation and a very long construction period would not be necessary when good soil conditions are considered. According to a survey study carried out by a private company, the depths of the foundations are not bigger than 6.20 m in most of the locations.

Within the framework of the research activities being carried out by Boğaziçi University Kandilli Observatory and Earthquake Research Institute, a soil survey was carried out by the Geophysical Department. During this study, seismic refraction measures were recorded in the garden surrounding the mosque. Measurements could not be taken at İstanbul University site since there is a graveyard in this location. Therefore, three locations of different lengths could be studied. The lengths of the profiles are limited to 60 m due to the energy source used which was a hammer. Beyond 60 m, the ratio of signal noise is decreased which makes difficult to read the first arrivals. In order to improve the quality of the records, several readings were realized at each measurement point which were piled up afterwards. Seismic measurements were recorded by two ABEM digital recorder with 24 channels. The total number of records is 27.

The study is gathered in 3 profiles. Profile-1 shows the front of the mosque while profile-2 and profile-3 show the Golden Horn side and the rear of the mosque respectively. From the delay time and the apparent velocity which is obtained from the time-distance curves on the profiles, the structure of the underground was estimated. The media appears to be two layered in some places and three layered in others.

There is a fill layer on top, The velocity of which is varying between 500 and 700 m/s. The second layer appears everywhere in all three profiles. The seismic velocity of the third layer varies between 2800 m/s and 3270 m/s. The foundations lay on the rock layer. The

depths to the layer vary in each profile. Although the values of depths vary between 5m and 13m, they may increase due to the slope of the layer.

High values of seismic wave-P show that the rock layer of the foundation is strong.

3. STRUCTURAL ANALYSIS BY FINITE ELEMENT MODEL

The numerical model used for Süleymaniye Mosque is created by LUSAS package program. LUSAS[9] is a general purpose finite element analysis system which incorporates facilities for : linear and non-linear; creep, natural frequency, buckling, spectral response, harmonic response, fourier analysis; steady field and transient field analysis and coupled thermomechanical analysis.

A range of linear and non-linear constitutive models are available, covering most commonly used engineering materials. The constitutive geometrical non-linear formulations are available for modelling large deformations and both small and large strains. The geometrical non-linearities may be accounted for by using the equations: Total Lagrangian, Updated Lagrangian, Eulerian, Co-rotational.

The LUSAS element library contains over 100 element types, enabling a wide range of engineering applications to be efficiently modelled. The elements types currently available include bars, beams, 2-D continuum, plates, shells, membranes, field, joints.

Boundary conditions may be applied to the finite element model as: restrained/prescribed values, springs, slidelines, conduction/radiation.

The method of solving the equilibrium equations in LUSAS is the frontal technique, to which random access techniques and machine code inner loops have been incorporated. This solution systems of simultaneous equations commonly encountered in finite element analysis.

The finite element model in this study was obtained through various analysis. In order to assure the precision of the results, the number of elements were kept as high as possible which increase the run time of the computer. But, using fast processors and big computer memories helped reducing the run-time.

3.1 STRUCTURAL MODEL PROPERTIES

The art of finite element analysis lies in the development of a suitable model idealisation. The element discretisation, or mesh must be neither too fine, making the preparation of data, execution computer time, and interpretation of results excessively difficult, nor too coarse, rendering the accuracy of the results unacceptable. The problem is thus one of balance.

Taking into consideration the above mentioned criteria, total number of elements and nodes in the model are:

- Total number of elements :3989
- Total number of nodes :6980

In order to increase the precision, the elements with high degree of integration were used which are explained in detail in this chapter.

A previous study was carried out with the purpose of investigating the dynamic characteristics of the Süleymaniye Mosque [5] and a numerical three dimensional finite element model was constructed. During this study, the first intention was to use SHELL elements for the domes, SOLID elements for the piers, BEAM elements for the lateral dome buttress. This selection of elements created problems at the dome level such as:

- The beam elements used at side of the dome windows increased the actual window opening width.
- The use of beam type element for the lateral dome bracing would increase total stress on the connection node on the arch.
- The problem of where to connect the dome base arised.

Considering the above mentioned problems, and to maintain the homogeneity in the element types; lateral dome braccings and the short columns between the dome windows are simulated as 3D SOLID element which is actually the case in the real structure.

3.1.1. Solid Elements

The solid elements whic are used when the bar and shell elements can not be used in the model due to geometrical considerations of the structure. There are three different types of groups of solid elements whic are defined as 8-noded, 6-noded, and 4-noded. These groups of solid elements are called hexahedral (HX8M), pentahedral (PN6), and tetrahedral (TH4) respectively.

The HX8M element is a low order enhanced strain element exhibiting improved accuracy in coarse meshes, particularly if bending predominates.

The solid elements may be utilised for analysing flat and curved 3-D shell structures where it is necessary to account for transverse shear. This typically involves thick shell structures where transverse shear deformation can have a considerable influence on response.

The elements may be used for modelling intersecting shells (branched shell junctions). In this instance the nodal rotation freedoms are transformed to relate to the global axis. For modelling stiffend shell structures, the shells may be connected to beam elements BMS to BTS3.

The element output obtained at the element nodes and Gauss points consists of:

Stress Resultant Output

N_x, N_y, N_{xy} :the membrane stress resultants/unit width in the local cartesian system,

M_x, M_y, M_{xy} :the moments/unit width in the local cartesian system,

S_x, S_y :the shear stress resultants/unit width in the local cartesian system.

3.2 STRUCTURAL IDEALIZATION

The structural finite element model which was used in a previous A.Selahiye's study on Süleymaniye Mosque [5]

- A detailed study was carried out to determine an optimum number of structural elements. For this purpose the total number of elements were raised to 3989 and the corresponding total number of nodes to 6980.
- Small domes were added to the model which were previously excluded.
- Foundation level was lowered 2.5 m below ground level
- Four different boundary conditions were analysed for a different combinations of material properties.

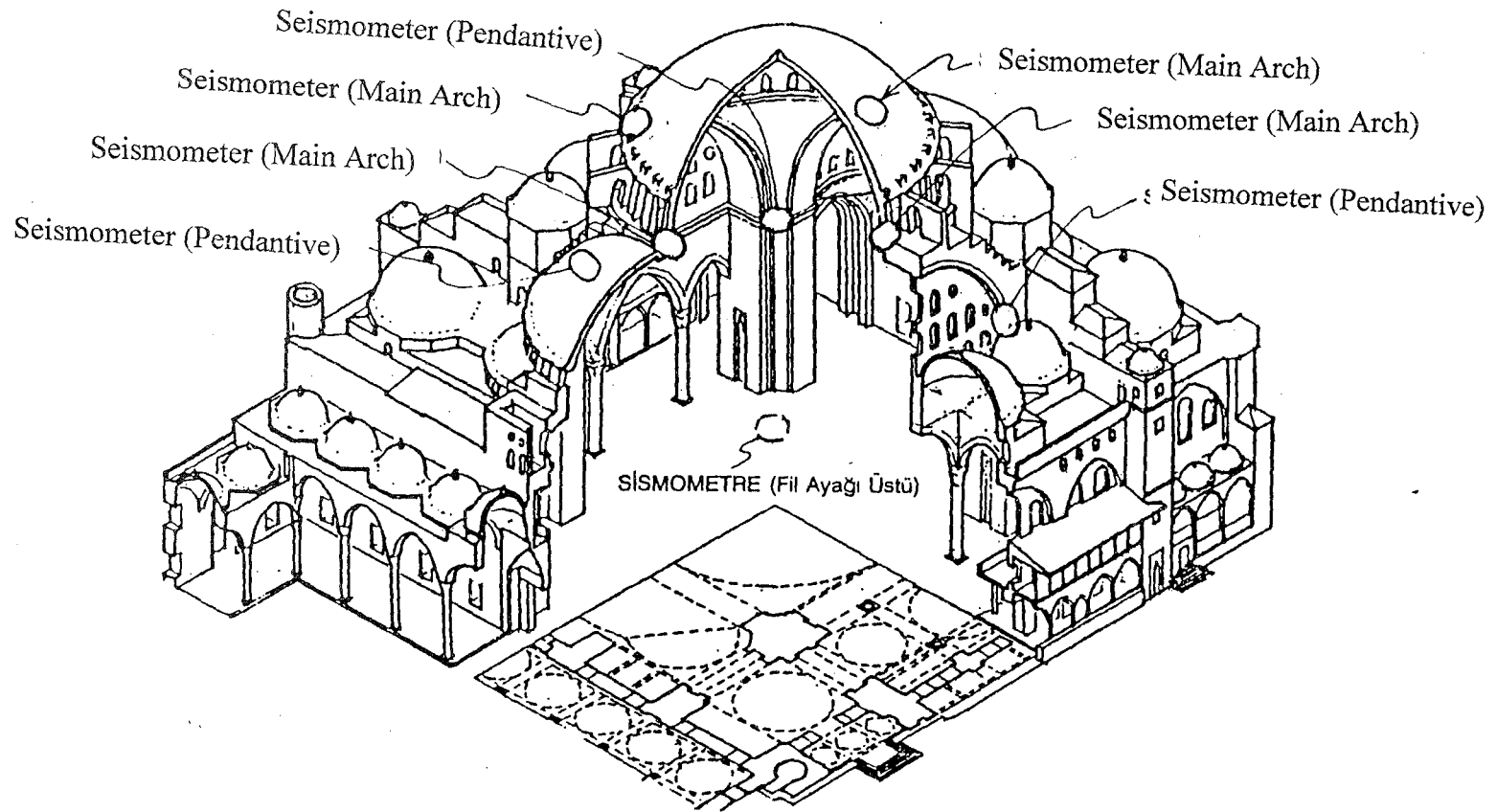
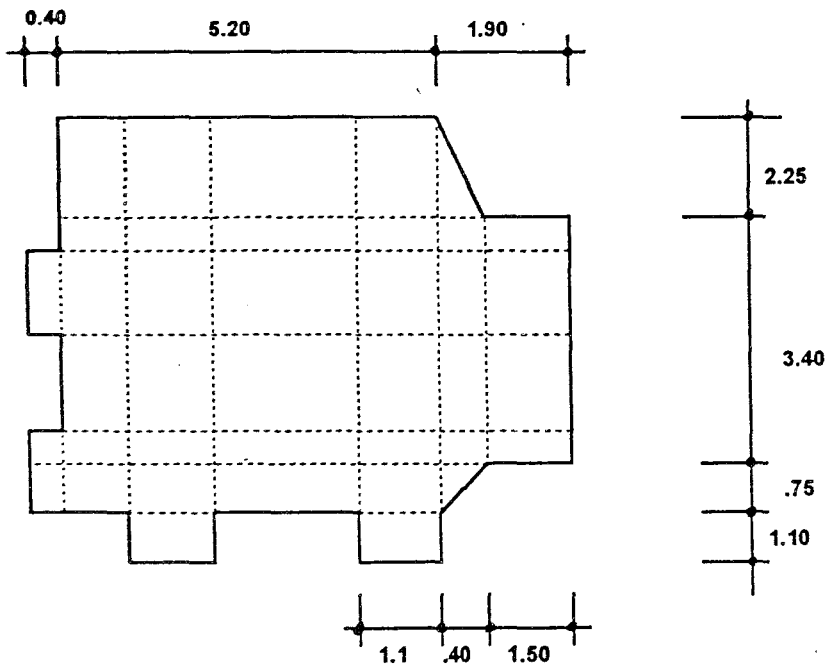


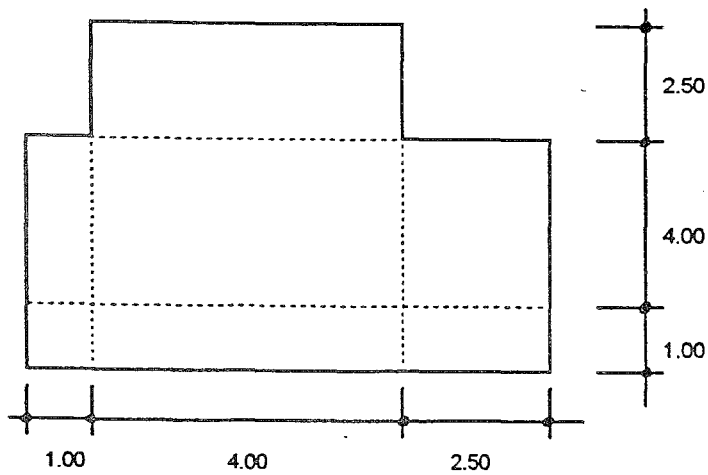
Fig.2.2.1.1 3-Dimensional View of the Accelerometer Positions on the Mosque [6]

FIGURE 3.2.1 Cross Section of the Main Pier

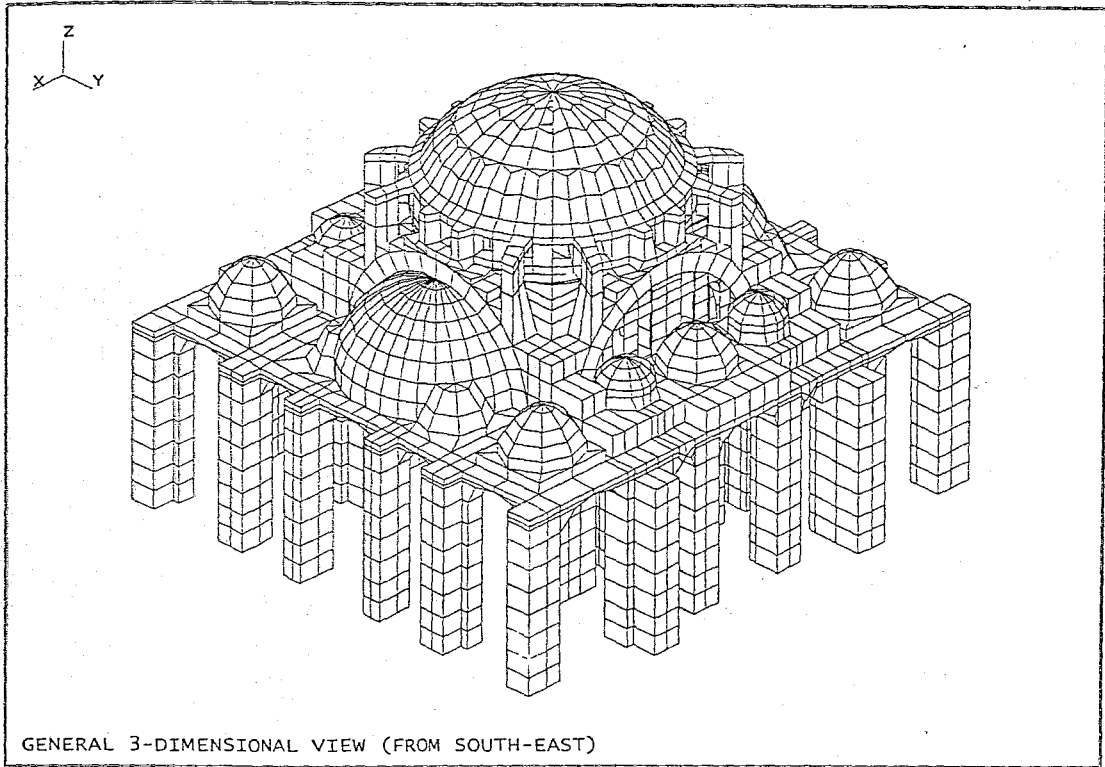


TOTAL CROSS SECTIONAL AREA IS 43.64 cm^2

FIGURE 3.2.2 Cross Section of the Simplified Piers

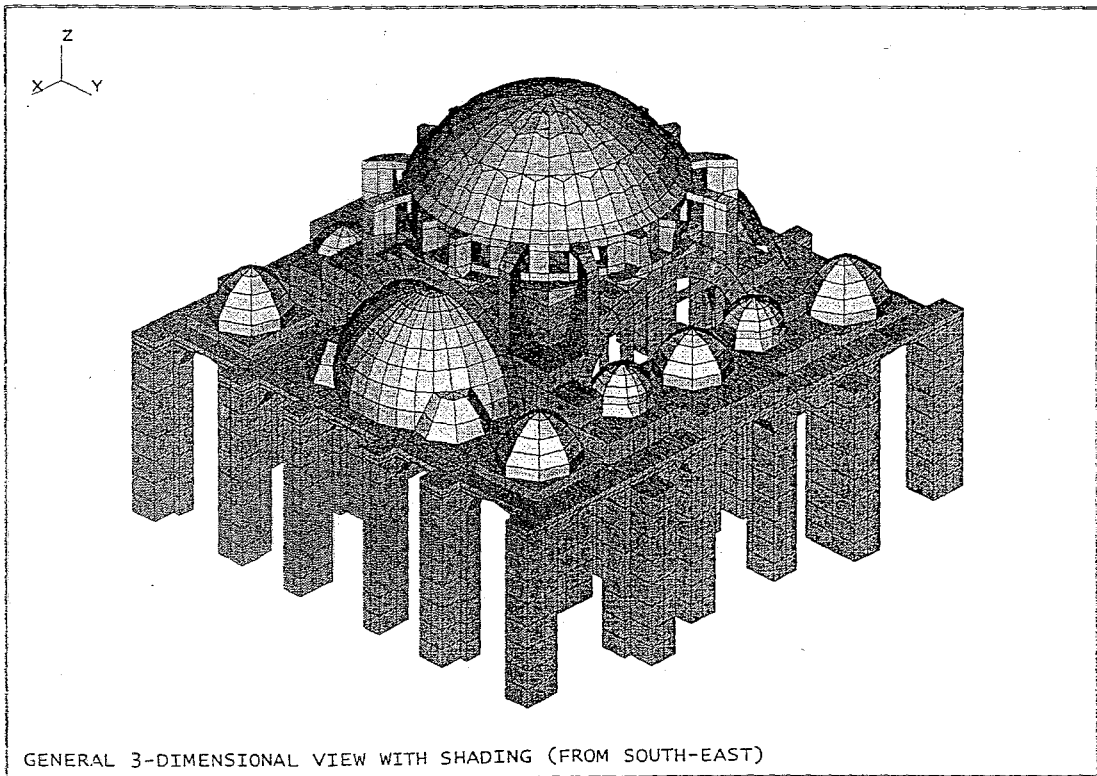


TOTAL CROSS SECTIONAL AREA IS 47.5 cm^2



GENERAL 3-DIMENSIONAL VIEW (FROM SOUTH-EAST)

FIGURE 3.2.3 General 3-Dimensional View From South-East



GENERAL 3-DIMENSIONAL VIEW WITH SHADING (FROM SOUTH-EAST)

FIGURE 3.2.4 General 3-Dimensional View from South-East

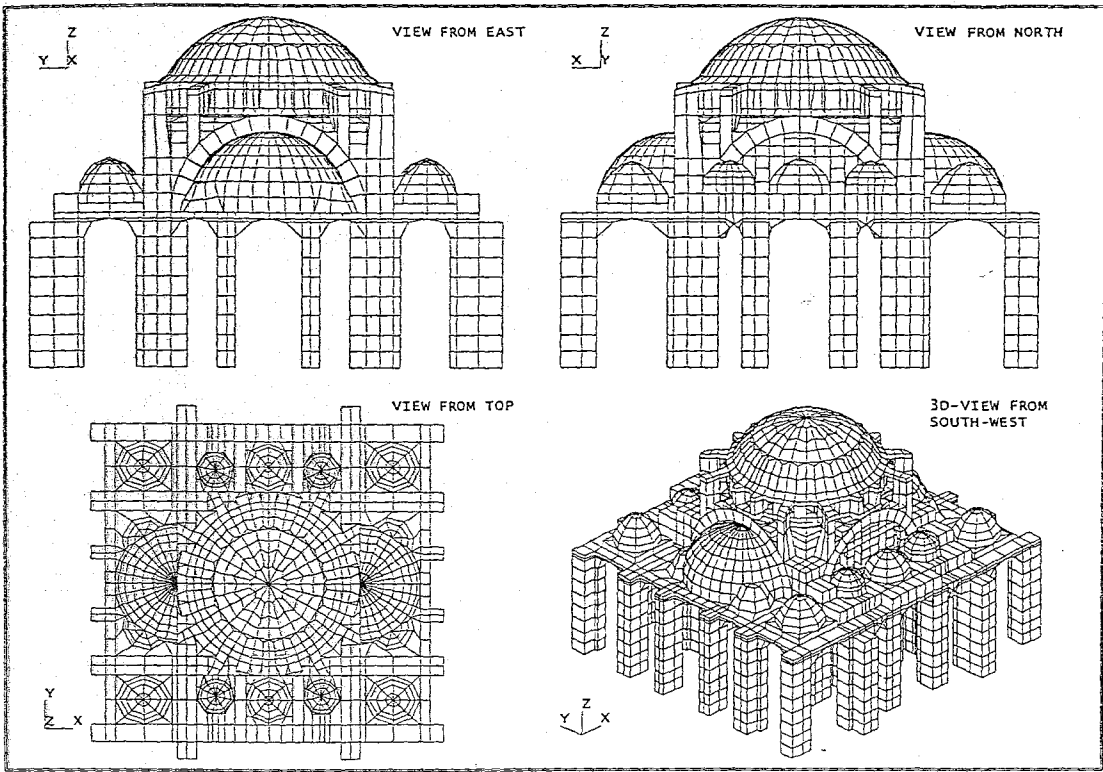


FIGURE 3.2.5 View from East, North, top and 3D view from South-West

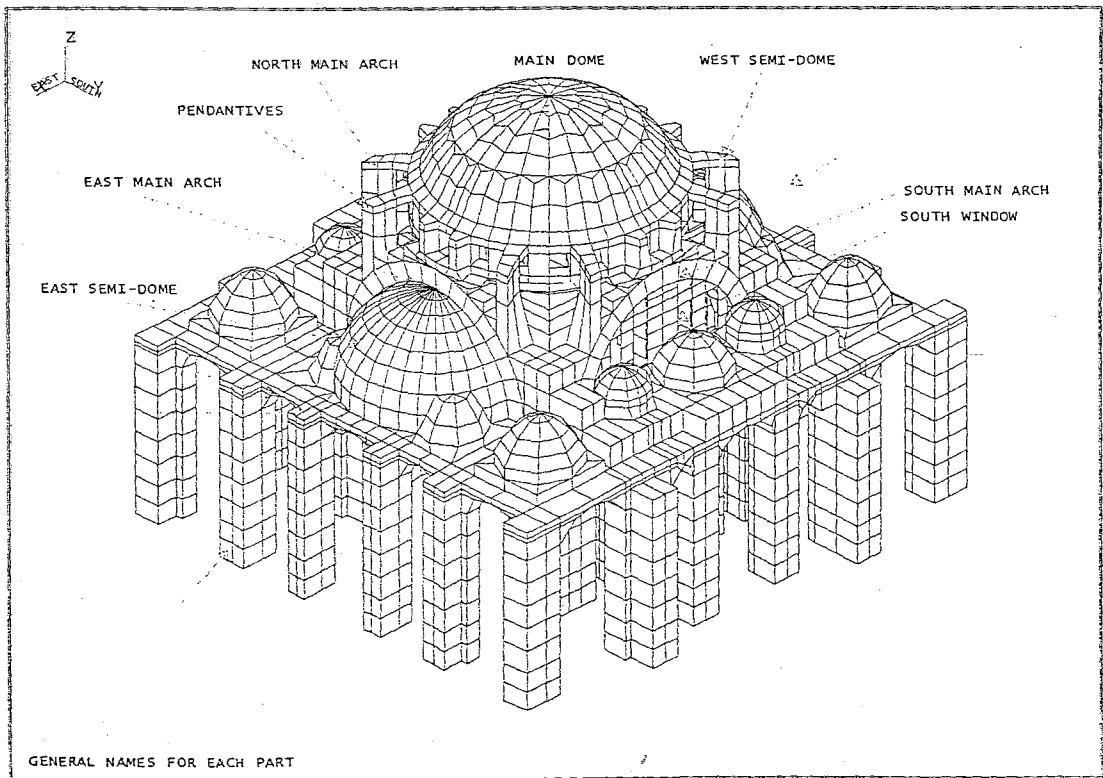


FIGURE 3.2.6 General Names for Each Part

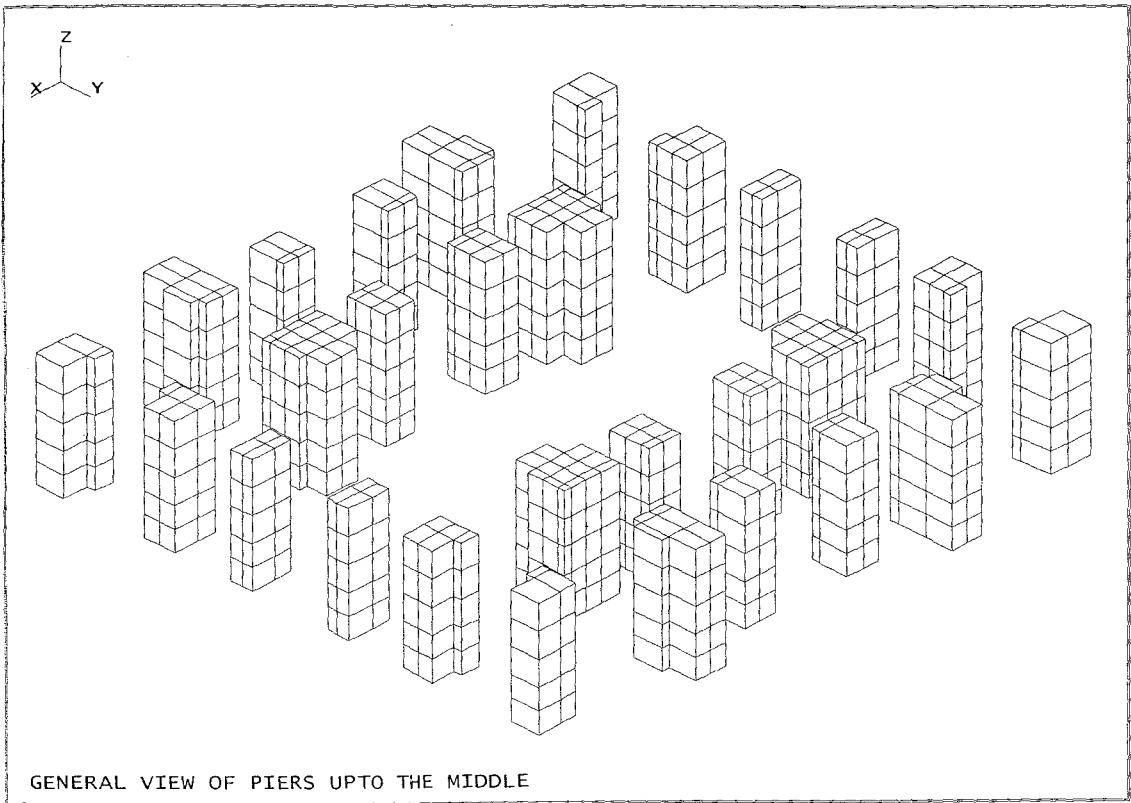


FIGURE 3.2.7 General View of the Piers upto the Middle

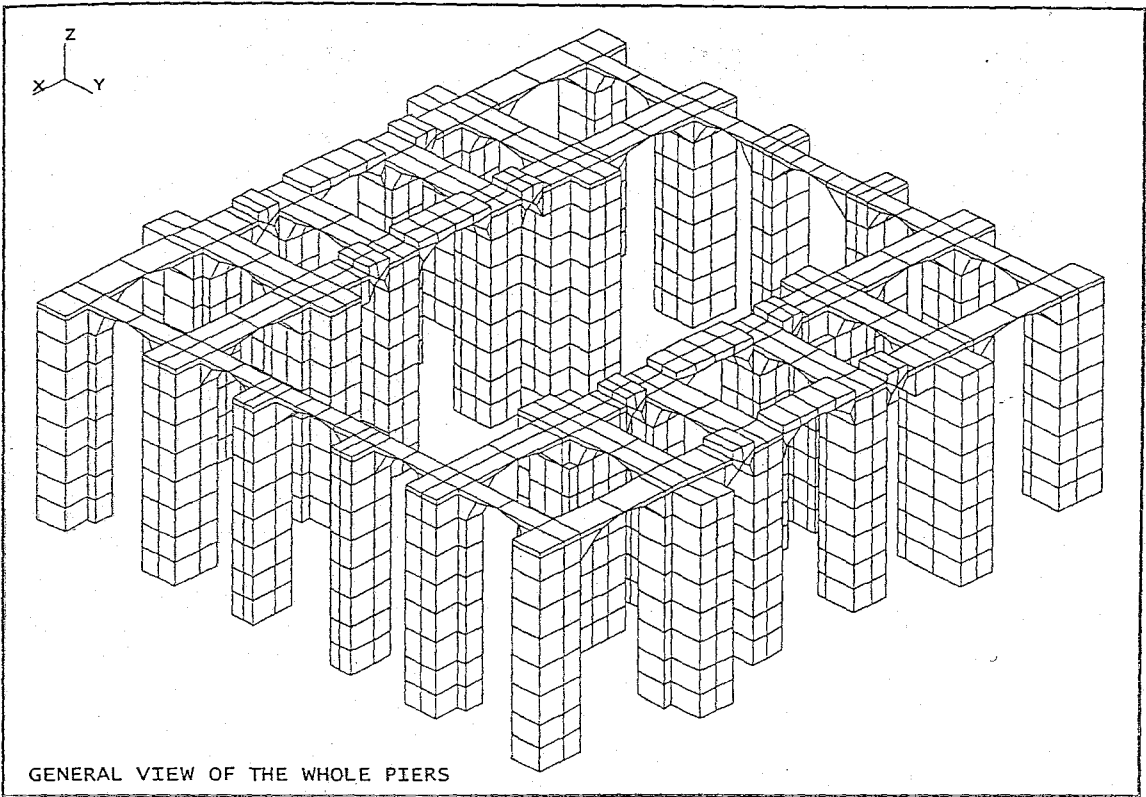


FIGURE 3.2.8 General View of the Whole Piers

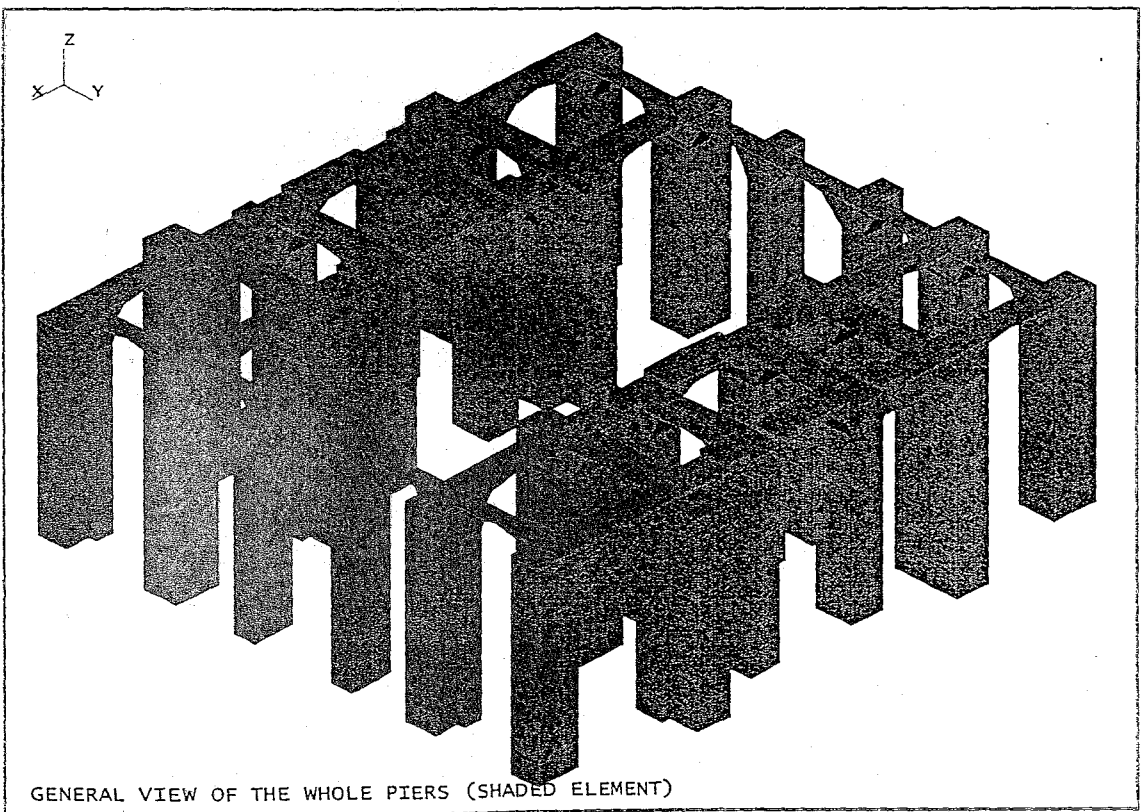


FIGURE 3.2.9 General View of the Whole Piers

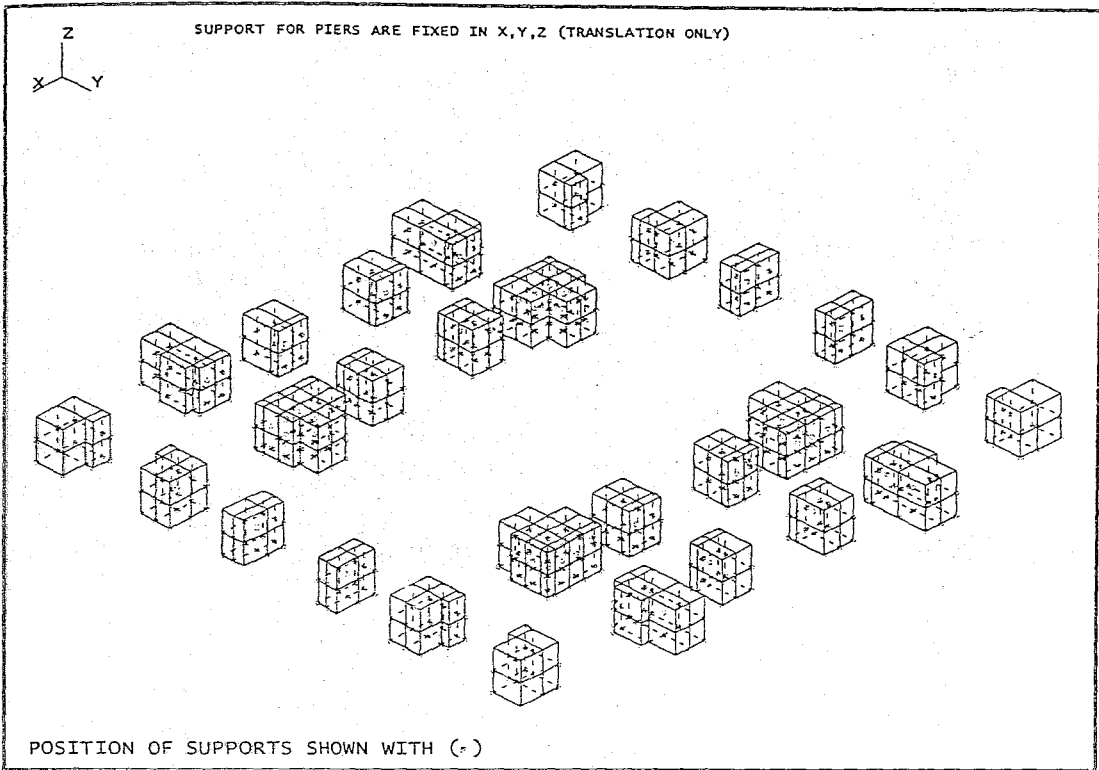


FIGURE 3.2.10 Position of Supports shown with (-)

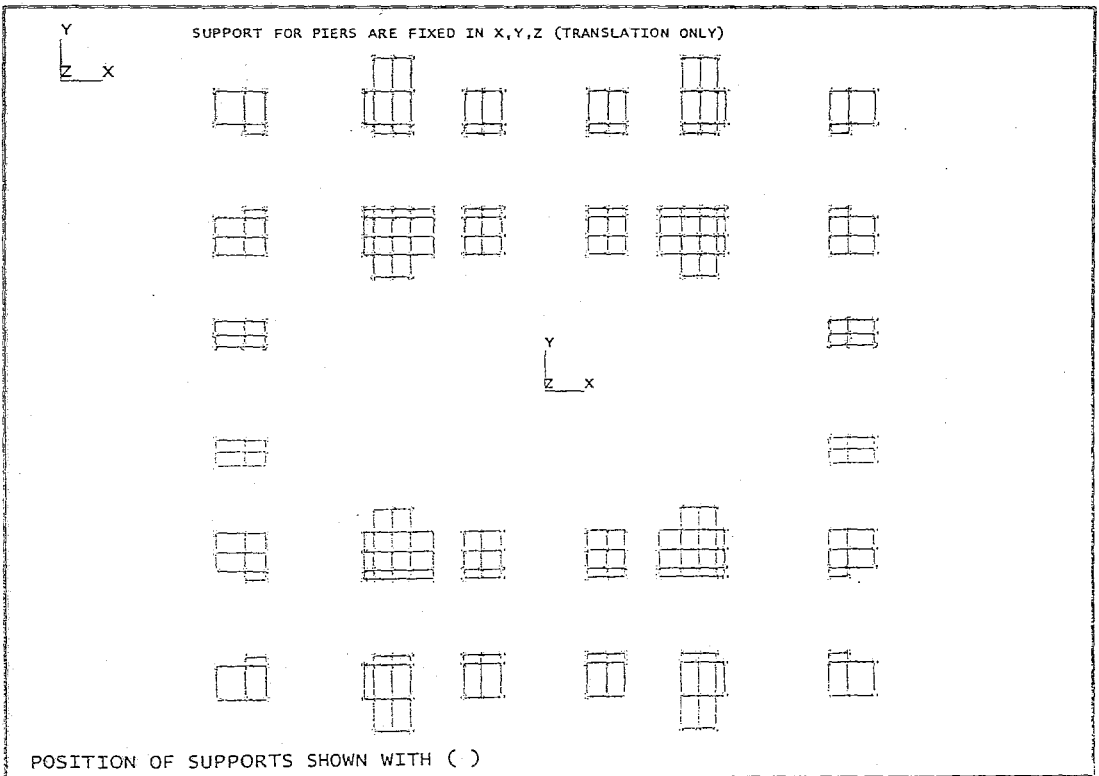


FIGURE 3.2.11 Position of Supports shown with (+)

3.3 ANALYSIS UNDER DEAD LOAD

The earthquake analysis necessitates the structure to be investigated under its own dead loads. For linear static analysis, it is assumed that the loaded body instantaneously develops a state of internal stress so as to equilibrate the total applied loads.

The main aim from static analysis is to investigate the possible stress distributions; the deflections and possible crack locations on the structure.

The static analysis of a structure involves the solution of the system of linear equations represented by:

$$KU=R$$

K is the stiffness matrix

U is the vector of resulting displacements,

R is the vector of applied loads

The three dimensional view of the deformed structure is given in figure 3.3.1 and the plan view is given in figure 3.3.1

The resultant deformations of the linear static analysis are shown in figures 3.3.1-3.3.4. These deformations are the linear short term deformations that would occur in a linear elastic homogeneous system under its own weight.

Figure 3.3.4 shows deformations in global Z direction in meter with displacement contours. Dark areas indicate the higher values of deformations. Observed deformations can be interpreted as follows.

-Due to existence of semi domes, east and west arches have less deflection than the others.

-From figure 3.3.4 it can be easily observed that the deformations mainly concentrates in the middle are at dome and arches.

Stresses

The stresses under dead load are generally below the stresses that can be resisted by the material. However, this analysis gives satisfactory results to determine the critical areas. The stresses and deformations output are in KN/m^2 and meter respectively for the solid elements. For the shell elements, the forces are in KN. Therefore, the real stresses are obtained by dividing the force by the thickness of the shell for each element.

It is easier to observe the stresses in half of the model. For the solid elements, the stresses are in global axis which are shown at top left of figures. The horizontal stresses S_X, S_Y, S_Z in east-west direction are shown in Figure 3.3.19 and S_Y and S_Z show respectively the stresses in north-south direction and vertical direction (as shown in figure 3.3.18.)

The following interpretations can be done for the stresses experienced by the structure under dead load.

The distribution of vertical stress SY which is the most important stress component for the dead load analysis shows that:

- Bottom fibres of the main arches are in compression and the upper fibers in tension.
- There are local high compressive stress concentrations at the base of the lateral dome bracings. These bracings at the top of the arches try to rotate the arches outwards.

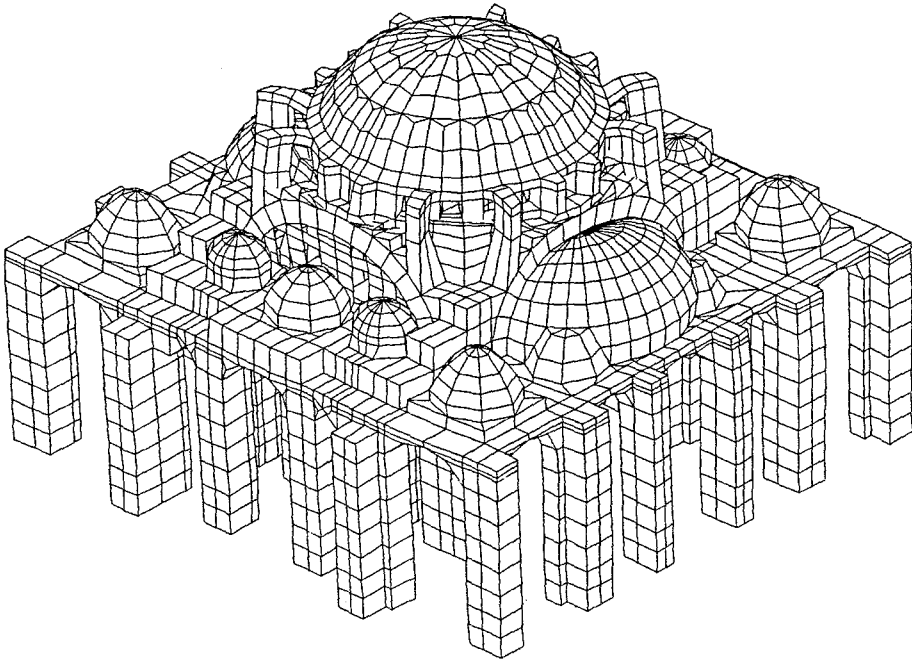
The maximum and minimum principal stresses are given in table 3.3.1

Table 3.3.1 Maximum and Minimum Stresses

Name of the element	Max.Maximum Principal Value	Min.Minimum Principal Value
Pier	$2,1765 \times 10^2$	$-1,1183 \times 10^2$
Arch (east-west)	$2,0252 \times 10^2$	$-1,0461 \times 10^2$
Arch (south-north)	$2,5124 \times 10^2$	$-8,2973 \times 10^2$
Dome	$5,3813 \times 10^2$	$-5,2725 \times 10^2$



MAGINIFICATION FACTOR = 650

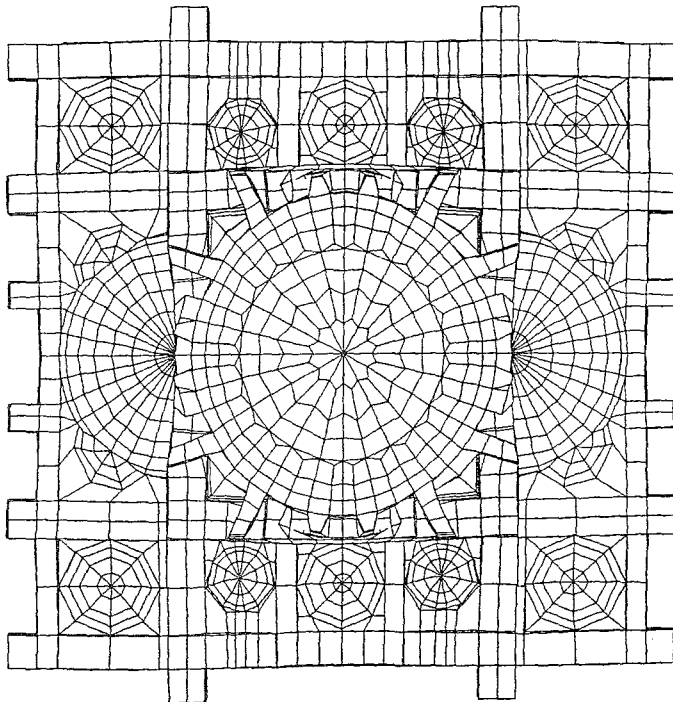


GENERAL DEFORMED CONFIGURATION (3-D VIEW FROM SOUTH-EAST)
SIMPLE STATIC ANALYSIS UNDER SELF WEIGHT

FIGURE 3.3.1 General Deformed Configuration (3-D View from South-East)
Simple Static Analysis Under Self Weight



MAGINIFICATION FACTOR = 650



GENERAL DEFORMED CONFIGURATION (VIEW FROM TOP)
SIMPLE STATIC ANALYSIS UNDER SELF WEIGHT

FIGURE 3.3.2 General Deformed Configuration (View from Top)

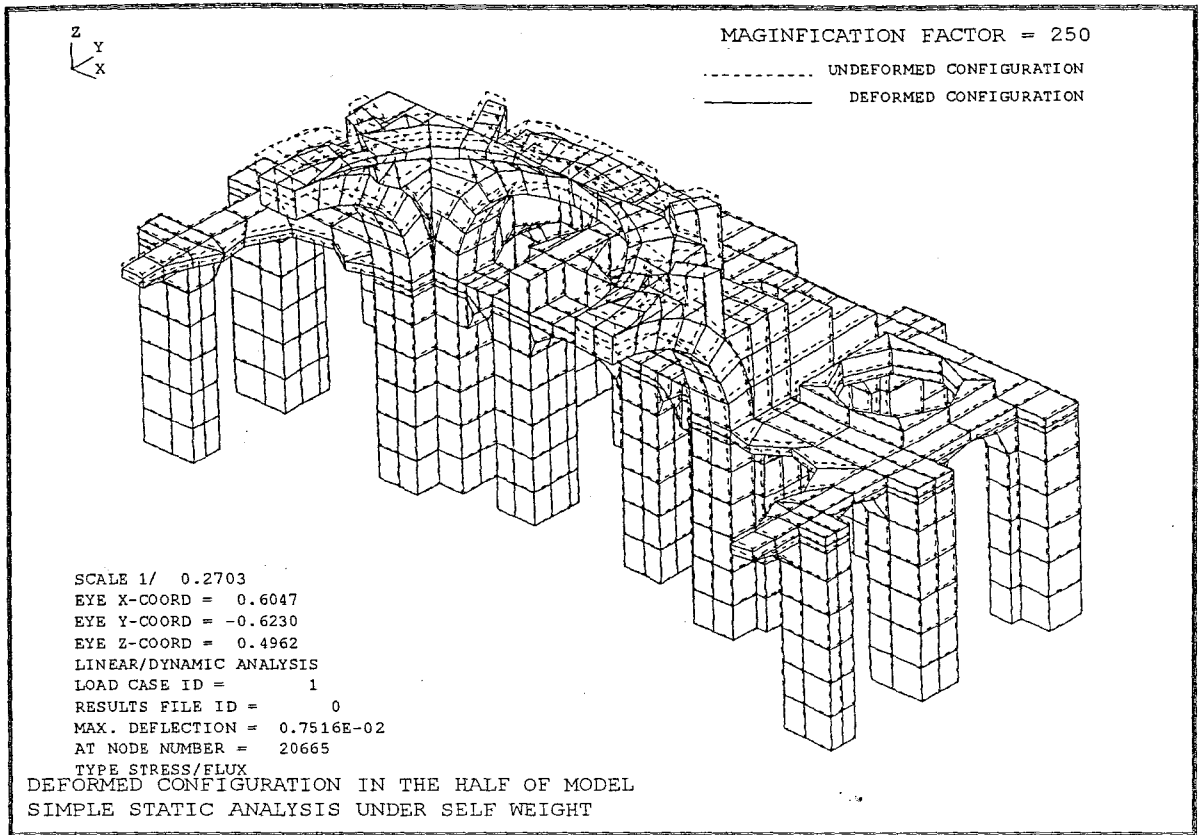


FIGURE 3.3.3 Deformed Configuration in the Half of the Model
 Simple Static Analysis Under Self Weight

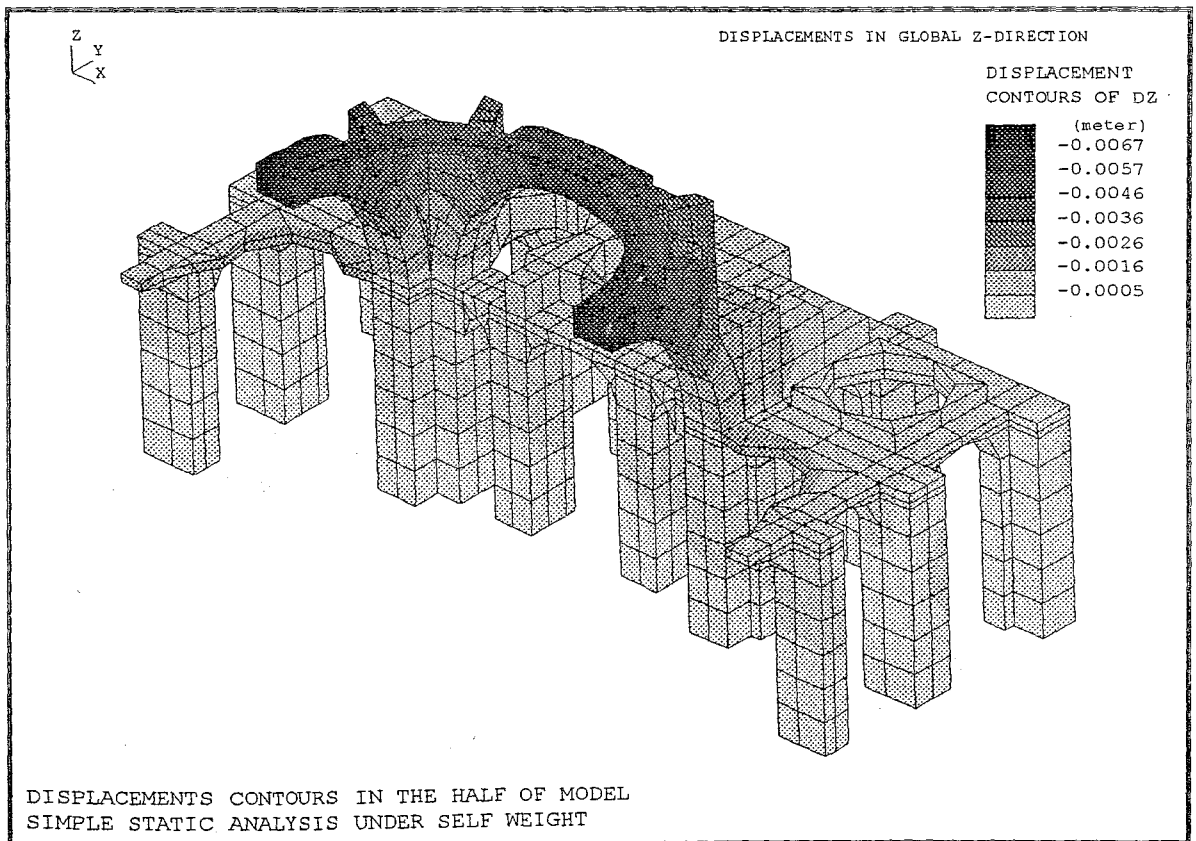


FIGURE 3.3.4 Displacement Contours in the Half of the Model
 Simple Static Analysis Under Self Weight

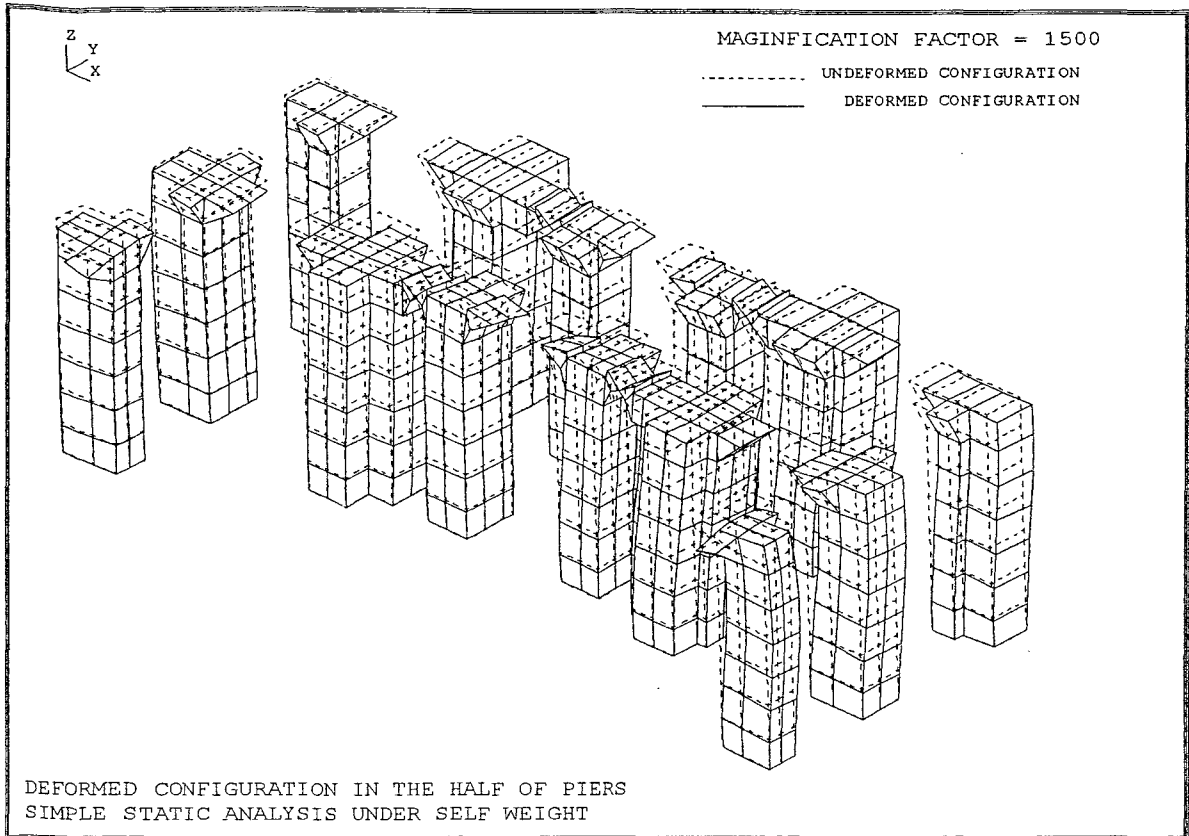


FIGURE 3.3.5 Deformed Configuration in the Half of Piers
 Simple Static Analysis Under Self Weight

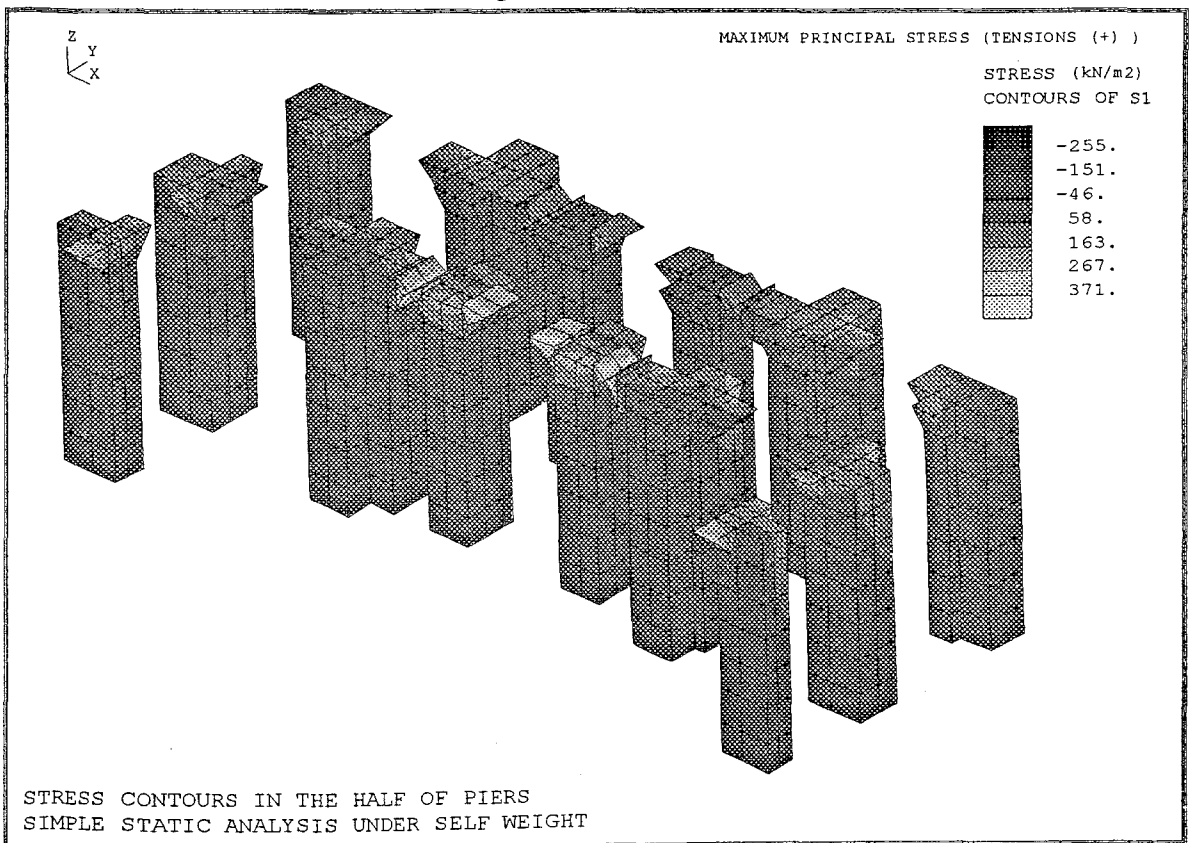


FIGURE 3.3.6 Stress Contours in the Half of Piers
 Simple Static Analysis Under Self Weight

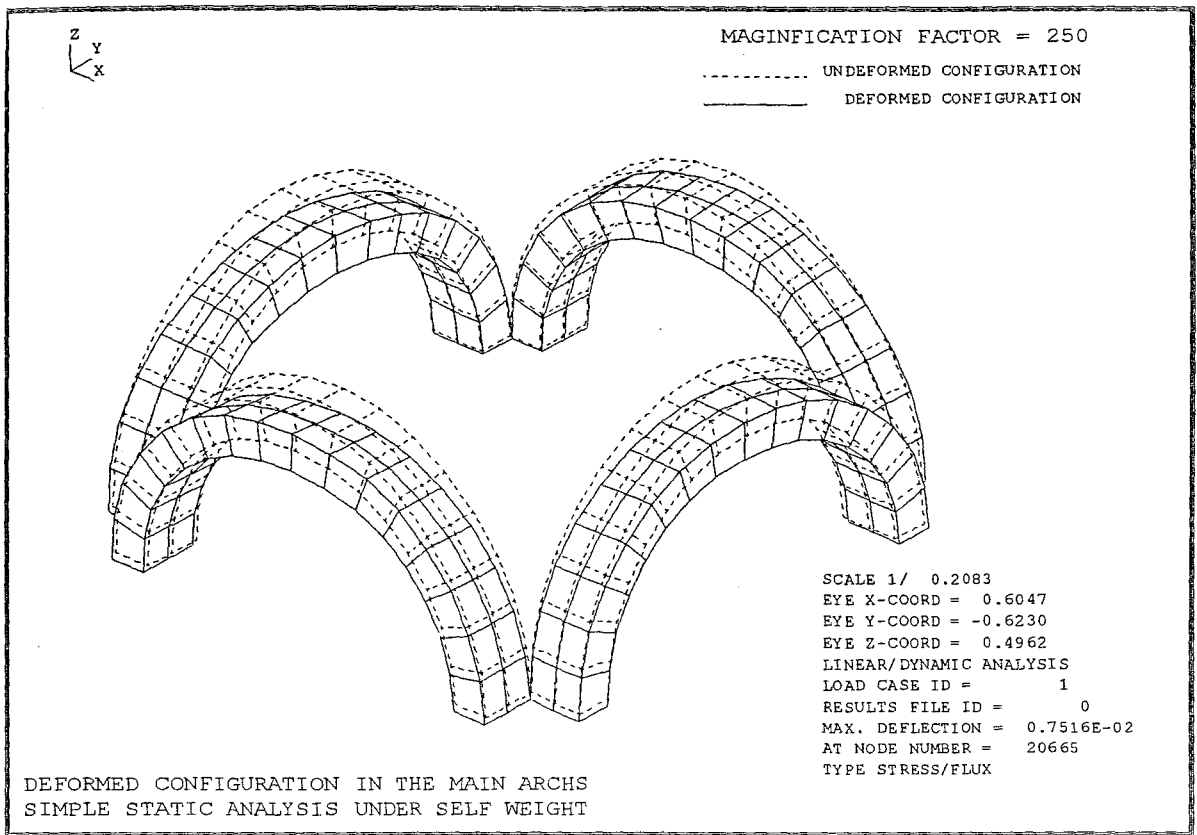


FIGURE 3.3.7 Deformed Configuration in the Main Arches
 Simple Static Analysis Under Self Weight

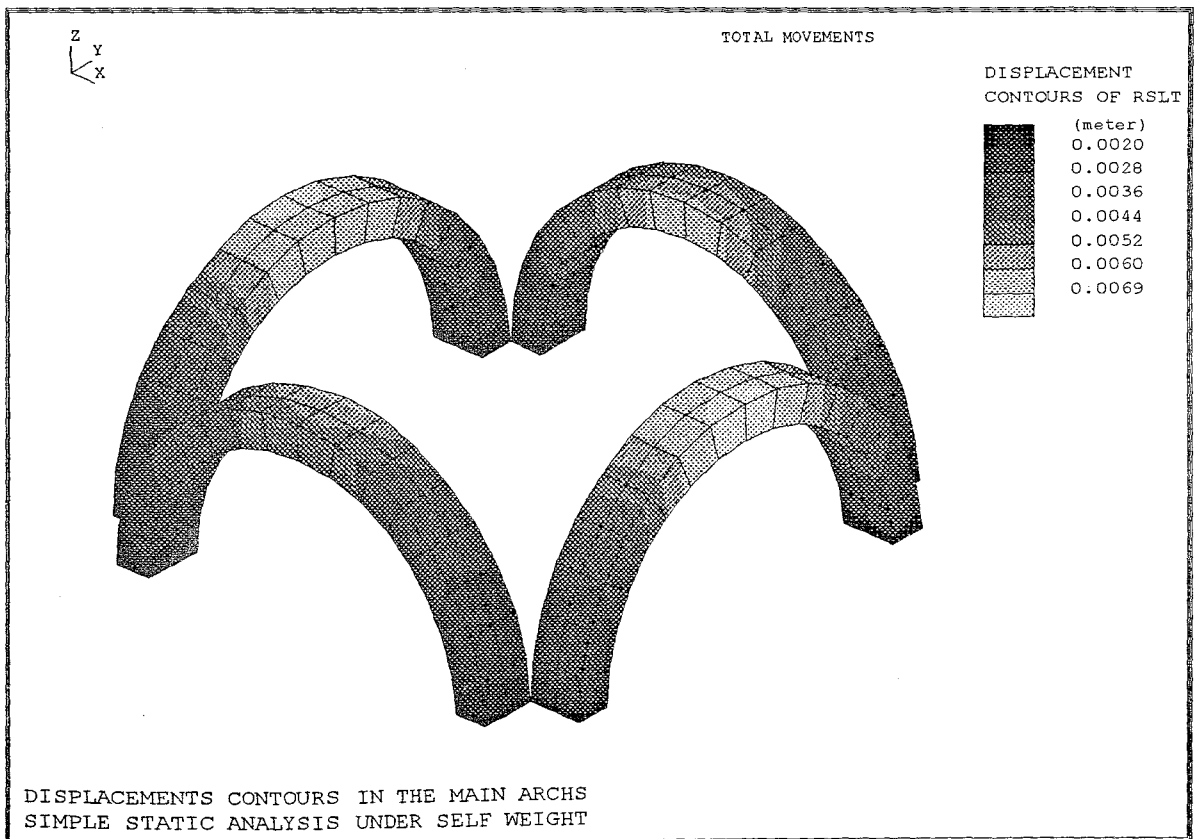


FIGURE 3.3.8 Displacement Contours in the Main Arches
 Simple Static Analysis Under Self Weight

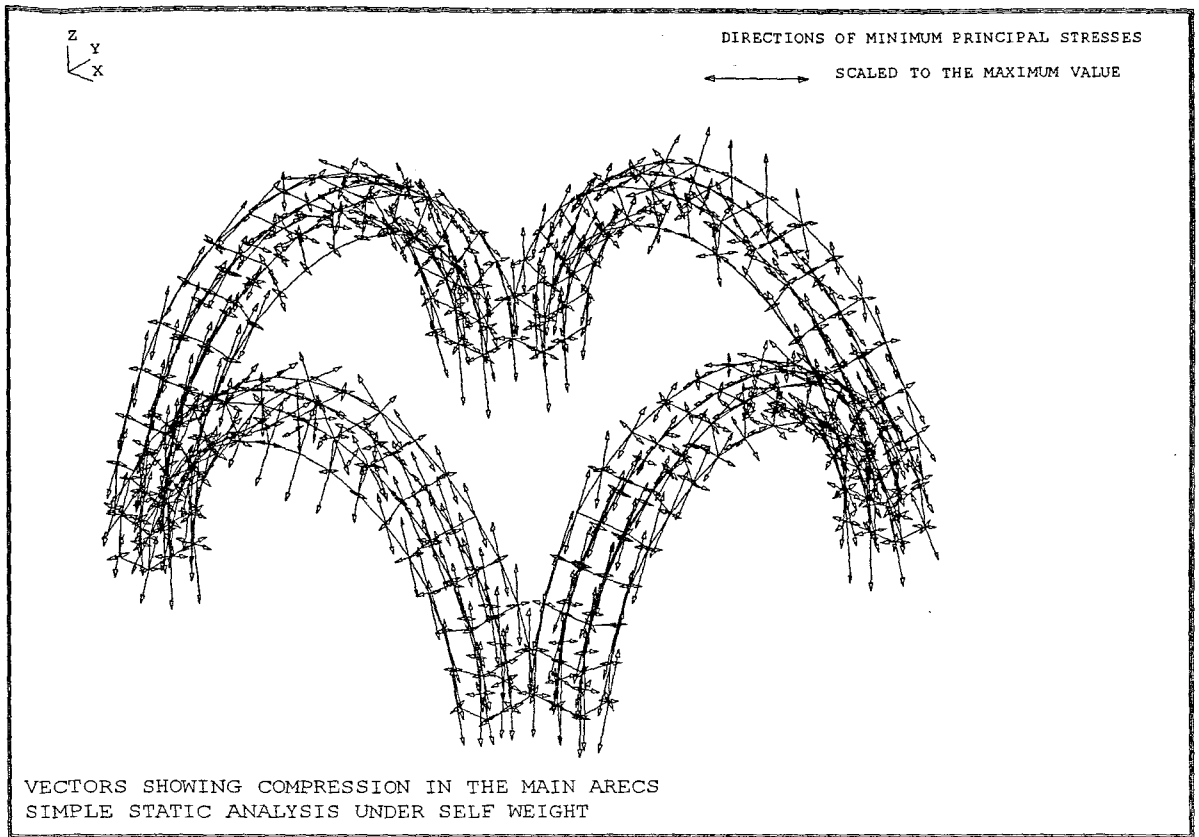
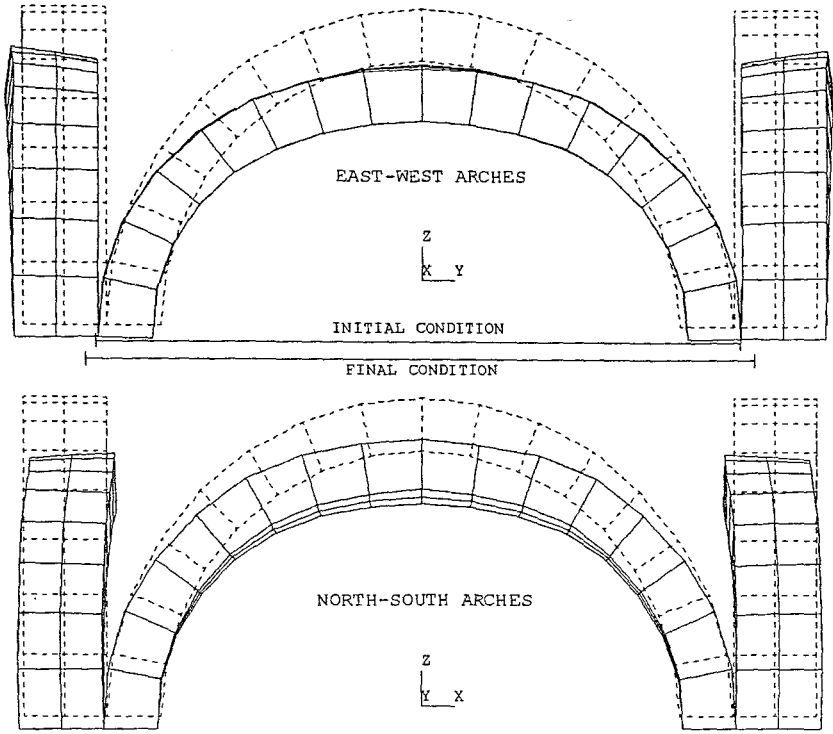


FIGURE 3.3.9 Vectors Showing Compression in the Main Arches
Simple Static Analysis Under Self Weight

MAGNIFICATION FACTOR = 400



GENERAL DEFORMED CONFIGURATION OF MAIN ARCHES
SIMPLE STATIC ANALYSIS UNDER SELF WEIGHT

FIGURE 3.3.10 General Deformed Configuration of Main Arches
Simple Static Analysis Under Self Weight

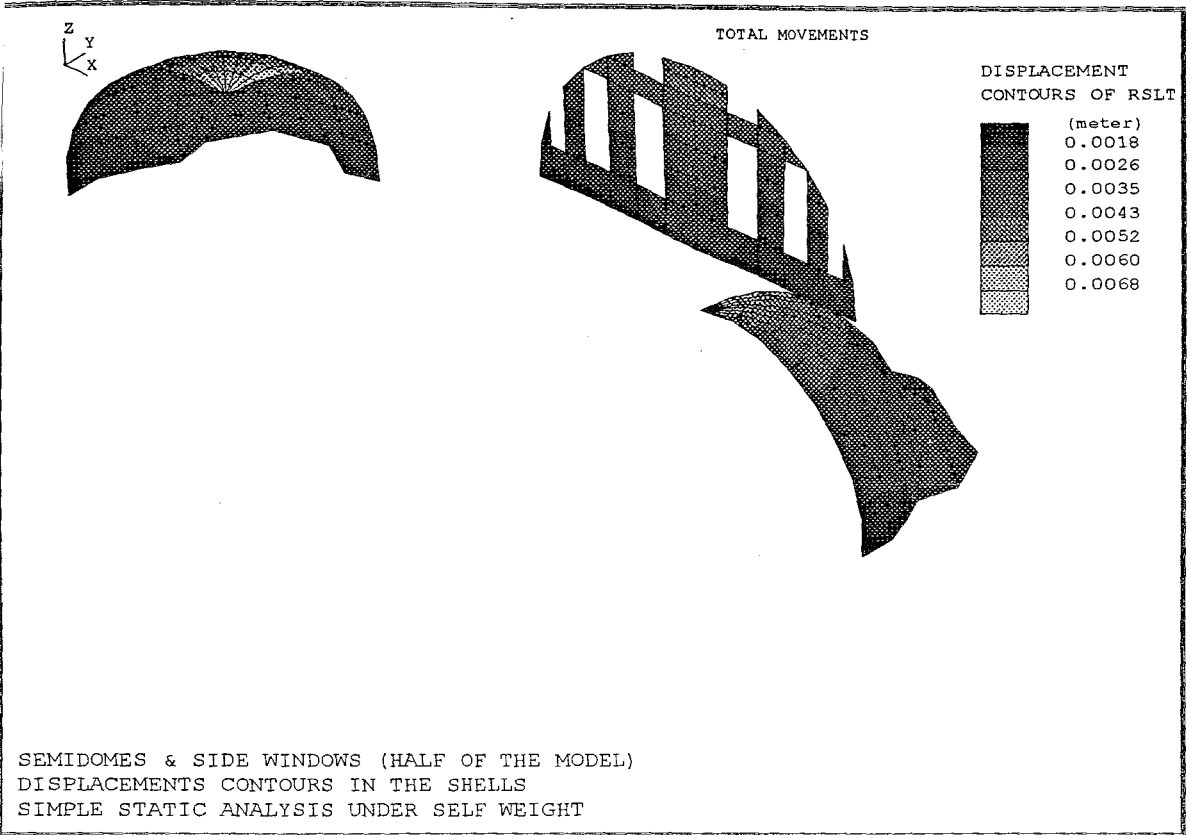


FIGURE 3.3.11 Semidomes&Side Windows (Half of the Model) Displacement Contours in the Shells,Simple Static Analysis Under Self Weight

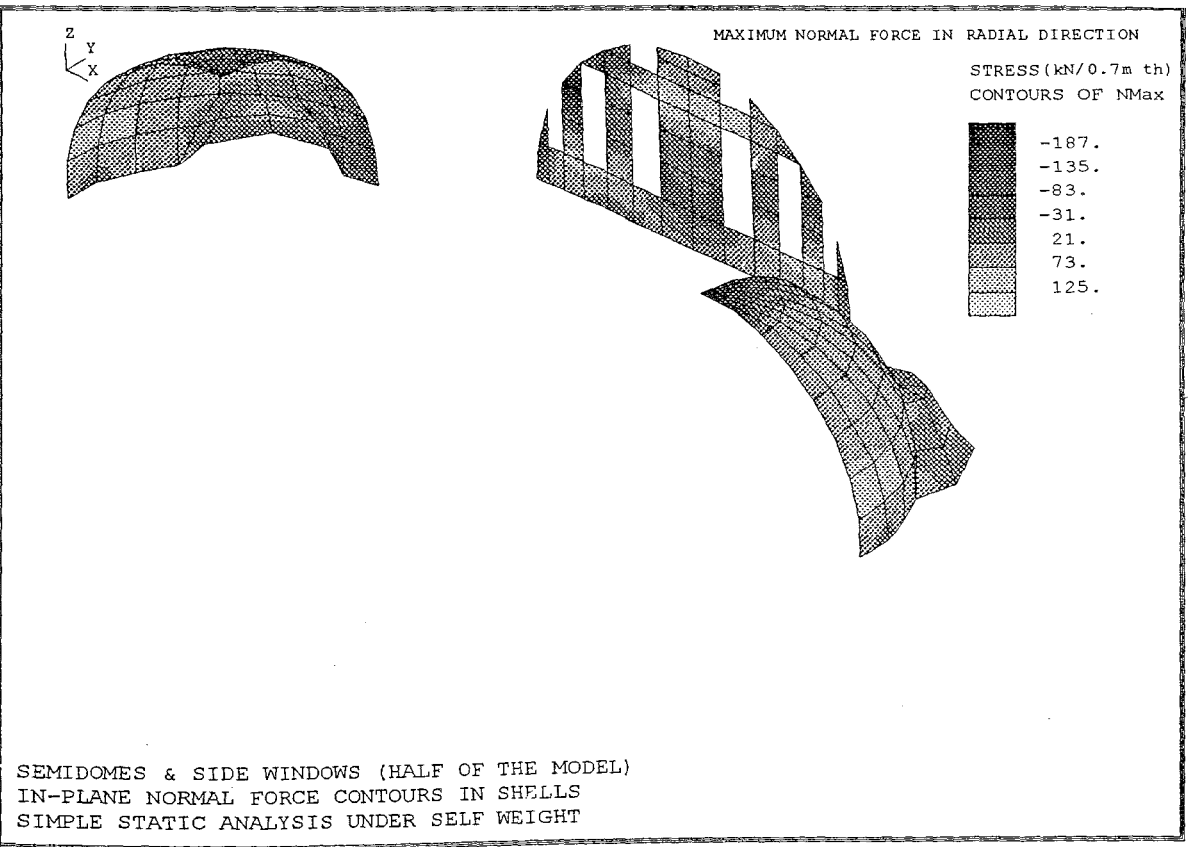


FIGURE 3.3.12 Semidomes&Side Windows (Half of the Model).In Plane Normal Force Contours in Shells-Simple Static Analysis Under Self Weight.

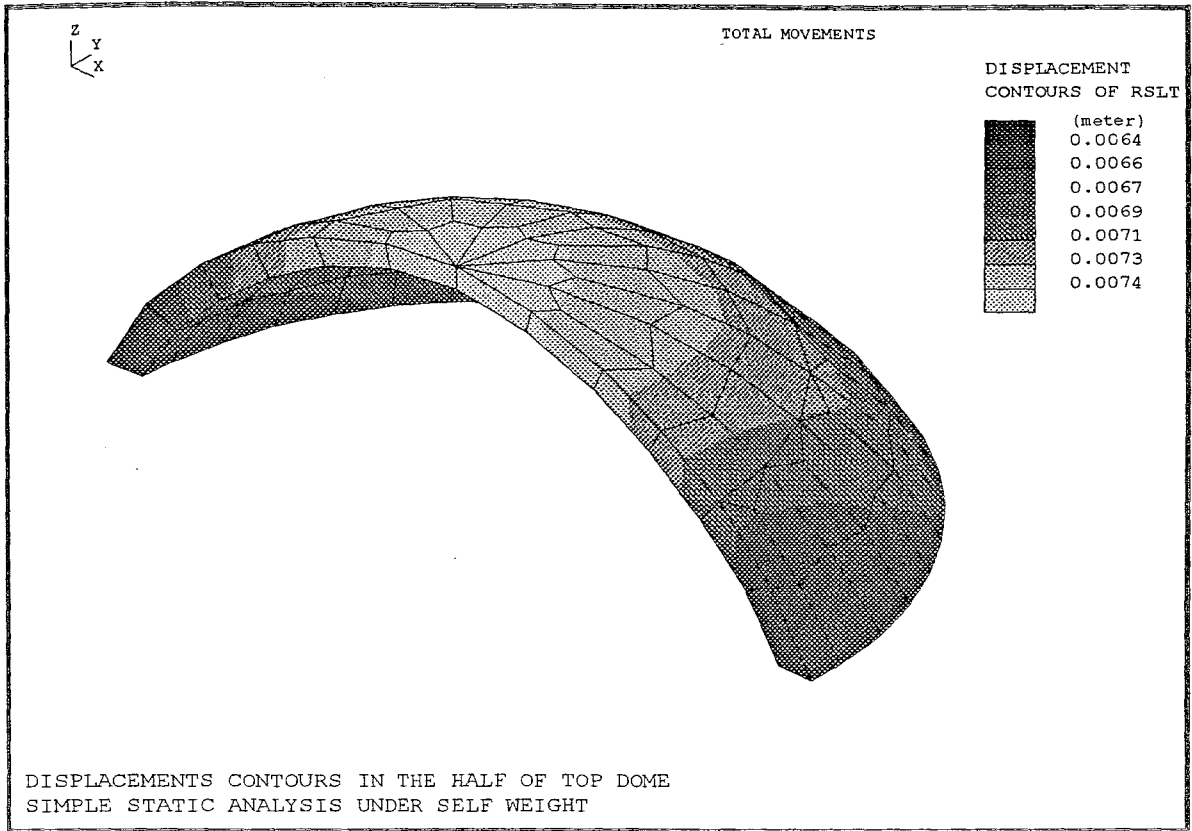


FIGURE 3.3.13 Displacement Contours in the Half of Top Dome
Simple Static Analysis Under Self Weight

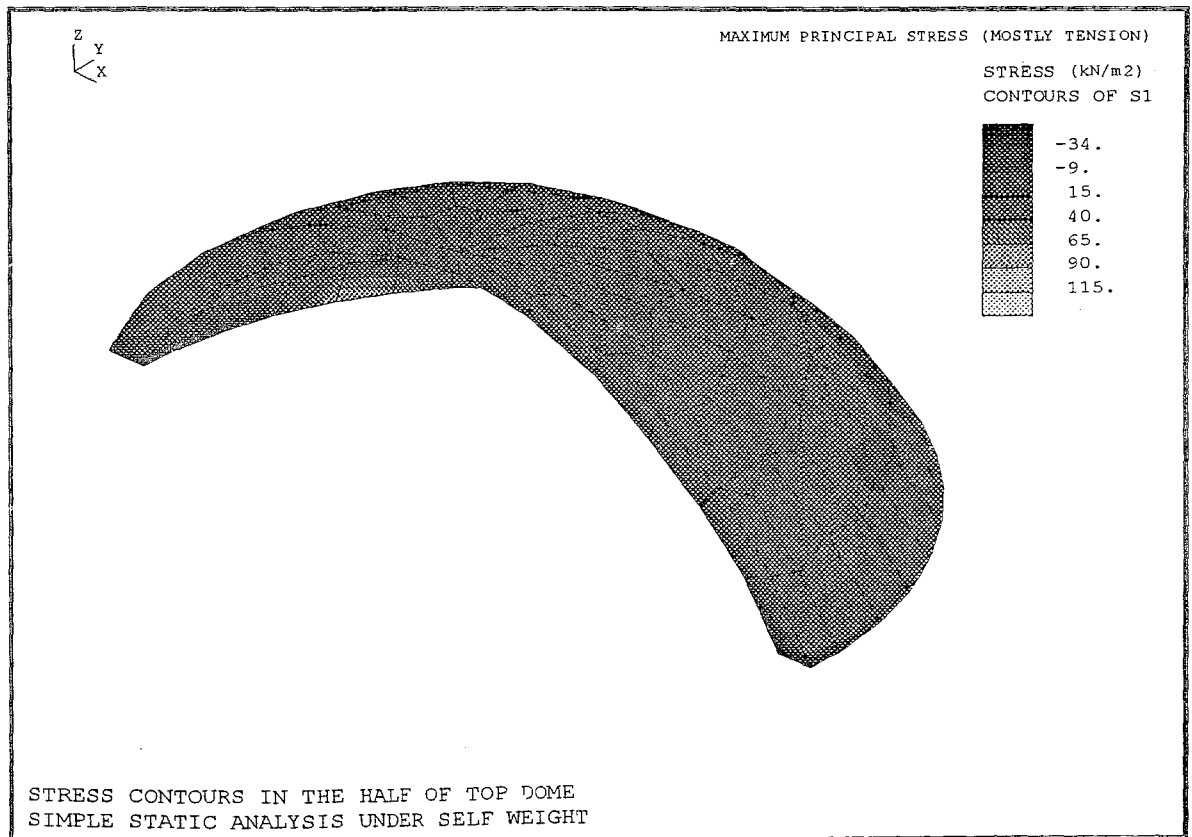


FIGURE 3.3.14 Stress Contours in the Half of Top Dome
Simple Static Analysis Under Self Weight

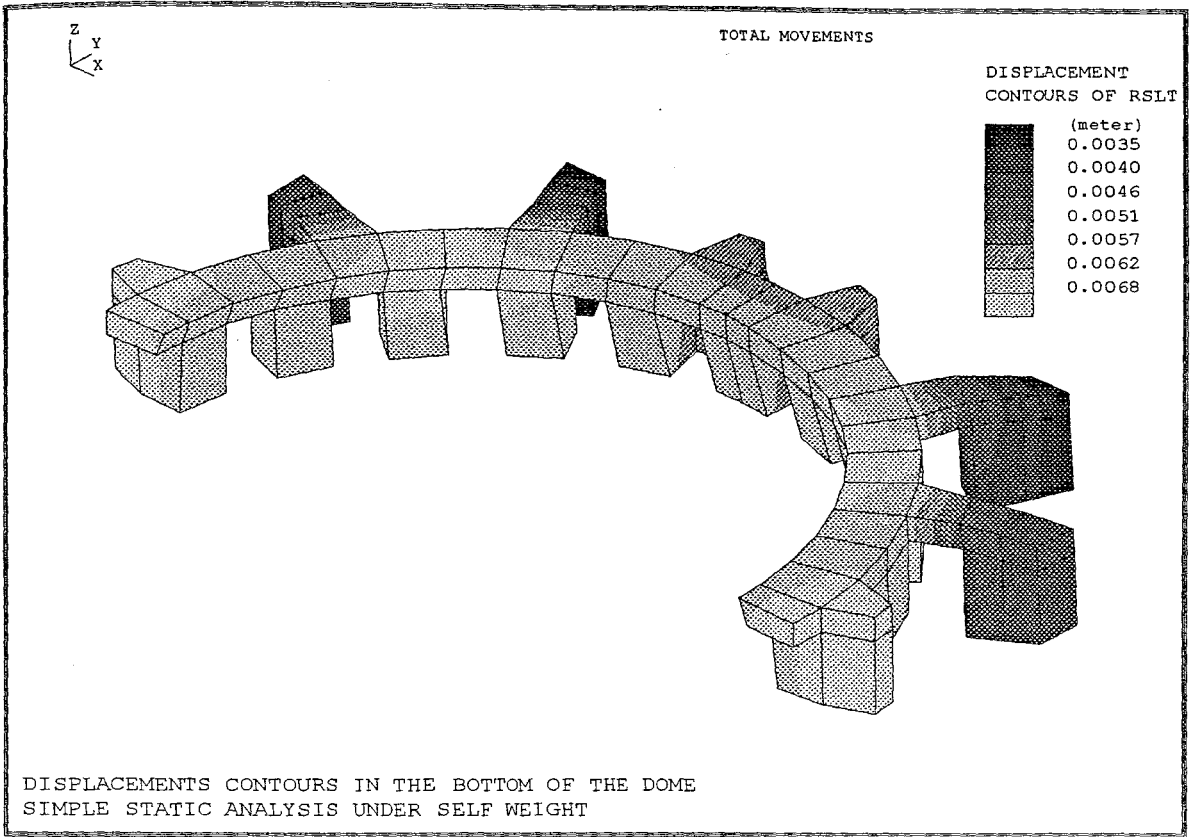


FIGURE 3.3.15 Displacement Contours in the Bottom of Dome
Simple Static Analysis Under Self Weight

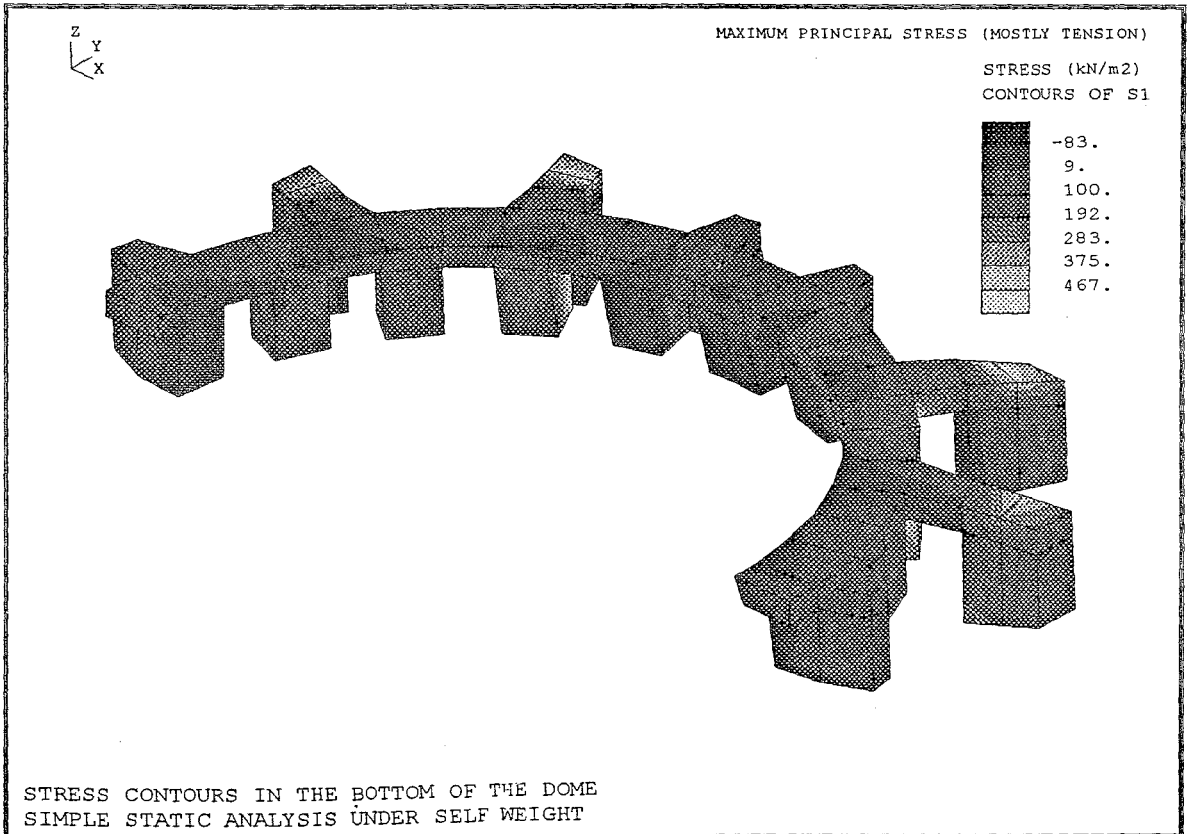


FIGURE 3.3.16 Stress Contours in the Bottom of the Dome
Simple Static Analysis Under Self Weight

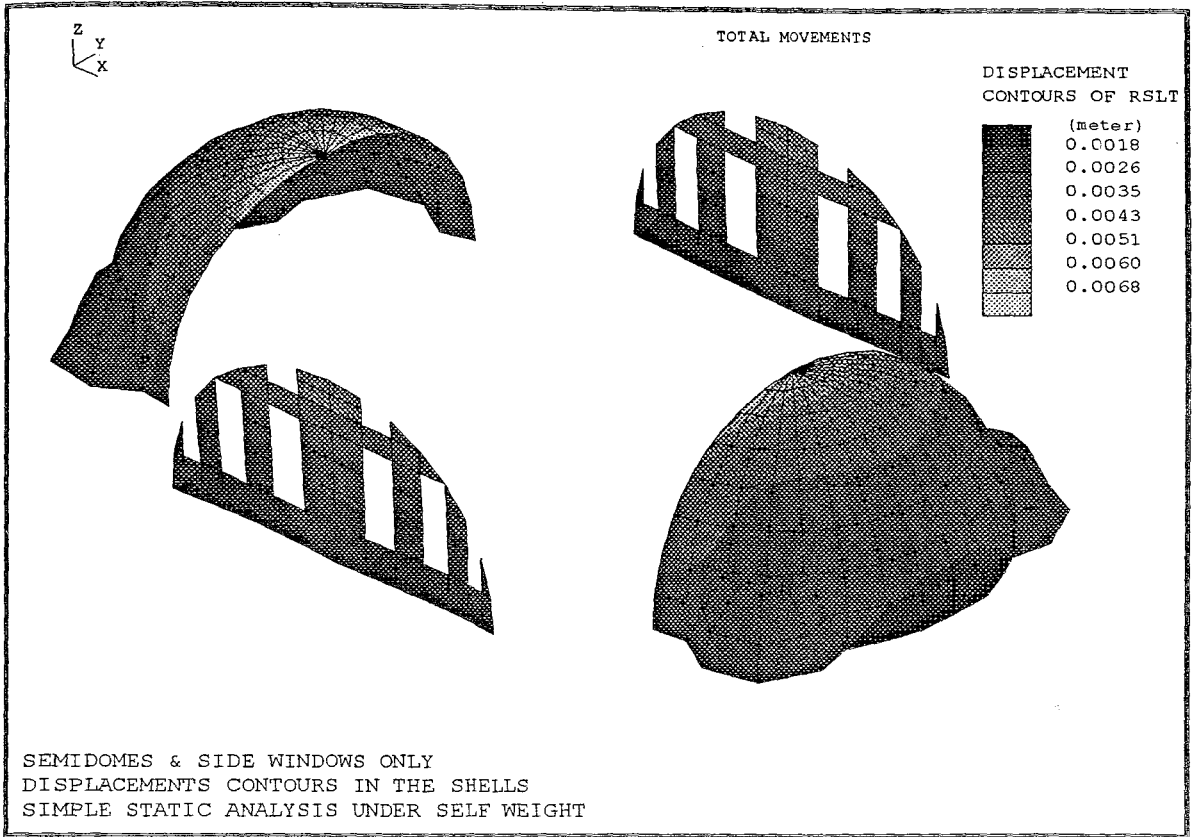


FIGURE 3.3.17 Semidomes&Side Windows Only.Displacement Contours in the Shells
Simple Static Analysis Under Self Weight

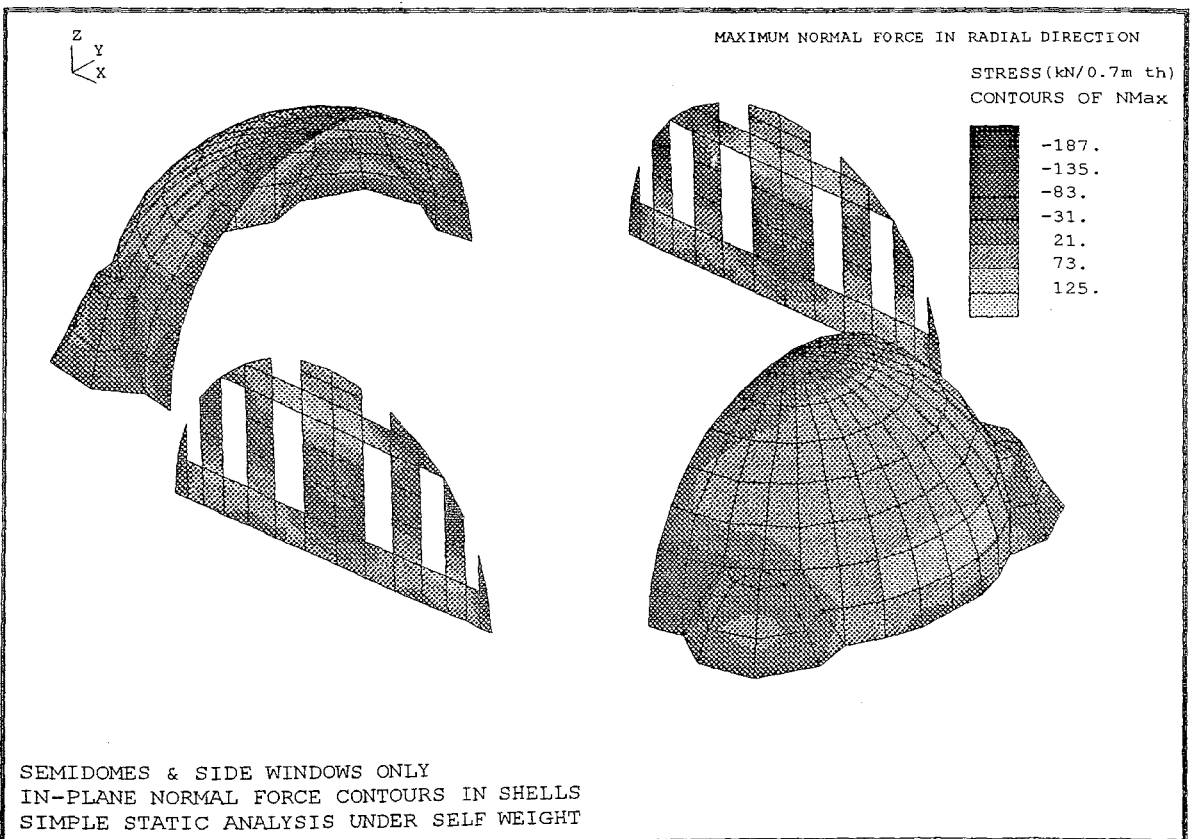


FIGURE 3.3.18 Stress Contours in the Half of Model
Simple Static Analysis Under Self Weight. Stress in Global X Direction.

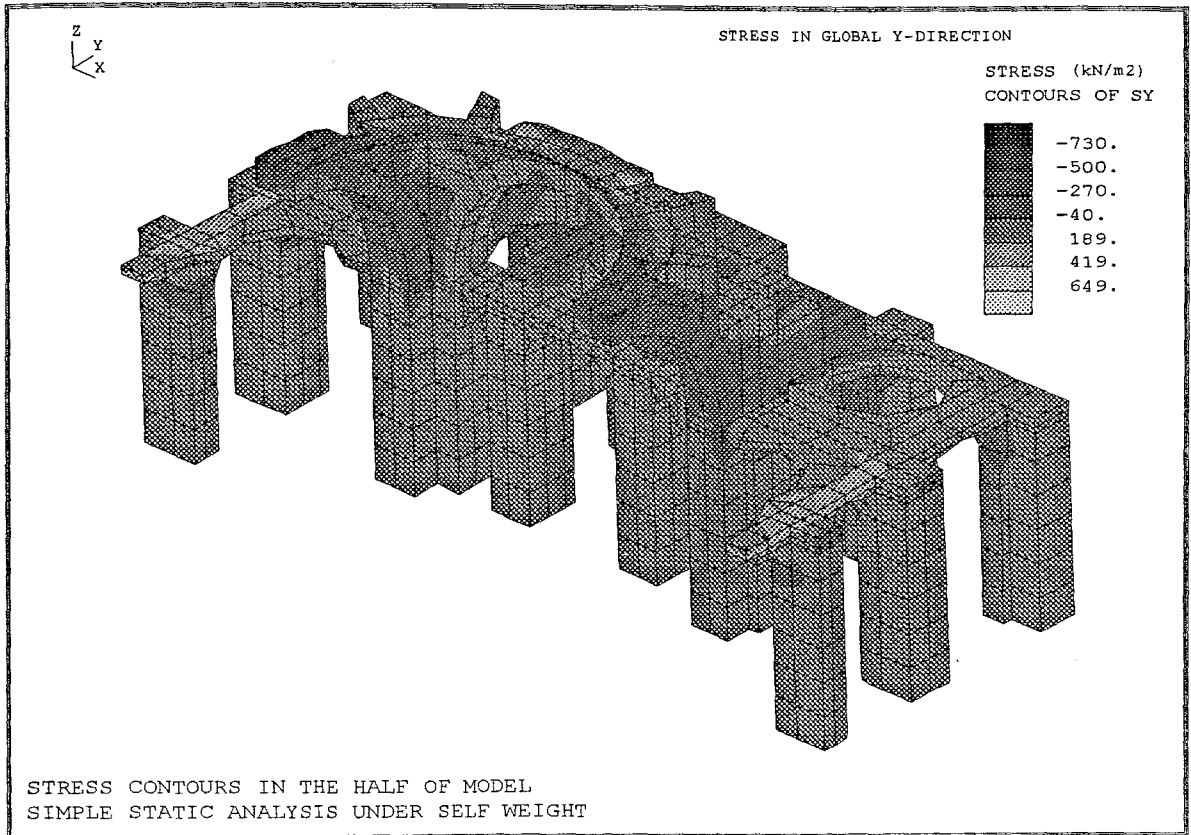


FIGURE 3.3.19 Stress Contours in the Half of Model
Simple Static Analysis Under Self Weight. Stress in Global Y Direction.

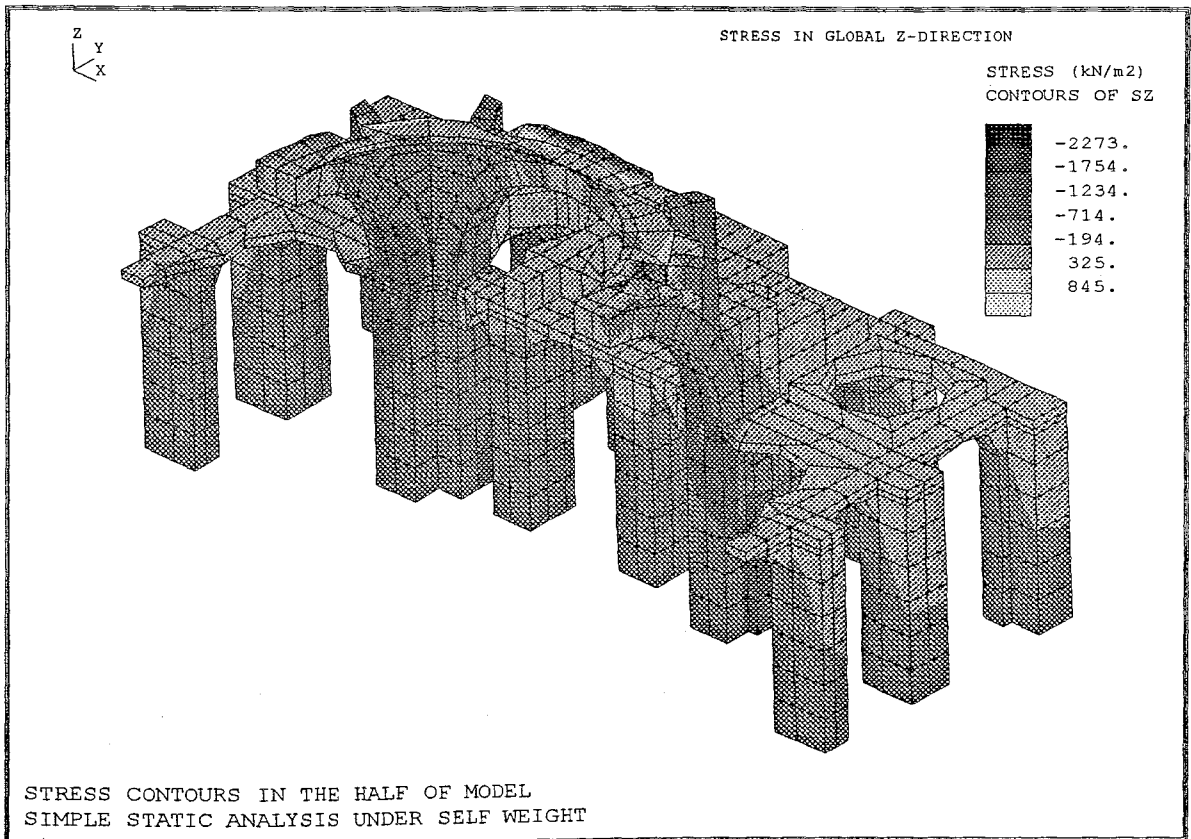


FIGURE 3.3.20 Stress Contours in the Half of Model
Simple Static Analysis Under Self Weight. Stress in Global Z Direction.

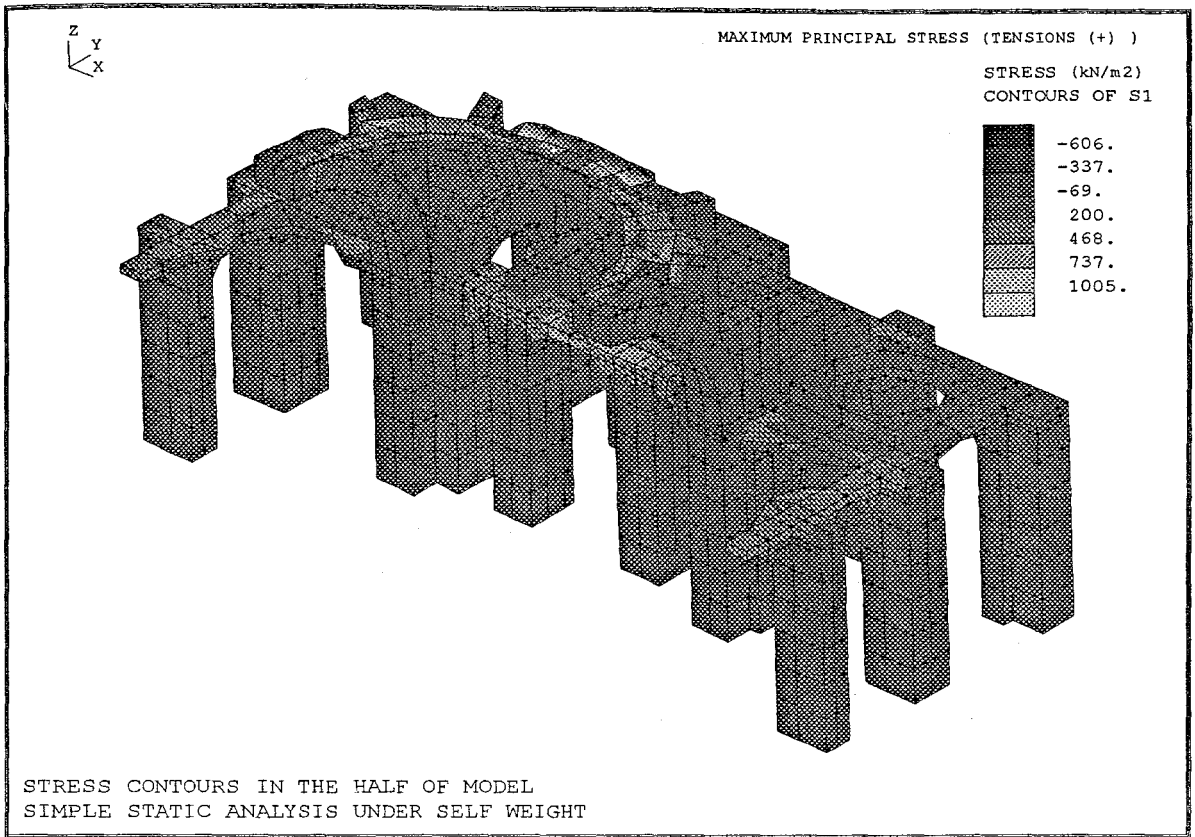


FIGURE 3.3.21 Stress Contours in the Half of Model
Simple Static Analysis Under Self Weight. Maximum Principal Stress (Tension+).

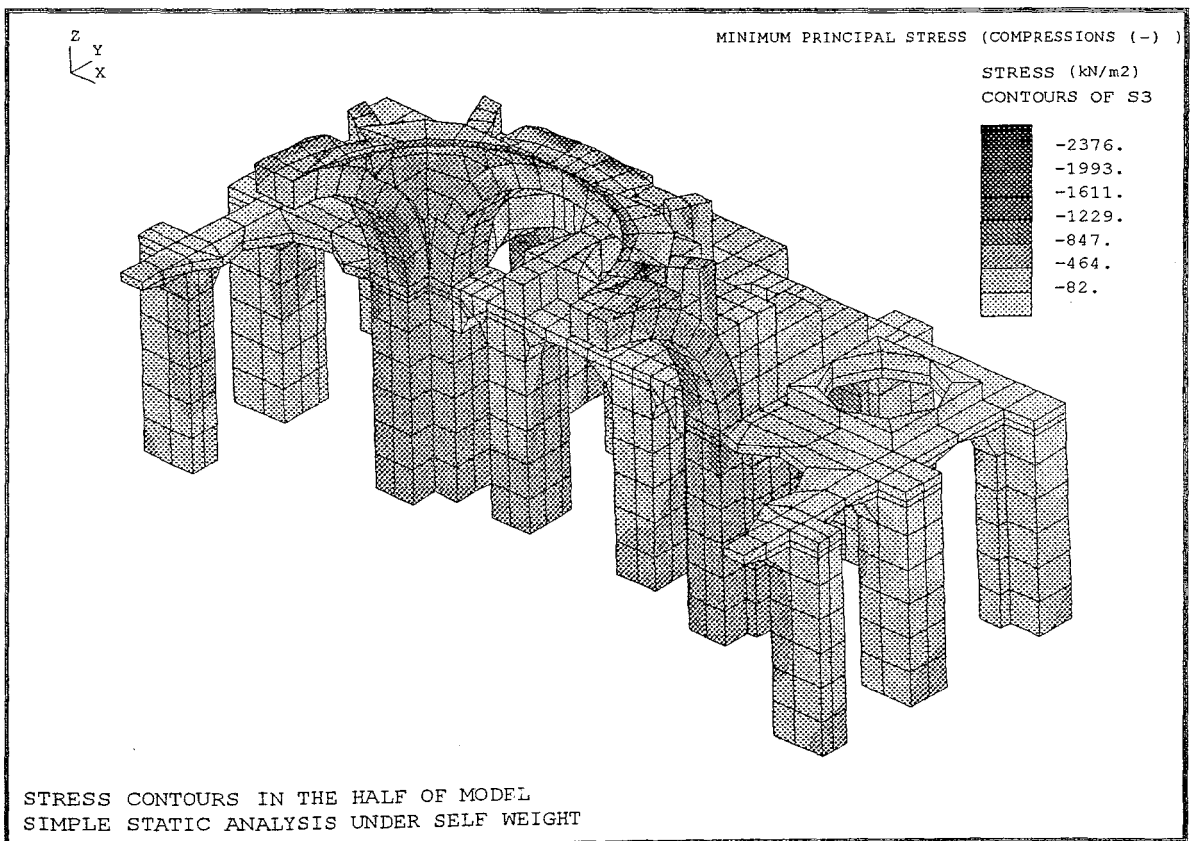


FIGURE 3.3.22 Stress Contours in the Half of Model
Simple Static Analysis Under Self Weight. Minimum Principal Stress (Compression-).

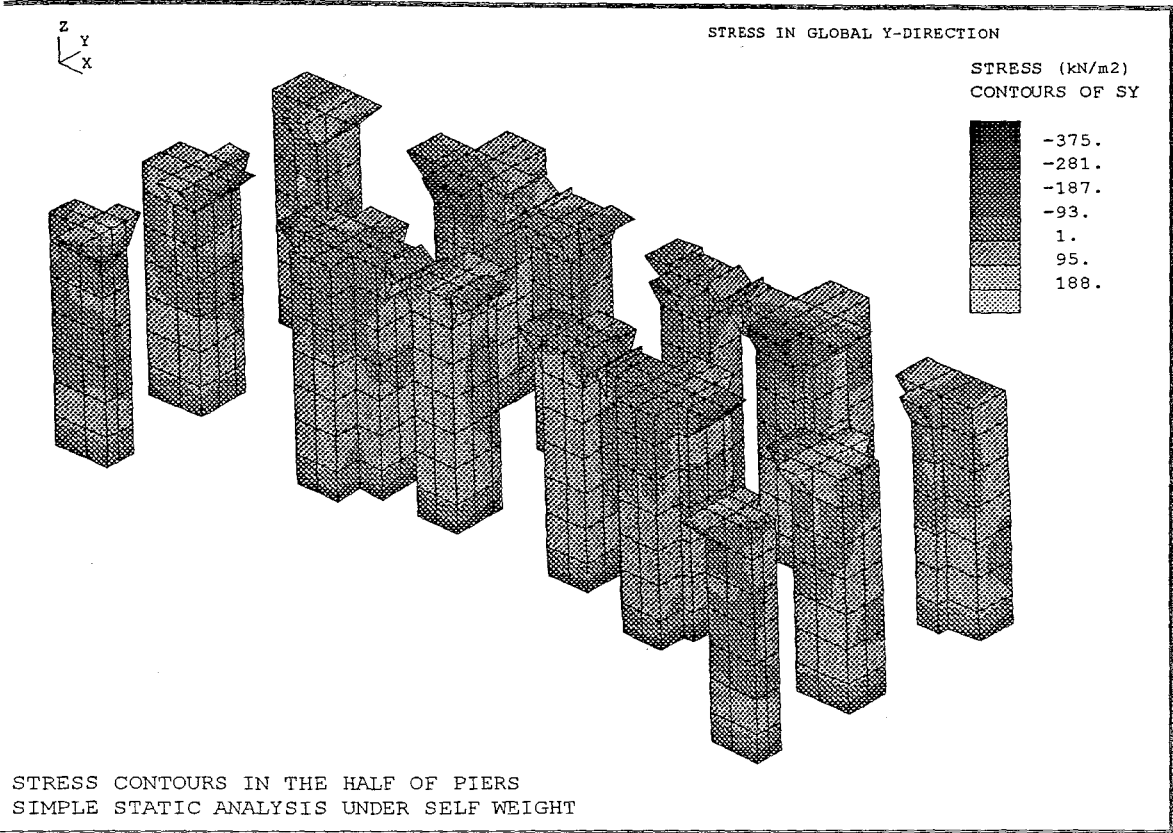


FIGURE 3.3.23 Stress Contours in the Half of Piers
Simple Static Analysis Under Self Weight. Stress Contours in Global Y Direction.

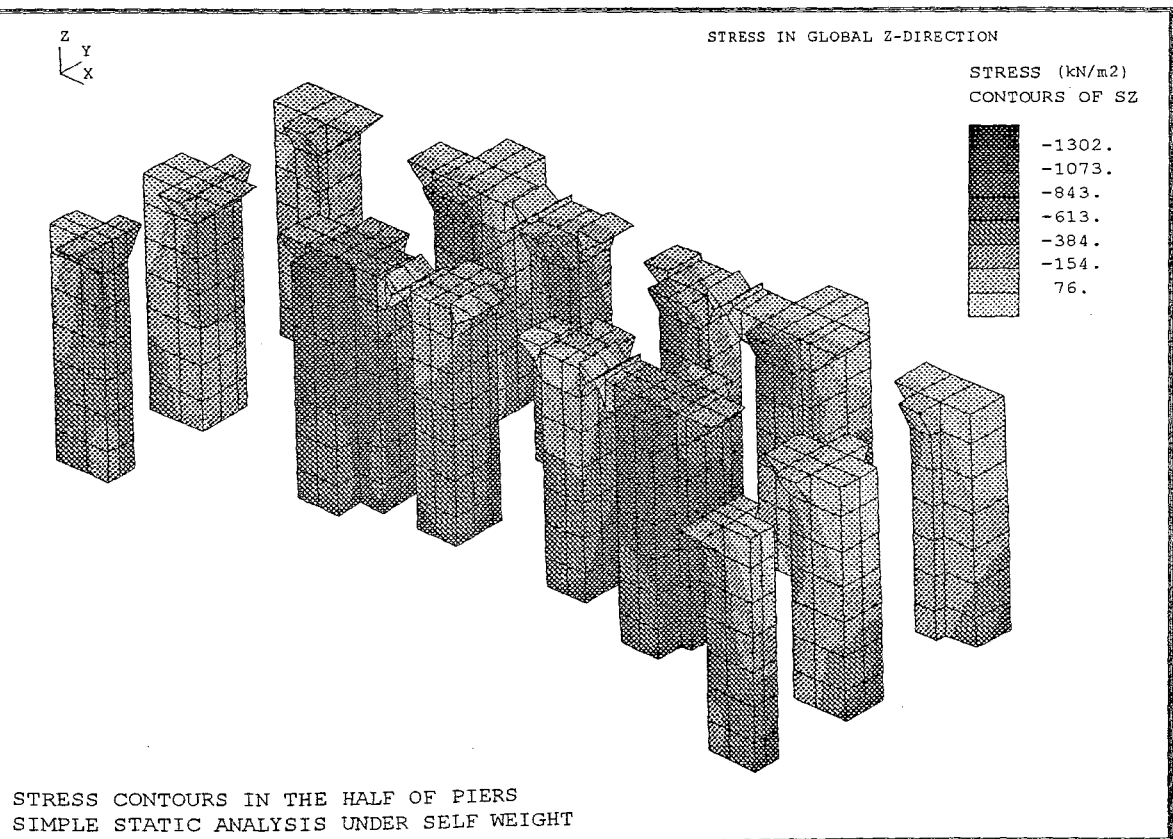


FIGURE 3.3.24 Stress Contours in the Half of Piers
Simple Static Analysis Under Self Weight. Stress Contours in Global Z Direction.

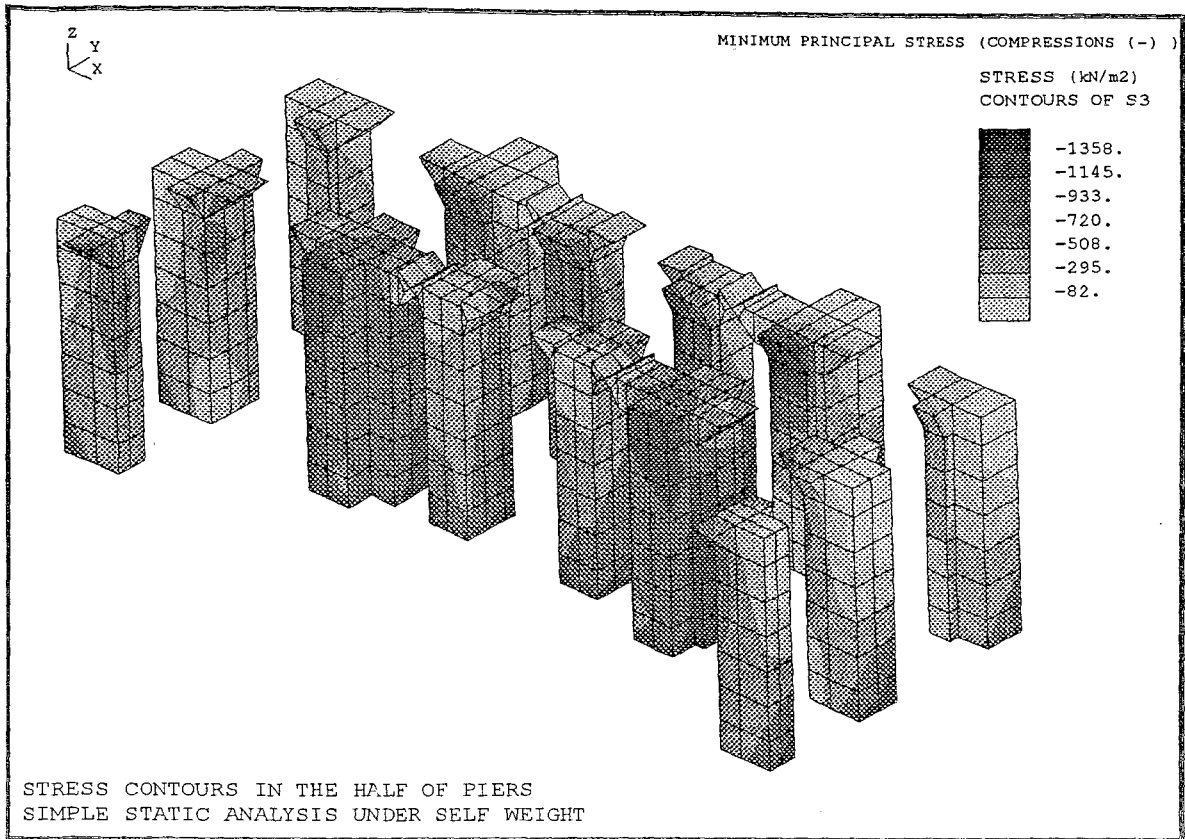


FIGURE 3.3.25 Stress Contours in the Half of Piers
Simple Static Analysis Under Self Weight. Minimum Principal Stress (Compression -)

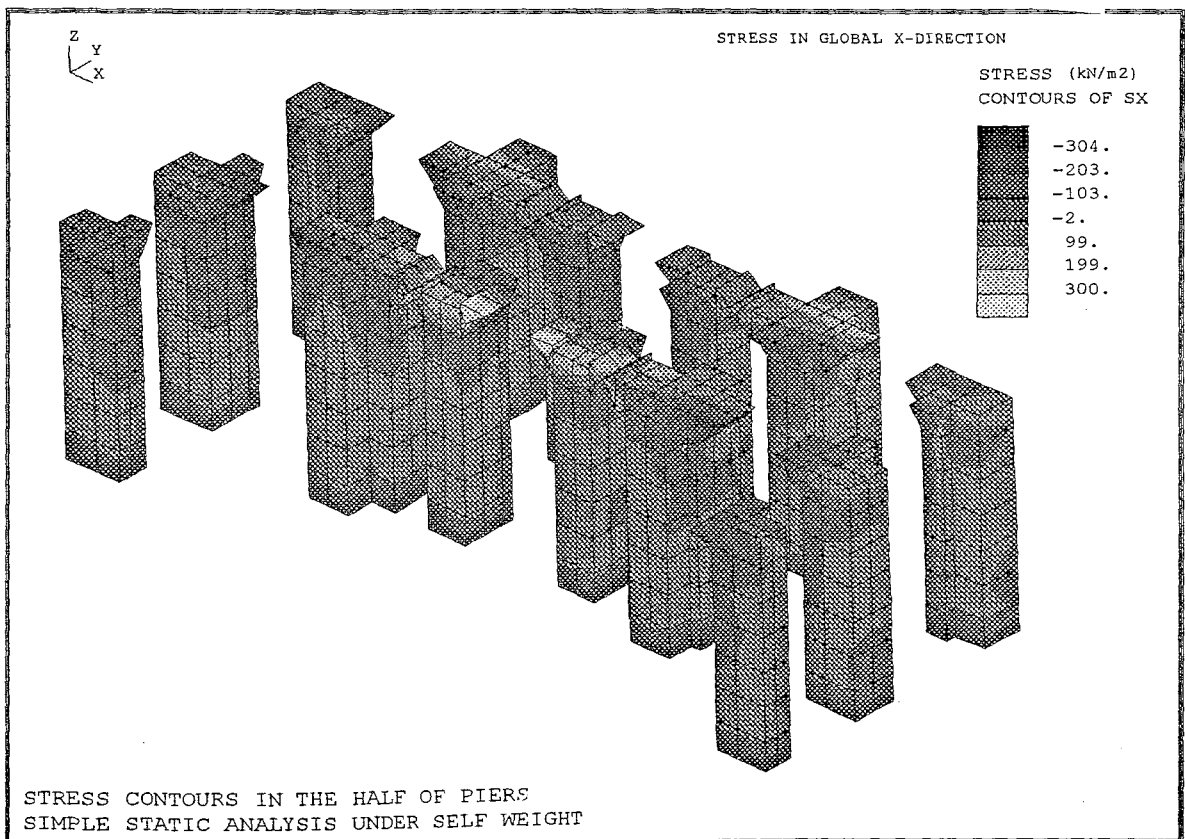


FIGURE 3.3.26 Stress Contours in the Half of Piers
Simple Static Analysis Under Self Weight. Stress in Global X Direction

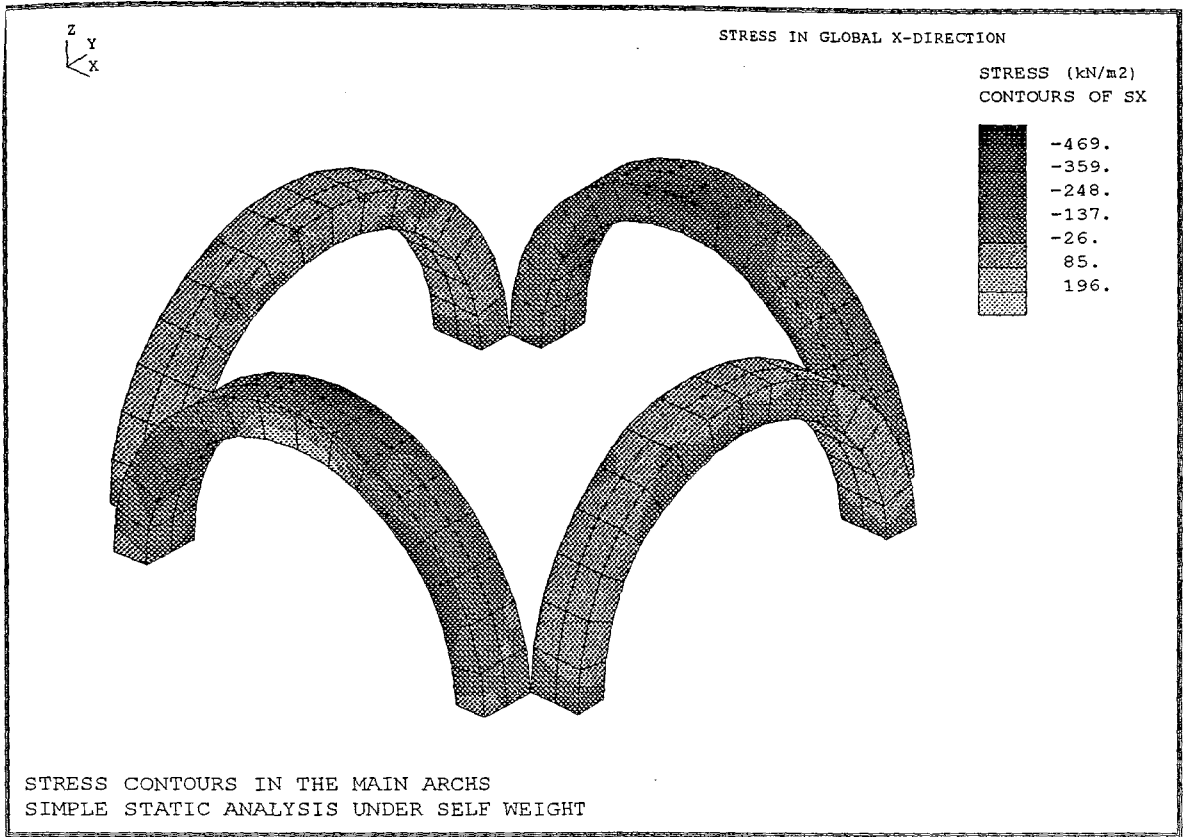


FIGURE 3.3.27 Stress Contours in the Main Arches
Simple Static Analysis Under Self Weight. Stress in Global X Direction

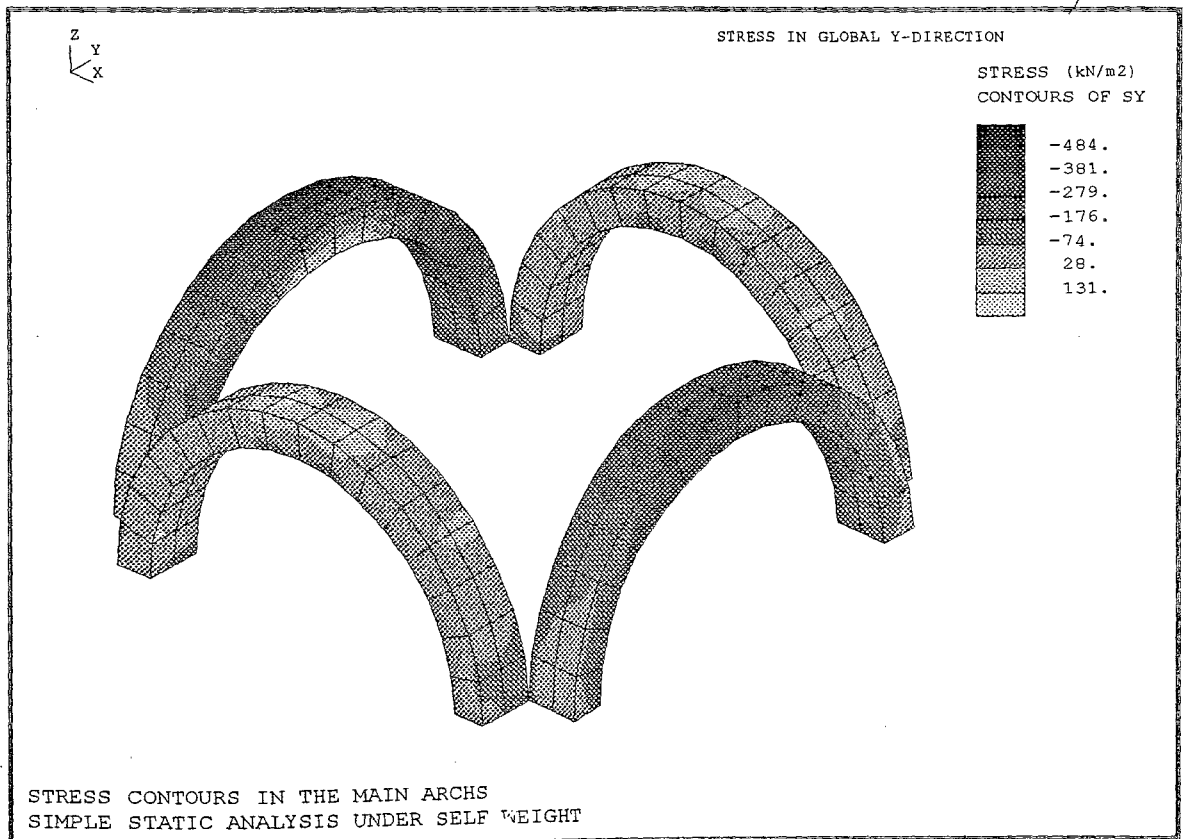


FIGURE 3.3.28 Stress Contours in the Main Arches
Simple Static Analysis Under Self Weight. Stress in Global Y Direction

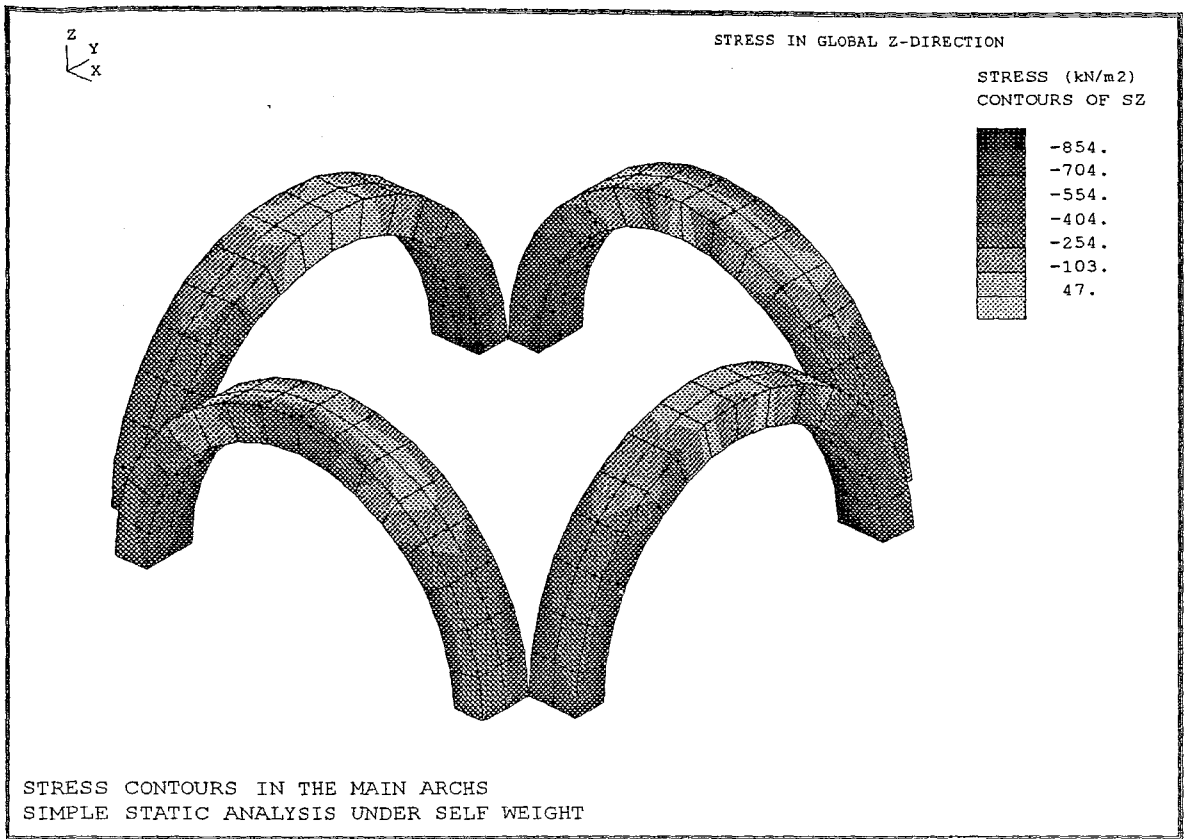


FIGURE 3.3.29 Stress Contours in the Main Arches
Simple Static Analysis Under Self Weight. Stress in Global Z Direction

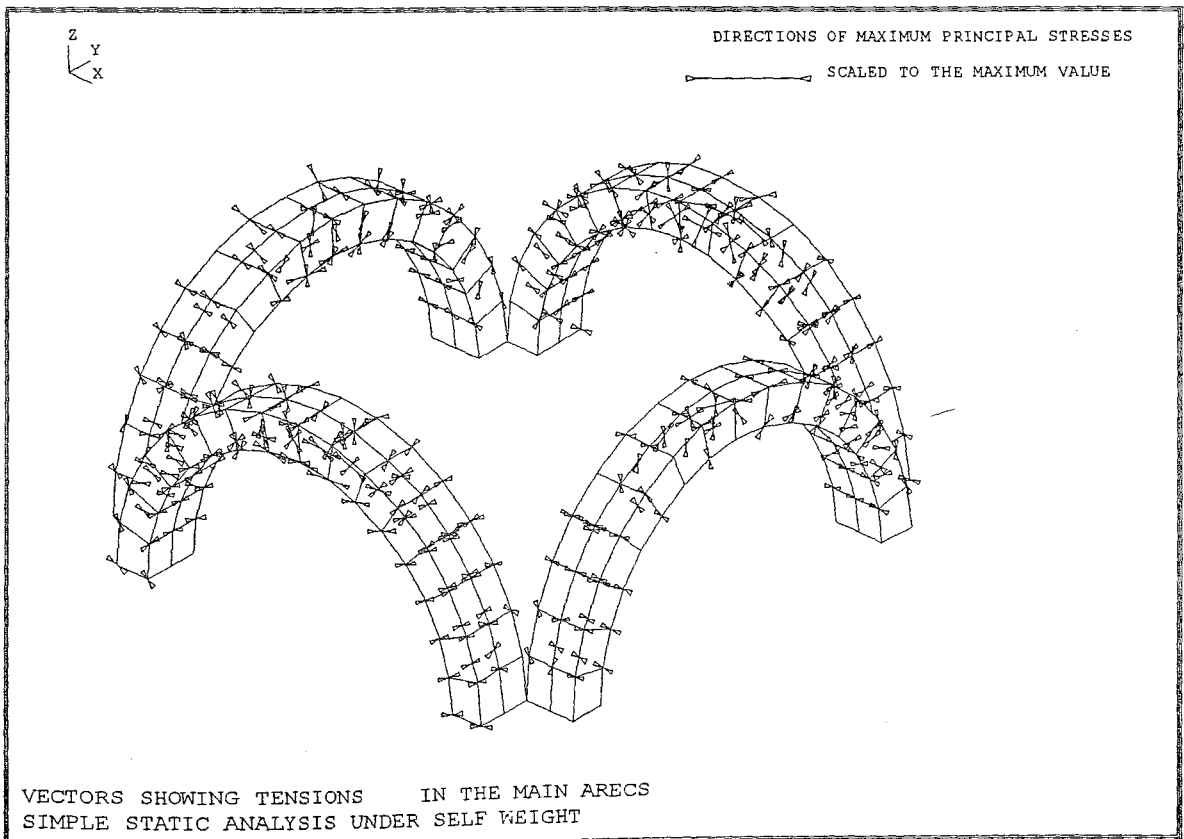


FIGURE 3.3.30 Stress Contours in the Main Arches
Simple Static Analysis Under Self Weight. Directions of Maximum Principal Stresses

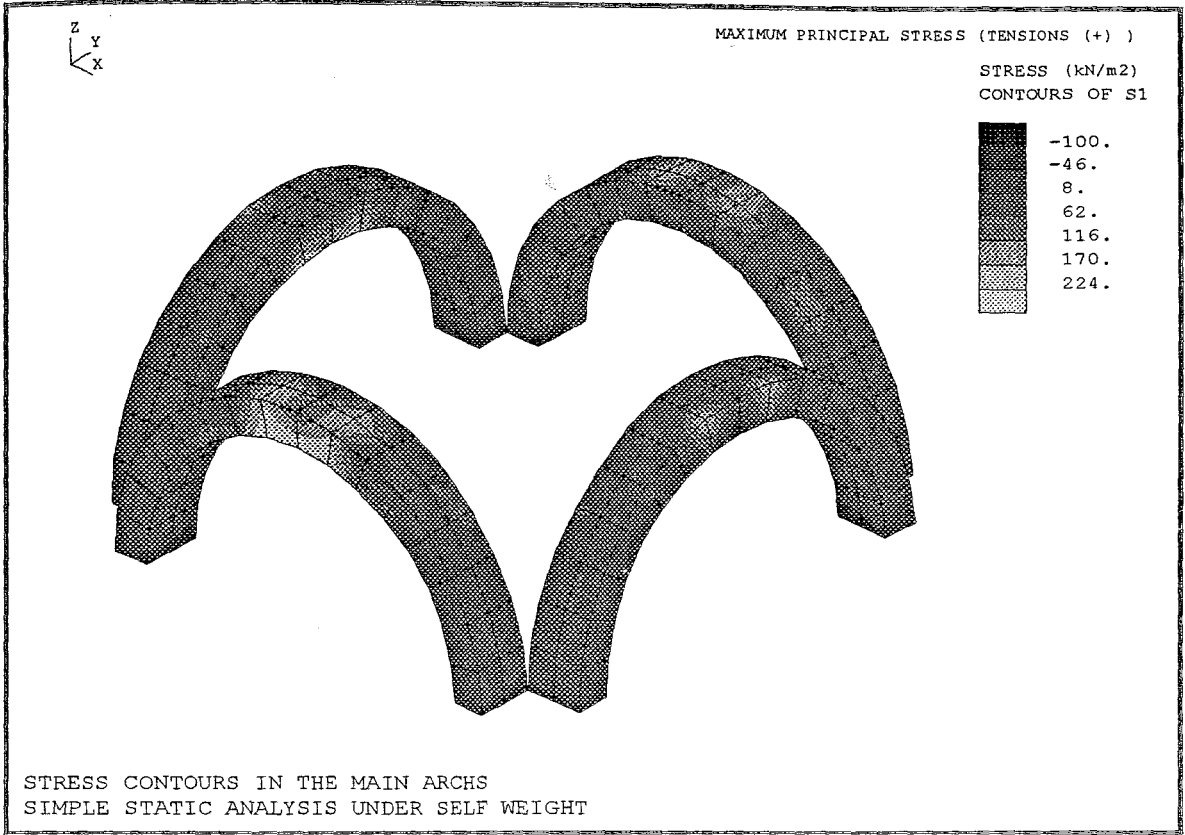


FIGURE 3.3.31 Stress Contours in the Main Arches
Simple Static Analysis Under Self Weight. Maximum Principal Stress (Tensions+)

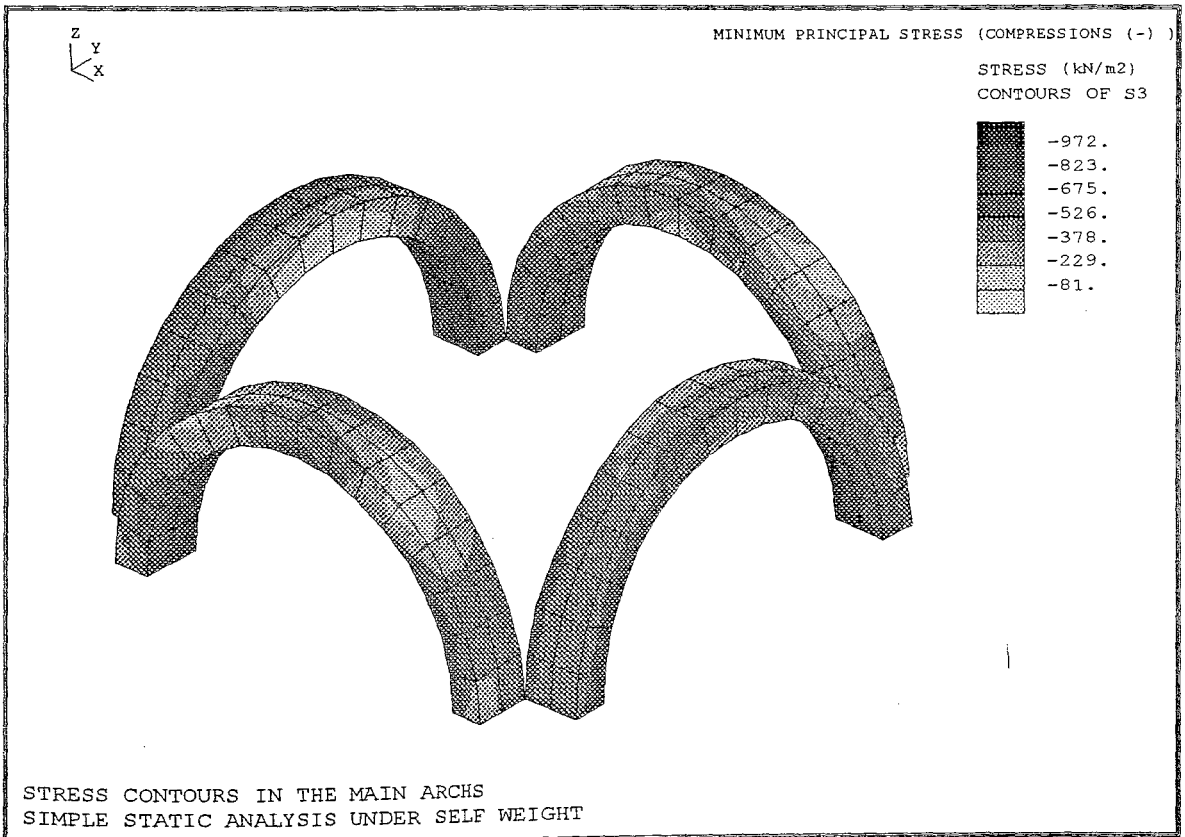


FIGURE 3.3.32 Stress Contours in the Main Arches
Simple Static Analysis Under Self Weight. Minimum Principal Stress (Compressions-)

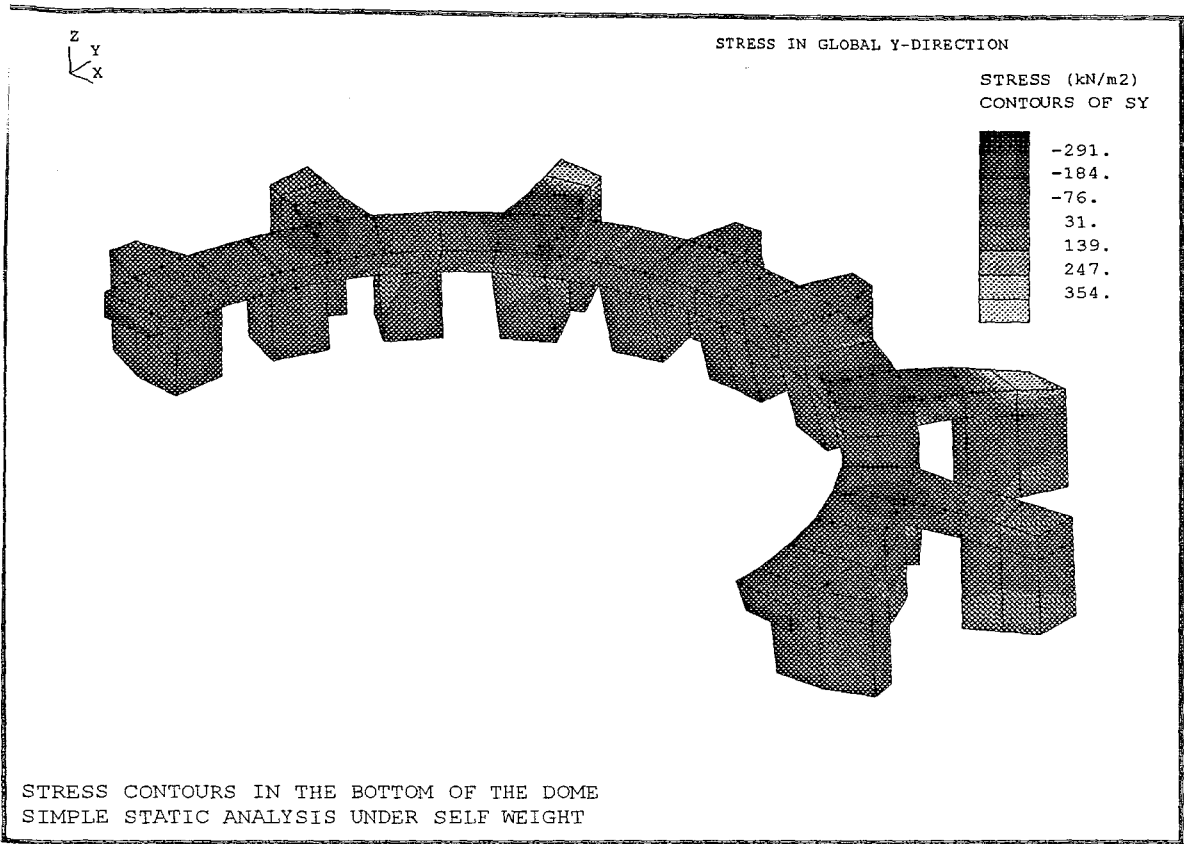


FIGURE 3.3.33 Stress Contours in the Bottom of the Dome
Simple Static Analysis Under Self Weight. Stress in Global Y Direction

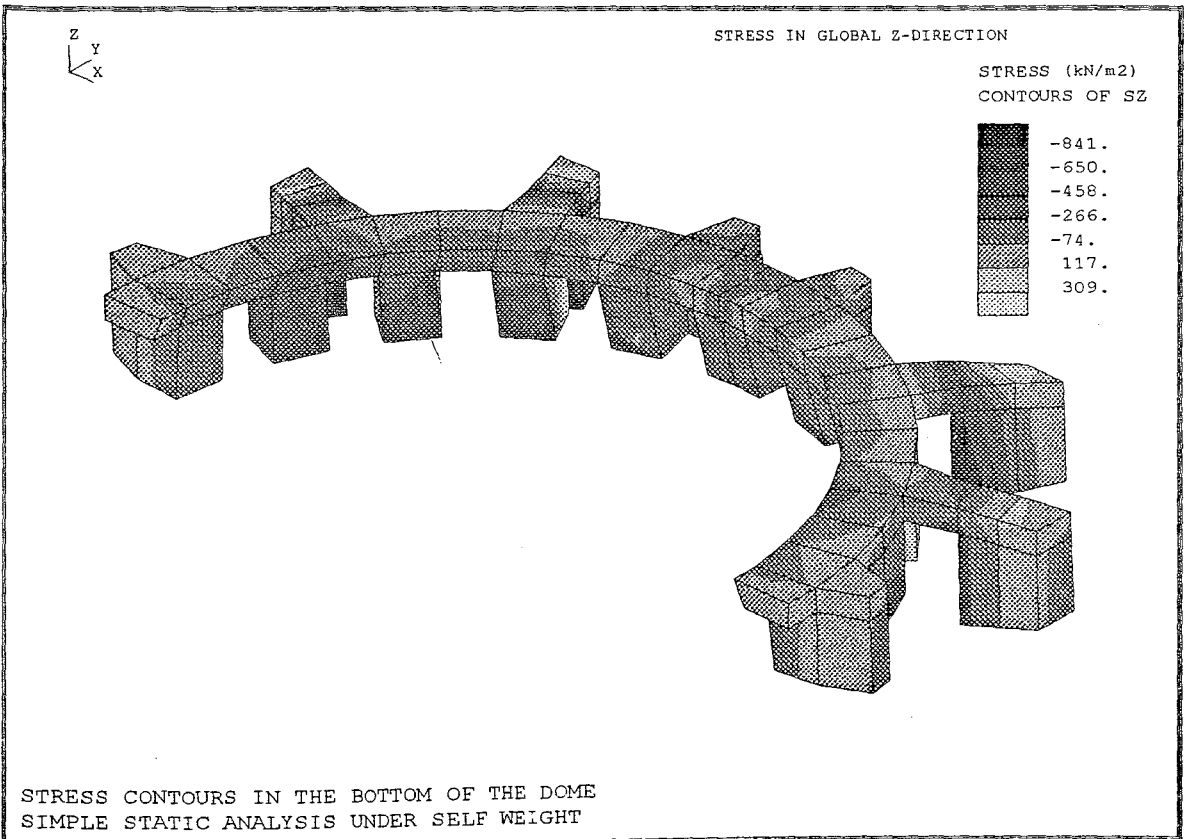


FIGURE 3.3.34 Stress Contours in the Bottom of the Dome
Simple Static Analysis Under Self Weight. Stress in Global Z Direction

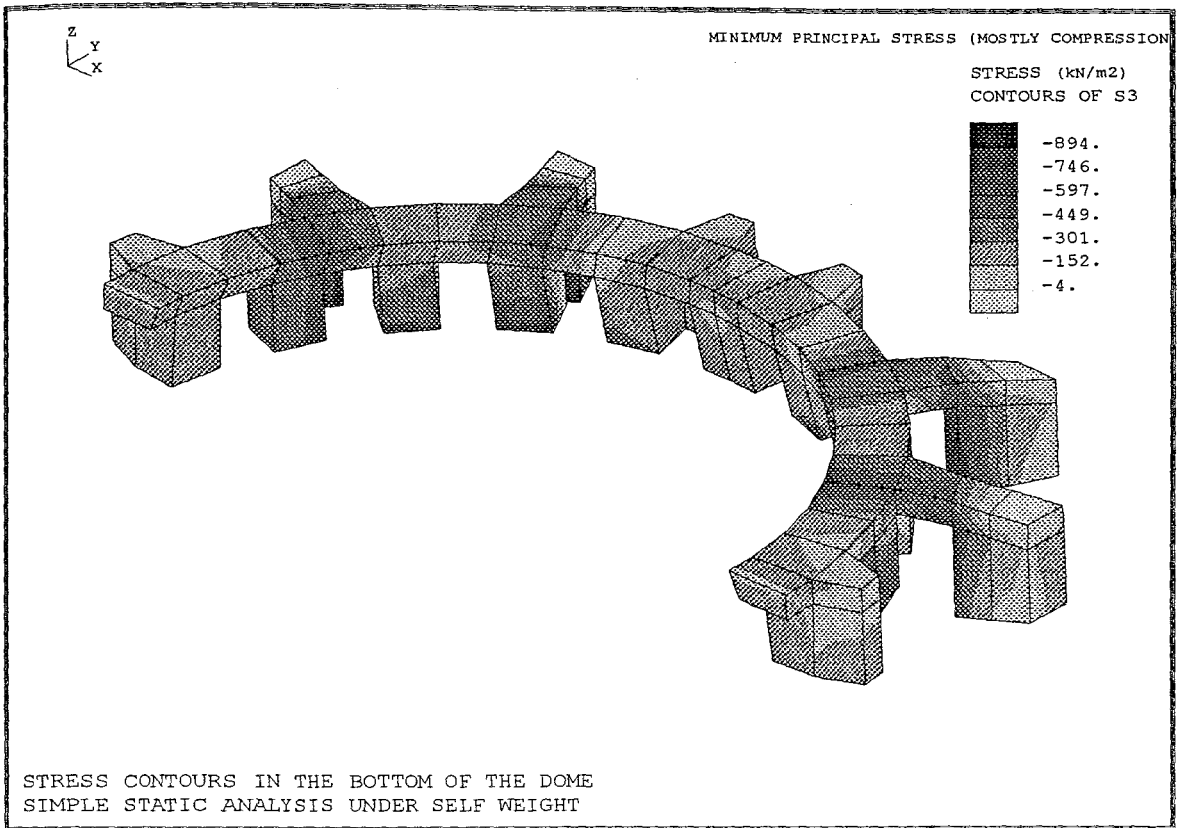


FIGURE 3.3.35 Stress Contours in the Bottom of the Dome
Simple Static Analysis Under Self Weight. Minimum Principal Stress

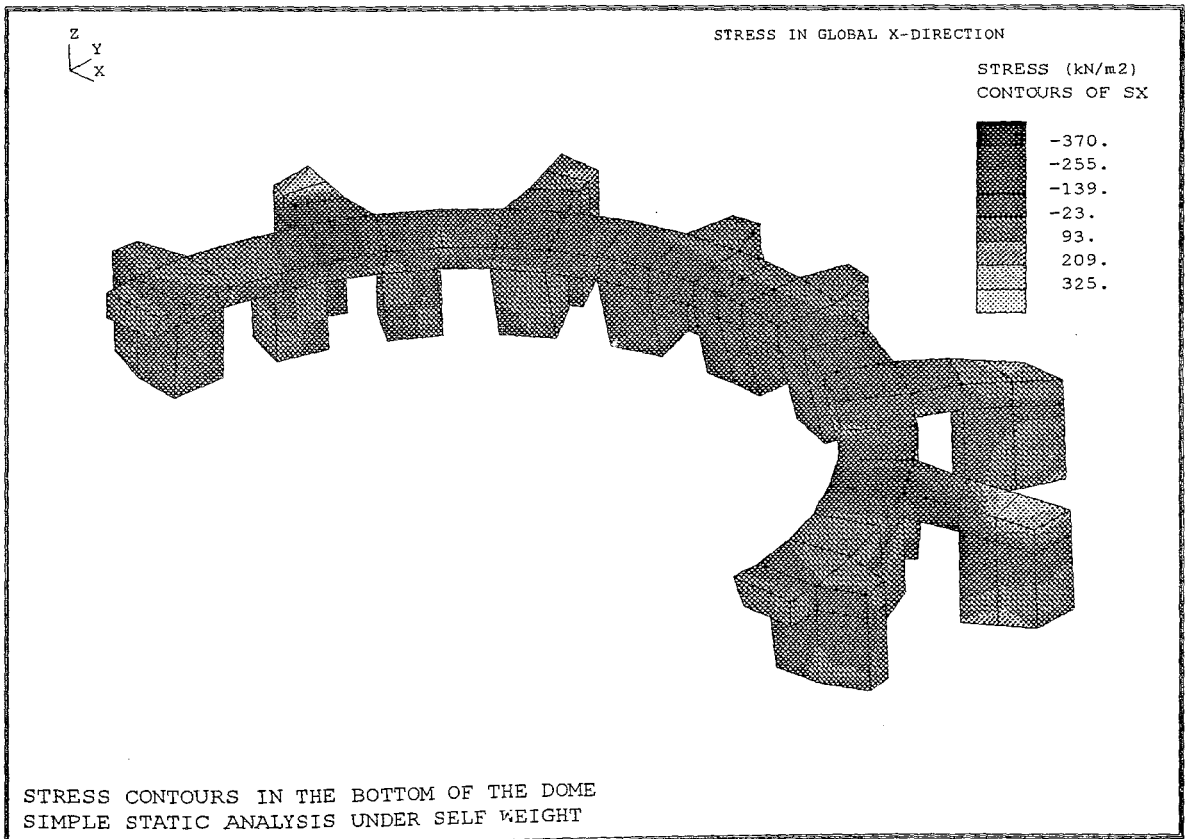


FIGURE 3.3.36 Stress Contours in the Bottom of the Dome
Simple Static Analysis Under Self Weight. Stress in Global X Direction

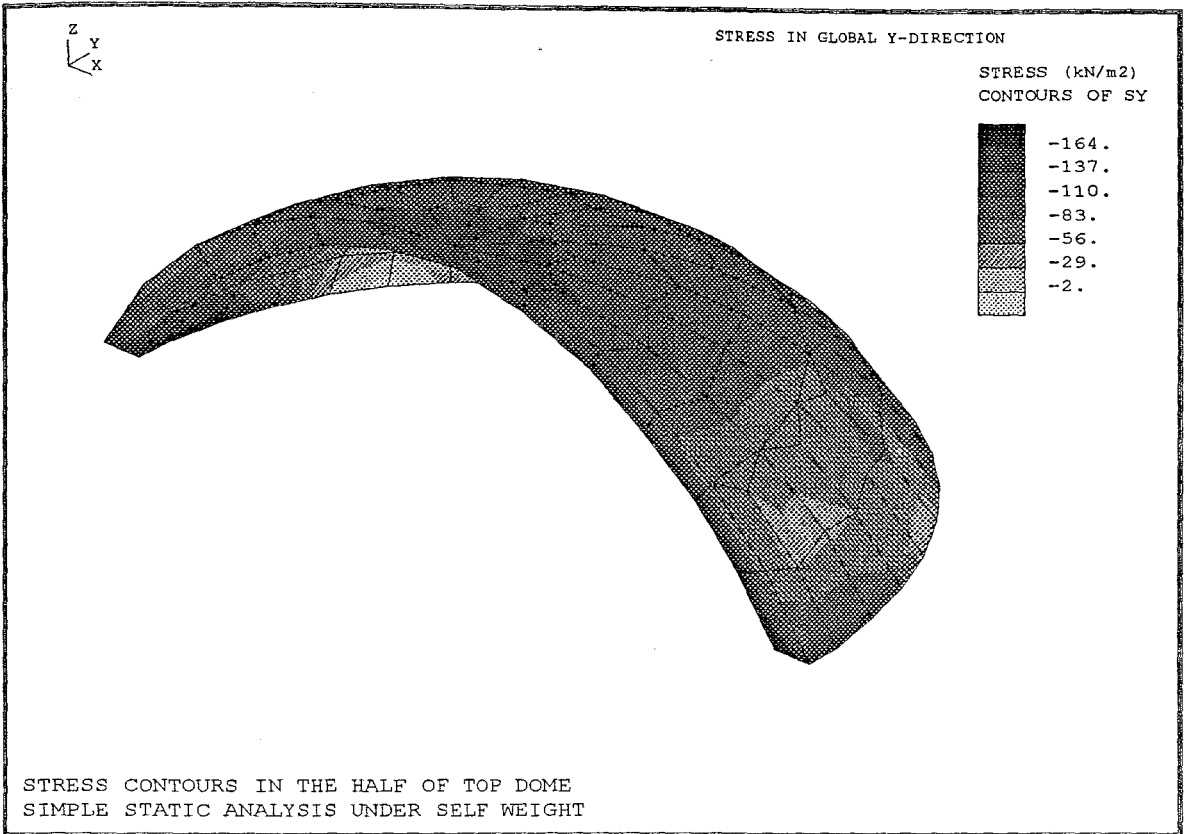


FIGURE 3.3.37 Stress Contours in the Bottom of the Dome
Simple Static Analysis Under Self Weight. Stress in Global Y Direction

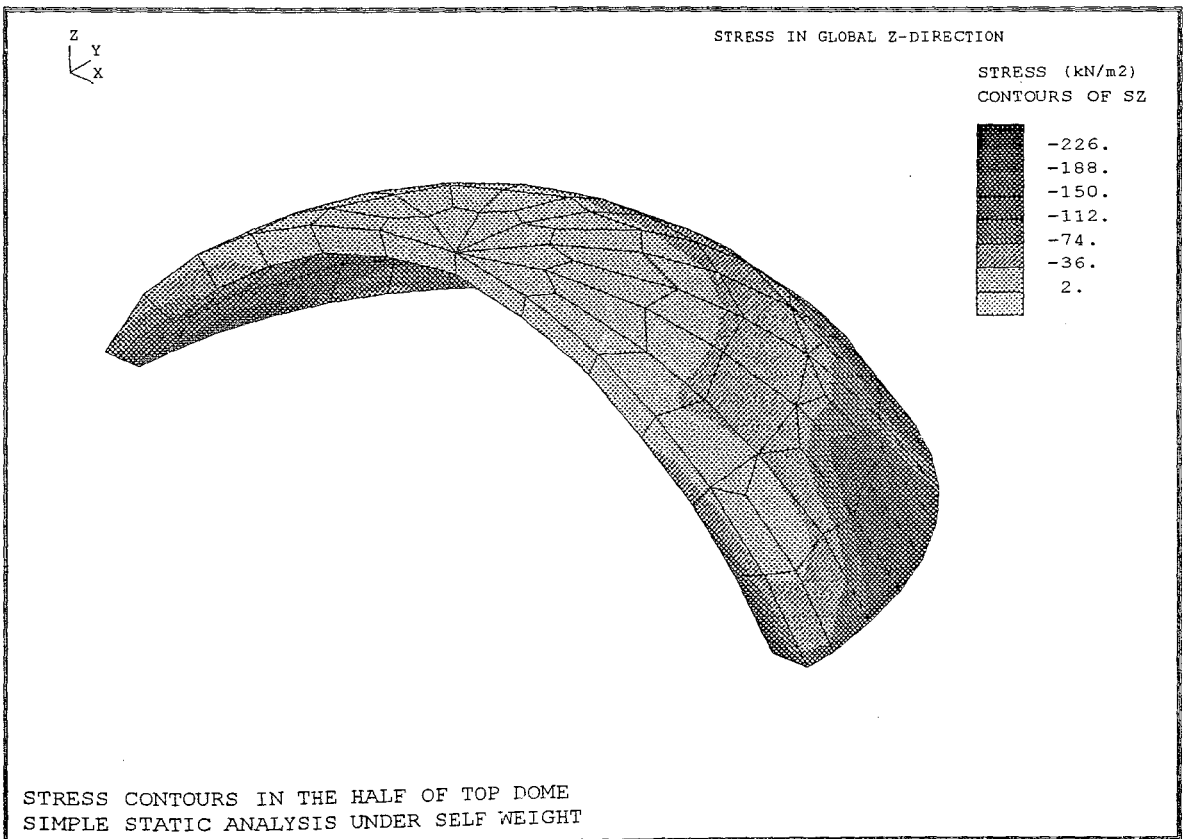


FIGURE 3.3.38 Stress Contours in the Bottom of the Dome
Simple Static Analysis Under Self Weight. Stress in Global Z Direction

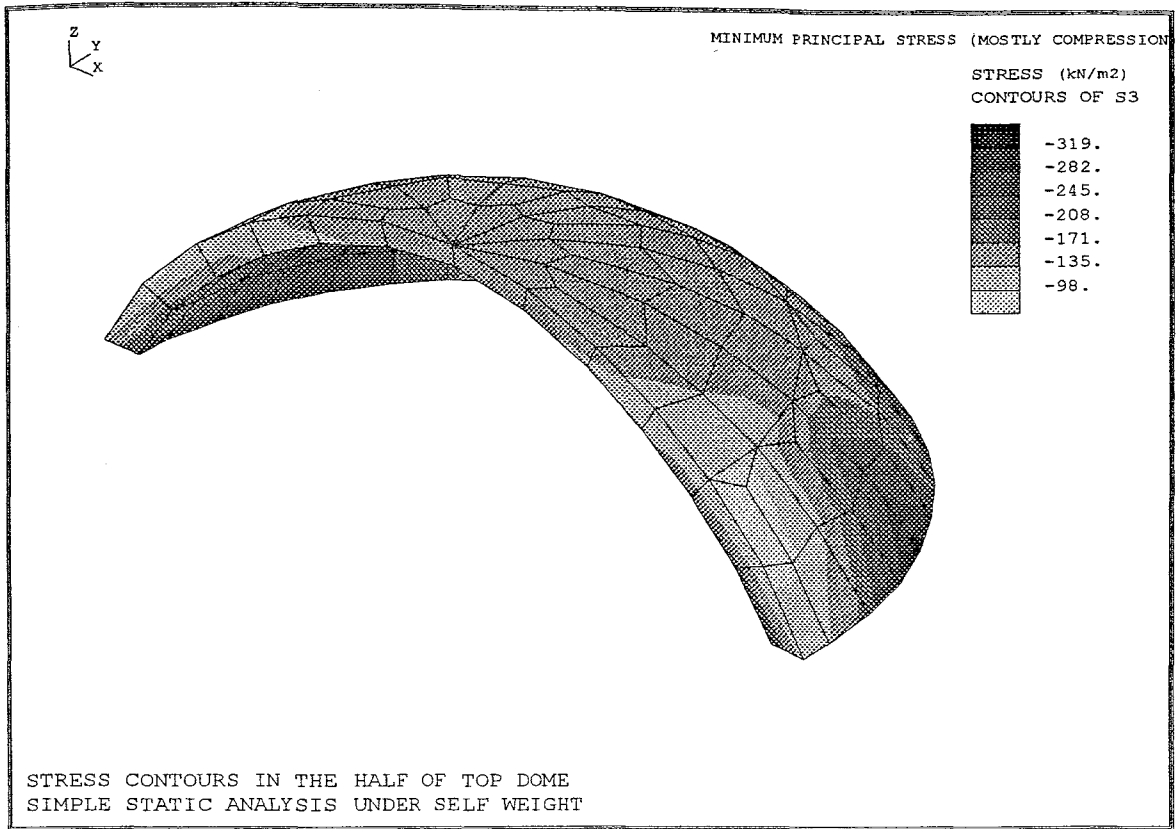


FIGURE 3.3.39 Stress Contours in the Half of Top Dome
Simple Static Analysis Under Self Weight. Minimum Principal Stress

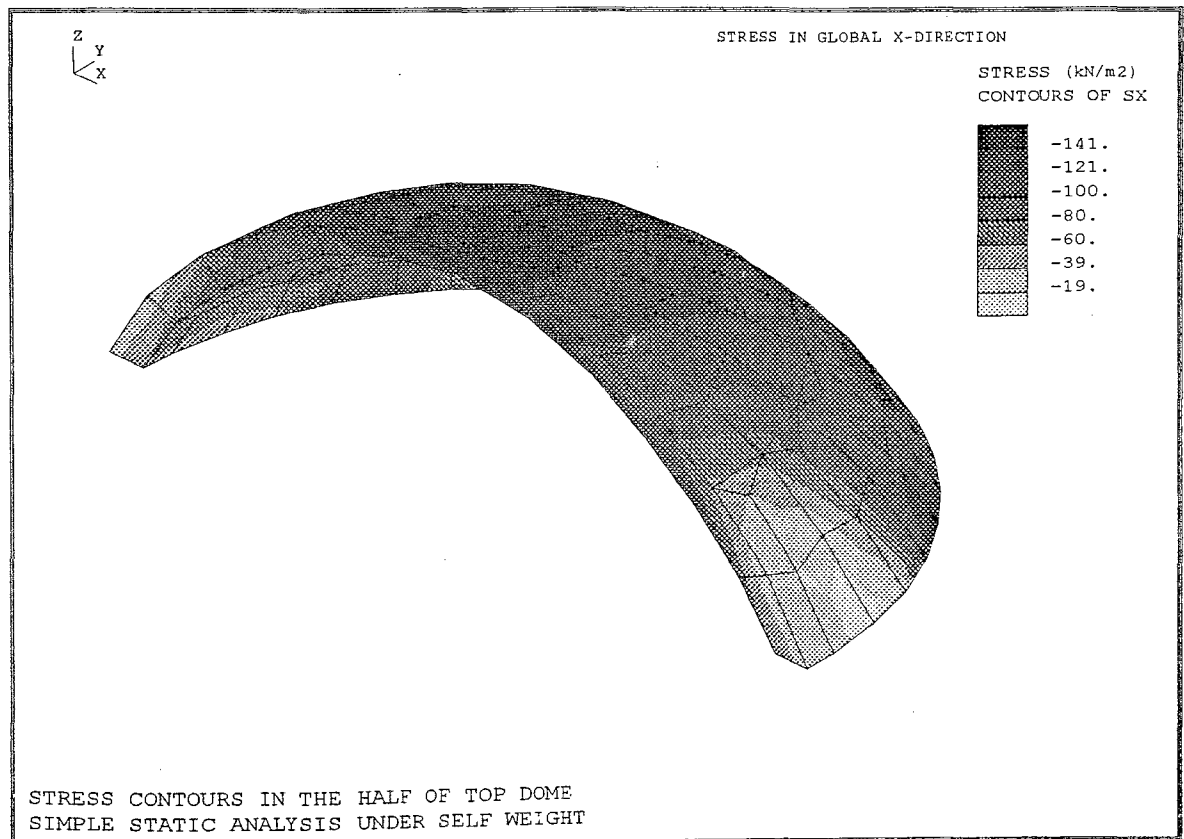


FIGURE 3.3.40 Stress Contours in the Half of Top Dome
Simple Static Analysis Under Self Weight. Stress in Global X Direction

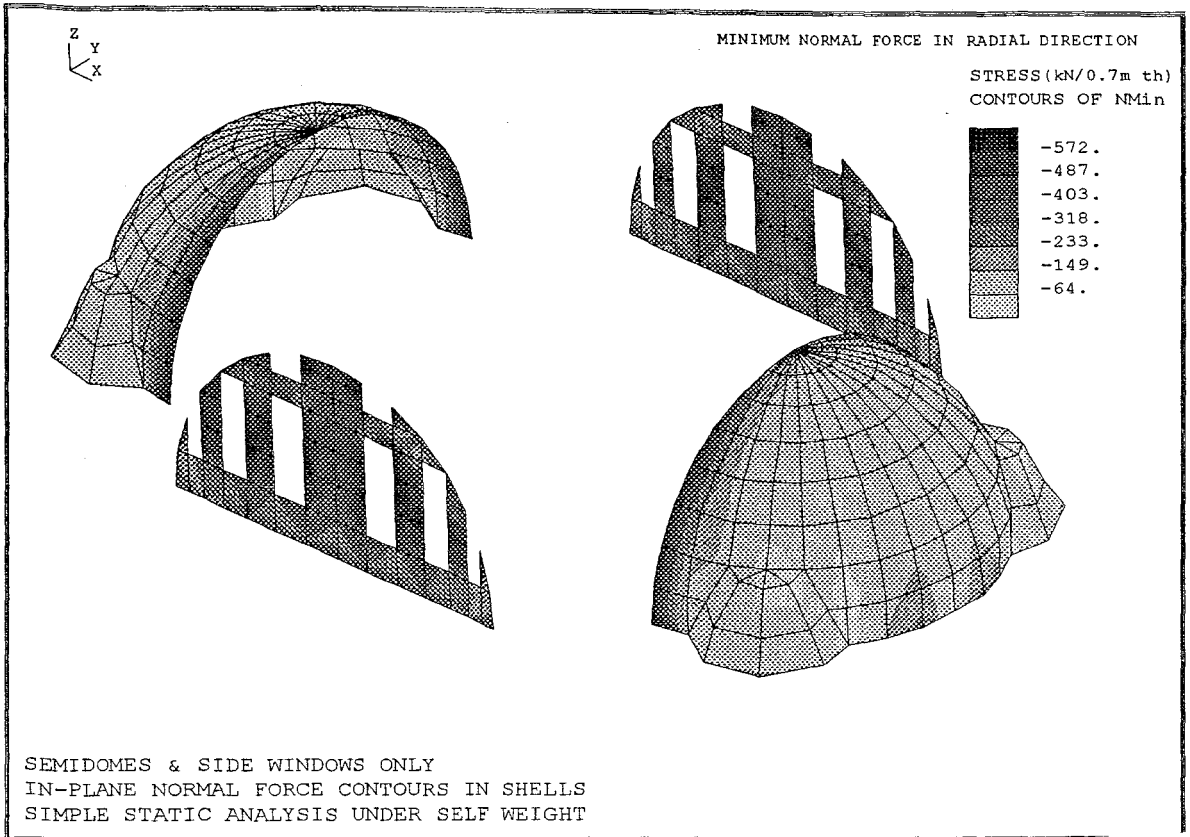


FIGURE 3.3.41 Semidomes&Side Windows Only.In Plane Normal Force Contours in Shells Simple Static Analysis Under Self Weight.Minimum Normal Force in Radial Direction

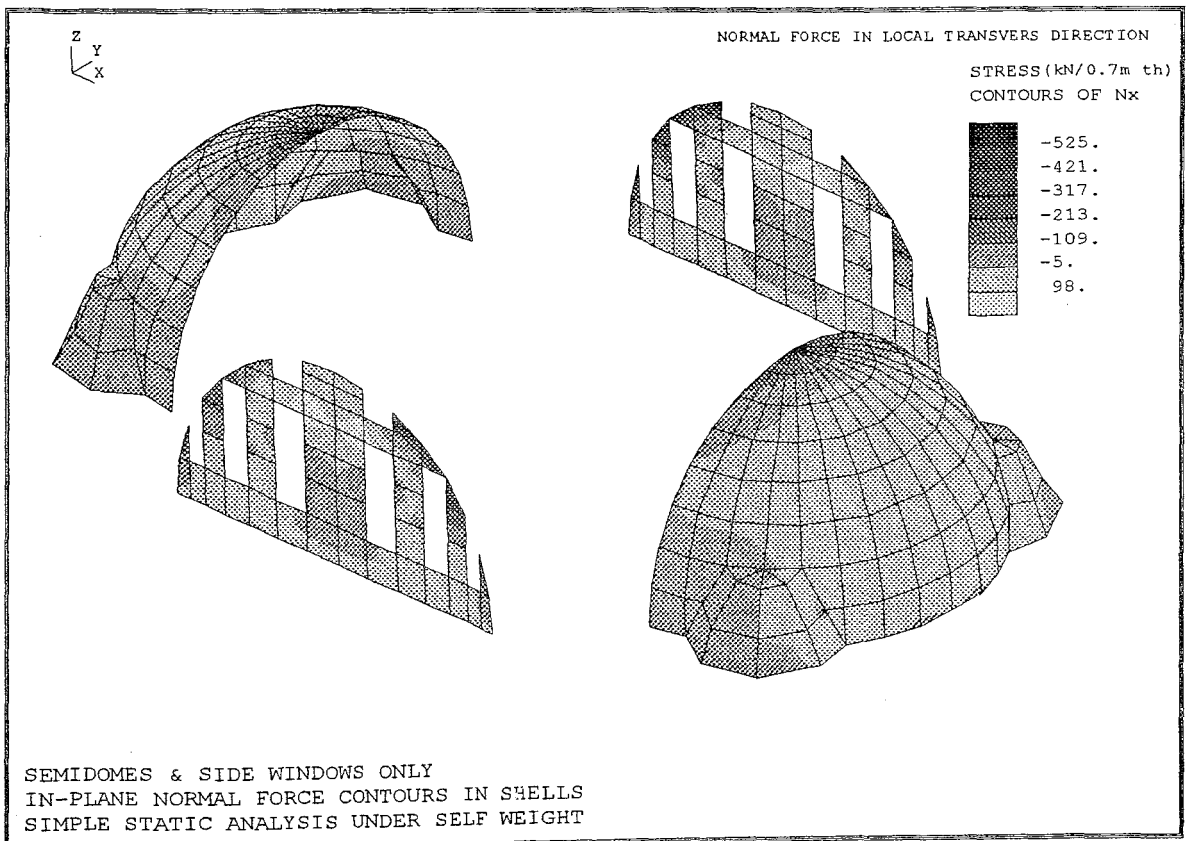


FIGURE 3.3.42 Semidomes&Side Windows Only.In Plane Normal Force Contours in Shells Simple Static Analysis Under Self Weight.Minimum Normal Force in Transverse Direction

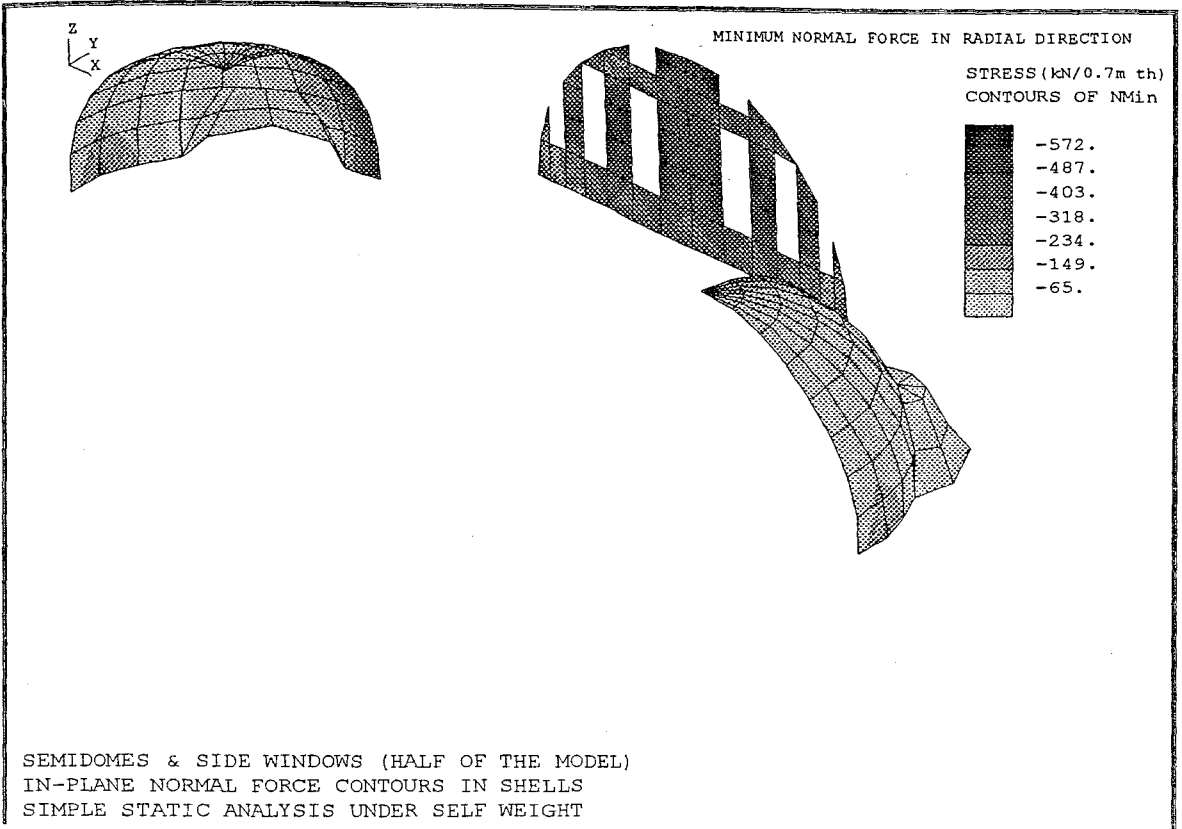


FIGURE 3.3.43 Semidomes&Side Windows in the Half of the Model.In Plane Normal Force Contours in Shells.Simple Static Analysis Under Self Weight.Minimum Normal Force in radial Direction

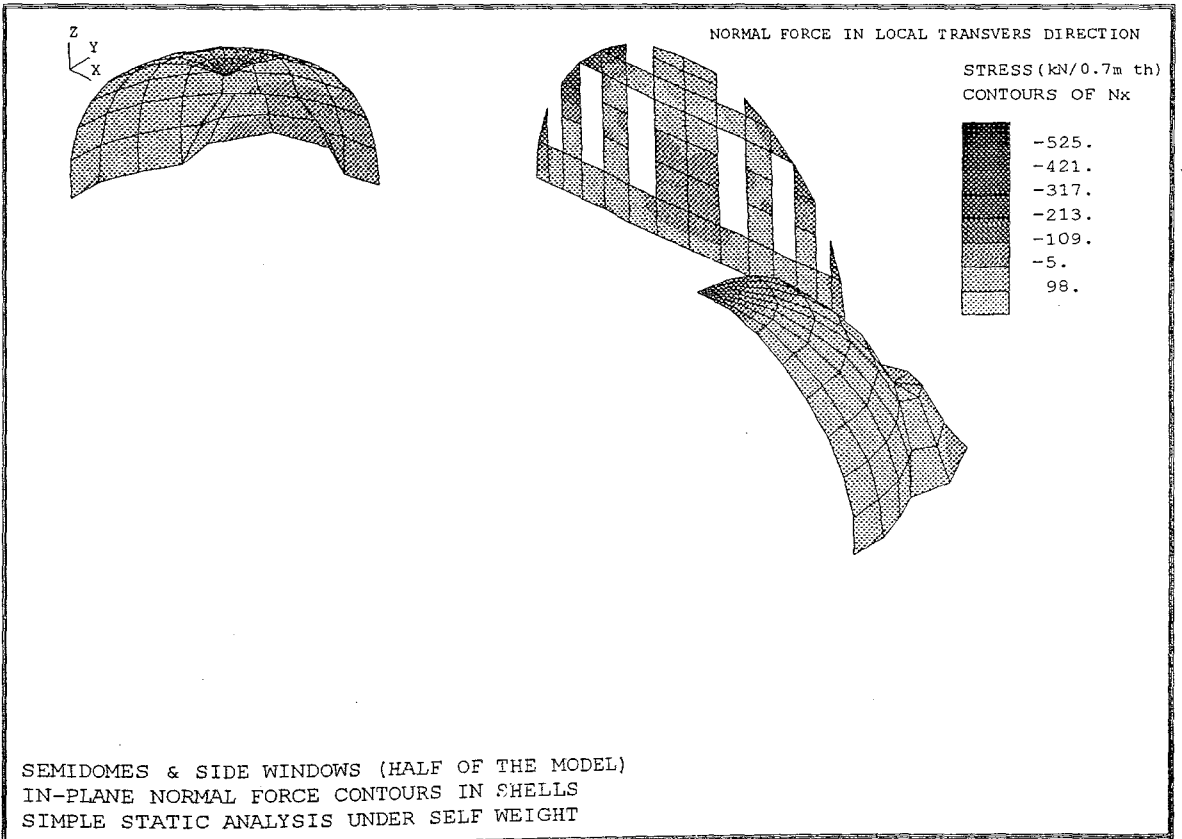


FIGURE 3.3.44 Semidomes&Side Windows in the Half of the Model.In Plane Normal Force Contours in Shells.Simple Static Analysis Under Self Weight.Minimum Normal Force in radial Direction

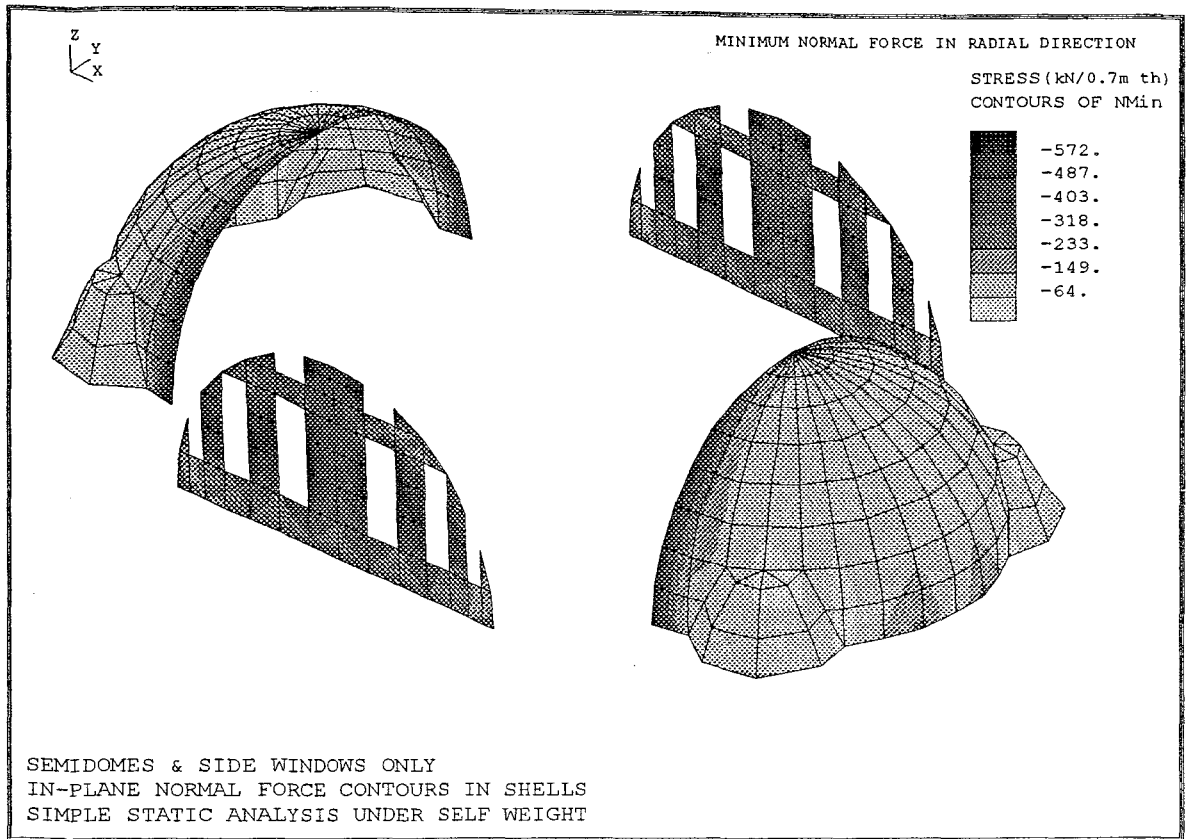


Figure 3.2.2.28 Semidomes & Side Windows Only- In-Plane Normal Force Contours in Shells Simple Static Analysis Under Self Weight-Minimum Normal Force Radial Direction

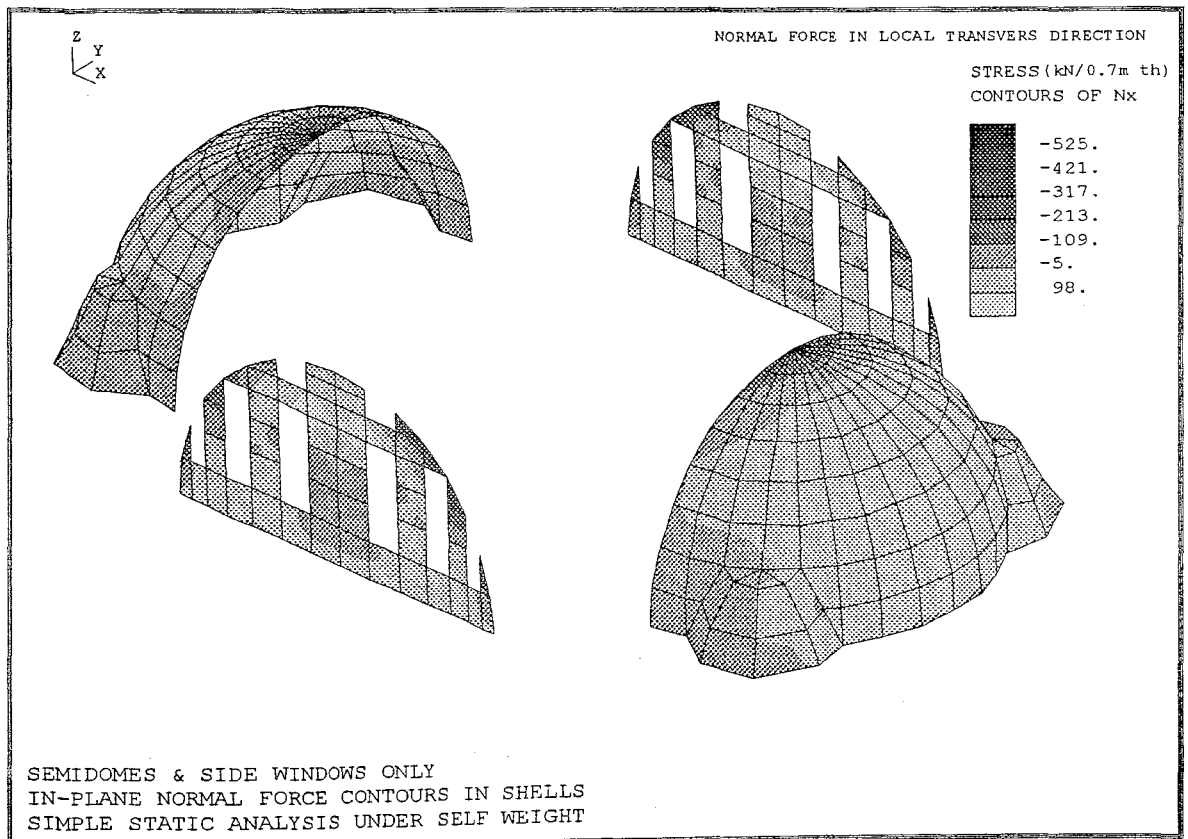


FIGURE 3.3.45 Semidomes&Side Windows Only. In Plane Normal Force Contours in Shells.Simple Static Analysis Under Self Weight.Minimum Normal Force in radial Direction

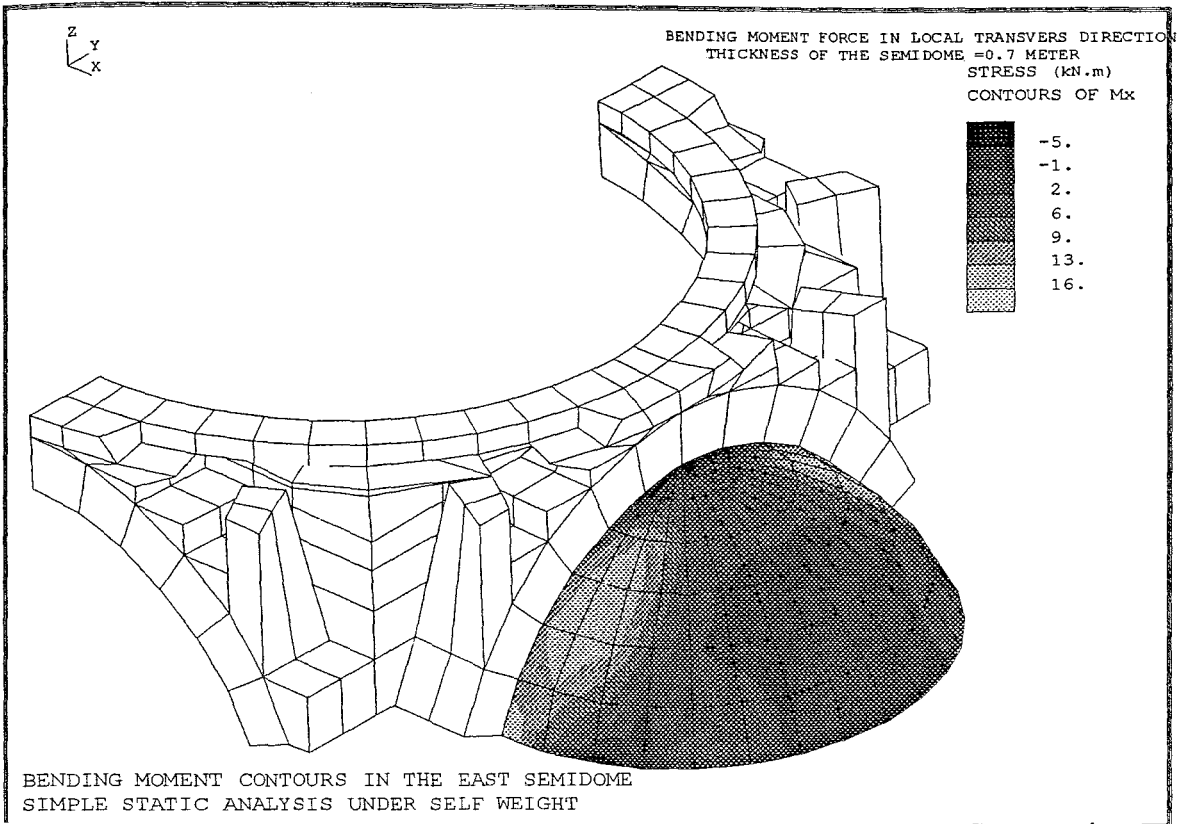


FIGURE 3.3.46 Semidomes&Side Windows Only. In Plane Normal Force Contours in Shells.Simple Static Analysis Under Self Weight.Minimum Normal Force in Local Transverse Direction

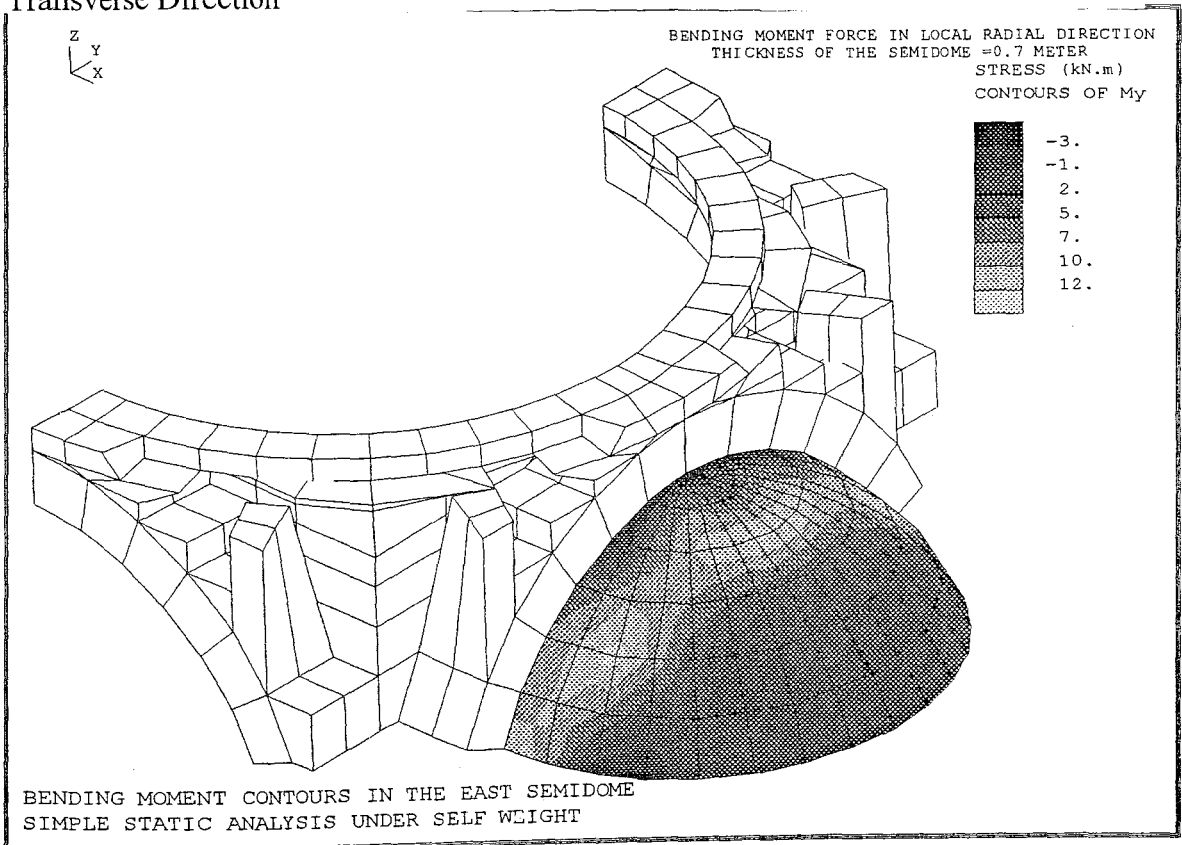


FIGURE 3.3.47 Bending Moment Contours in the East Semidome.Simple Static Analysis Under Self Weight.Bending Moment Force in Local Transverse Direction

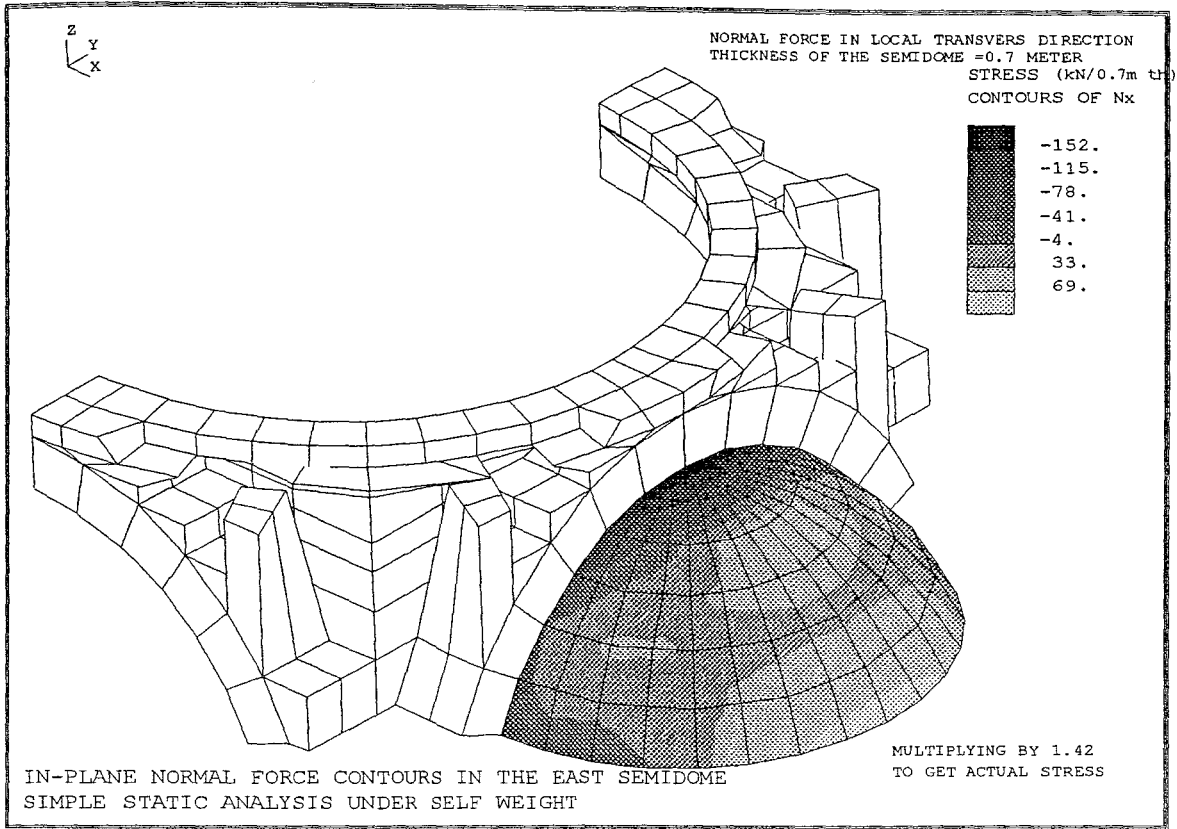


FIGURE 3.3.48 Bending Moment Contours in the East Semidome. Simple Static Analysis Under Self Weight. Bending Moment Force in Local Radial Direction

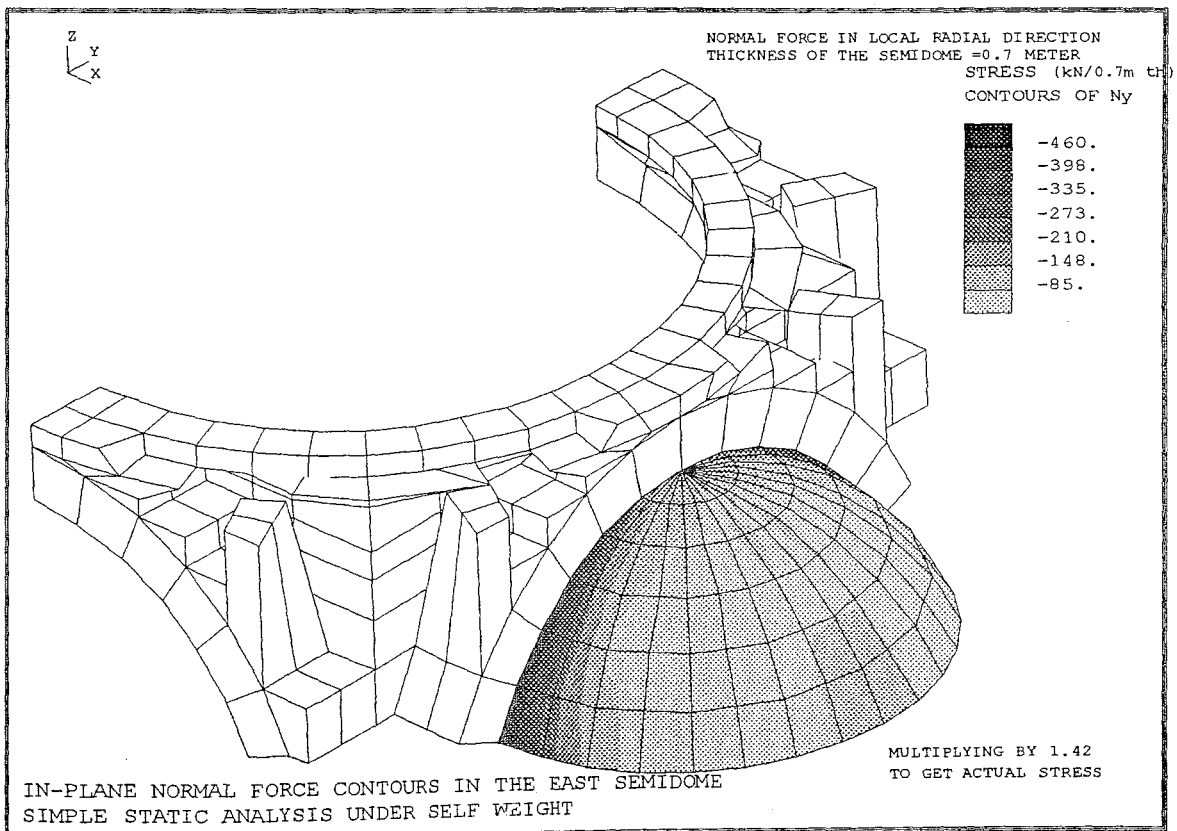


FIGURE 3.3.49 In Plane Normal Force Contours in the East Semidome. Simple Static Analysis Under Self Weight. Normal Force in Local Transverse Direction

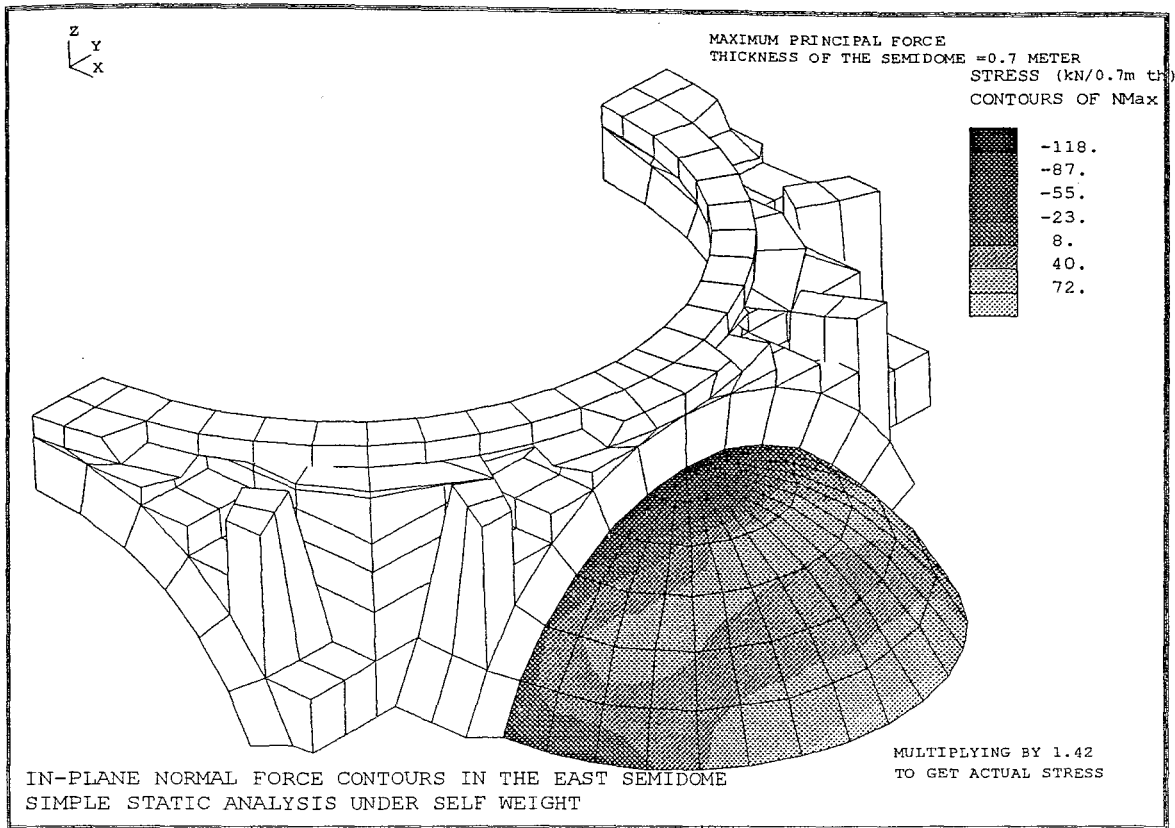


FIGURE 3.3.50 In Plane Normal Force Contours in the East Semidome.Simple Static Analysis Under Self Weight.Normal Force in Local Radial Direction

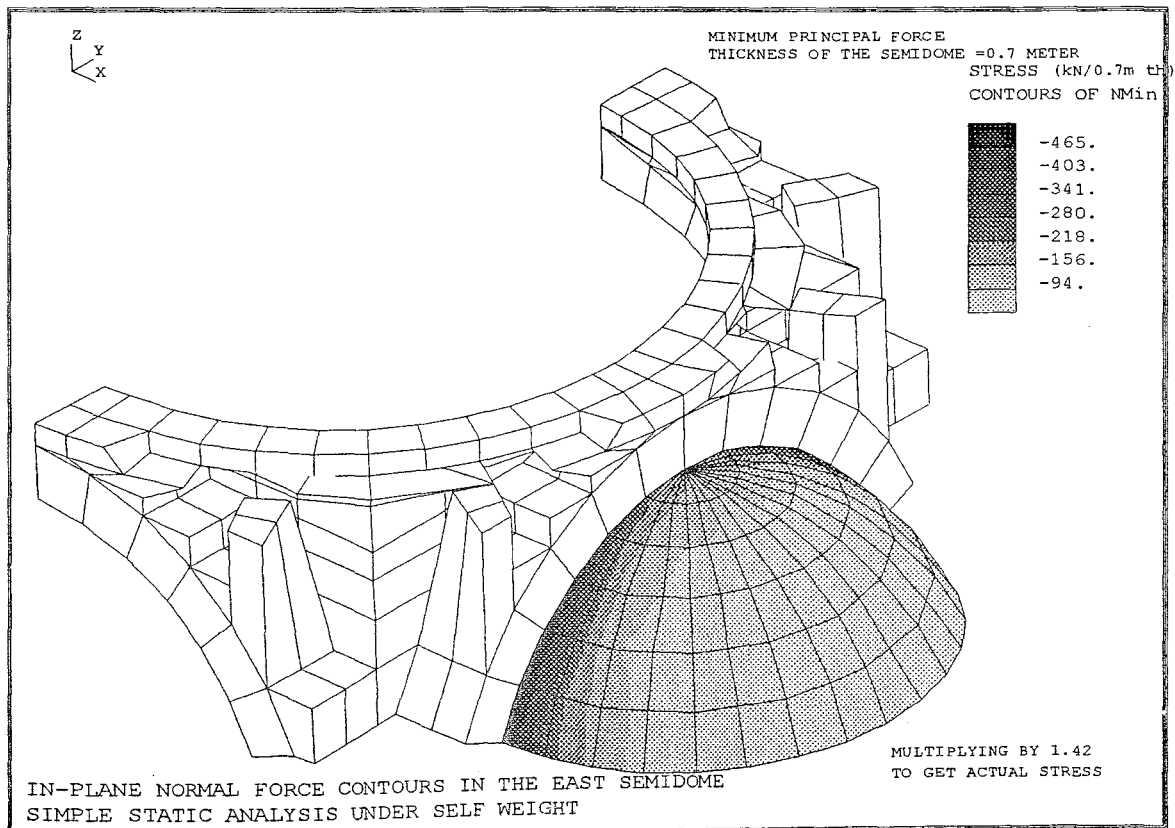


FIGURE 3.3.52 In Plane Normal Force Contours in the East Semidome.Simple Static Analysis Under Self Weight.Minimum Principal Force

3.4 ANALYSIS UNDER DYNAMIC LOADS

3.4.1 PAST STUDIES

In 1975, E. Arıoğlu and K. Anadol [10] made a dynamic model for Süleymaniye Mosque. In their simple dynamic model, they used 4 lumped mass, showing the 4 main piers which are connected by means of springs forming a square in the plan. In the middle an infinitely rigid mass is placed, representing the dome. The four piers are connected to the outer buttress piers via the springs and the semi domes are modelled with beam elements. In their research they found the longest natural period of the mosque as 0.76 seconds for both horizontal directions in the plan.

In 1994, A. Selahiye carried out a thesis study [6] on the identification of structural configuration of structural configuration, earthquake response and performance of the Süleymaniye Mosque. Natural frequencies and mode shapes of the structure are determined by ambient vibration tests and finite element analysis. The same dynamic characteristics are further obtained by processing a small intensity earthquake data recorded in 1994 by nine strong motion accelerographs installed in the mosque. A satisfactory correlation is observed between experimental and analytical results. Table 3.3.4.1 gives the calculated and measured frequencies of this study.

Table 3.4.1.1 Calculated and Measured Dynamic Properties

Mode	Ambient Test	Model Result	Earthquake Result
1	3,38	3,26	3,38
2	3,44	3,65	3,42
3	4,26	4,58	4,3
4	4,71	5,21	*
5	5,85	5,35	*
Vertical	9,71	*	9,6

* Could not be computed

3.4.2 VIBRATION ANALYSIS

Eigenvector analysis involved the solution of the generalized eigenvalue problem:

$$|K - \Omega^2 M| \Phi = 0$$

Where K is the stiffness matrix, M is the diagonal mass matrix, Ω is the diagonal matrix of eigenvalues, and Φ is the matrix of corresponding eigenvectors (mode shapes).

Each eigenvalue-eigenvector pair is called a natural vibration mode of the structure.

In LUSAS (Ref 9), two methods are available to extract the eigenvalues and eigenvectors from large equation systems.

- (i) Subspace iteration
- (ii) Guyan reduction

Both techniques have been designed for structural applications in which the lowest eigenvalues and eigenvectors are typically required and both algorithms have similarities.

- (i) Both methods start by examining which degrees of freedom will provide the greatest contribution to the structural response, i.e. the q degrees of freedom with the highest mass to stiffness ratios.
- (ii) A transformation matrix is formed, and a reduced set of q equations are formed.
- (iii) The reduced set of equations are solved using either the implicit QL or Jacobi iteration to obtain the eigenvalues and eigenvectors of the reduced system.
- (iv) The eigenvectors of the full system are obtained using the transformation matrix.

In general, subspace iteration is more effective than Guyan reduction.

In the subspace iteration procedure which is used in this study, efficient evaluation of the lowest p eigenvalues and corresponding eigenvectors is achieved by performing simultaneous inverse iteration using a set of iteration vectors, followed by a projection of the problem matrices on to the subspace formed by these vectors. This produces a reduced eigen-problem which is solved using Jacobi iteration. The eigenvectors of the reduced problem are then transformed back to the full space to form new iteration vectors. The process is then repeated until the iteration vectors converge on the lowest p eigenvectors of the full problem.

3.4.3 MODE SHAPES AND FREQUENCIES

The first 20 modes calculated in this thesis study (Fig 3.4.3.1-thru Fig 3.4.3.14) are given in table 3.4.2.1. Total mass and participating mass values for each direction are also given in this table.

3.5 ANALYSIS UNDER DIFFERENT COMBINATIONS OF MATERIAL PROPERTIES AND BOUNDARY CONDITIONS

Table 3.5.1 gives the material characteristics for each model input.

The results of the various dynamic runs under different combinations of material properties and boundary conditions are summarized in Table 3.5.2

Table 3.5.1 Material Properties Used in the Analysis

INPUT NO	Modulus of Elasticity Values ($N/m^2 \cdot 10^9$)		
	Piers(Stone)	Dome(Brick)	Arches(Brick)
1	10	5	8,5
2	10	3	3
3	3,5	3	3
4	10	3,5	3,5

Four different boundary conditions were analysed for four different combinations of material properties (Table 3.5.3). Several dynamic runs were carried out and finally a model with nearest frequency values to those of ambient vibration tests was selected as the improved model which was used for the spectral response analysis under a scenario earthquake for İstanbul.

3.4.2.1 Results of Modal Analysis

Mod No	Eigen-value	Frequency	X -Axis		Y -Axis		Z -Axis	
			Part. Mass	Total Part. Mass	Part. Mass	Total Part. Mass	Part. Mass	Total Part. Mass
1	415.398	3.244	0.574	0.574	$0.949 \cdot 10^{-3}$	$0.949 \cdot 10^{-3}$	$0.489 \cdot 10^{-9}$	$0.489 \cdot 10^{-9}$
2	461.763	3.420	$0.1 \cdot 10^{-4}$	0.574	0.595	0.595	$0.190 \cdot 10^{-6}$	$0.190 \cdot 10^{-6}$
3	731.807	4.305	$0.2 \cdot 10^{-7}$	0.574	$0.336 \cdot 10^{-3}$	0.595	$0.202 \cdot 10^{-6}$	$0.393 \cdot 10^{-6}$
4	884.654	4.734	$0.127 \cdot 10^{-6}$	0.574	$0.16 \cdot 10^{-3}$	0.595	$0.697 \cdot 10^{-2}$	$0.697 \cdot 10^{-2}$
5	888.950	4.745	$0.461 \cdot 10^{-6}$	0.574	$0.595 \cdot 10^{-3}$	0.595	$0.167 \cdot 10^{-3}$	$0.713 \cdot 10^{-2}$
6	1463.72	6.089	$0.944 \cdot 10^{-1}$	0.668	$0.427 \cdot 10^{-4}$	0.595	$0.237 \cdot 10^{-6}$	$0.714 \cdot 10^{-2}$
7	1492.88	6.149	$0.542 \cdot 10^{-4}$	0.668	0.122	0.718	$0.710 \cdot 10^{-6}$	$0.714 \cdot 10^{-2}$
8	1552.89	6.271	$0.662 \cdot 10^{-1}$	0.734	$0.594 \cdot 10^{-3}$	0.718	$0.368 \cdot 10^{-4}$	$0.717 \cdot 10^{-2}$
9	1622.37	6.410	$0.593 \cdot 10^{-4}$	0.735	$0.171 \cdot 10^{-6}$	0.718	$0.784 \cdot 10^{-1}$	$0.856 \cdot 10^{-1}$
10	1854.89	6.854	$0.441 \cdot 10^{-7}$	0.735	$0.455 \cdot 10^{-2}$	0.722	$0.485 \cdot 10^{-6}$	$0.856 \cdot 10^{-1}$
11	1872.82	6.887	$0.214 \cdot 10^{-6}$	0.735	$0.499 \cdot 10^{-4}$	0.722	$0.145 \cdot 10^{-6}$	$0.856 \cdot 10^{-1}$
12	2183.44	7.437	$0.824 \cdot 10^{-6}$	0.735	$0.550 \cdot 10^{-6}$	0.722	$0.481 \cdot 10^{-1}$	0.134
13	2201.60	7.468	$0.341 \cdot 10^{-7}$	0.735	$0.366 \cdot 10^{-7}$	0.722	$0.130 \cdot 10^{-4}$	0.134
14	2212.49	7.486	$0.339 \cdot 10^{-3}$	0.735	$0.201 \cdot 10^{-10}$	0.722	$0.114 \cdot 10^{-4}$	0.134
15	2342.30	7.703	$0.324 \cdot 10^{-7}$	0.735	$0.127 \cdot 10^{-1}$	0.735	$0.543 \cdot 10^{-3}$	0.134
16	2359.80	7.731	$0.220 \cdot 10^{-6}$	0.735	$0.428 \cdot 10^{-3}$	0.735	$0.513 \cdot 10^{-1}$	0.185
17	2616.39	8.141	$0.681 \cdot 10^{-6}$	0.735	$0.154 \cdot 10^{-2}$	0.737	$0.141 \cdot 10^{-9}$	0.185
18	2679.37	8.238	$0.309 \cdot 10^{-2}$	0.738	$0.330 \cdot 10^{-6}$	0.737	$0.127 \cdot 10^{-3}$	0.185
19	3055.13	8.797	$0.245 \cdot 10^{-2}$	0.740	$0.218 \cdot 10^{-7}$	0.737	$0.127 \cdot 10^{-6}$	0.185
20	3158.41	8.944	$0.346 \cdot 10^{-11}$	0.740	$0.223 \cdot 10^{-8}$	0.737	$0.135 \cdot 10^{-1}$	0.199

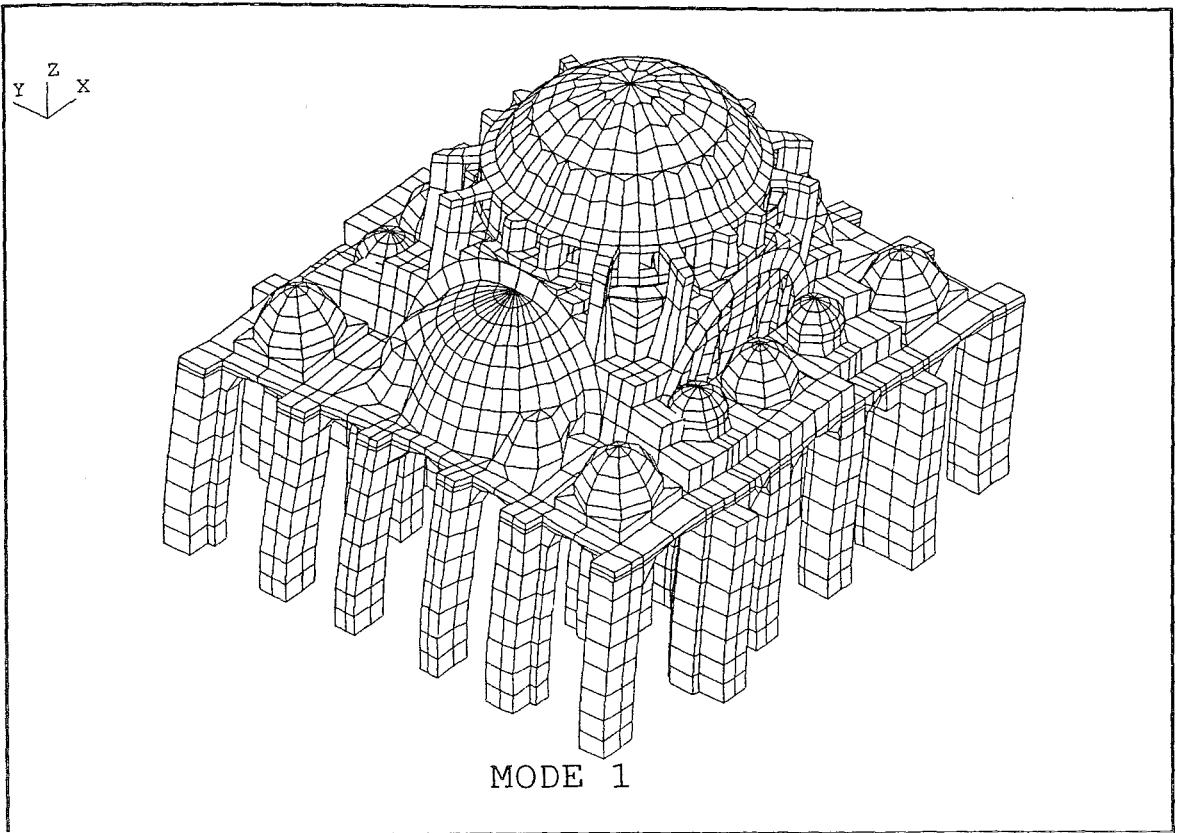


FIGURE 3.4.3.1 Modal Analysis 3-D View from South-East Mode1

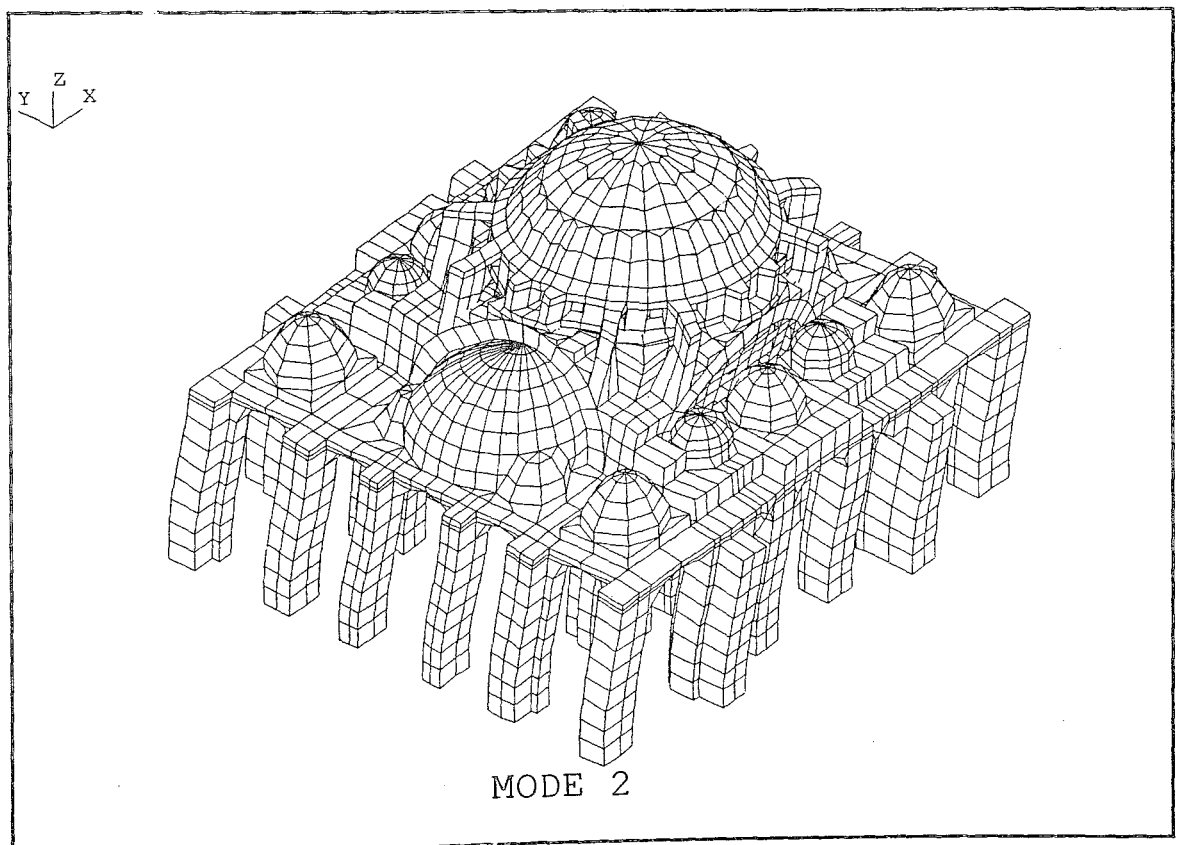


FIGURE 3.4.3.2 Modal Analysis 3-D View from South-East Mode2

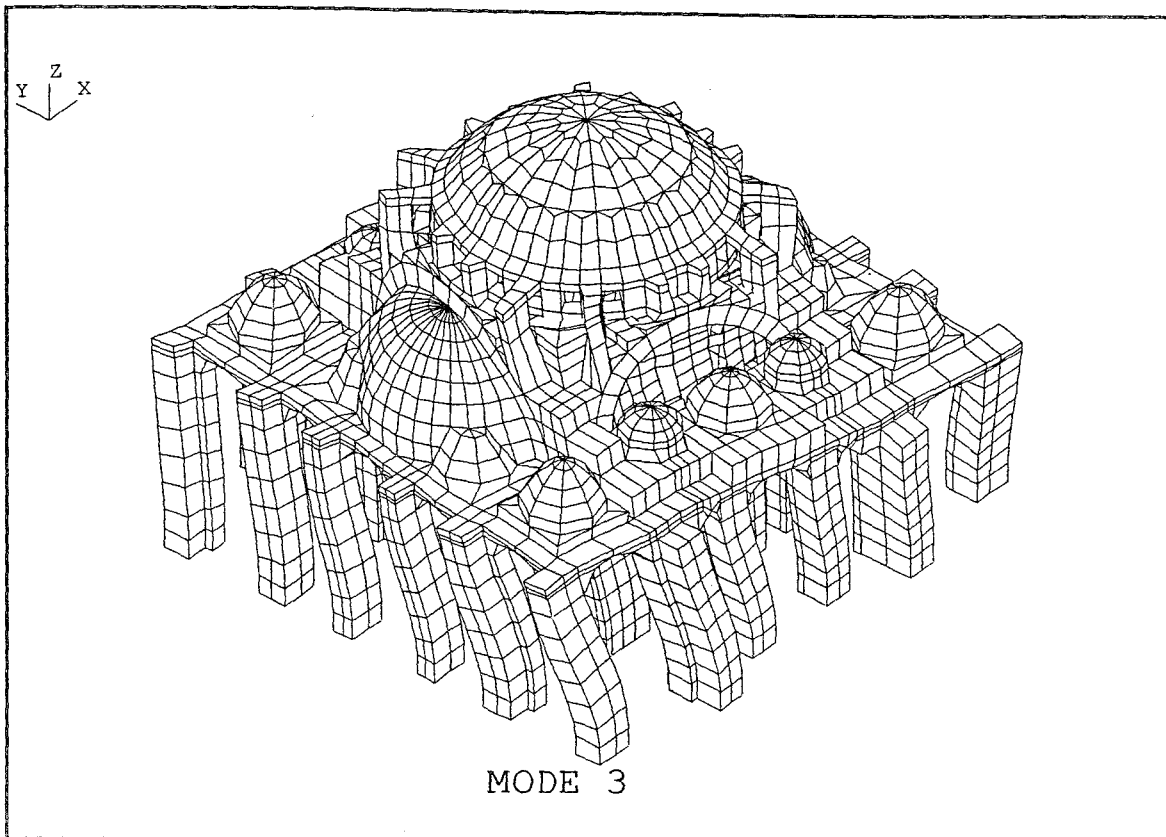


FIGURE 3.4.3.3 Modal Analysis 3-D View from South-East Mode3

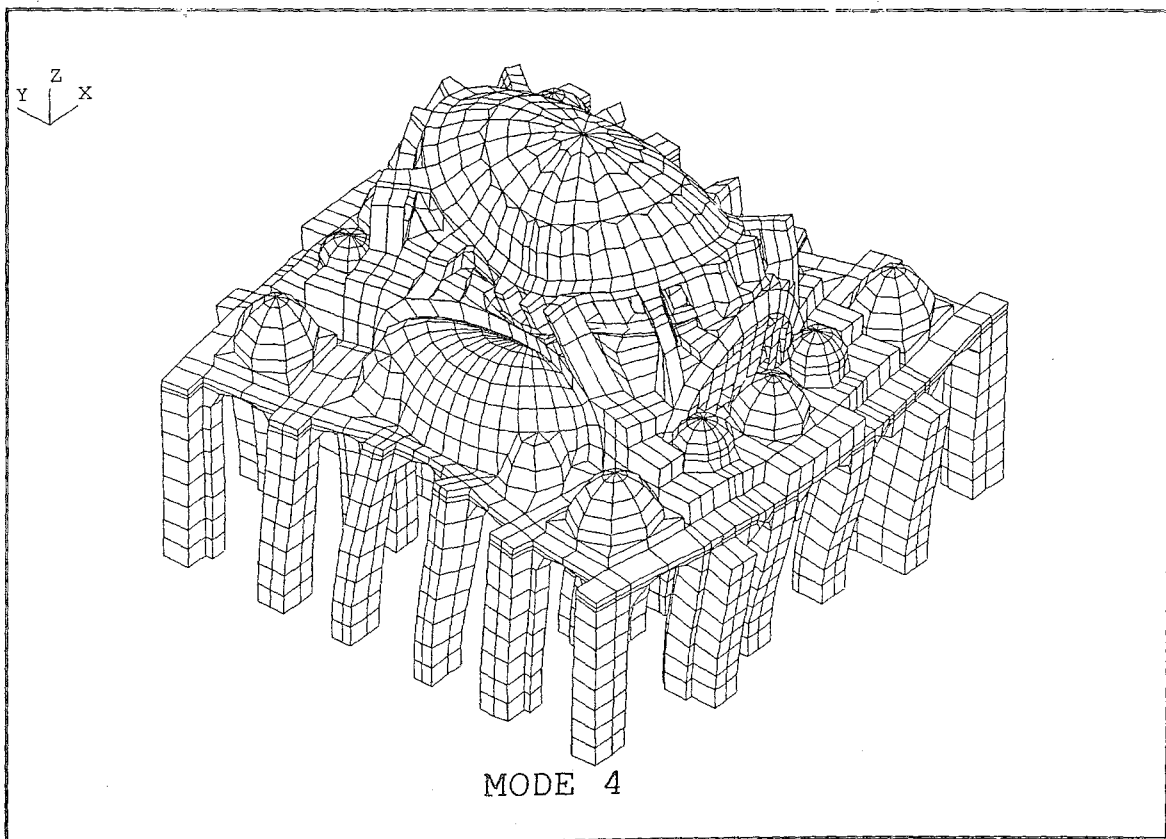


FIGURE 3.4.3.4 Modal Analysis 3-D View from South-East Mode4

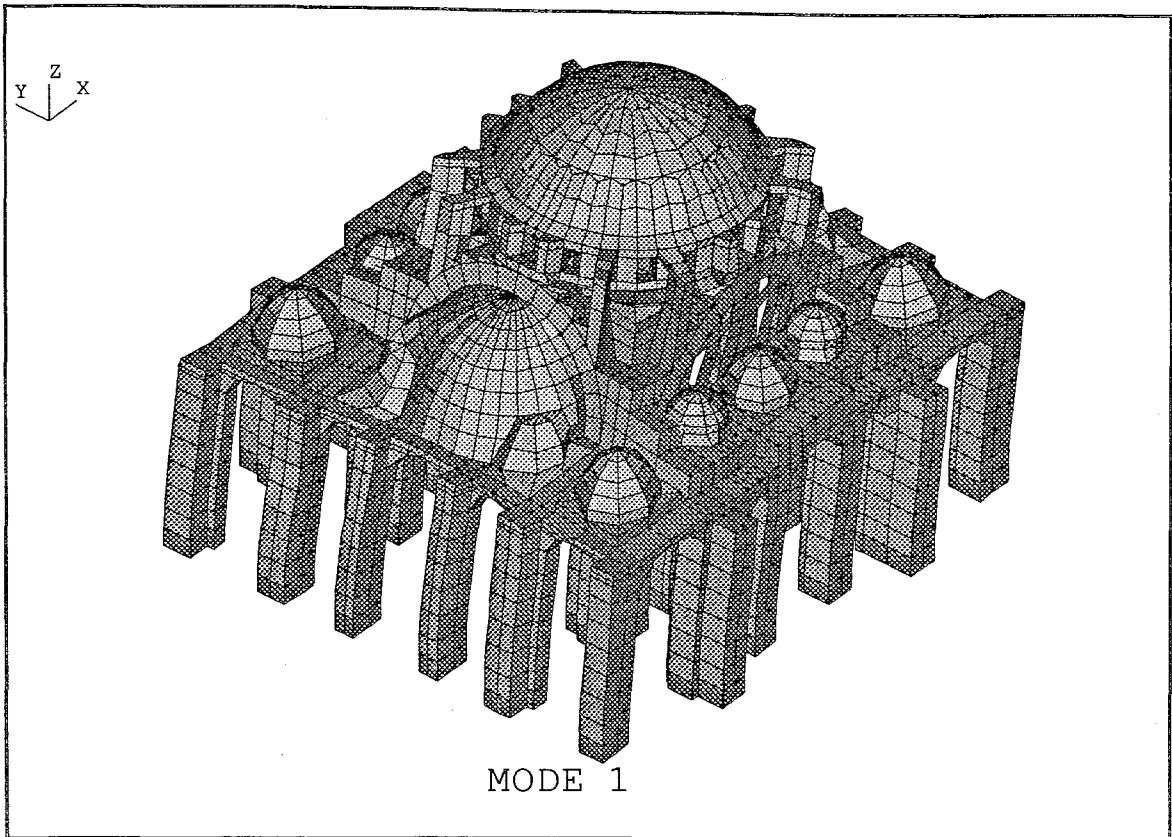


FIGURE 3.4.3.5 Modal Analysis Shaded 3-D View from South -East Model1

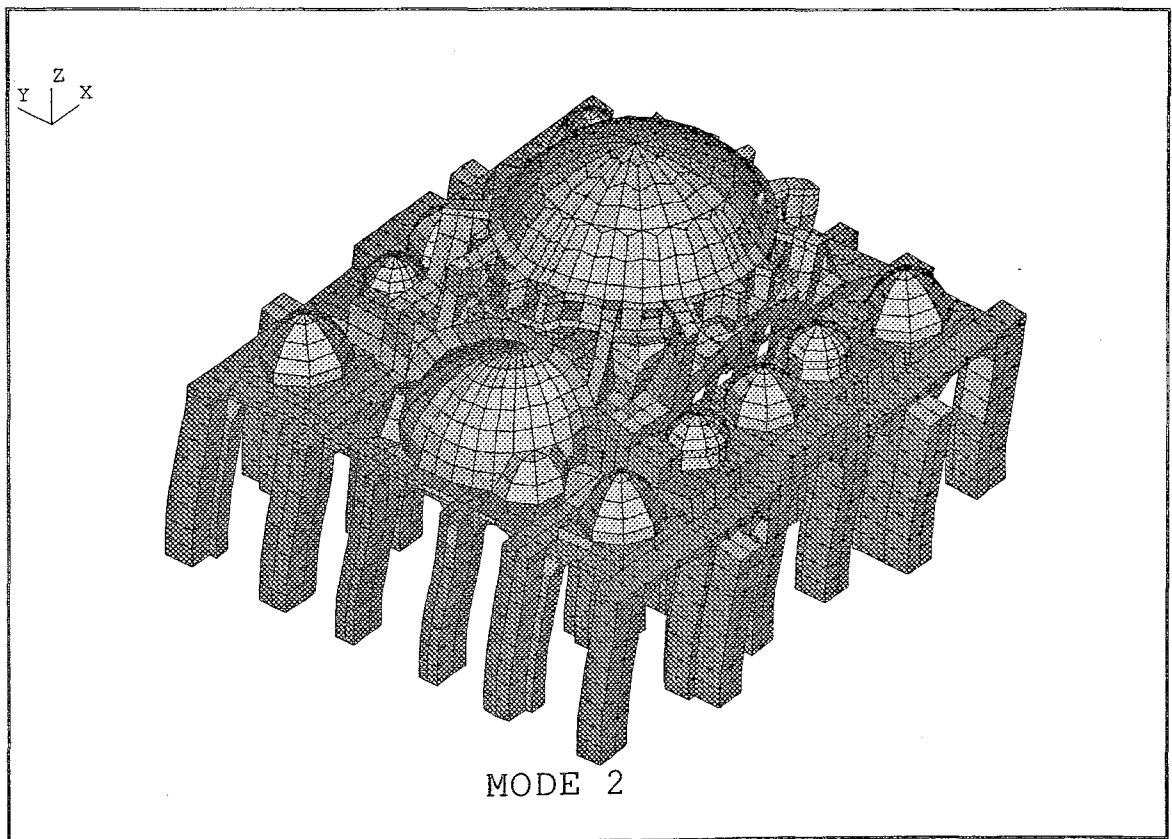


FIGURE 3.4.3.6 Modal Analysis Shaded 3-D View from South -East Mode2

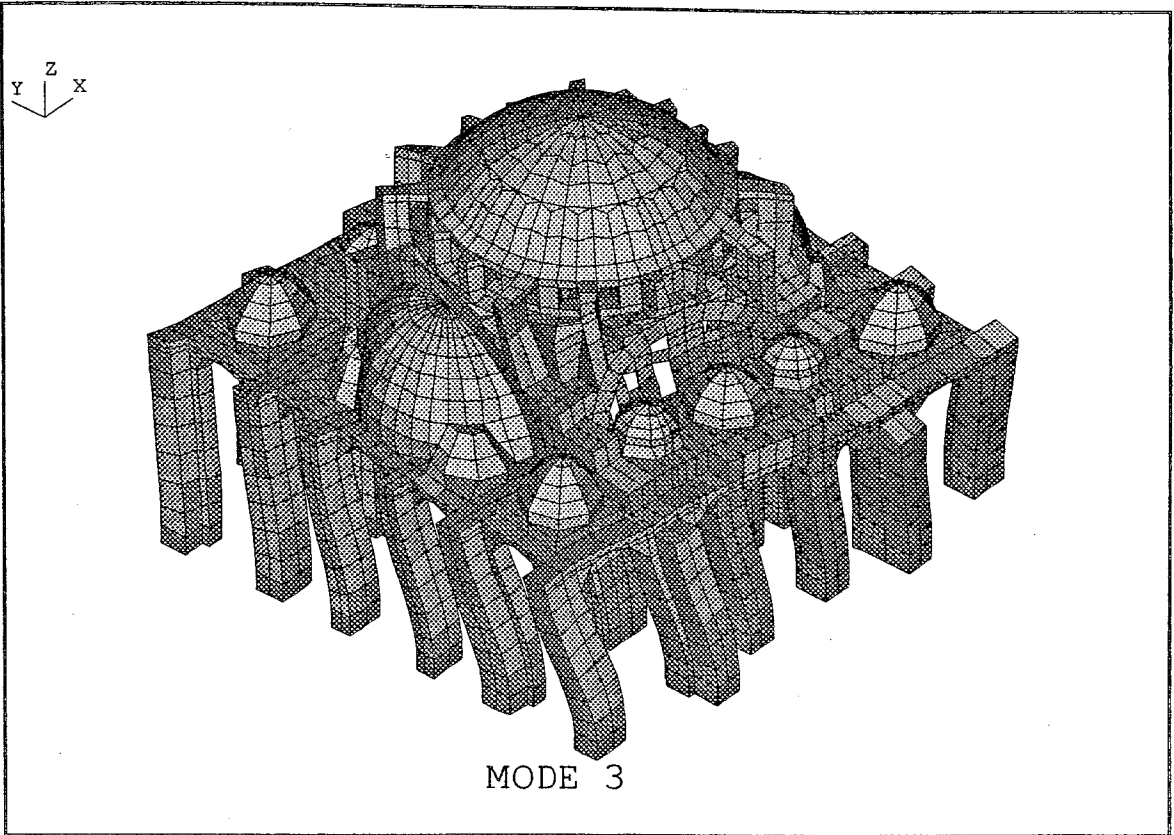


FIGURE 3.4.3.7 Modal Analysis Shaded 3-D View from South -East Mode3

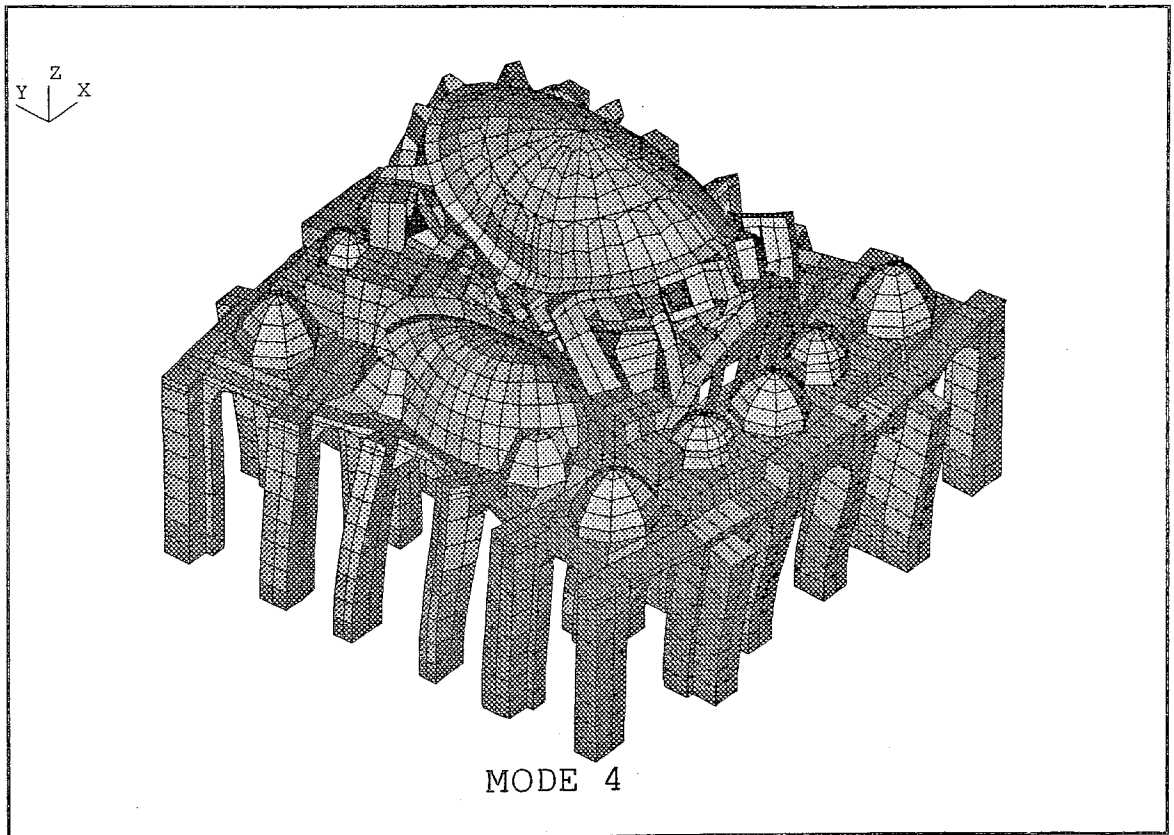


FIGURE 3.4.3.8 Modal Analysis Shaded 3-D View from South -East Mode4

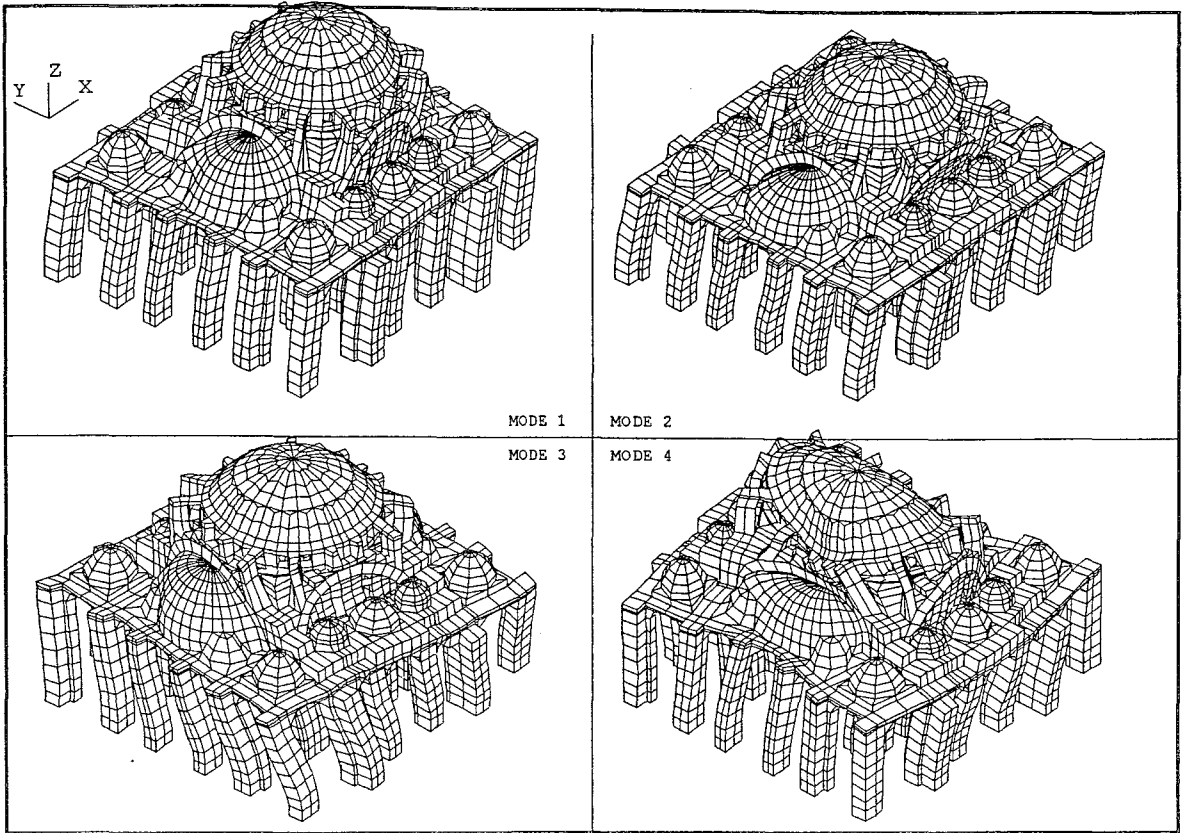


FIGURE 3.4.3.9 Modal Analysis Mode 1-2-3-4

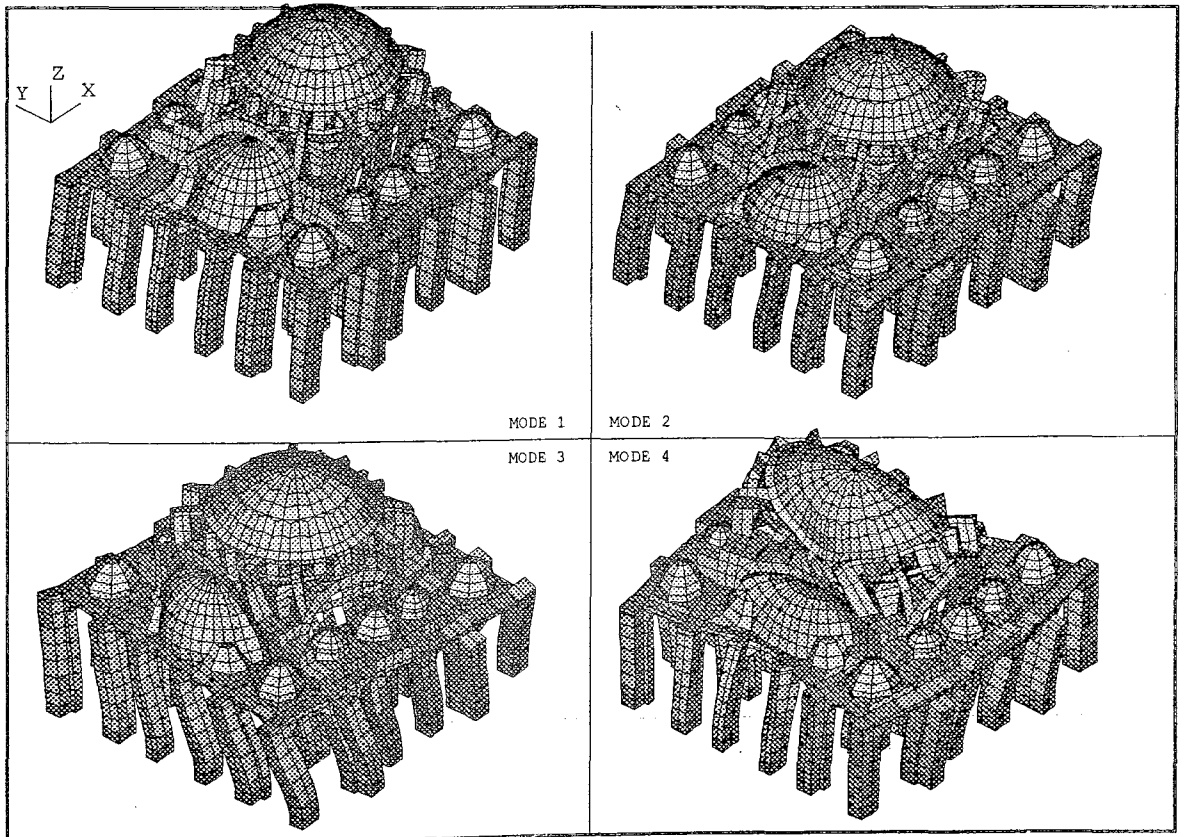


FIGURE 3.4.3.10 Modal Analysis Mode 1-2-3-4 ,shaded

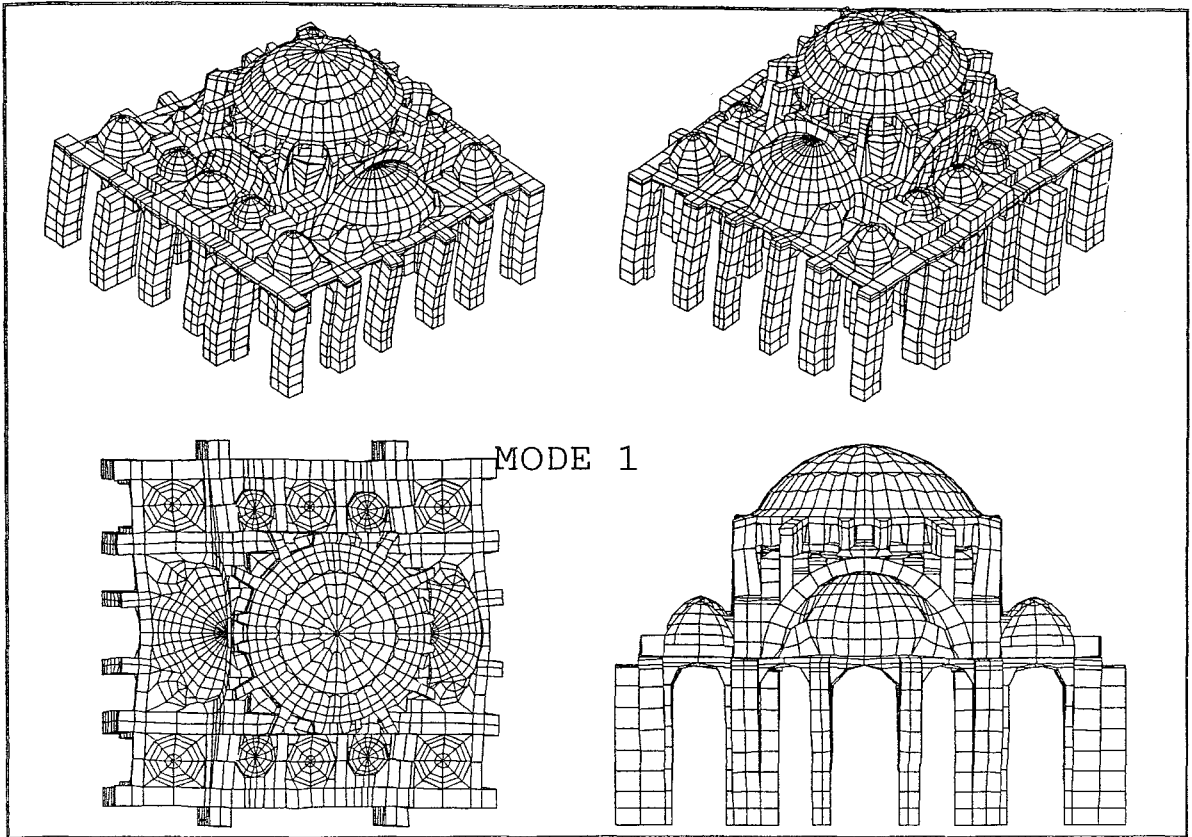


FIGURE 3.4.3.11 Modal Analysis 3-D View from South-East, South-West ,Top and Front Model1

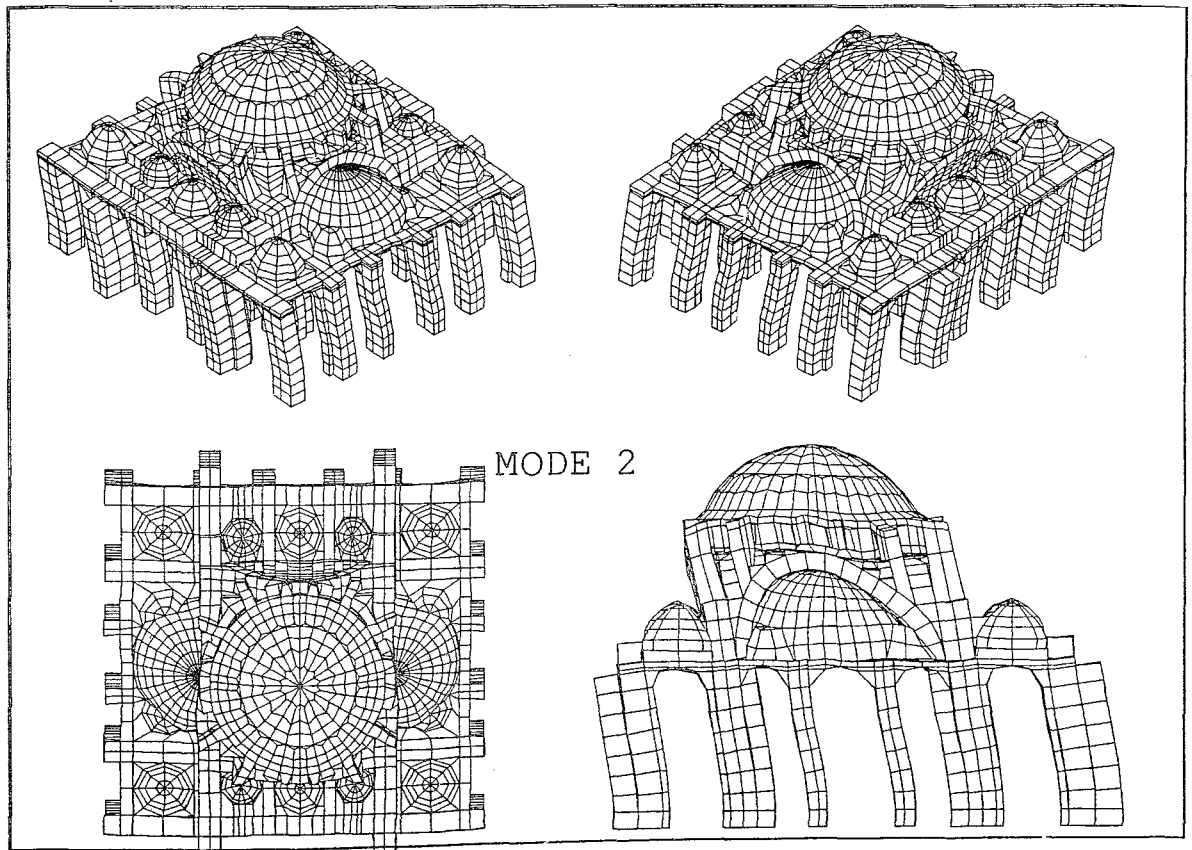


FIGURE 3.4.3.12 Modal Analysis 3-D View from South-East, South-West ,Top and Front Mode2

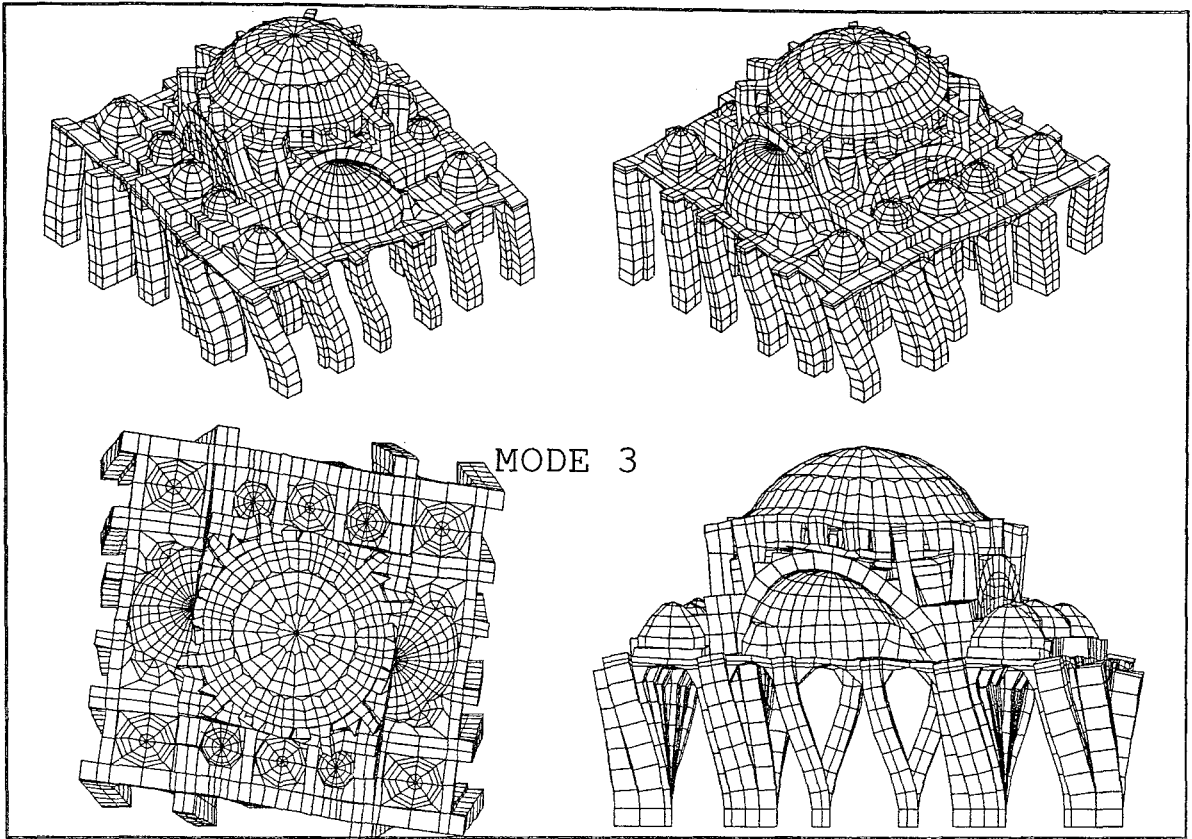


FIGURE 3.4.3.13 Modal Analysis 3-D View from South-East, South-West, Top and Front Mode 3

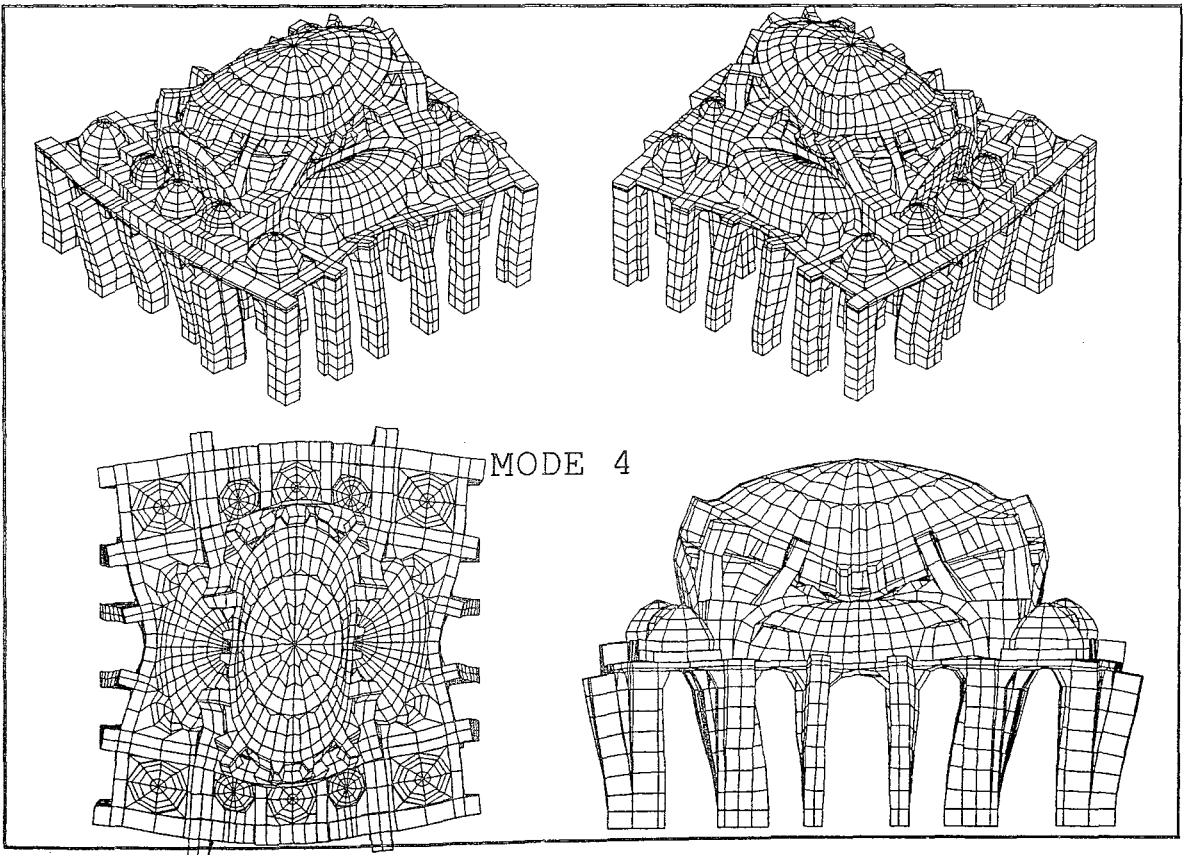


FIGURE 3.4.3.14 Modal Analysis 3-D View from South-East, South-West, Top and Front Mode 4

3.5 ANALYSIS UNDER DIFFERENT COMBINATIONS OF MATERIAL PROPERTIES AND BOUNDARY CONDITIONS

Table 3.5.1 gives the material characteristics for each model input.

The results of the various dynamic runs under different combinations of material properties and boundary conditions are summarized in Table 3.5.2

Table 3.5.1. Material Properties Used in the Analysis

INPUT NO	Modulus of Elasticity Values ($N/m^2 \cdot 10^9$)		
	Piers(Stone)	Dome(Brick)	Arches(Brick)
1	10	5	8,5
2	10	3	3
3	3,5	3	3
4	10	3,5	3,5

Four different boundary conditions were analysed for four different combinations of material properties (Table 3.5.3). Several dynamic runs were carried out and finally a model with nearest frequency values to those of ambient vibration tests was selected as the improved model which was used for the spectral response analysis under a scenario earthquake for İstanbul.

Table 3.5.3 Description of the Boundary Conditions

MODEL NAME	DESCRIPTION	DESCRIPTION
Sup A1	Fix in XYZ at -5.3m	
Sup2 A2	Fix in XYZ at -5.3m	
B2	Spring in XY at -2.8m A1	
Sup 3 A3 SELECTED MODEL	Fix in XYZ at -2.8m A1	
Sup A4	Fix in XYZ at -2.8m A1 Fix in XY at -0.3m	
B4	Spring in XYZ at -2.8m A1 Spring in XY at -0.3m	
A5	Fix in XYZ at -2.8m A1 Fix in XY at -0.3m	
B5	Fix in XYZ at -2.8m A5 Spring in XYZ at -0.3m	
A6	Fix in XYZ at -2.8m	

Table 3.5.2 Table of Dynamic Runs

Model Name	Description	Natural Frequencies (Hz)					
		f1	f2	f3	f4	F5	
Sup1 A1	Fix in XYZ at -5.3 m	3.07	3.23	3.76	4.81	4.93	Input1
		2.84	2.99	3.65	4.17	4.18	Input2
		2.89	3.03	3.67	4.28	4.30	Input3
Sup2 A2	Fix in XY at -2.8 m A1	3.24	3.41	4.02	5.01	5.12	Input1
		2.96	3.12	3.89	4.32	4.33	Input2
		3.02	3.17	3.91	4.44	4.44	Input3
B2	Spring in XY at -2.8m A1	3.08	3.29	3.82	4.85	4.91	Input1
		2.85	3.03	3.7	4.2	4.22	Input2
		2.90	3.08	3.72	4.31	4.34	Input3
Sup3 A3 (Selected Model)	Fix in XYZ at -2.8 m A1	3.52	3.75	4.45	5.35	5.44	Input1
		3.15	3.34	4.26	4.56	4.60	Input2
		3.24	3.41	4.30	4.71	4.73	Input3
		3.24	3.42	4.30	4.73	4.74	Input4
AMBIENT TEST MEASURMENTS		3.38	3.44	4.26	4.71	5.85	
Sup A4	Fix in XY at -2.8m A1 Fix in XY at -0.3m	3.63	3.82	4.66	5.47	5.55	Input1
		3.22	3.39	4.43	4.62	4.70	Input2
		3.31	3.47	4.47	4.78	4.84	Input3
B4	Spring in XY at -2.8m A1 Spring in XY at -0.3m	3.14	3.33	3.89	4.90	5.03	Input1
		2.89	3.06	3.78	4.25	4.26	Input2
		2.94	3.11	3.80	4.36	4.38	Input3
A5	Fix in XYZ at -2.8m A1 Fix in XY at -0.3m	3.72	3.74	4.47	5.36	5.45	Input1
		3.16	3.35	4.28	4.56	4.61	Input2
		3.37	3.56	4.59	4.88	4.93	Input3
B5	Fix in XYZ at -2.8 m A5 Spring in XYZ at -0.3m	3.53	3.74	4.47	5.36	5.45	Input1
		3.16	3.35	4.28	4.56	4.61	Input2
		3.24	3.42	4.31	4.71	4.74	Input3
A6	Fix in XYZ at -2.8 m	4.04	4.31	5.34	6.04	6.08	Input1
		3.46	3.68	4.94	4.94	5.06	Input2
		3.58	3.79	5.02	5.14	5.23	Input3

4.SPECTRAL RESPONSE ANALYSIS OF THE IMPROVED MODEL UNDER A SCENARIO EARTHQUAKE FOR ISTANBUL

İstanbul in general, is expected to be exposed to earthquakes occurring mainly as a result of the activity of the graben system in Marmara Sea associated with the North Anatolian Fault Zone. The nearest fault is about 20 km south of İstanbul.

The improved model (Table 3.5.2 Model No:Sup3-A3, Fix in XYZ at 2.8 m Input 4) is analysed under a scenario earthquake of magnitude 7 with an epicentral distance of 20 km to İstanbul

To study the effects of the ground motion excitations on structure it is necessary to measure the intensity of the motion. One practical measure can be obtained from a knowledge of the response spectra for a generic ground motion. The spectral response analysis seeks to estimate the maximum displacement or pseudo velocity or acceleration of the structure during a design earthquake without recourse to direct integration of the model over the complete duration of an event.

The relative motion of the structure with respect to earth arising from the earthquake is defined by the equation

$$M\{\ddot{u}\}+[c]\{\dot{u}\}+[K]\{u\}=-[K]\{\ddot{u}_g\}$$

Where $[M]$, $[C]$ and $[K]$ are mass, damping and rigidity and $\{\ddot{u}_g\}$ is ground vector respectively.

Earthquakes are unique events. Therefore, for design, spectra have been evaluated which envelope the peak response of one degree of freedom systems to a series of earthquakes. Such design spectra are given in terms of the maximum displacement or pseudo-velocity or acceleration of the structure for a range of circular frequencies.

As the modes do not necessarily occur at the same time they may not be superimposed directly to obtain design values. Therefore, two averaging methods have been incorporated in LUSAS: CQC (Complete Quadratic Combination and SRSS (Square-Root-of the Squares))

The numerical values of ground spectral acceleration are given in Table 4.1. Table 4.2 gives the distribution factors of spectral amplitude ratios in x, y and z direction. Figures 4.1 to 4.90 show the results of this analysis.

Modal frequencies obtained from ambient tests, 1994 Earthquake, Ahmet Selahiye's study [6] and finally this study using improved model are summarized in from Table 4.3

Table 4.1 Spectral Acceleration Values

Period (sec)	Acceleration (m/sec²)
0,04	7,250
0,05	6,870
0,10	7,583
0,13	7,227
0,14	7,138
0,17	7,807
0,20	7,227
0,25	6,692
0,33	6,246
0,50	5,353
0,67	4,193
1,00	3,413
1,11	2,453
1,25	2,208
1,43	1,963
1,67	1,686
2,00	1,419
2,50	1,138
2,56	0,875
	0,835

Table 4.2 Spectral Amplitude Ratios

Earthquake Direction	Amplitude Ratios
Xdirection (horizontal east -west)	%70
Y direction (horizontal south-north)	%70
Z direction (vertical)	%70

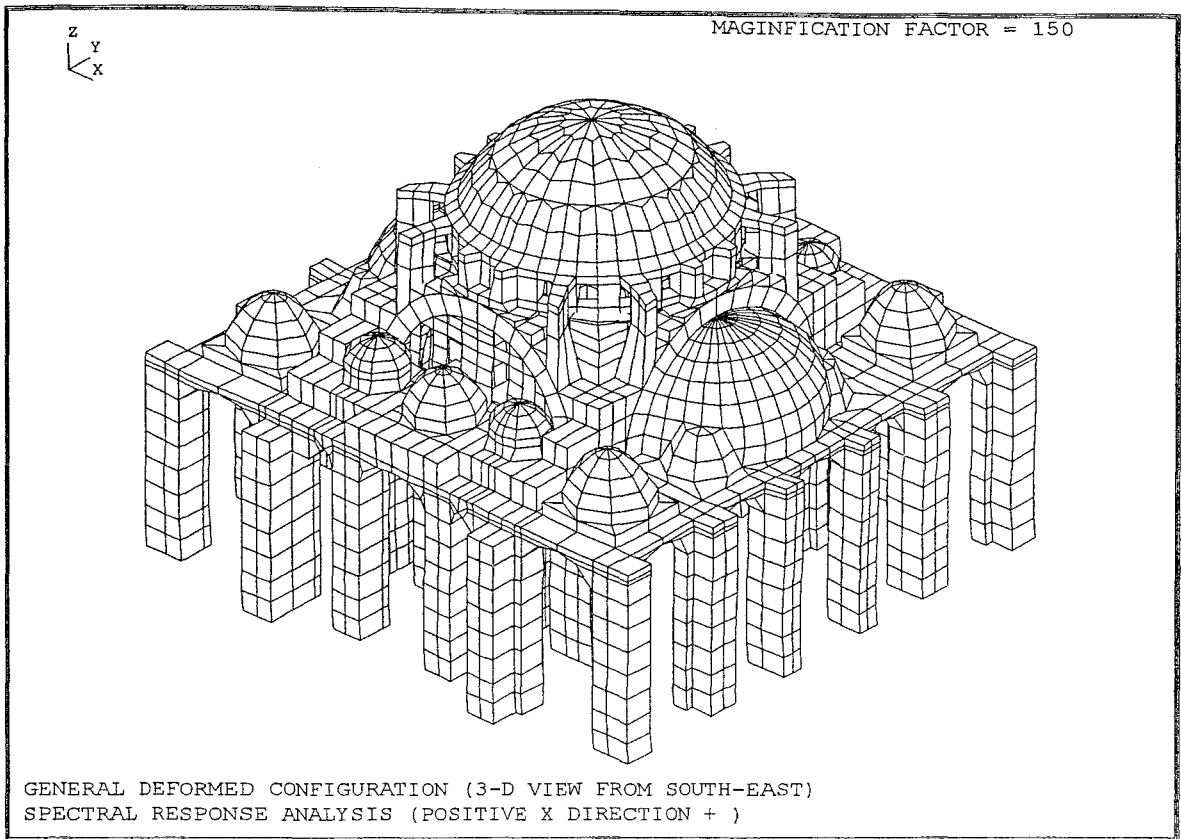


FIGURE 4.1 General Deformed Configuration (3-D View from South-East)
Spectral Response Analysis (Positive X Direction+)

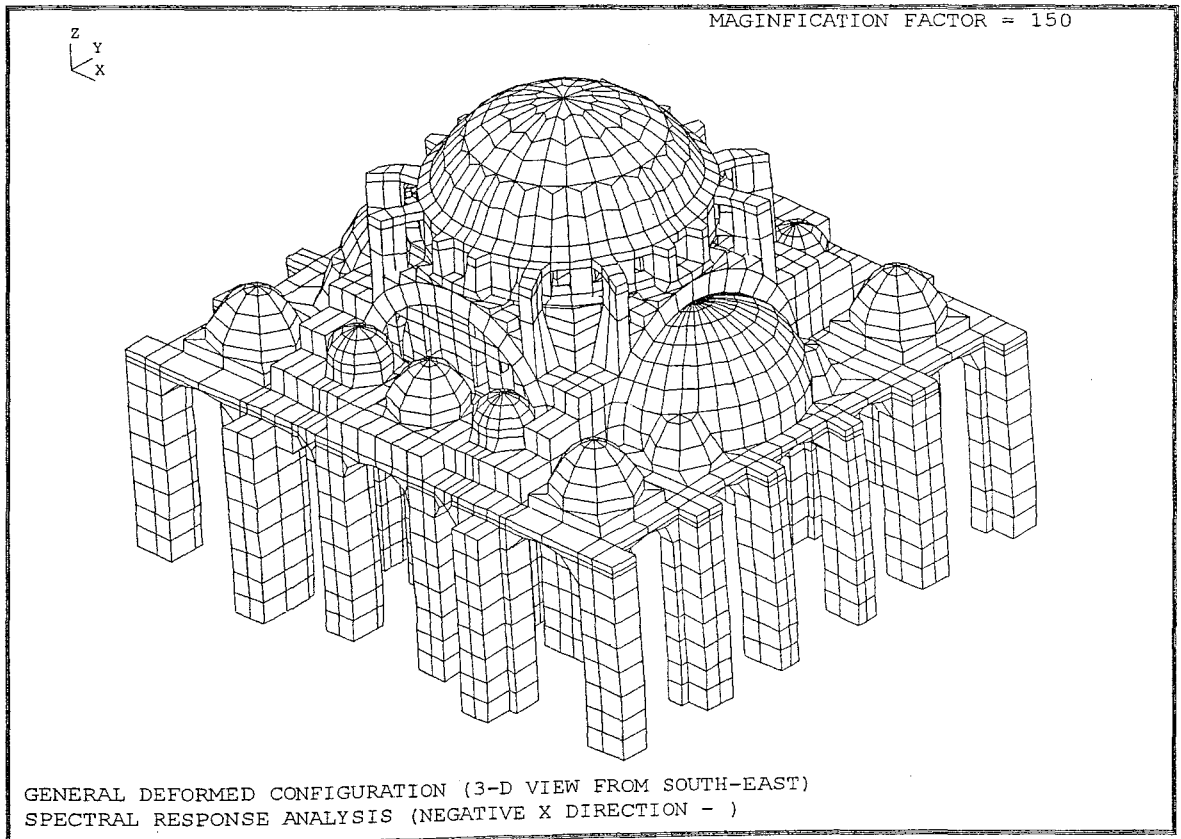


FIGURE 4.2 General Deformed Configuration (3-D View from South-East)
Spectral Response Analysis (Negative X Direction-)

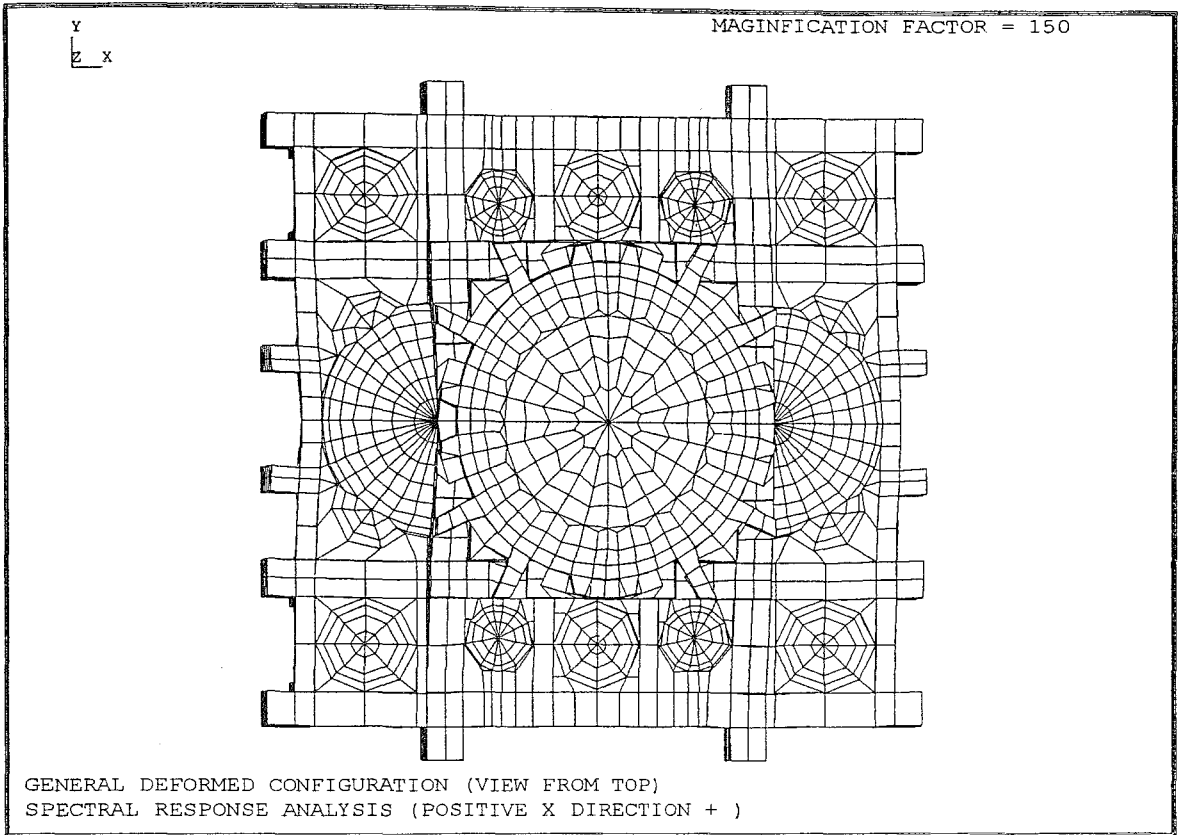


FIGURE 4.3 General Deformed Configuration (View from Top)
Spectral Response Analysis (Positive X Direction-)

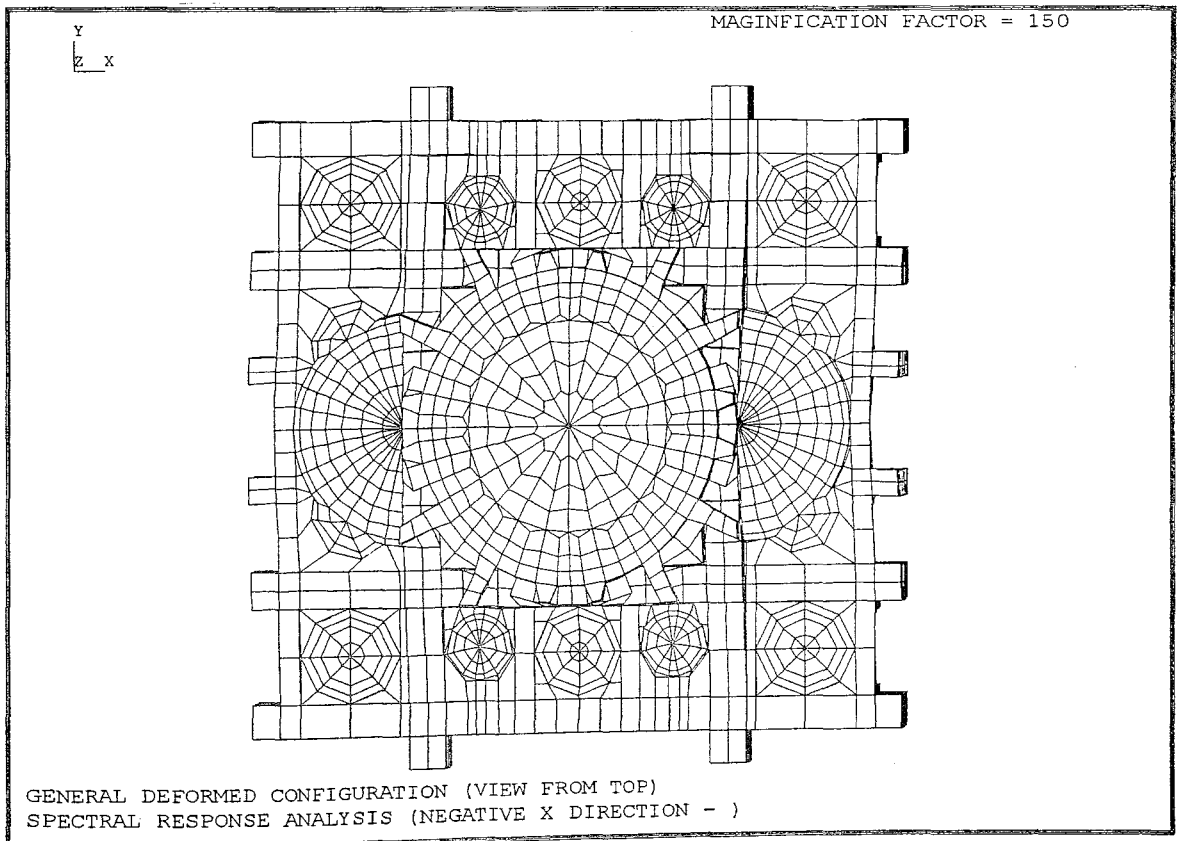


FIGURE 4.4 General Deformed Configuration (View from Top)
Spectral Response Analysis (Negative X Direction-)

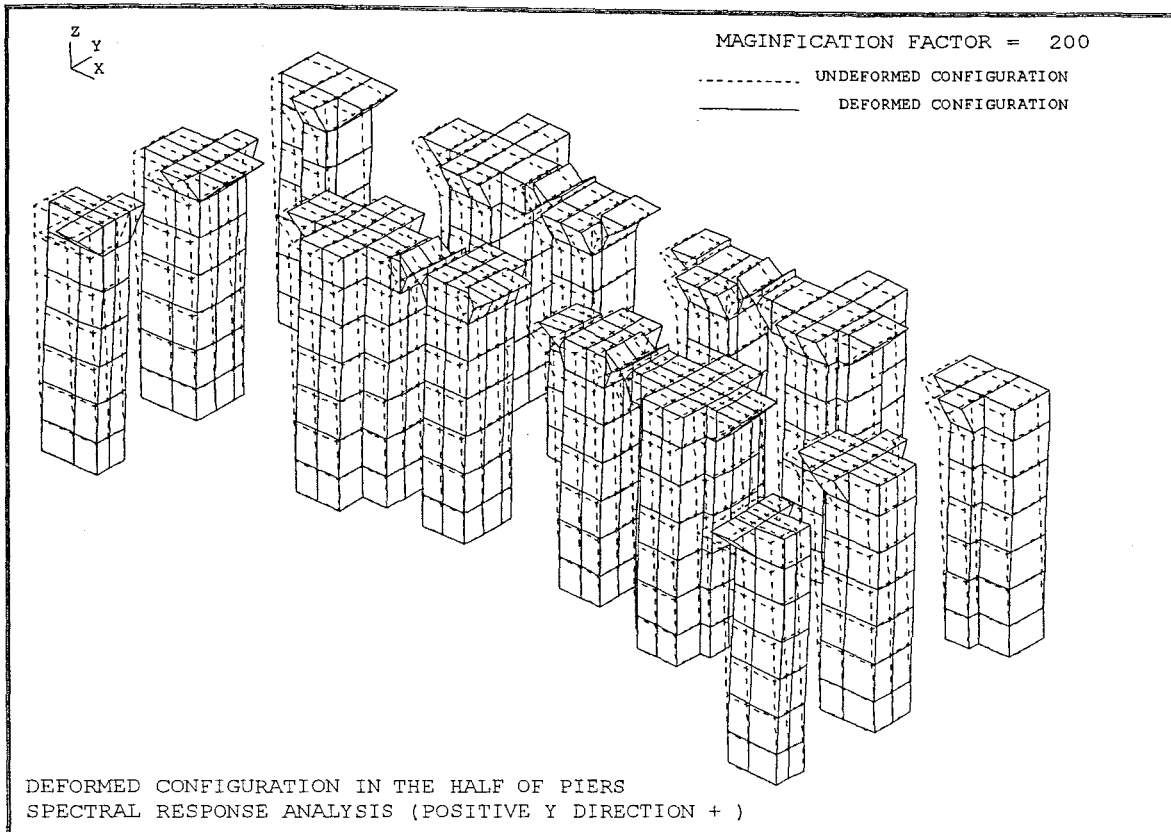


FIGURE 4.5 Deformed Configuration in the Half of Piers Spectral Response Analysis (Positive Y Direction+)

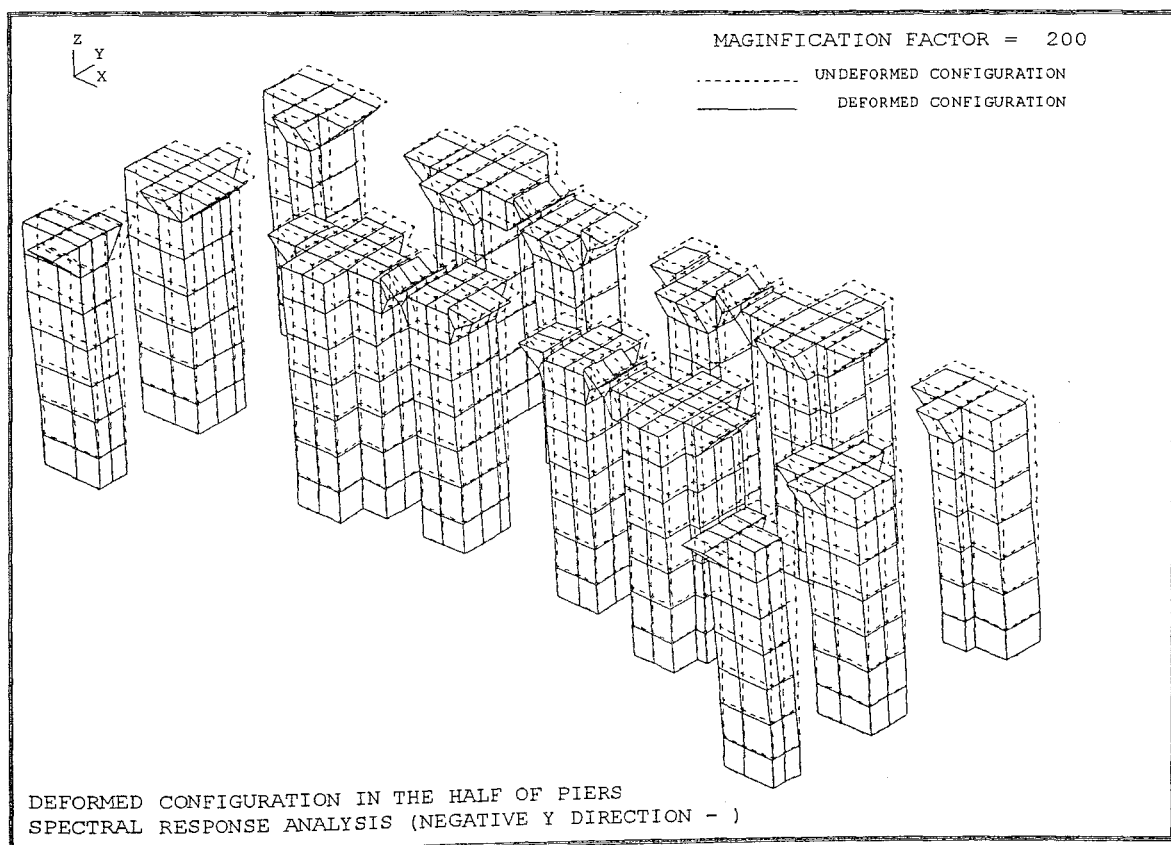


FIGURE 4.6 Deformed Configuration in the Half of Piers Spectral Response Analysis (Negative Y Direction-)

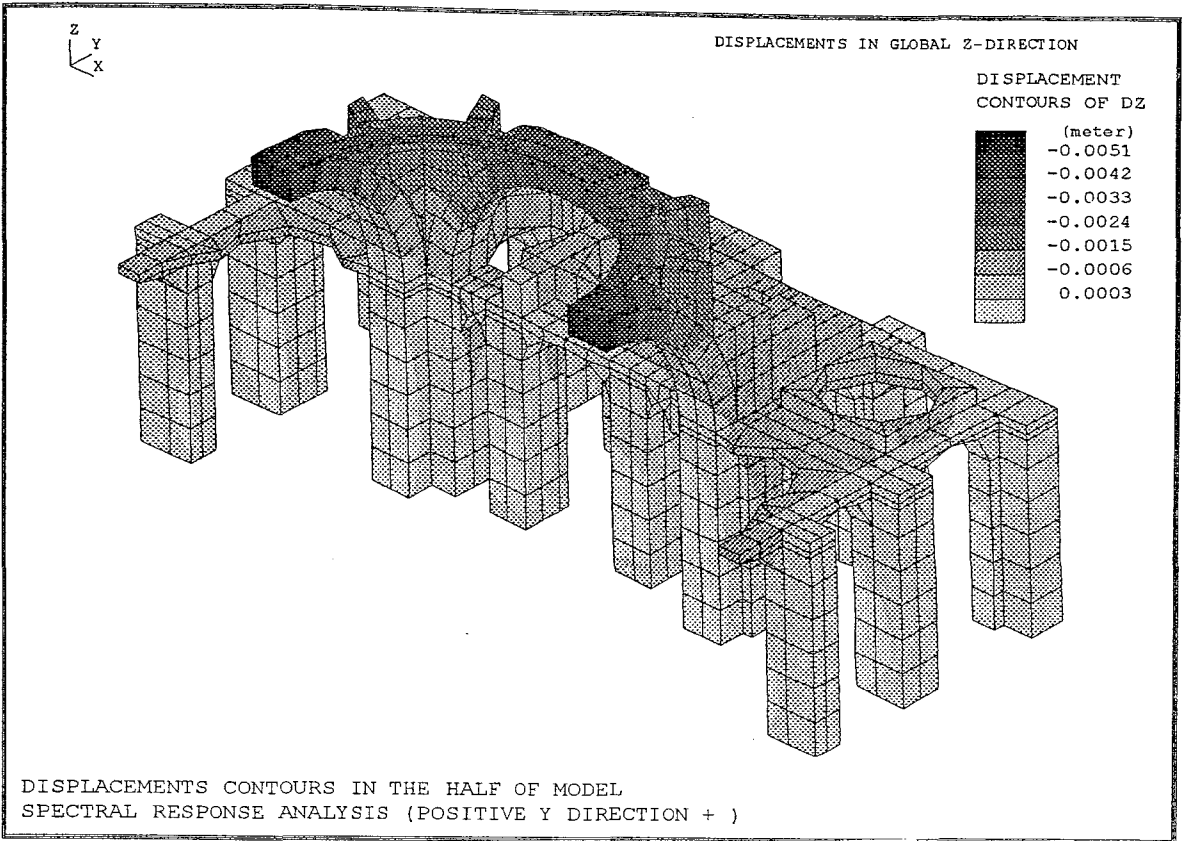


FIGURE 4.7 Displacement Contours in the Half of Model Spectral Response Analysis (Positive Y Direction+)

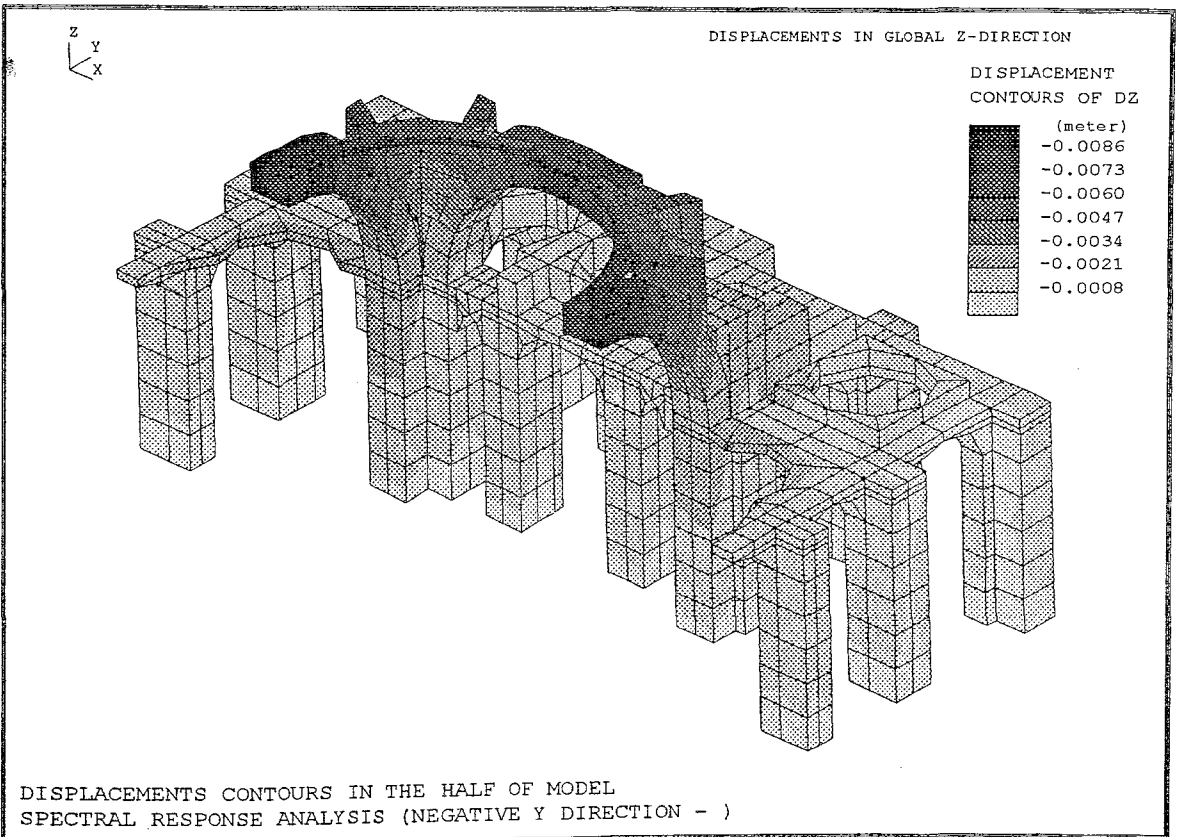


FIGURE 4.8 Displacement Contours in the Half of Model Spectral Response Analysis (Negative Y Direction-)

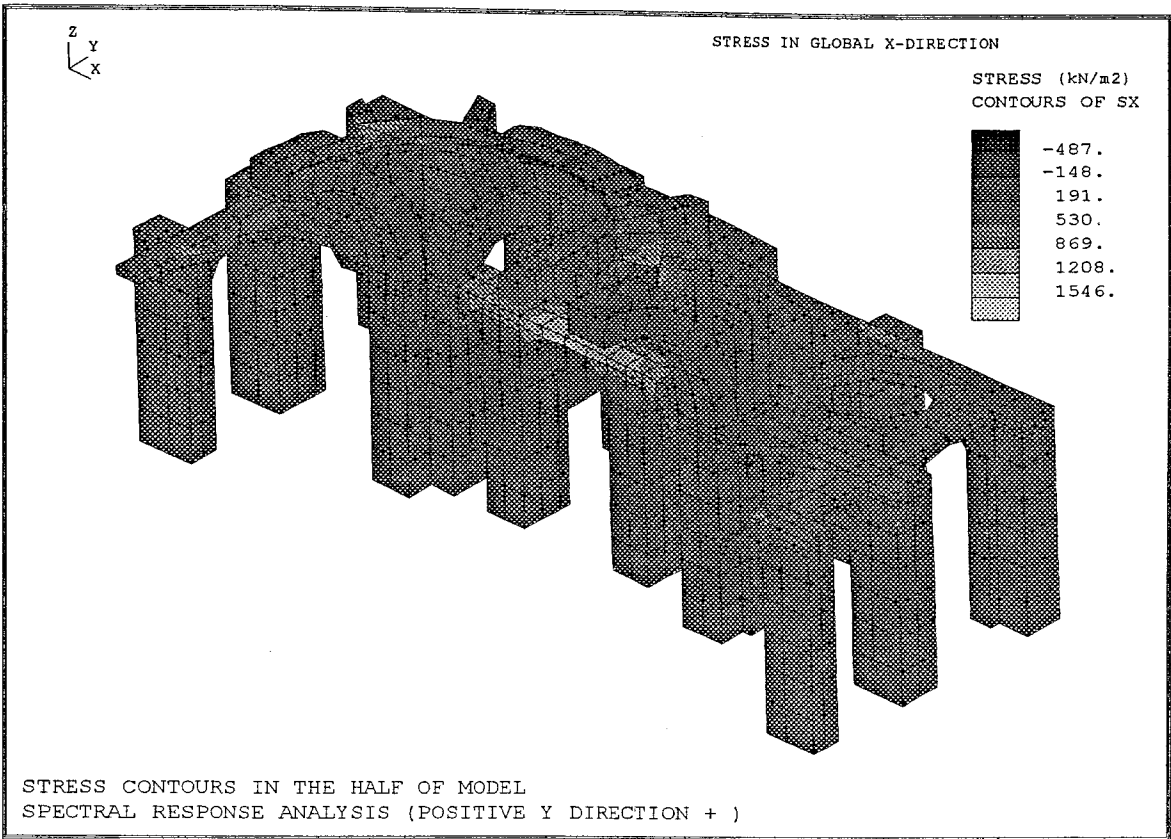


FIGURE 4.9 Stress Contours in the Half of Model Spectral Response Analysis (Positive Y Direction+)

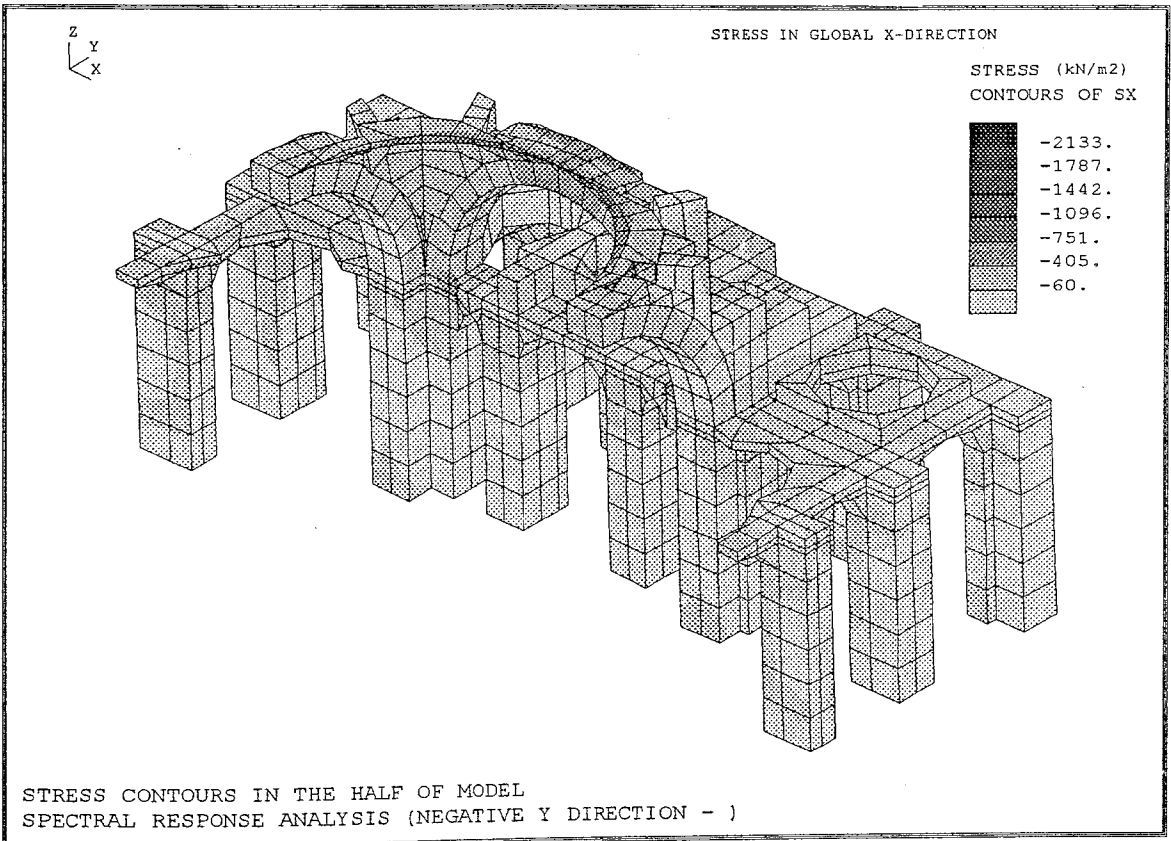


FIGURE 4.10 Stress Contours in the Half of Model Spectral Response Analysis (Negative Y Direction-)

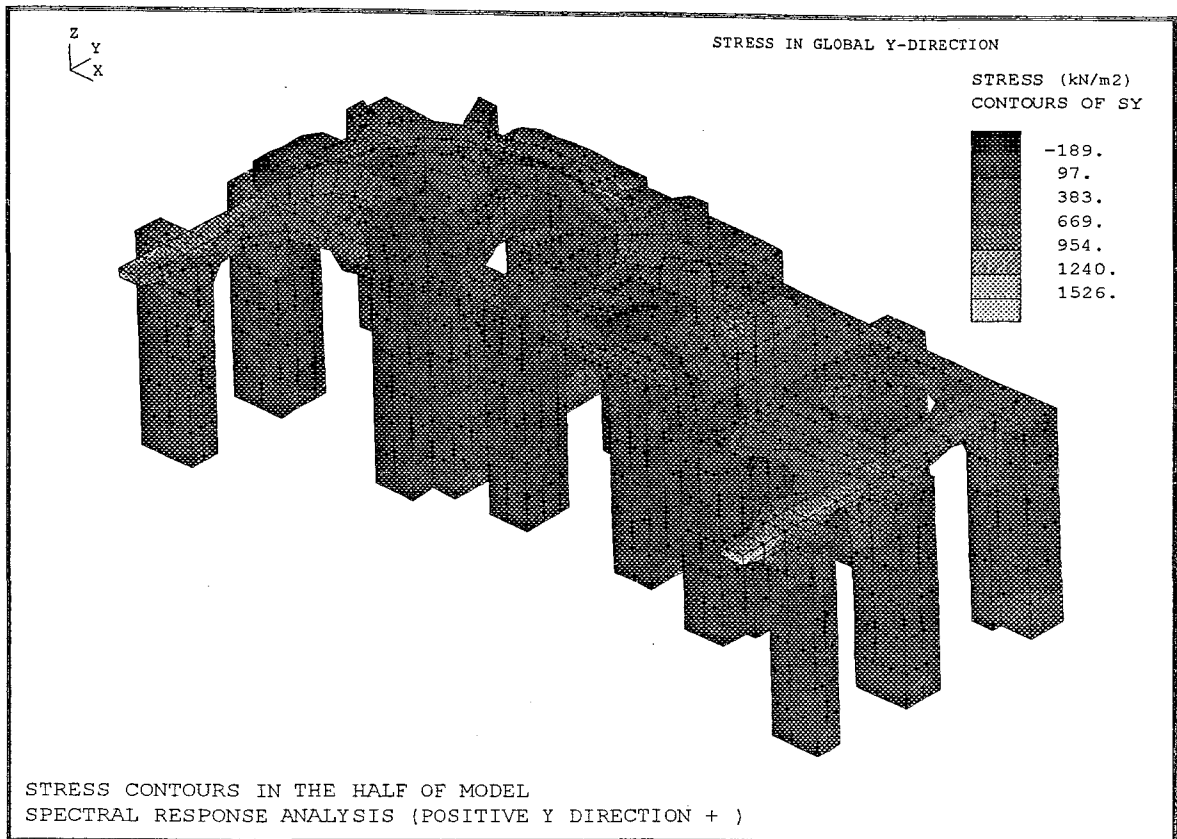


FIGURE 4.11 Stress Contours in the Half of Model
Spectral Response Analysis (Positive Y Direction+)

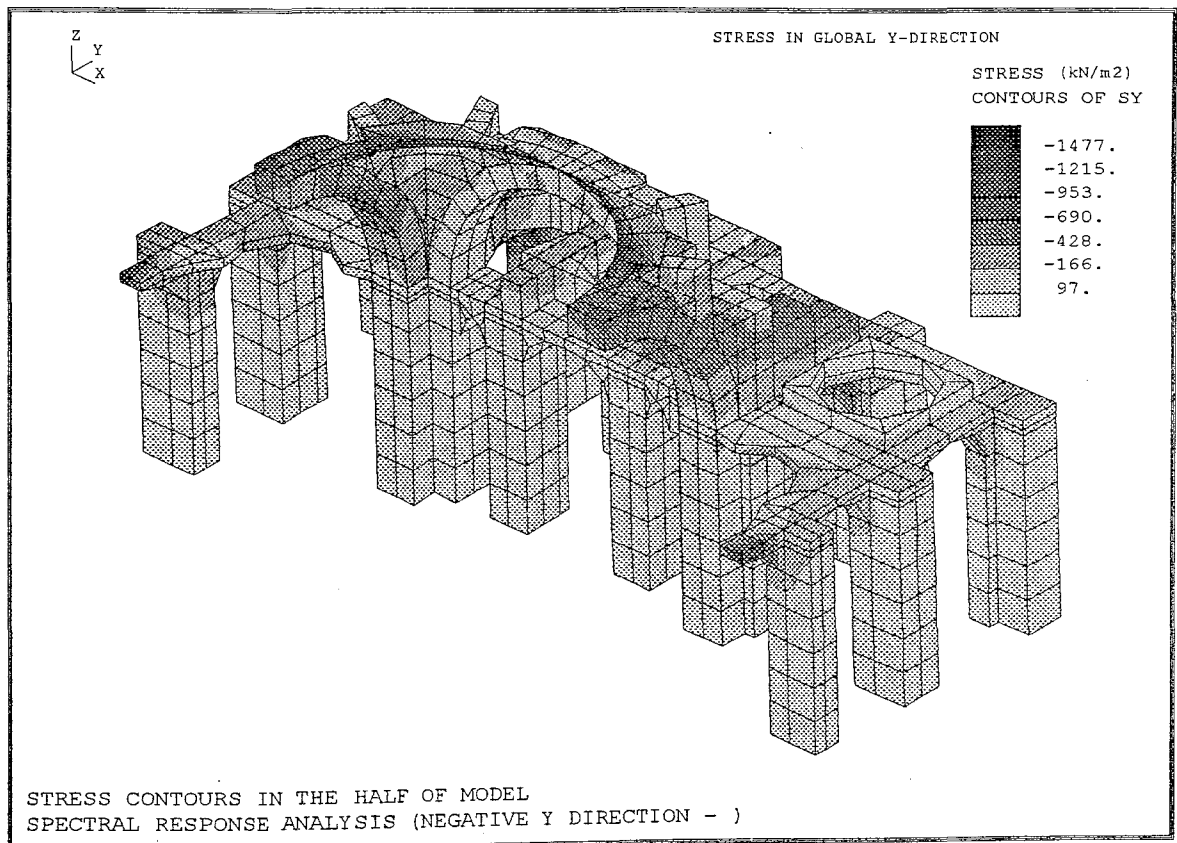


FIGURE 4.12 Stress Contours in the Half of Model
Spectral Response Analysis (Negative Y Direction-)

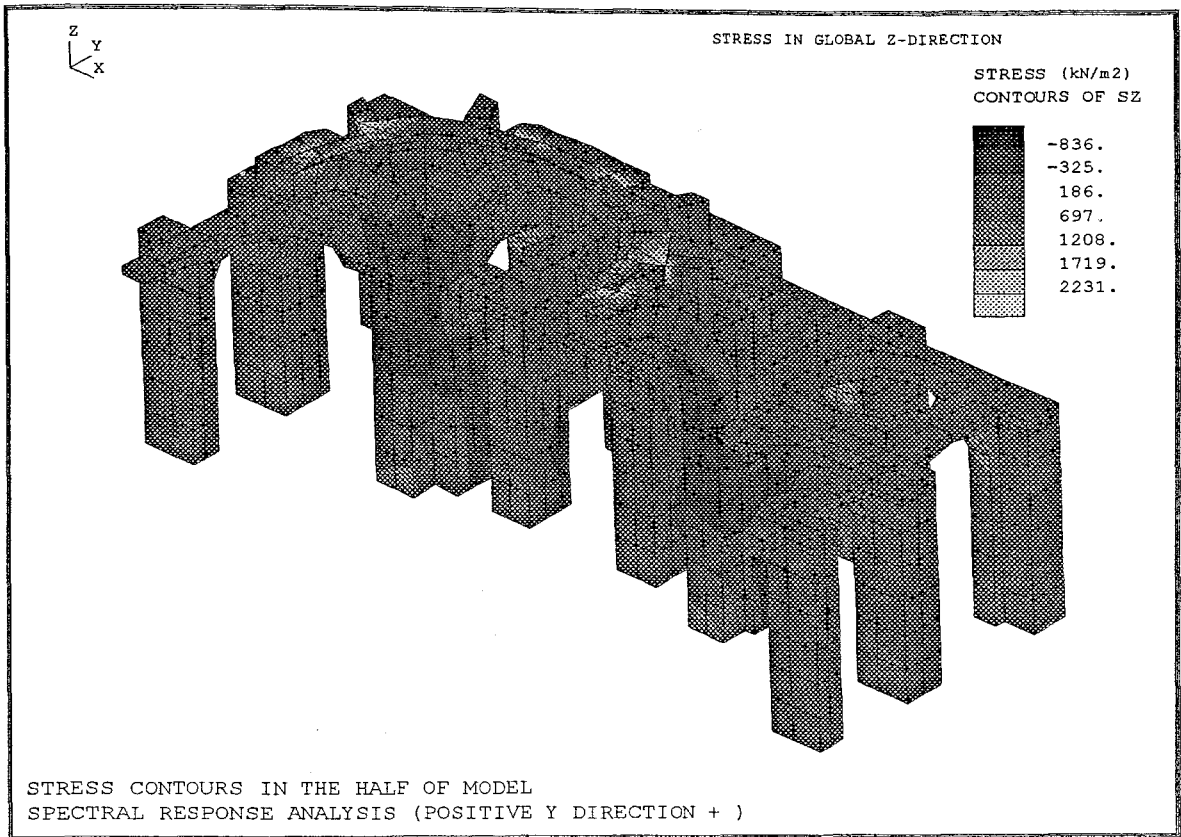


FIGURE 4.13 Stress Contours in the Half of Model Spectral Response Analysis (Positive Y Direction+)

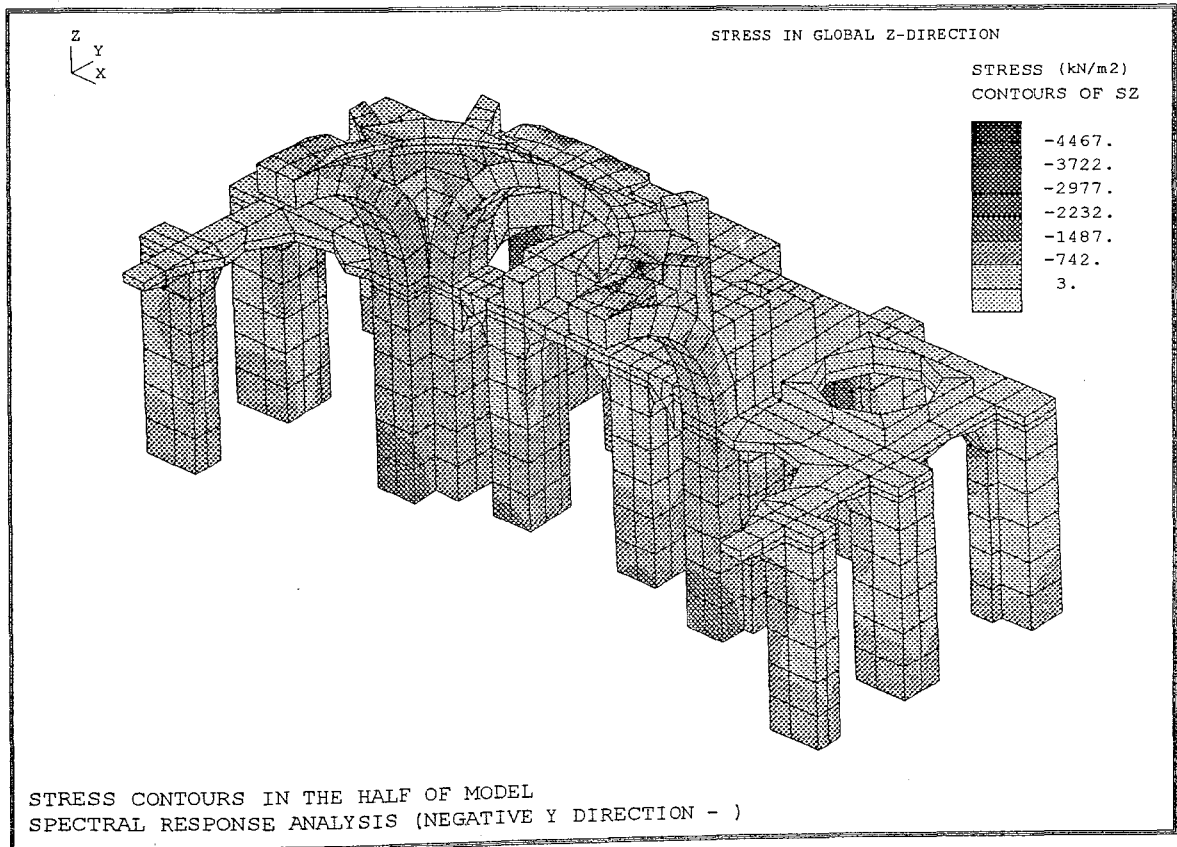


FIGURE 4.14 Stress Contours in the Half of Model Spectral Response Analysis (Negative Y Direction-)

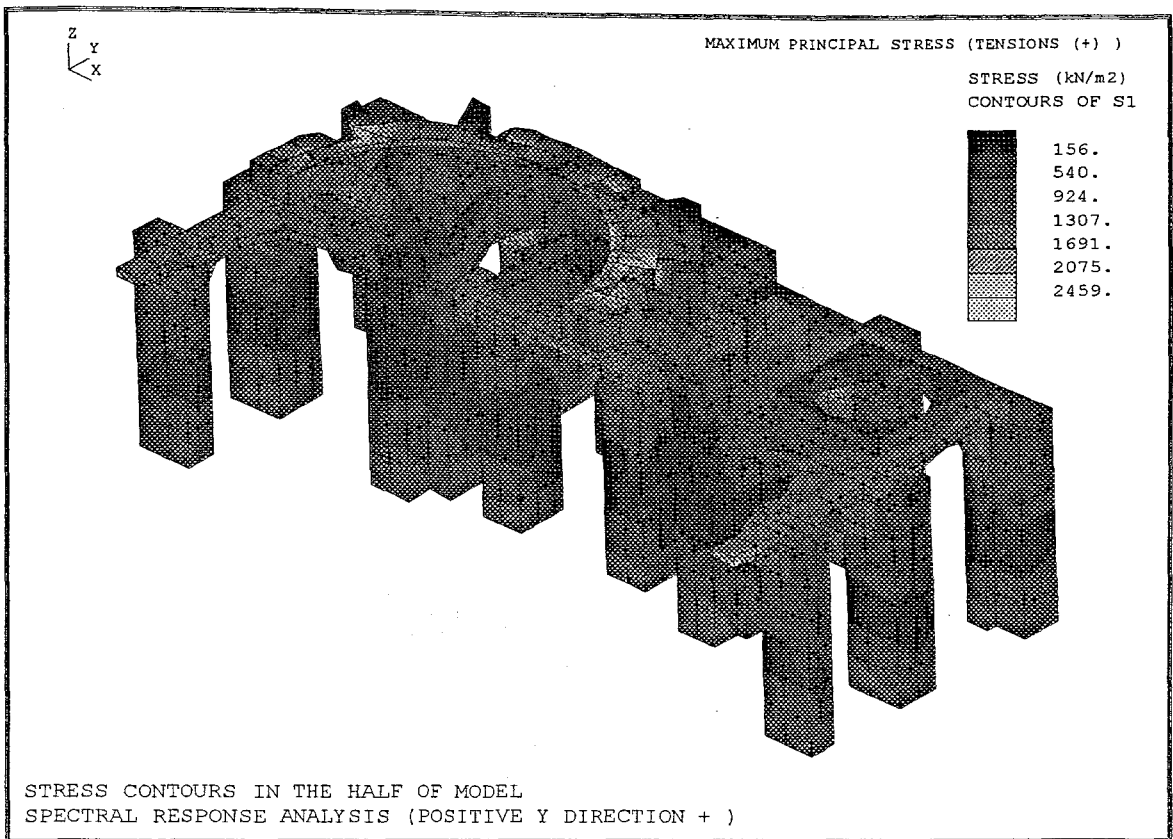


FIGURE 4.15 Stress Contours in the Half of Model Spectral Response Analysis (Positive Y Direction+).Maximum Principal Stress (Tensions+)

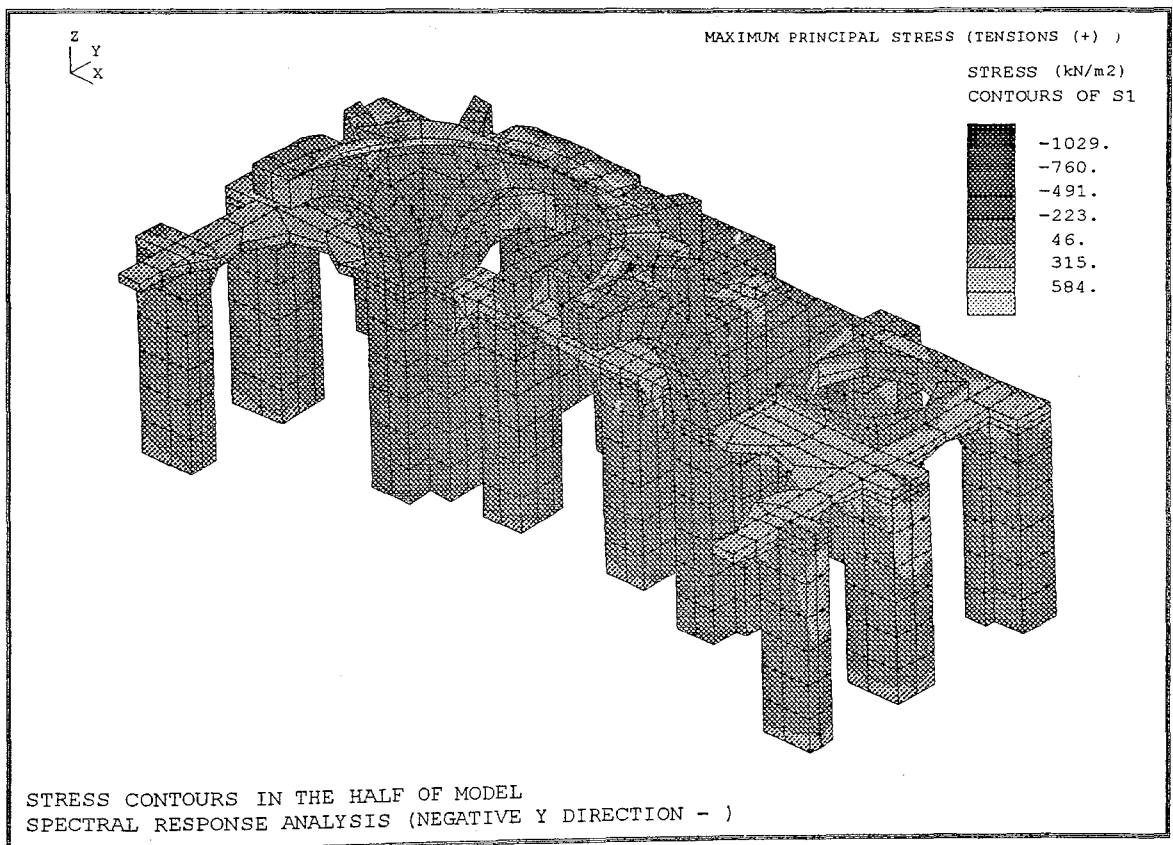


FIGURE 4.16 Stress Contours in the Half of Model Spectral Response Analysis (Negative Y Direction-).Maximum Principal Stress (Tensions+)

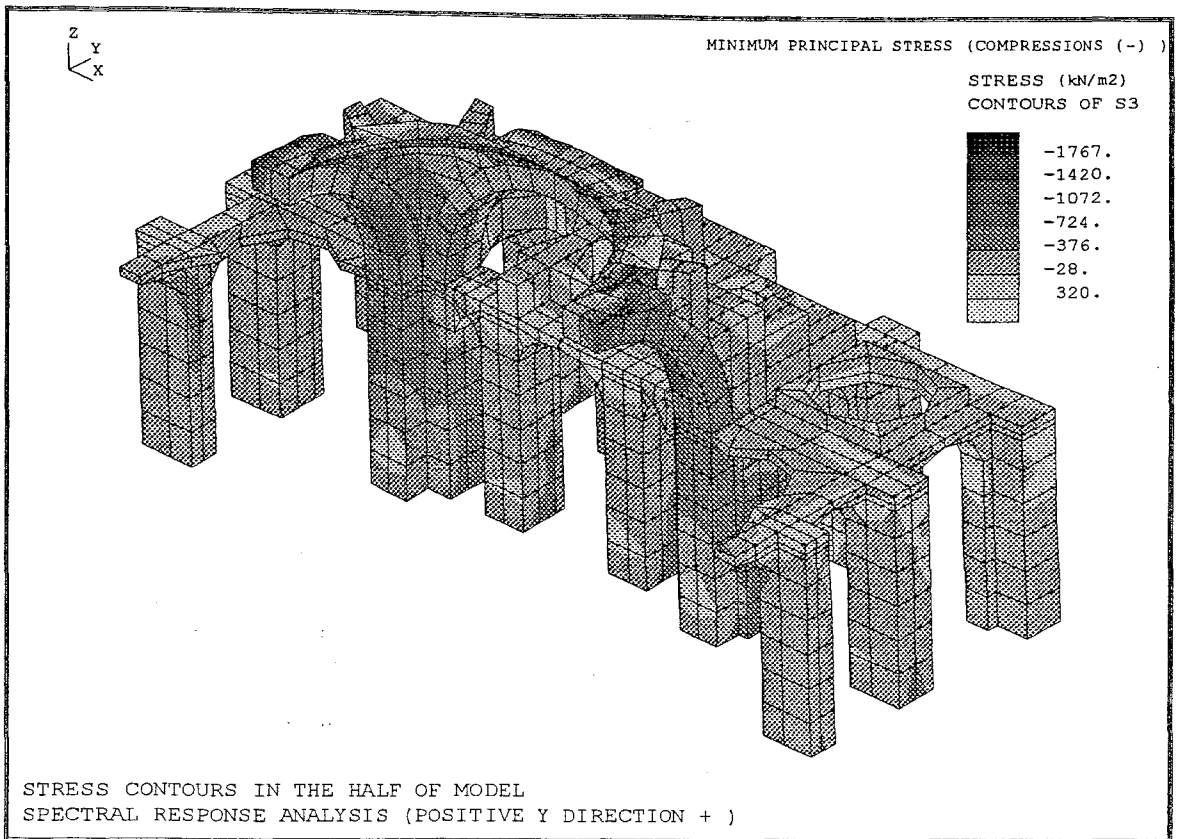


FIGURE 4.17 Stress Contours in the Half of Model.Spectral Response Analysis (Positive Y Direction+).Maximum Principal Stress Compression

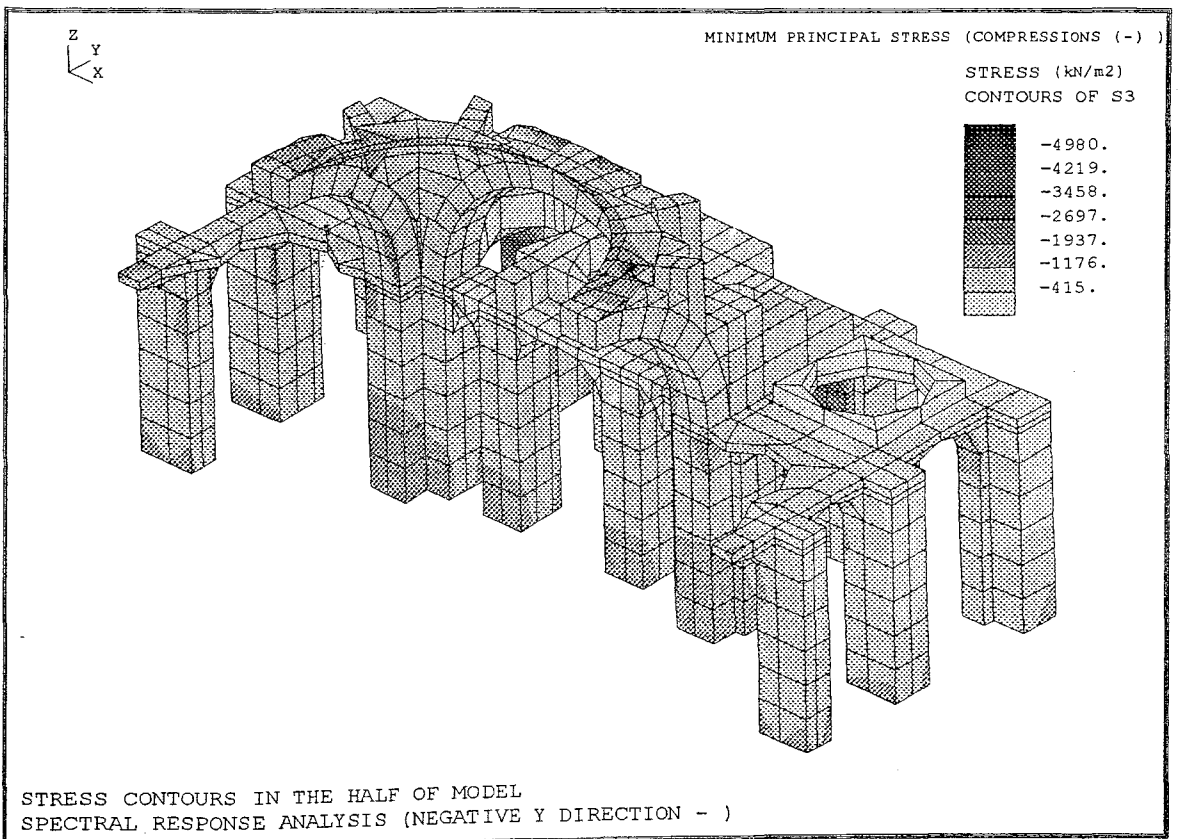


FIGURE 4.18 Stress Contours in the Half of Model.Spectral Response Analysis (Negative Y Direction-).Minimum Principal Stress Compression

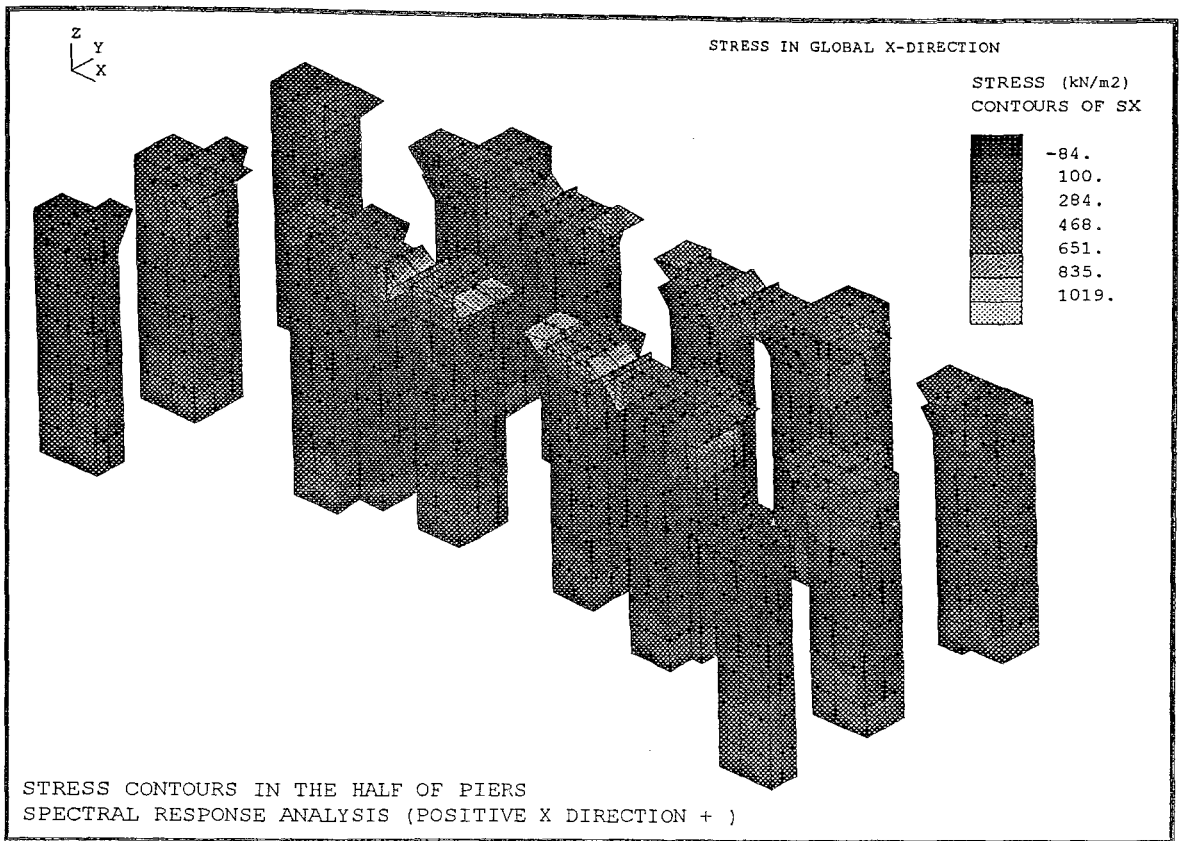


FIGURE 4.19 Stress Contours in the Half of Piers.Spectral Response Analysis (Positive X Direction+).Stress in Global X Direction

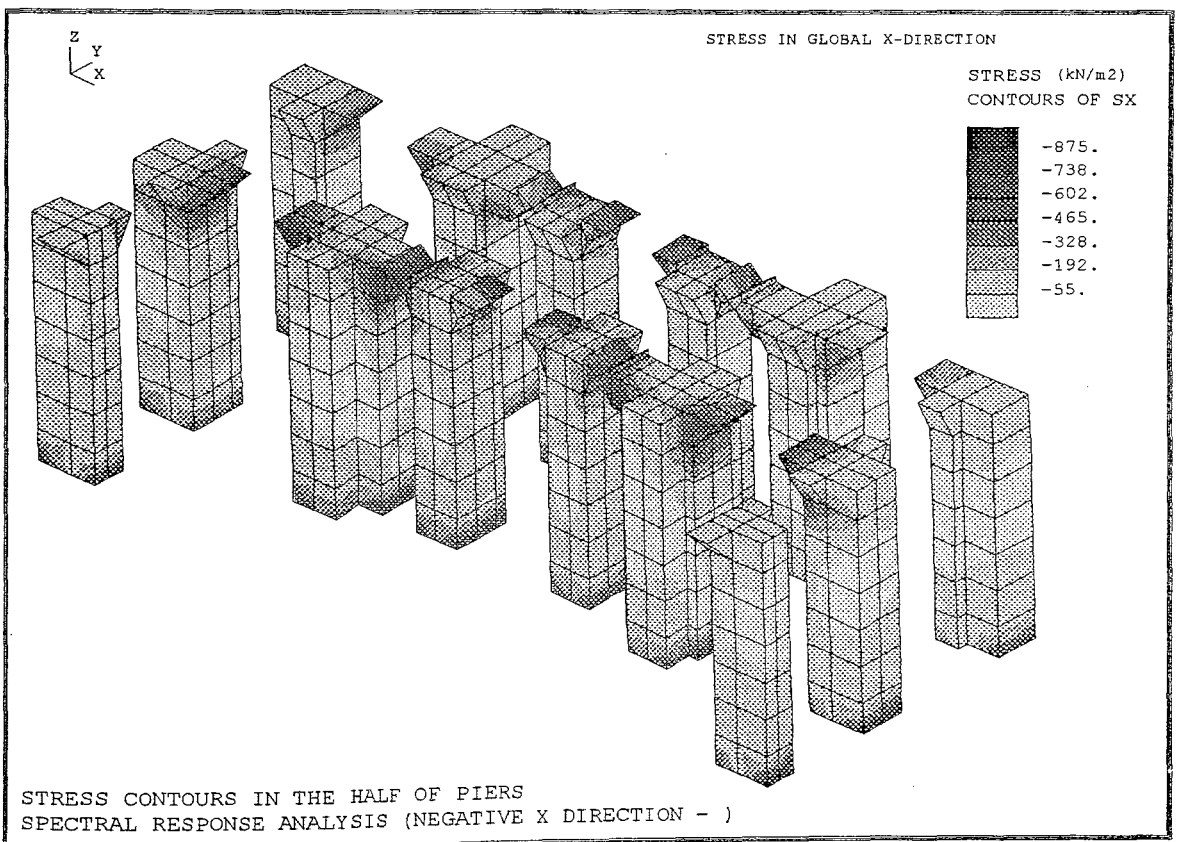


FIGURE 4.20 Stress Contours in the Half of Piers.Spectral Response Analysis (Negative X Direction-).Stress in Global X Direction

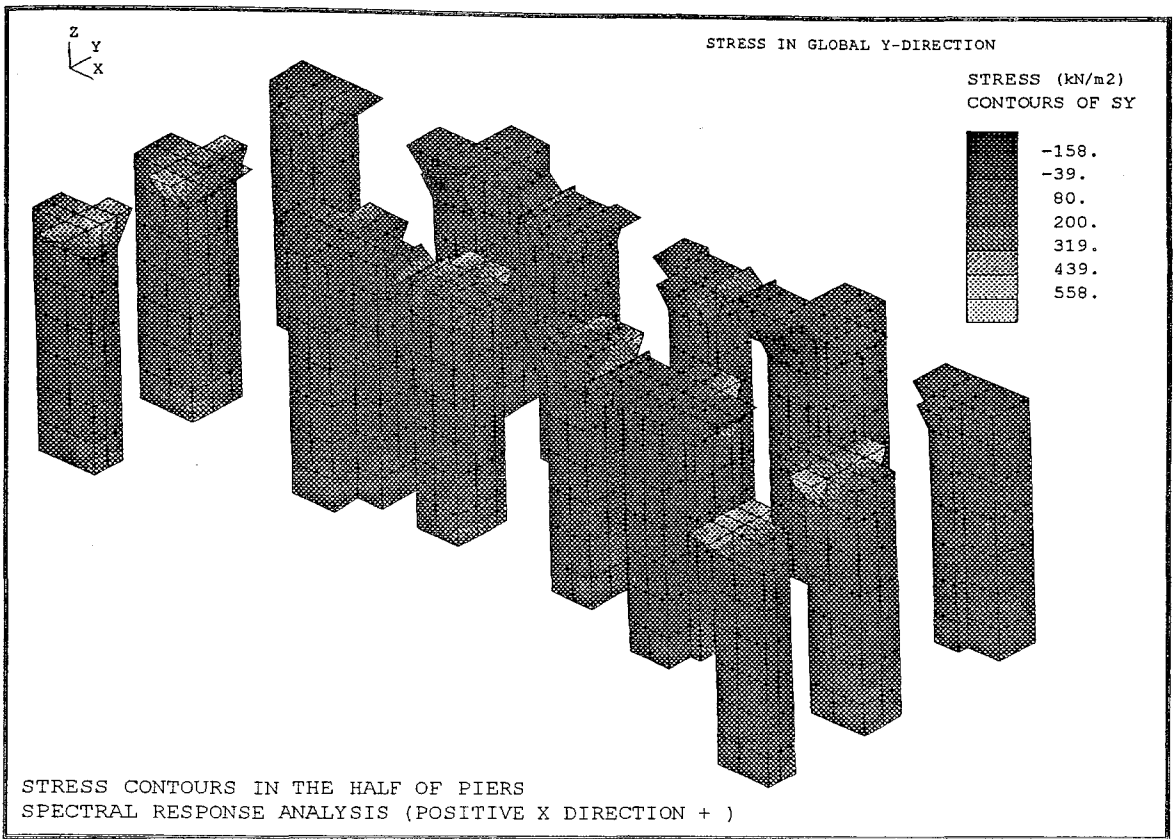


FIGURE 4.21 Stress Contours in the Half of Piers.Spectral Response Analysis (Positive X Direction+).Stress in Global Y Direction

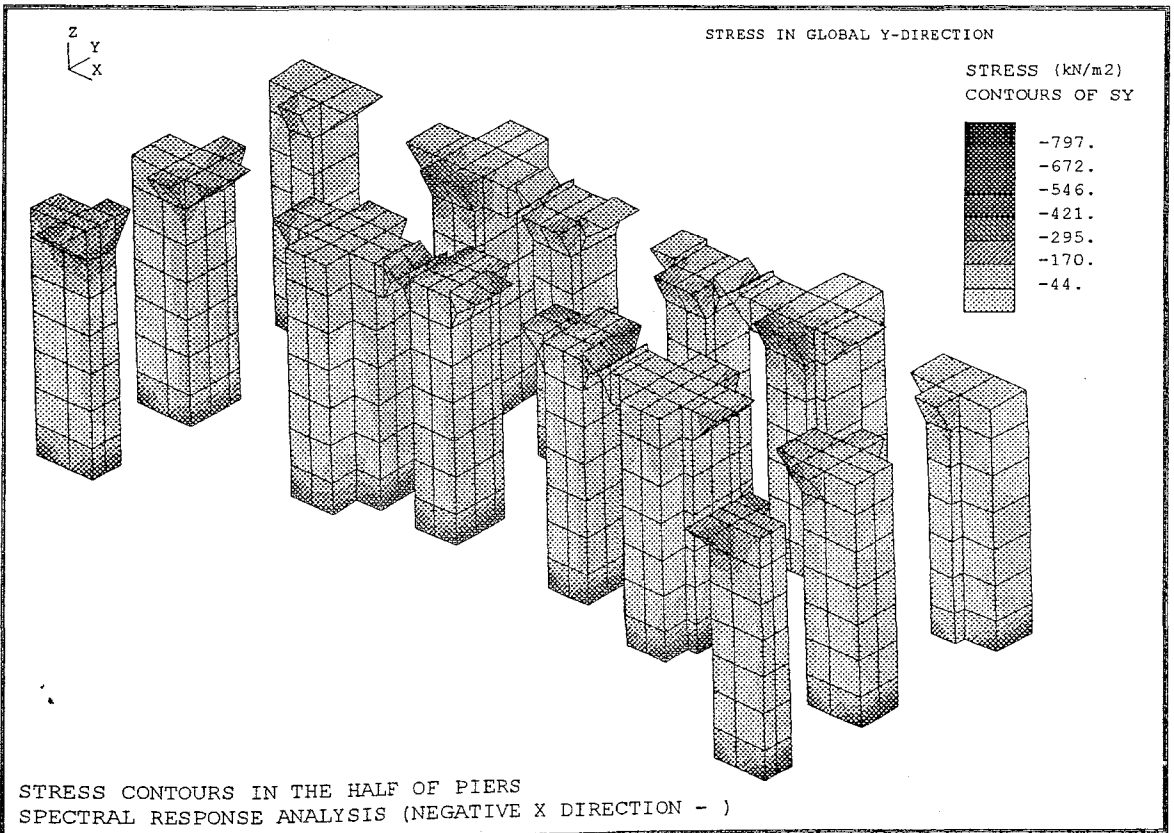


FIGURE 4.22 Stress Contours in the Half of Piers.Spectral Response Analysis (Negative X Direction-).Stress in Global Y Direction

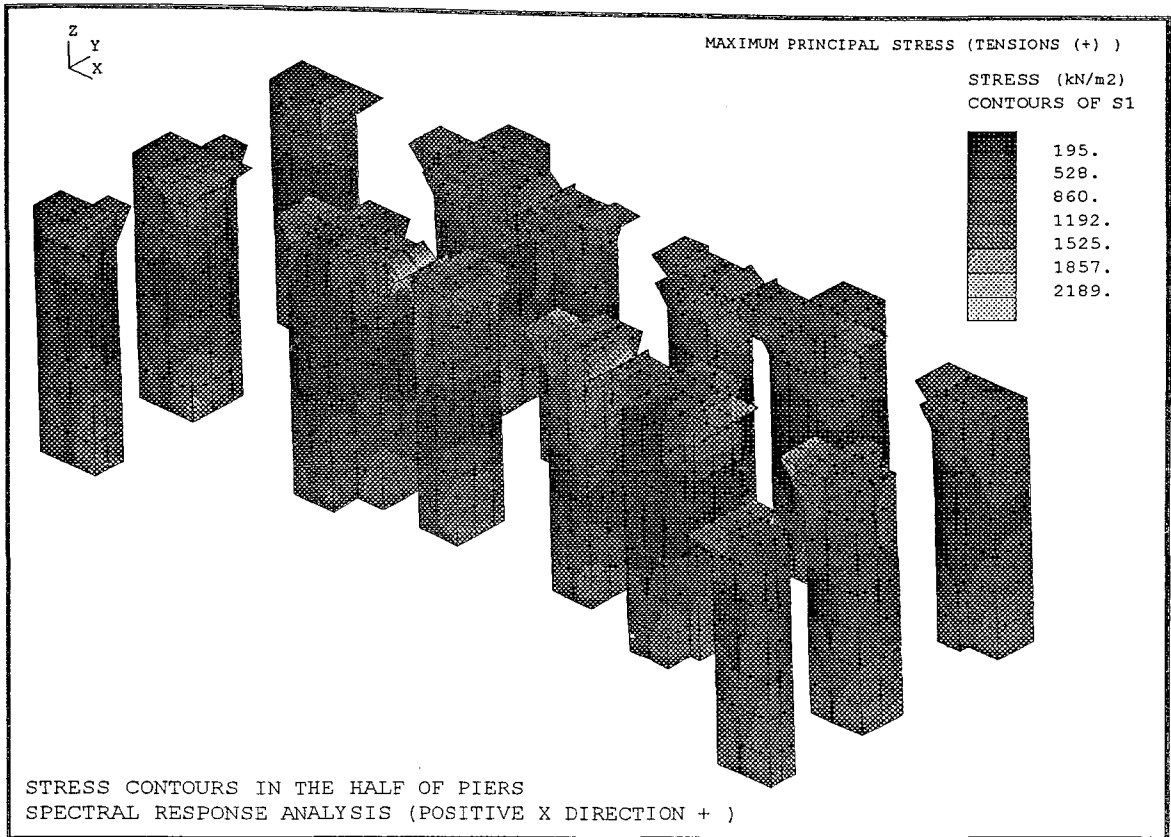


FIGURE 4.23 Stress Contours in the Half of Piers.Spectral Response Analysis (Positive X Direction+).Maximum Principal Stress in (Tensions+)

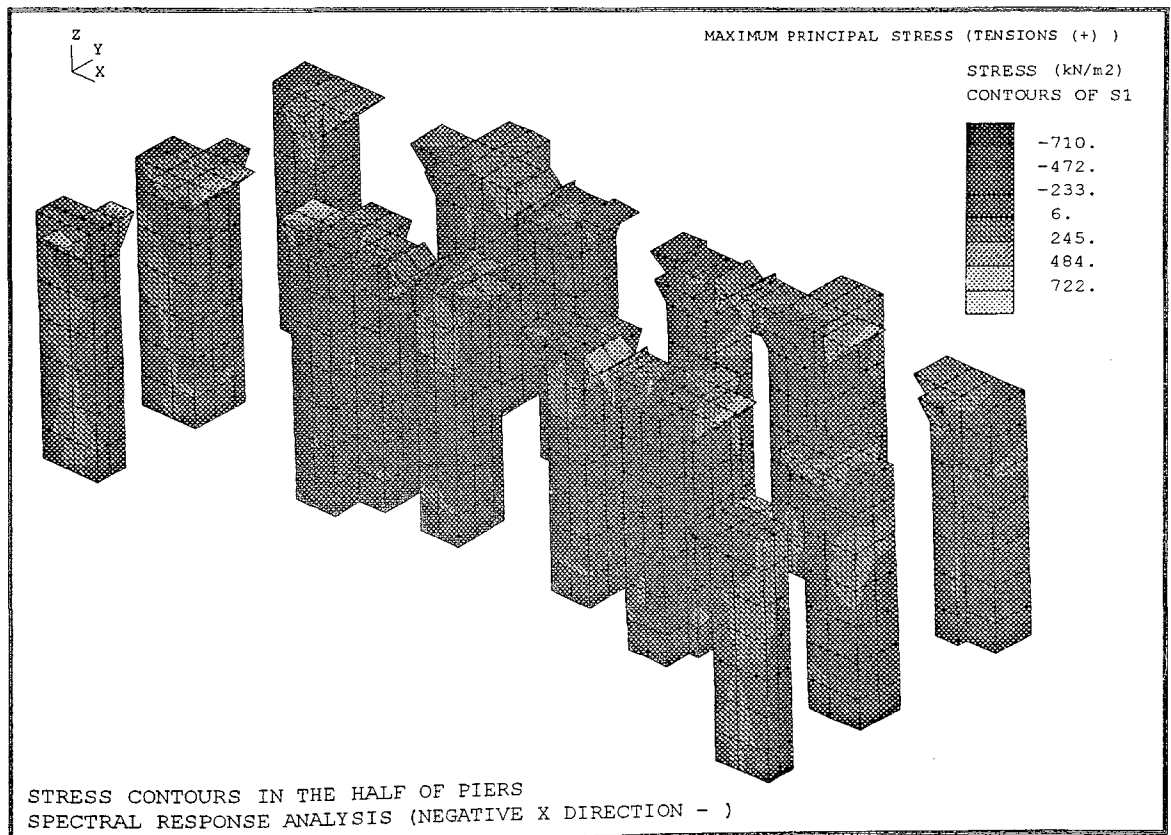


FIGURE 4.24 Stress Contours in the Half of Piers.Spectral Response Analysis (Negative X Direction-).Maximum Principal Stress in (Tensions+)

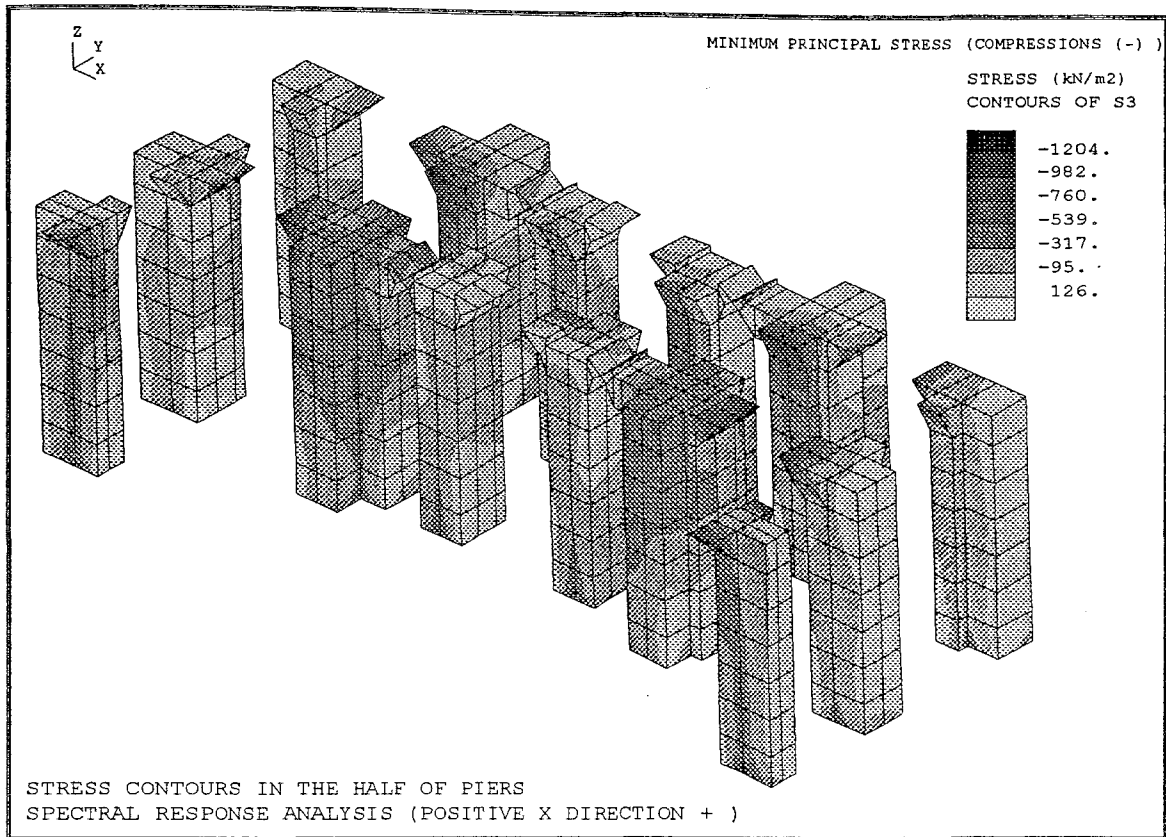


FIGURE 4.25 Stress Contours in the Half of Piers.Spectral Response Analysis (Positive X Direction+).Minimum Principal Stress (Compressions+)

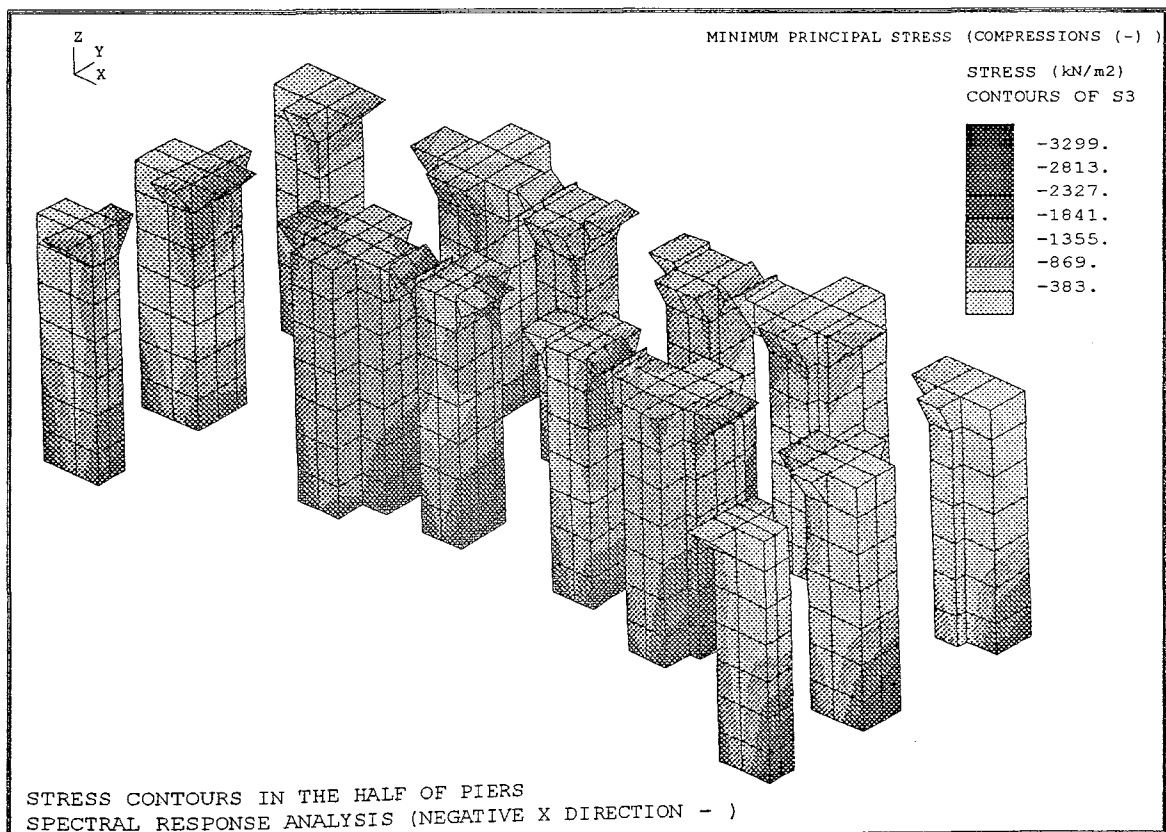


FIGURE 4.26 Stress Contours in the Half of Piers.Spectral Response Analysis (Negative X Direction-).Minimum Principal Stress (Compressions-)

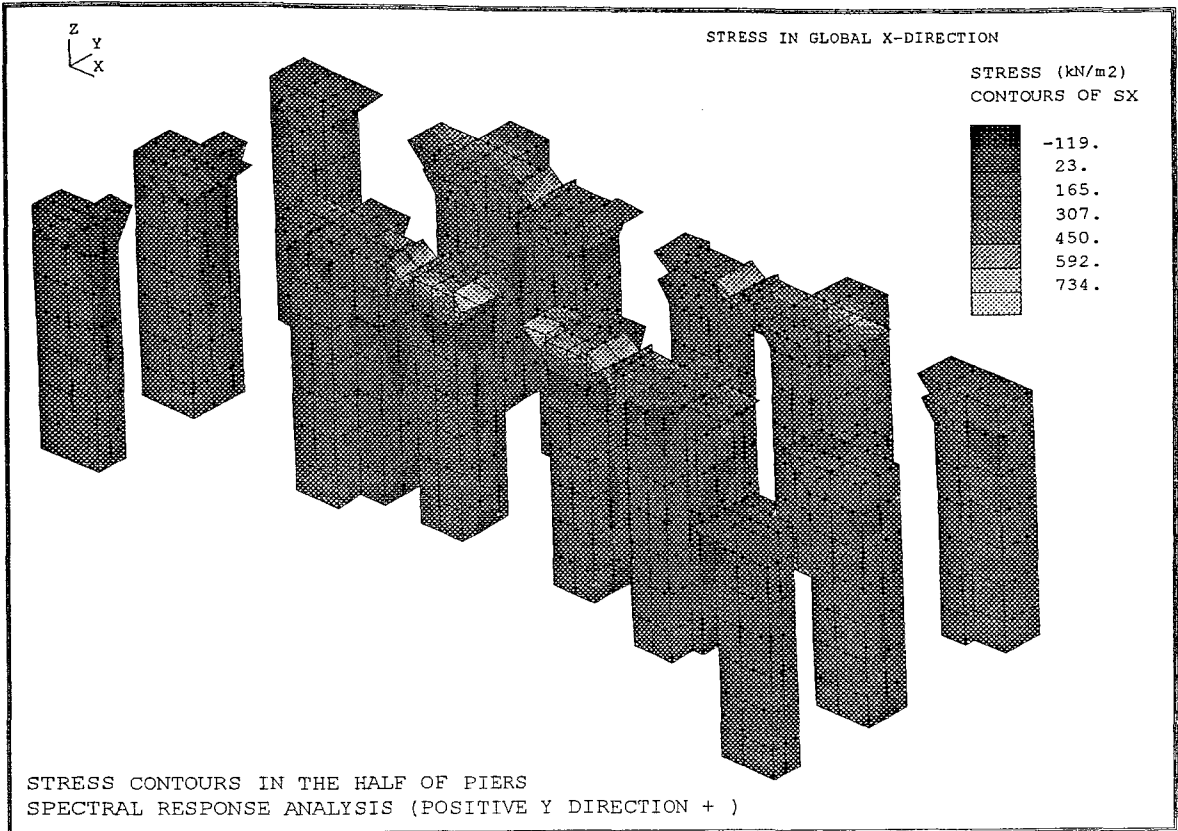


FIGURE 4.27 Stress Contours in the Half of Piers.Spectral Response Analysis (Positive Y Direction+).Stress in Global X Direction

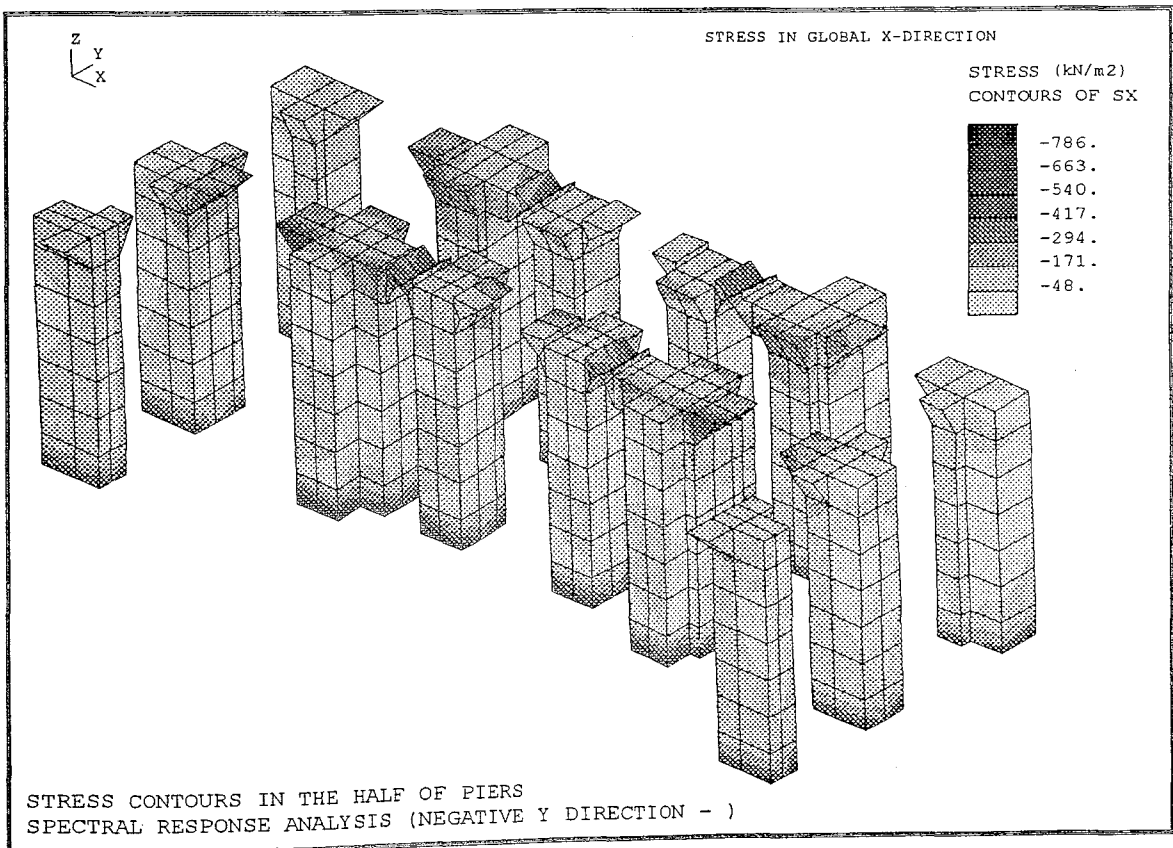


FIGURE 4.28 Stress Contours in the Half of Piers.Spectral Response Analysis (Negative Y Direction-).Stress in Global X Direction

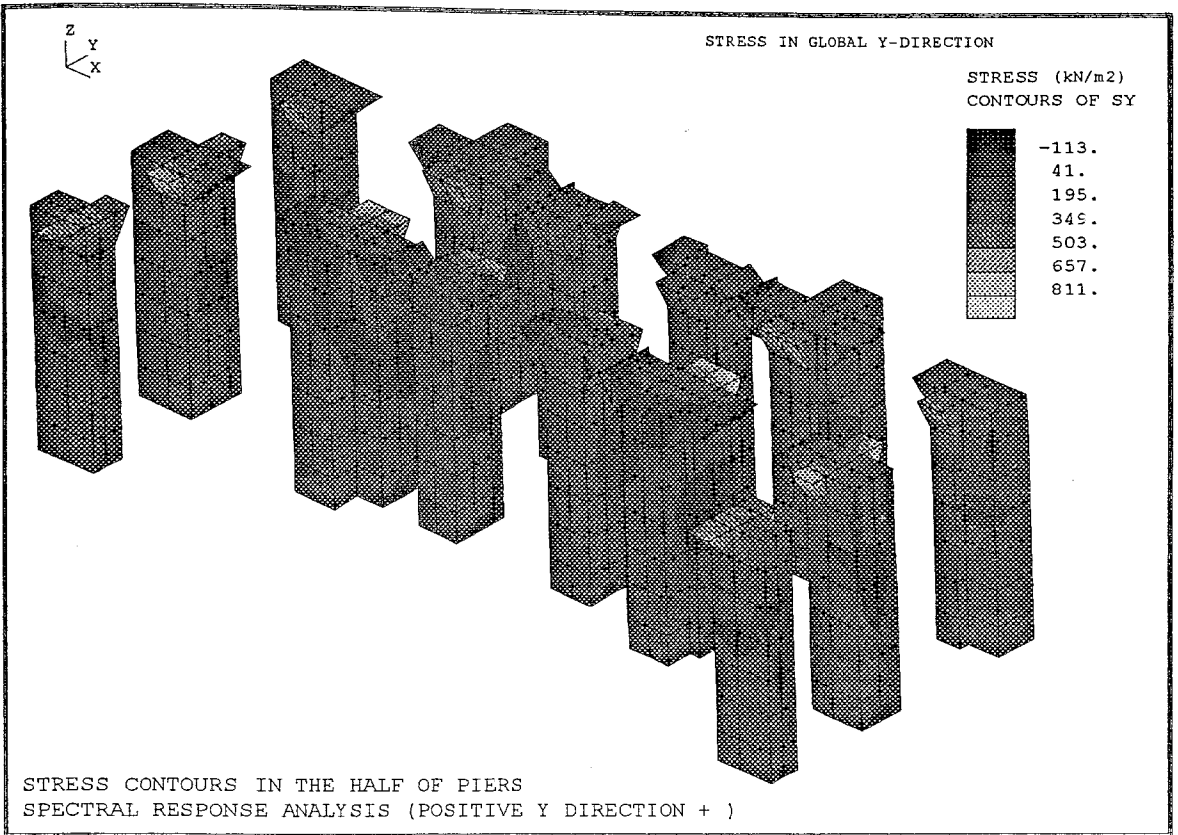


FIGURE 4.29 Stress Contours in the Half of Piers.Spectral Response Analysis (Positive Y Direction+).Stress in Global Y Direction

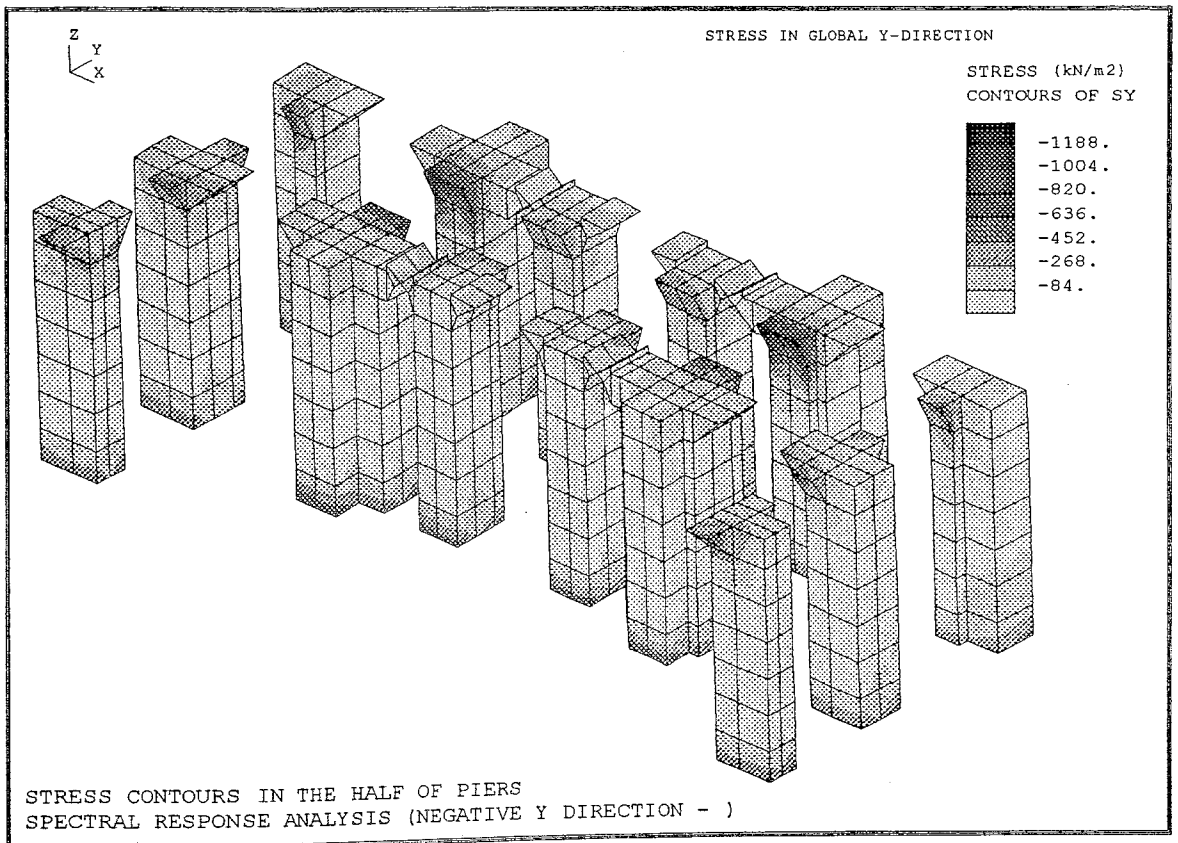


FIGURE 4.30 Stress Contours in the Half of Piers.Spectral Response Analysis (Negative Y Direction-).Stress in Global Y Direction

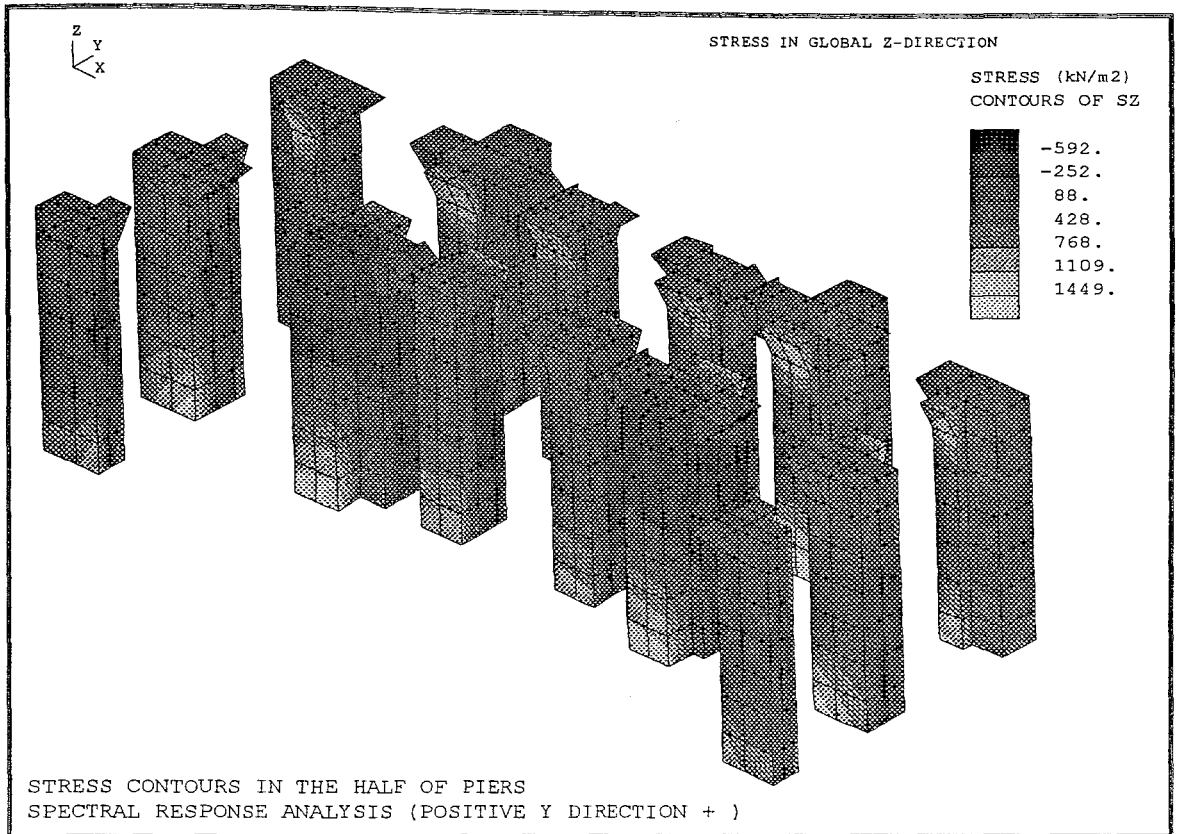


FIGURE 4.31 Stress Contours in the Half of Piers.Spectral Response Analysis (Positive Y Direction+).Stress in Global Z Direction

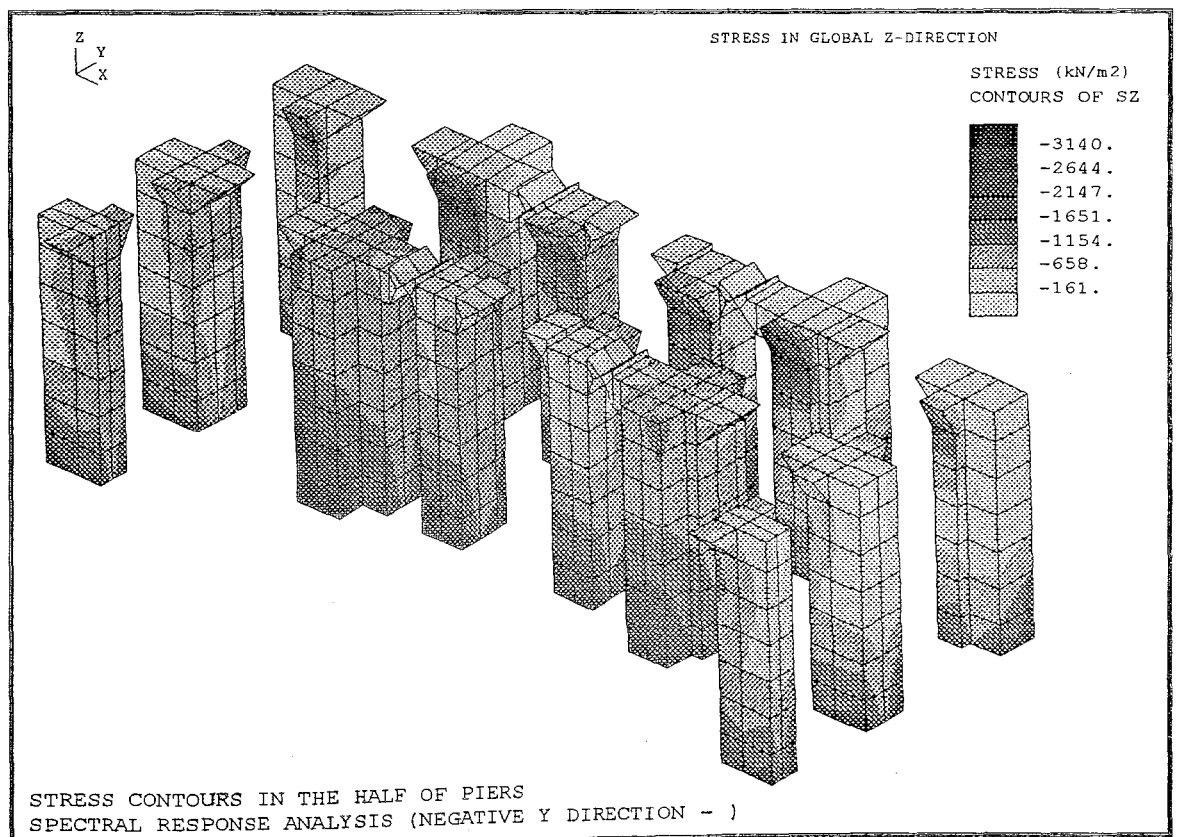


FIGURE 4.32 Stress Contours in the Half of Piers.Spectral Response Analysis (Negative Y Direction-).Stress in Global Z Direction

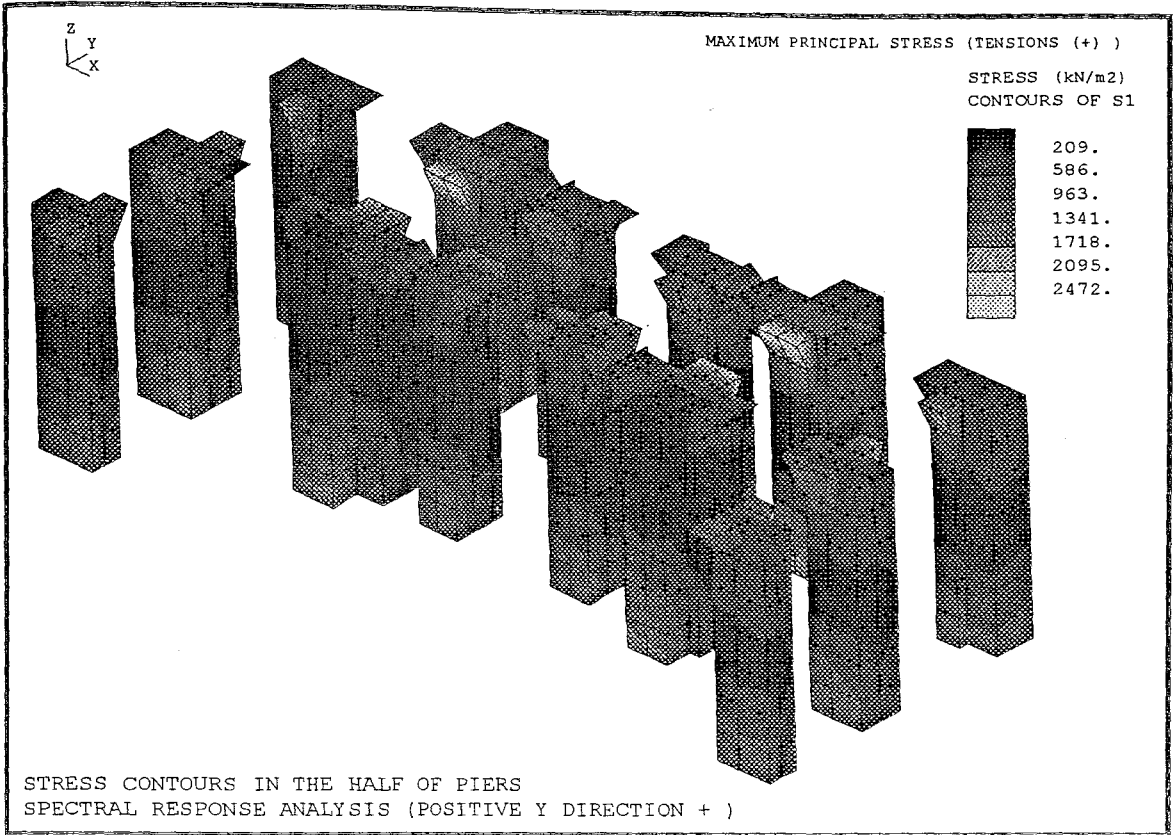


FIGURE 4.33 Stress Contours in the Half of Piers.Spectral Response Analysis (Positive Y Direction+). Maximum Principal Stress (Tensions+)

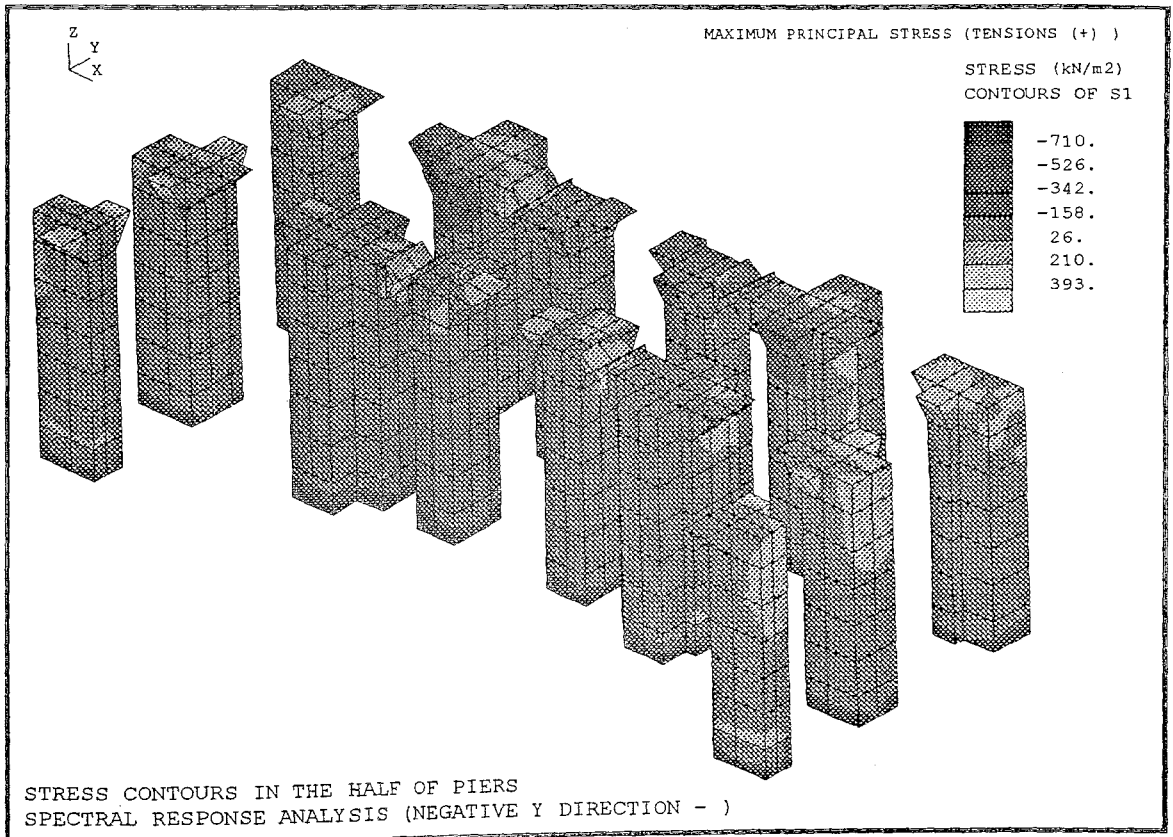


FIGURE 4.34 Stress Contours in the Half of Piers.Spectral Response Analysis (Negative Y Direction-).Maximum Principal Stress (Tensions+)

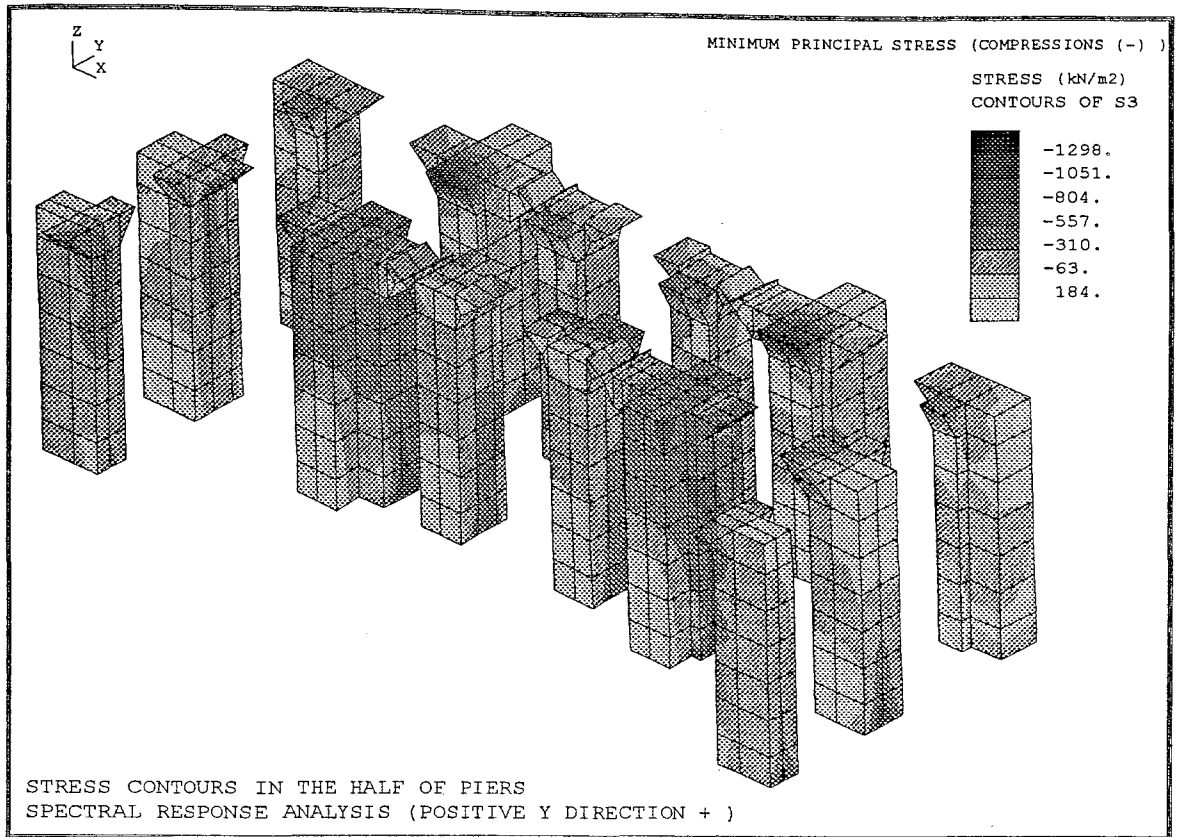


FIGURE 4.35 Stress Contours in the Half of Piers.Spectral Response Analysis (Positive Y Direction+).Minimum Principal Stress (Compressions-)

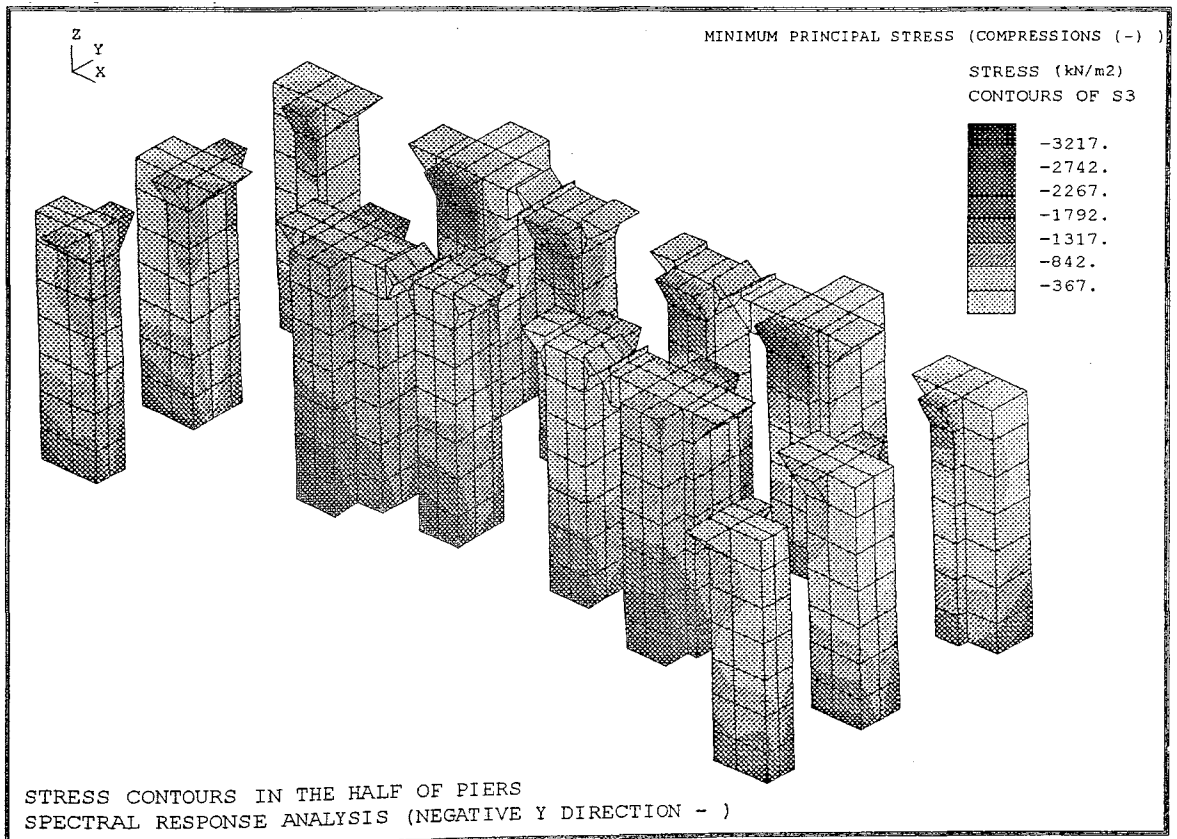


FIGURE 4.36 Stress Contours in the Half of Piers.Spectral Response Analysis (Negative Y Direction-).Minimum Principal Stress (Compressions-)

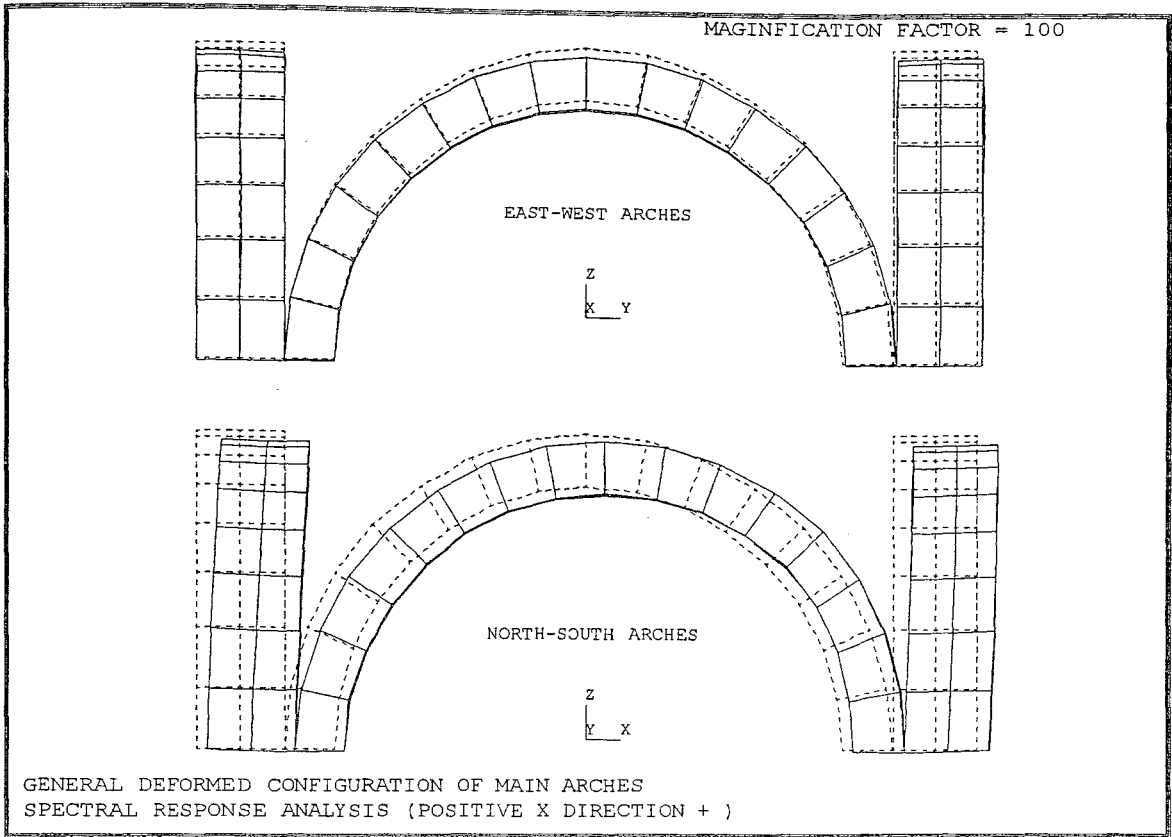


FIGURE 4.37 Stress Contours in the Half of Piers.Spectral Response Analysis (Positive X Direction+).

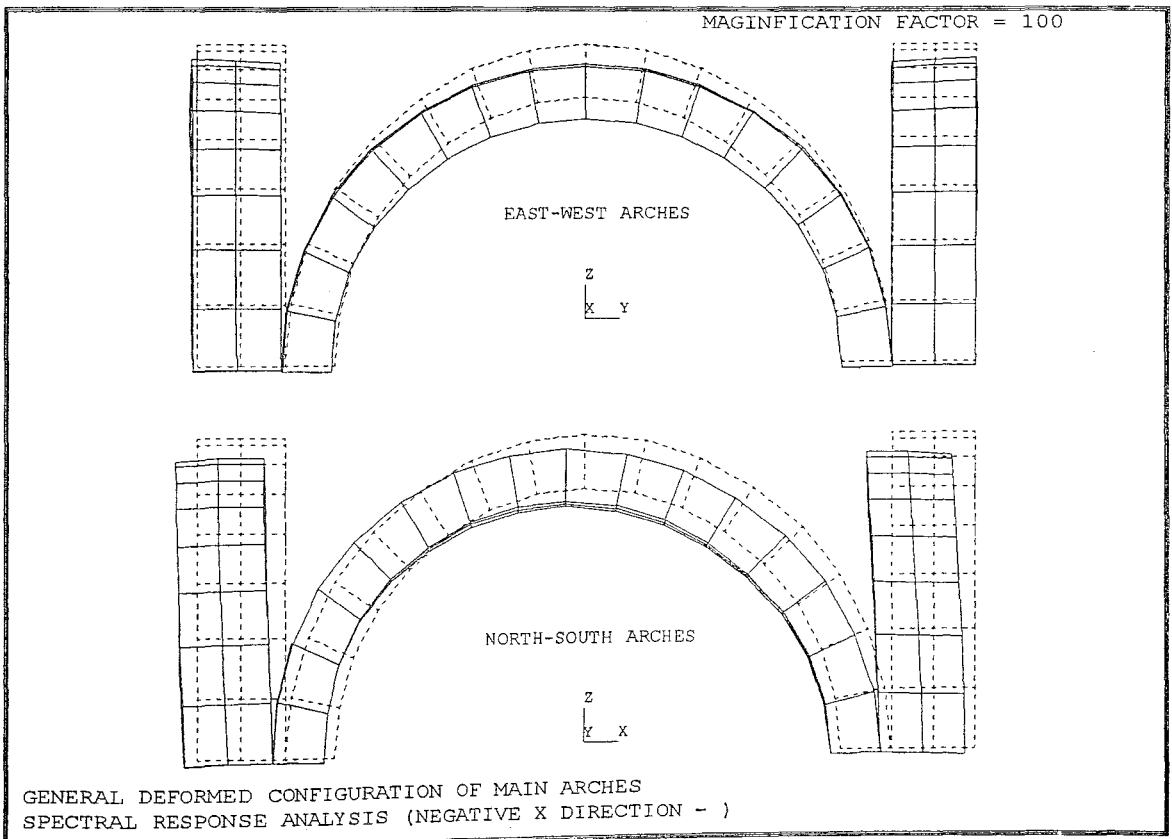


FIGURE 4.38 General Deformed Configuration of main Arches.Spectral Response Analysis (Negative X Direction-)

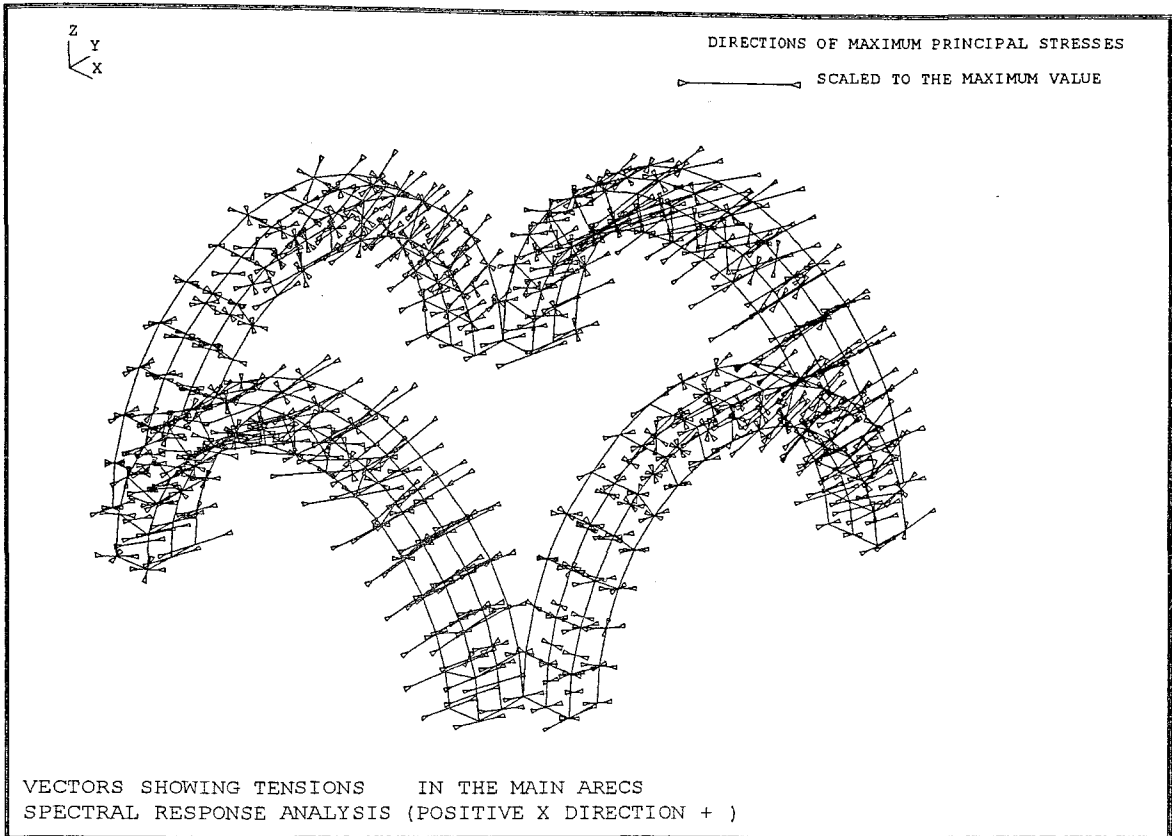


FIGURE 4.39 General Deformed Configuration of main Arches. Spectral Response Analysis (Positive X Direction+)

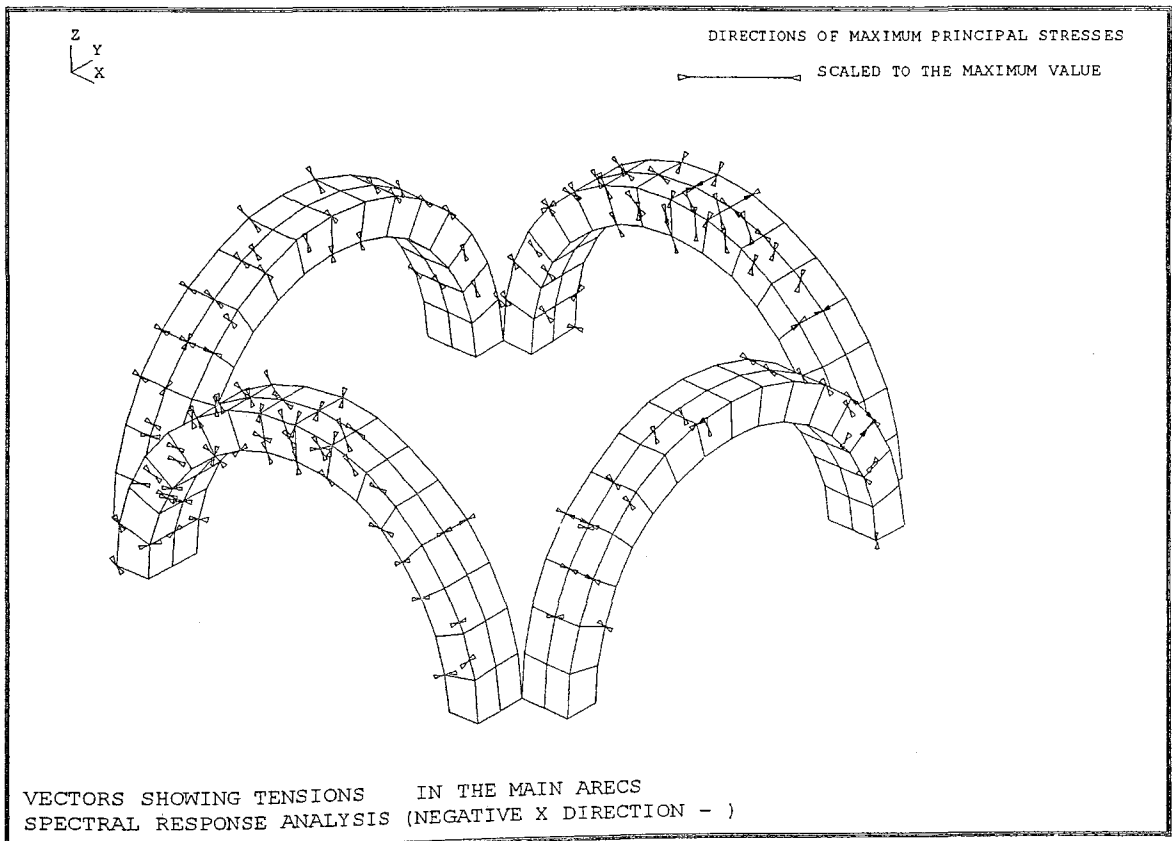


FIGURE 4.40 General Deformed Configuration of main Arches. Spectral Response Analysis (Negative X Direction-)

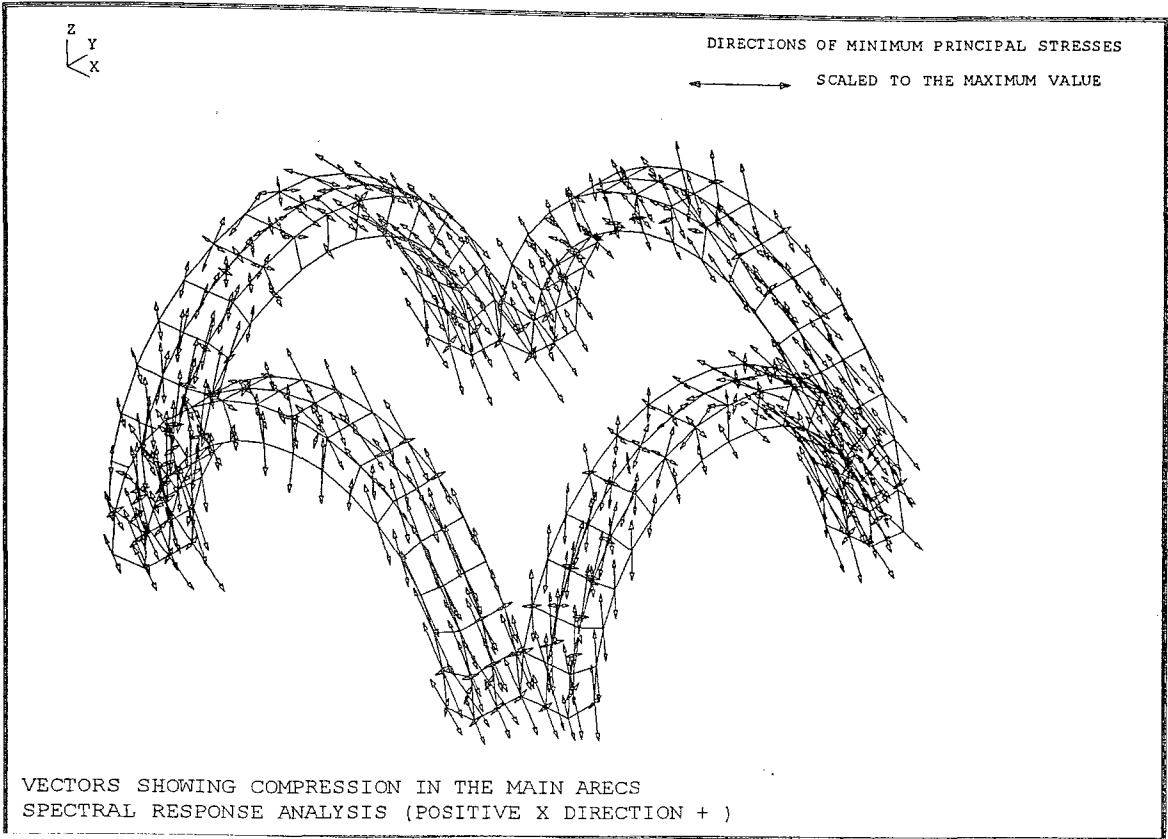


FIGURE 4.41 Vectors Showing Compression in the Main Arches.Spectral Response Analysis (Positive X Direction+)Directions of minimum Principal Stresses

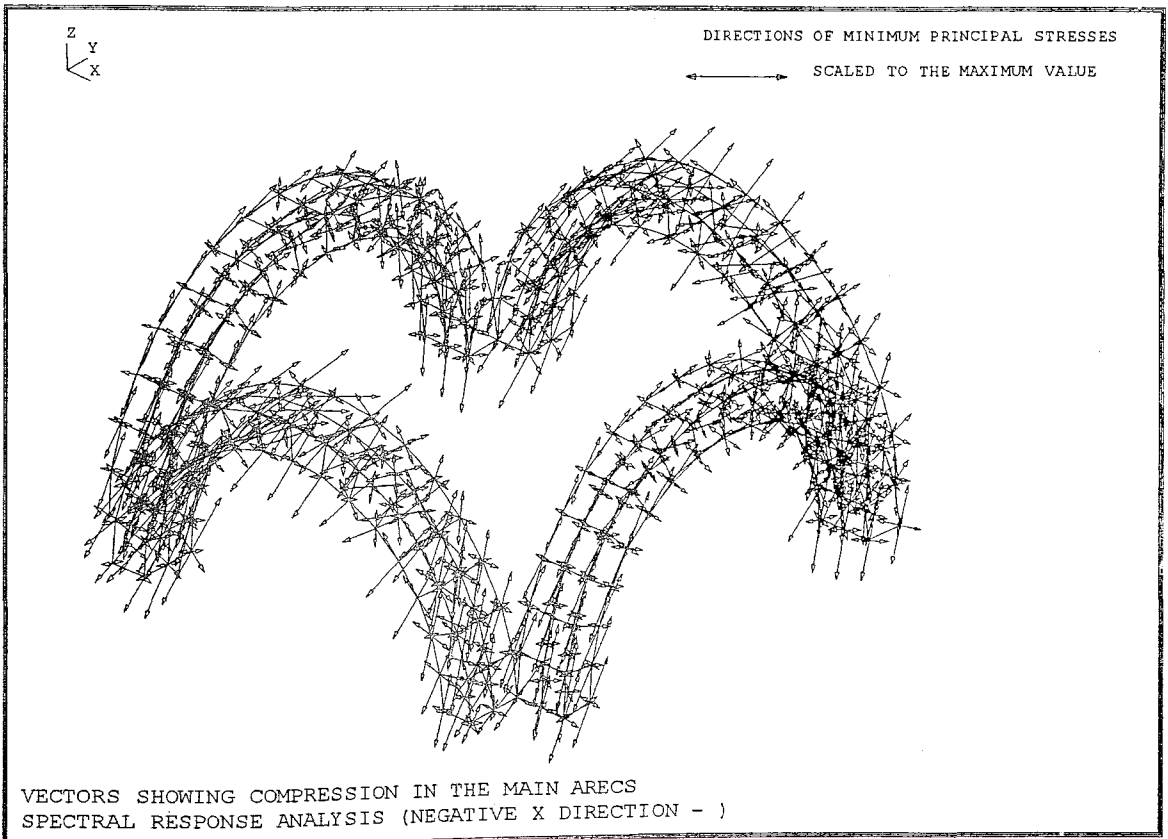


FIGURE 4.42 Vectors Showing Compression in the Main Arches.Spectral Response Analysis (Negative X Direction-)Directions of minimum Principal Stresses

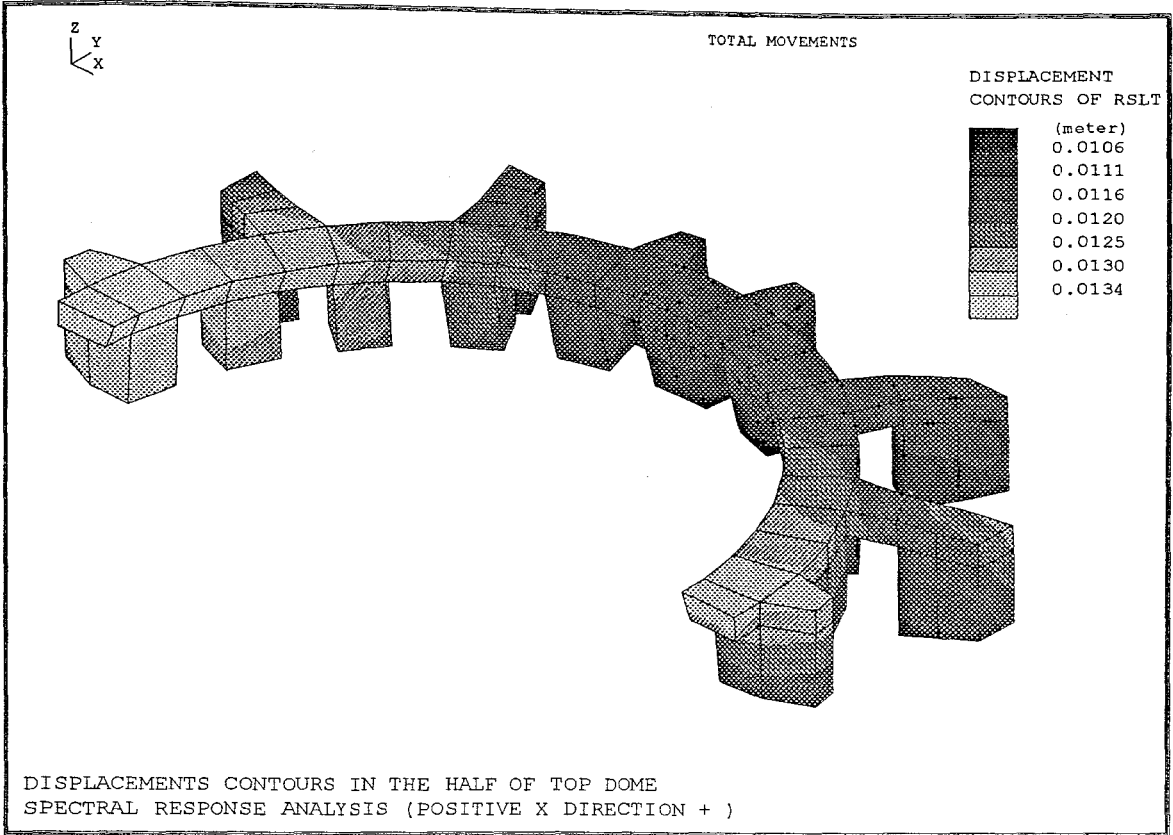


FIGURE 4.43 Displacement Contours in the Half of Top Model.Spectral Response Analysis (Positive X Direction+)Total Movements

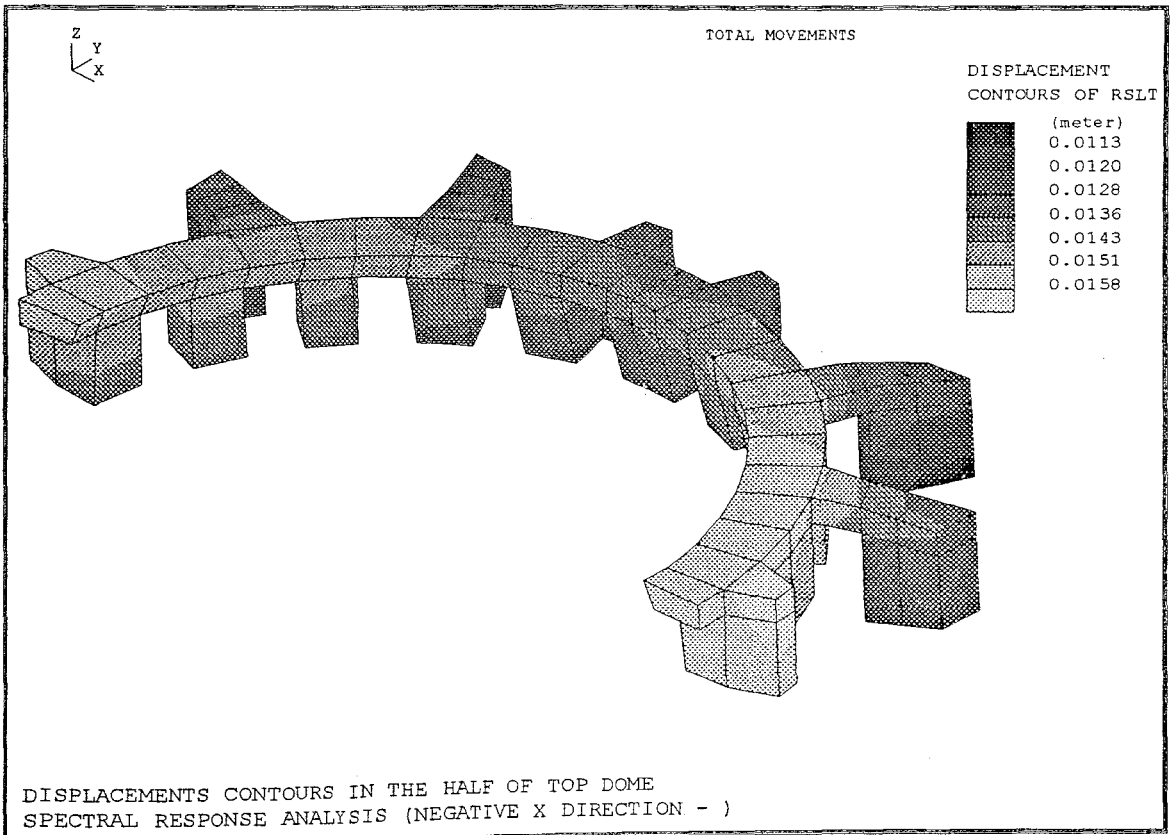


FIGURE 4.44 Displacement Contours in the Half of Top Model.Spectral Response Analysis (Negative X Direction-)Total Movements

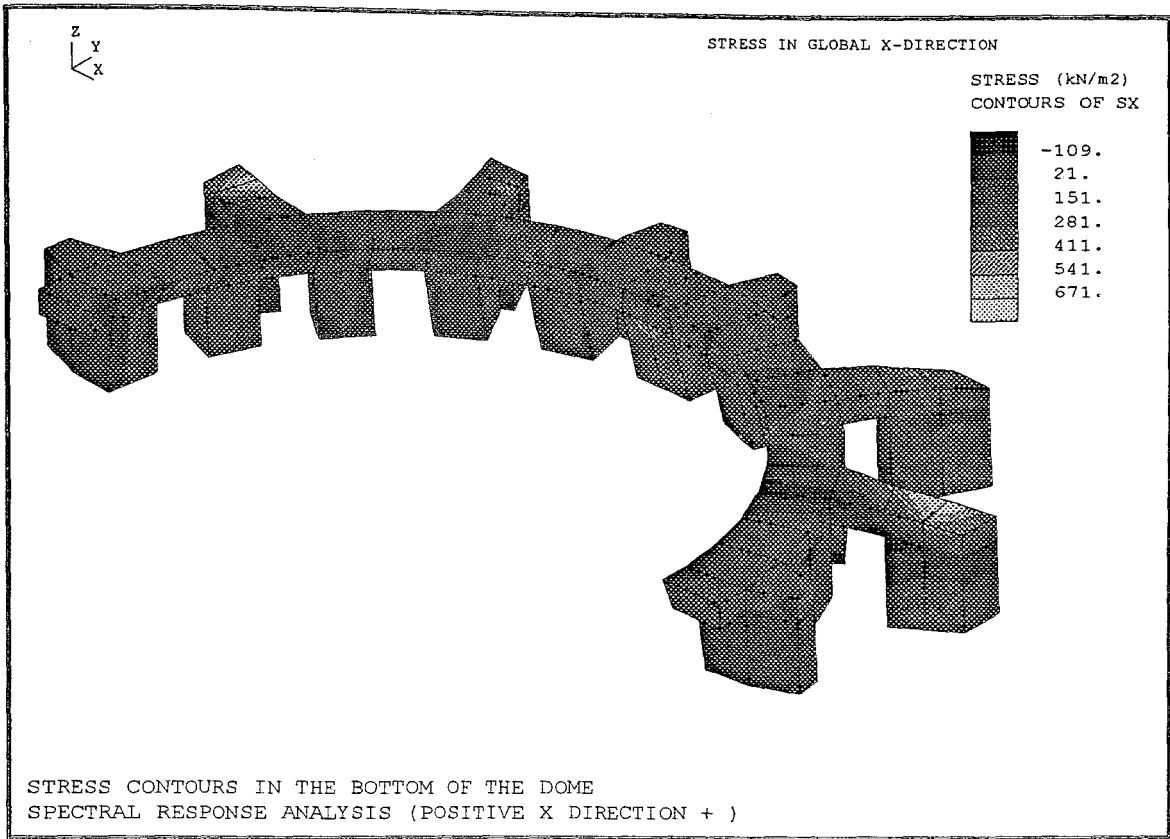


FIGURE 4.45 Stress Contours in the Bottom of the Dome.Spectral Response Analysis (Positive X Direction+)Stress in Global X Direction

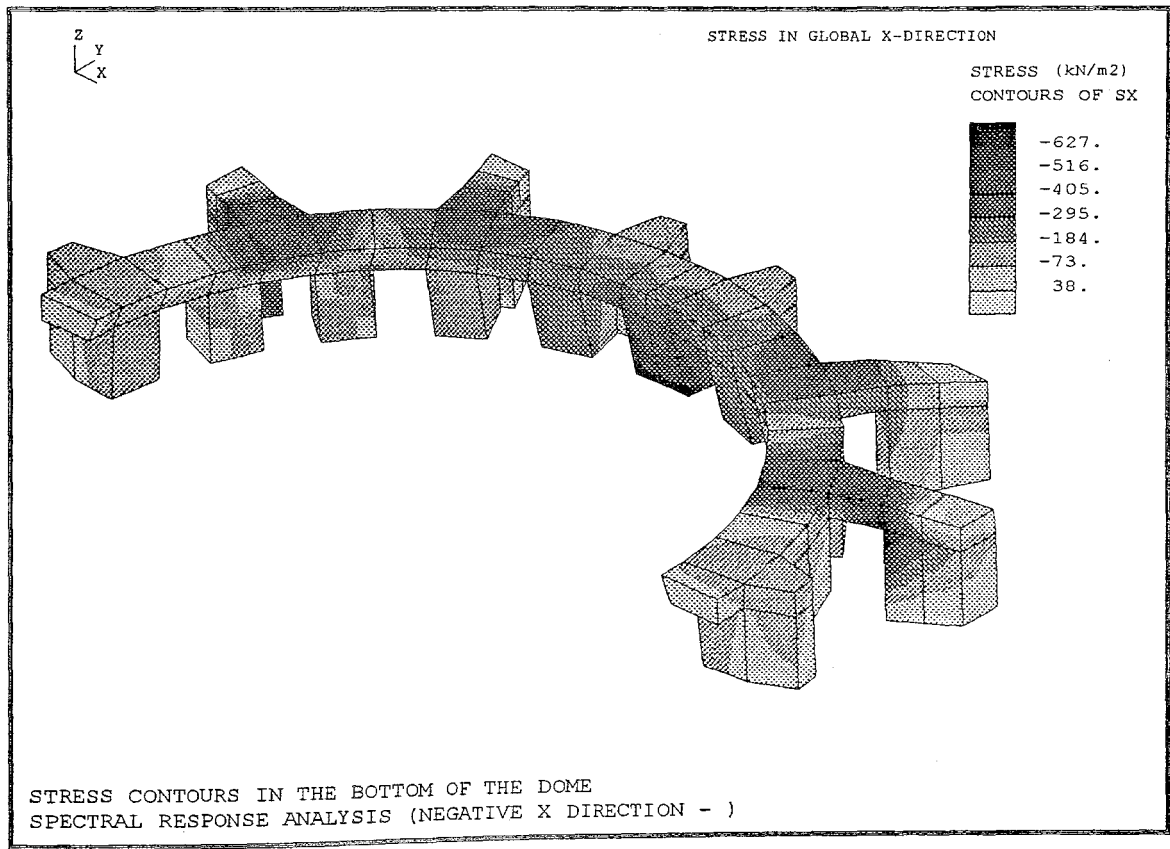


FIGURE 4.46 Stress Contours in the Bottom of the Dome.Spectral Response Analysis (Negative X Direction-)Stress in Global X Direction

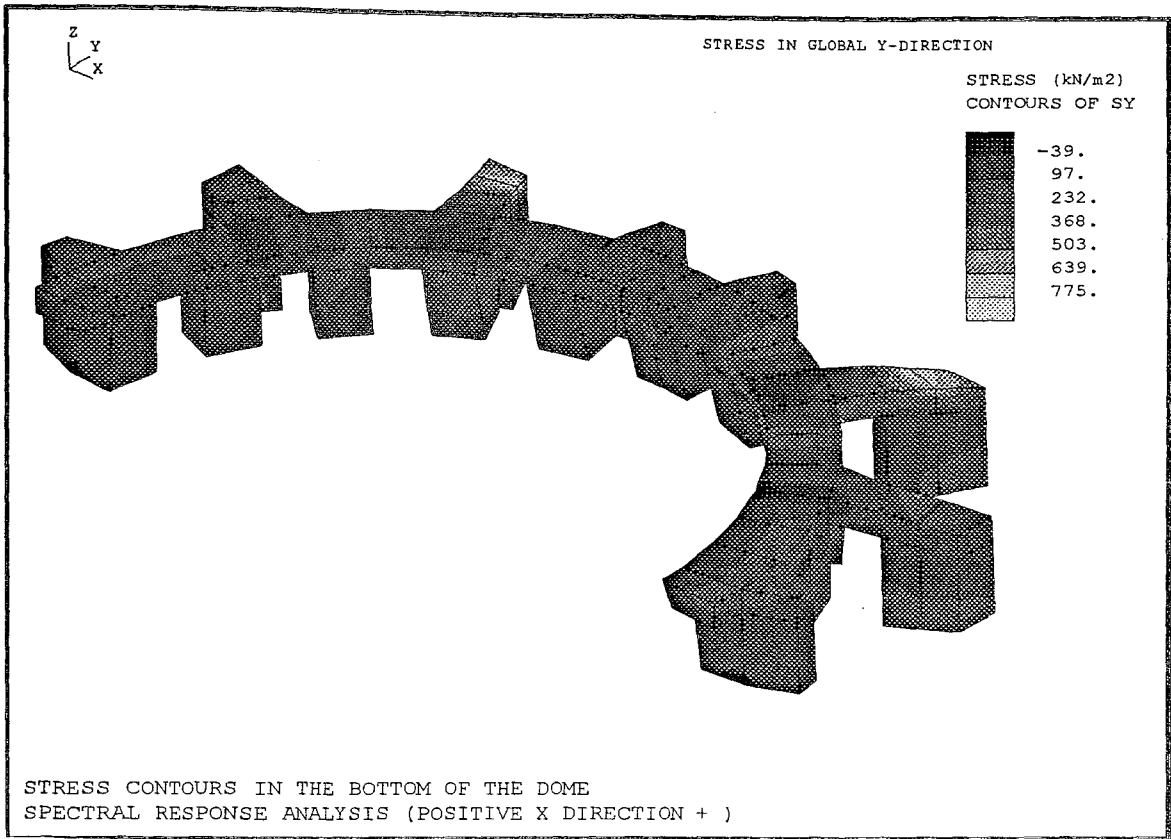


FIGURE 4.47 Stress Contours in the Bottom of the Dome.Spectral Response Analysis (Positive X Direction+)
Stress in Global Y Direction

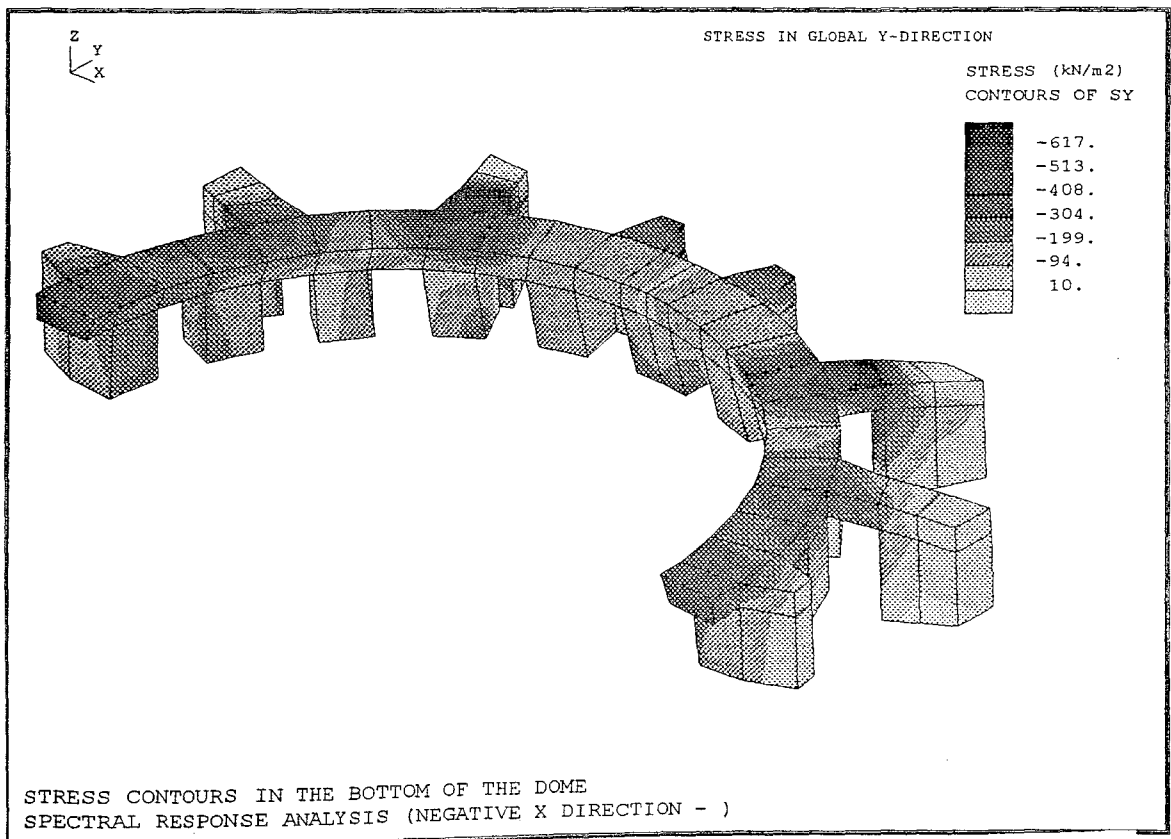


FIGURE 4.48 Stress Contours in the Bottom of the Dome.Spectral Response Analysis (Negative X Direction-)
Stress in Global Y Direction

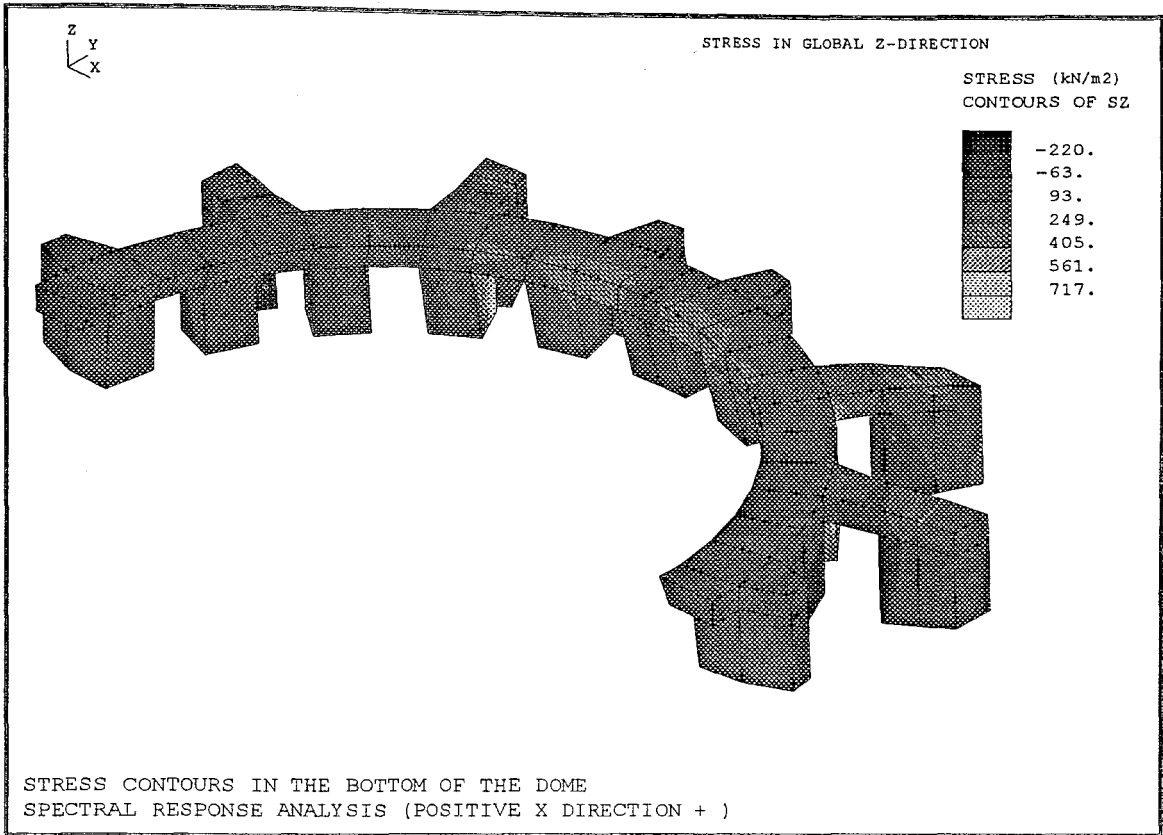


FIGURE 4.49 Stress Contours in the Bottom of the Dome.Spectral Response Analysis (Positive X Direction+)Stress in Global Z Direction

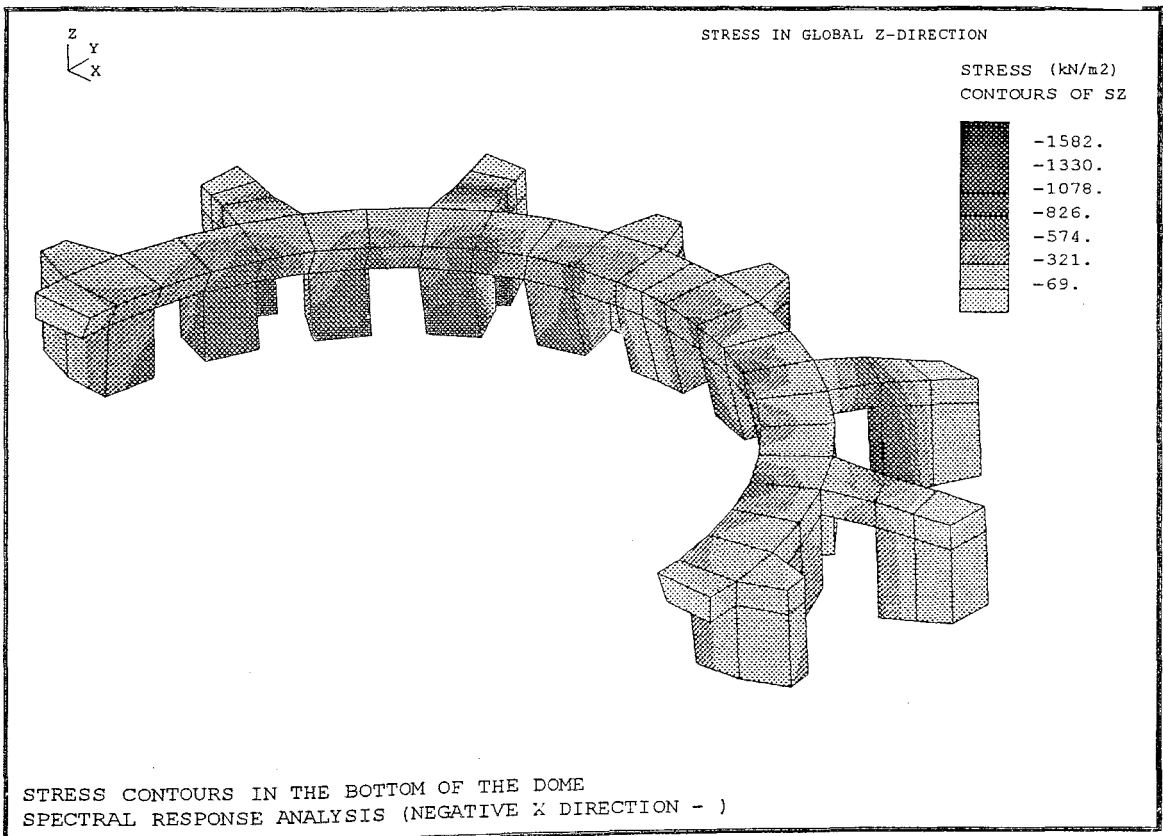


FIGURE 4.50 Stress Contours in the Bottom of the Dome.Spectral Response Analysis (Negative X Direction-) Stress in Global Z Direction

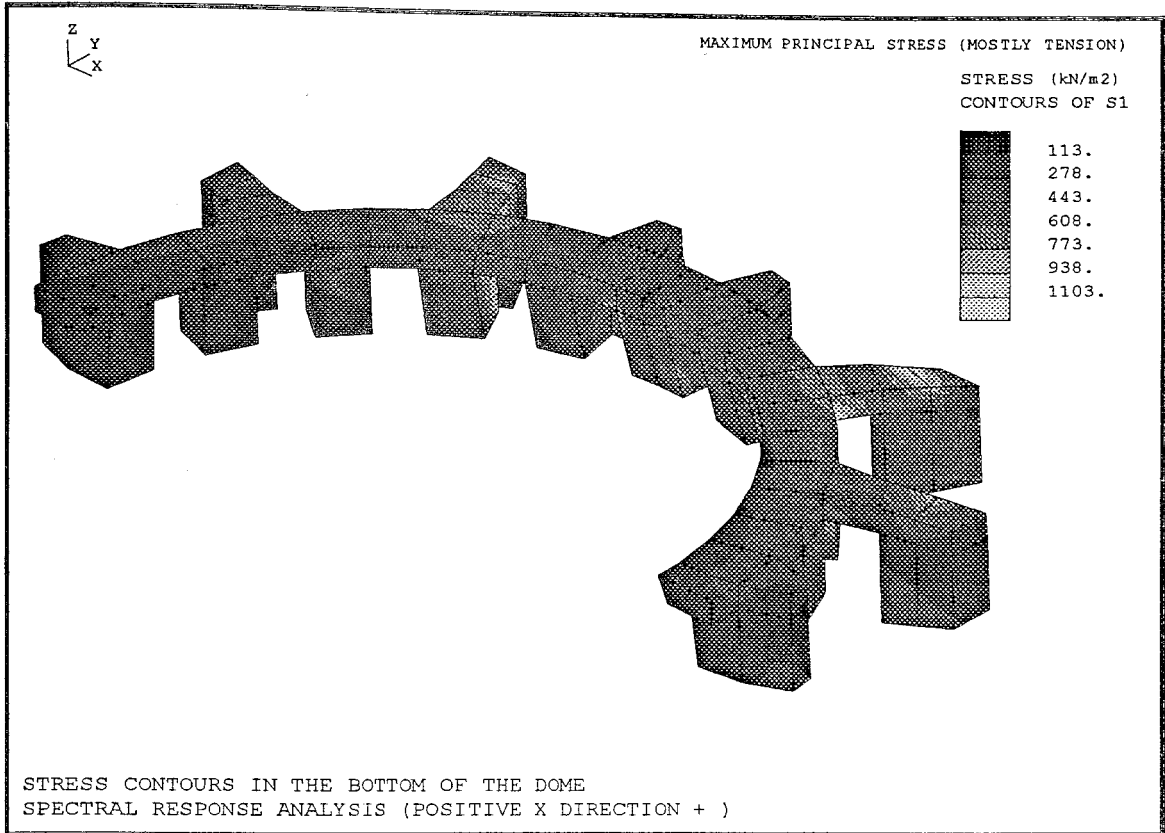


FIGURE 4.51 Stress Contours in the Bottom of the Dome.Spectral Response Analysis (Positive X Direction+) Maximum Principal Stress (Mostly Tension)

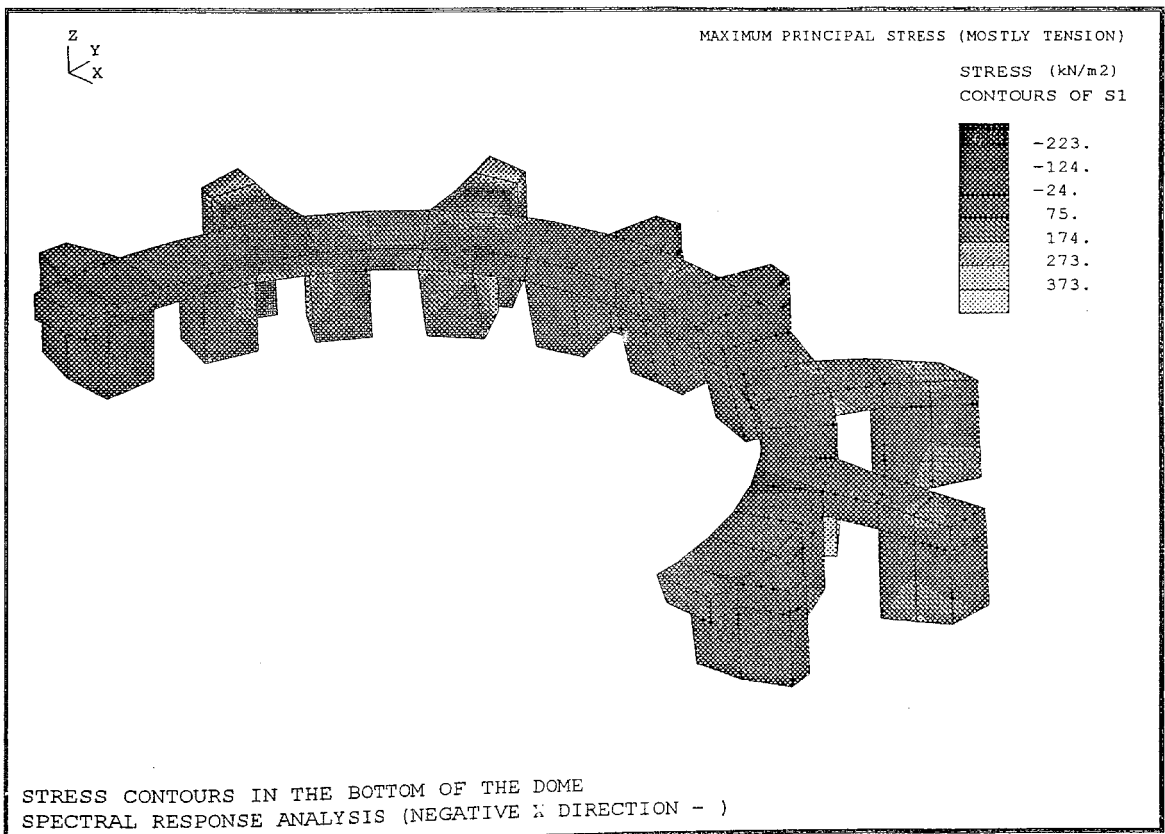


FIGURE 4.52 Stress Contours in the Bottom of the Dome.Spectral Response Analysis (Negative X Direction-) Maximum Principal Stress (Mostly Tension)

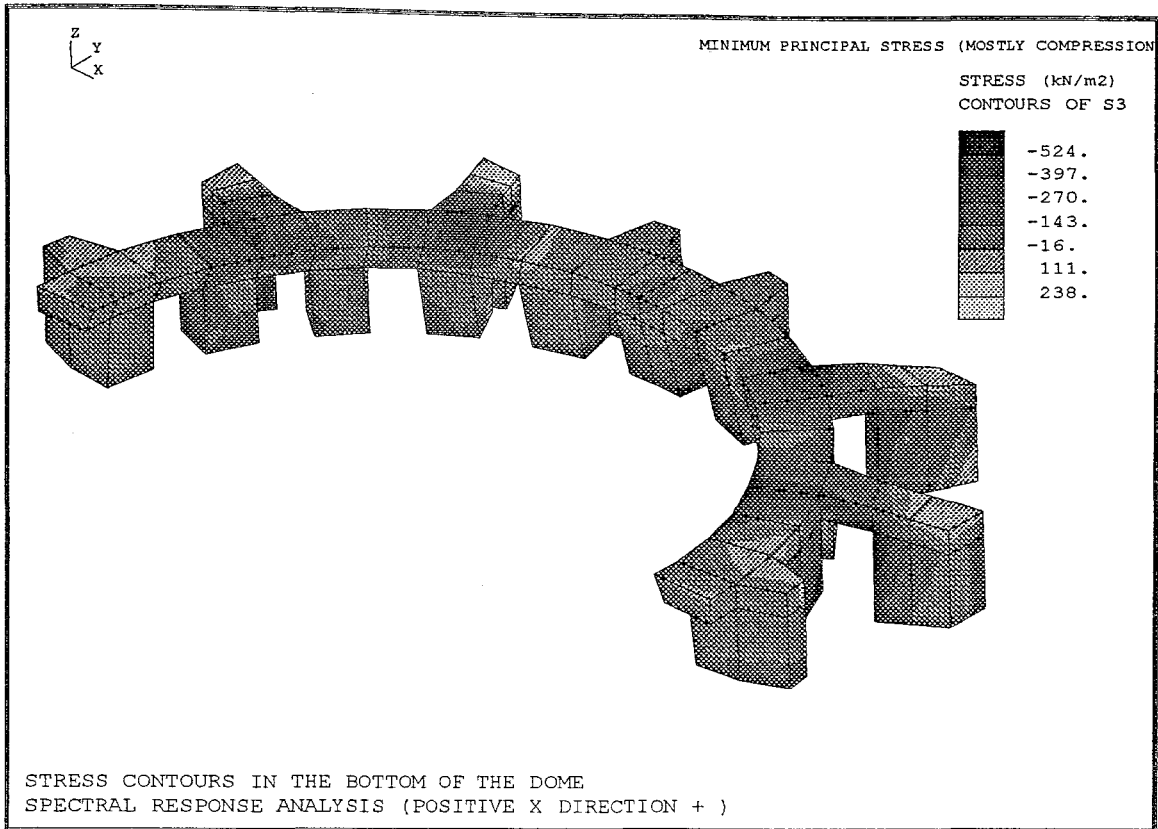


FIGURE 4.53 Stress Contours in the Bottom of the Dome.Spectral Response Analysis (Positive X Direction+) Minimum Principal Stress (Mostly Compression)

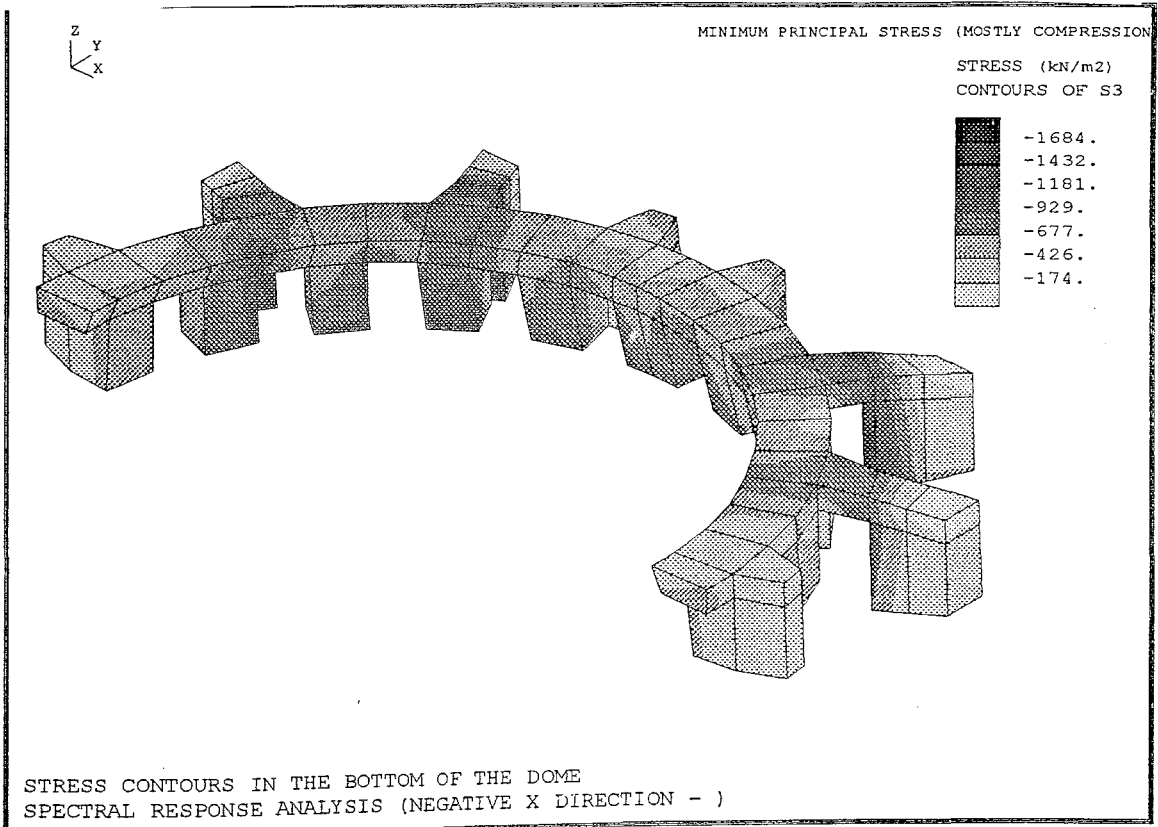


FIGURE 4.54 Stress Contours in the Bottom of the Dome.Spectral Response Analysis (Negative X Direction-) Minimum Principal Stress (Mostly Compression)

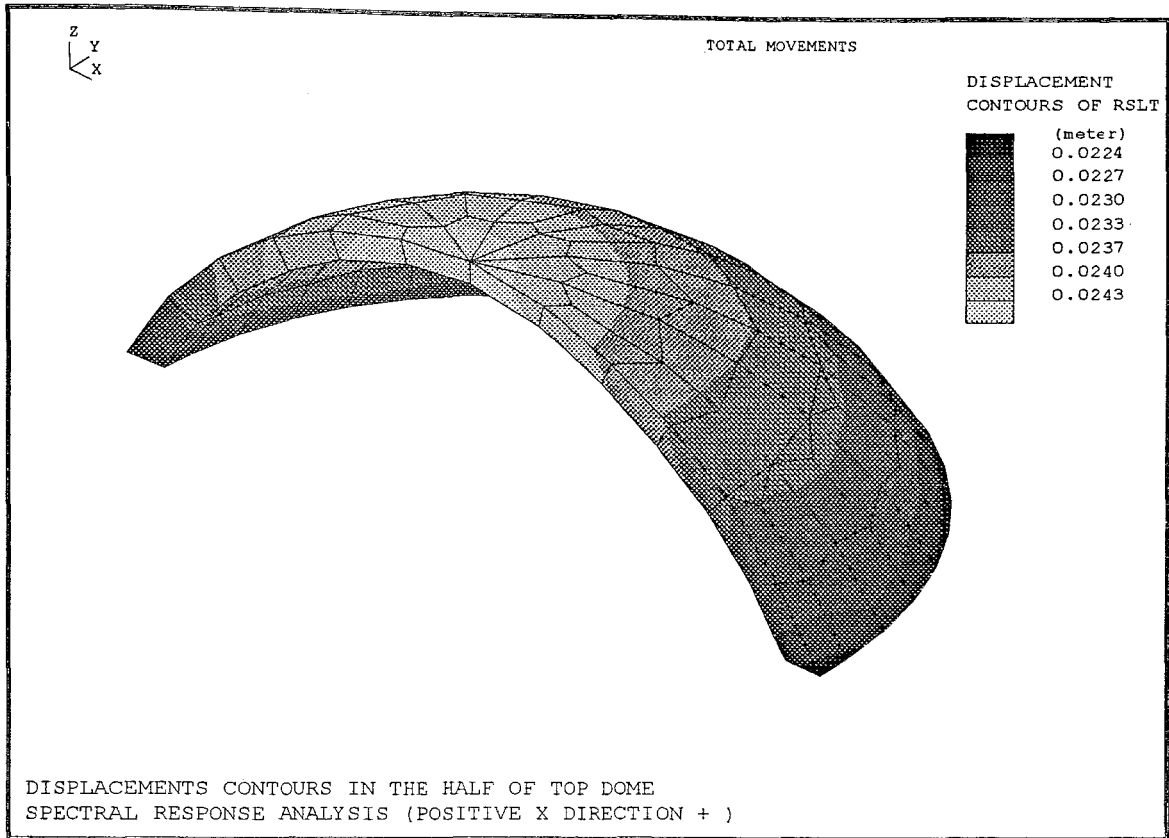


FIGURE 4.55 Displacement Contours in the Half of Top Dome.Spectral Response Analysis (Positive X Direction+) Minimum Principal Stress.Total Movements

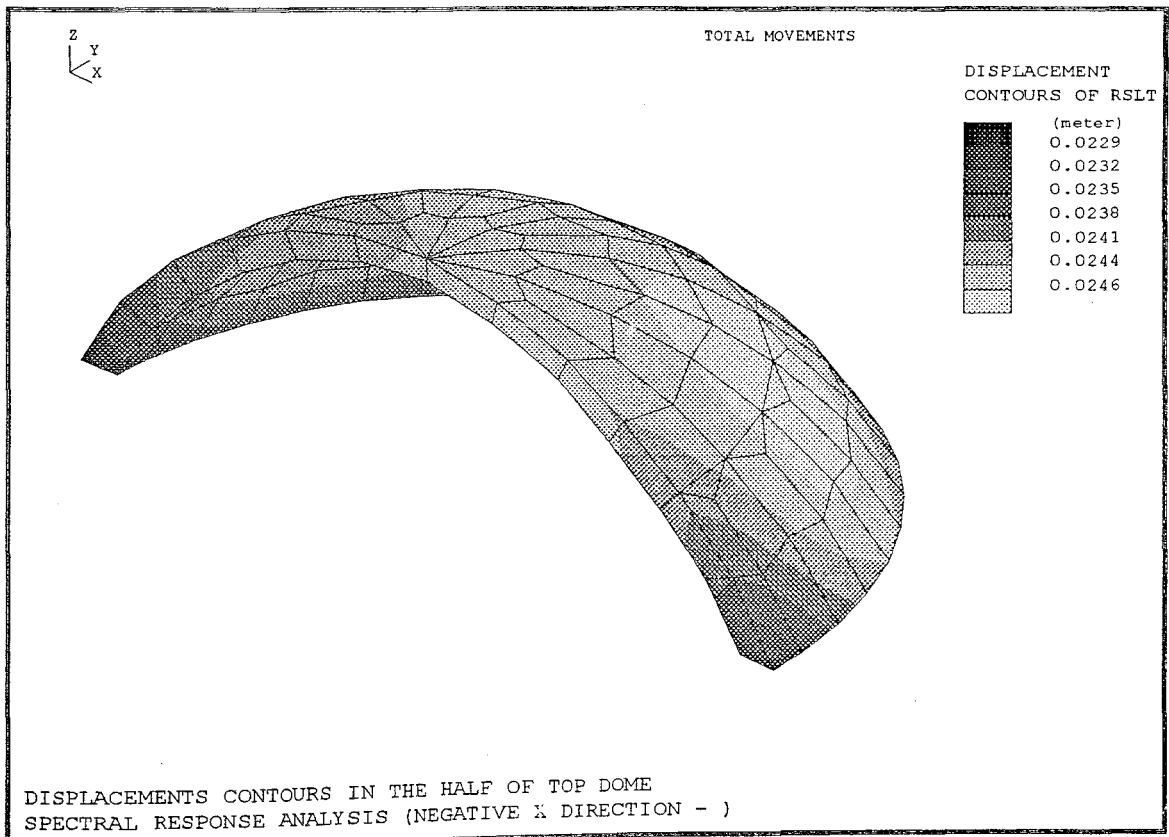


FIGURE 4.56 Displacement Contours in the Half of Top Dome.Spectral Response Analysis (Negative X Direction-) Minimum Principal Stress.Total Movements

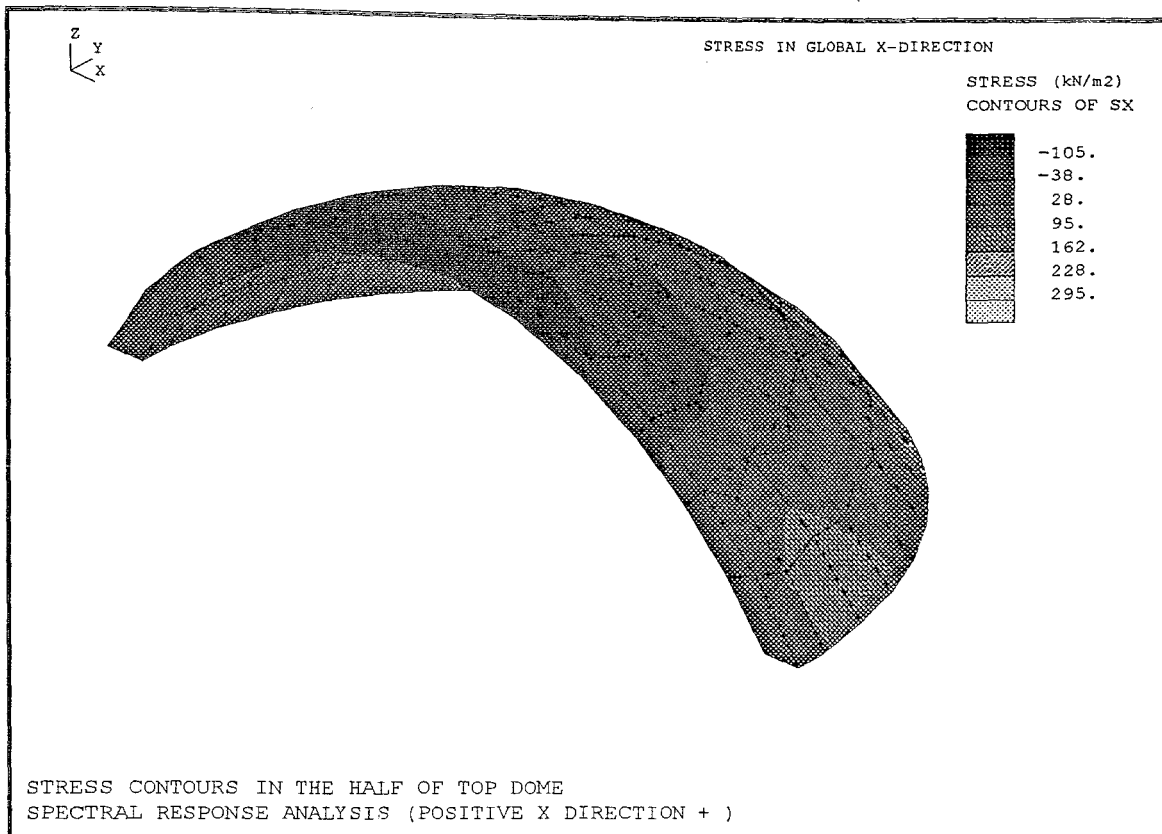


FIGURE 4.57 Displacement Contours in the Half of Top Dome.Spectral Response Analysis (Positive X Direction+) Minimum Principal Stress.Total Movements

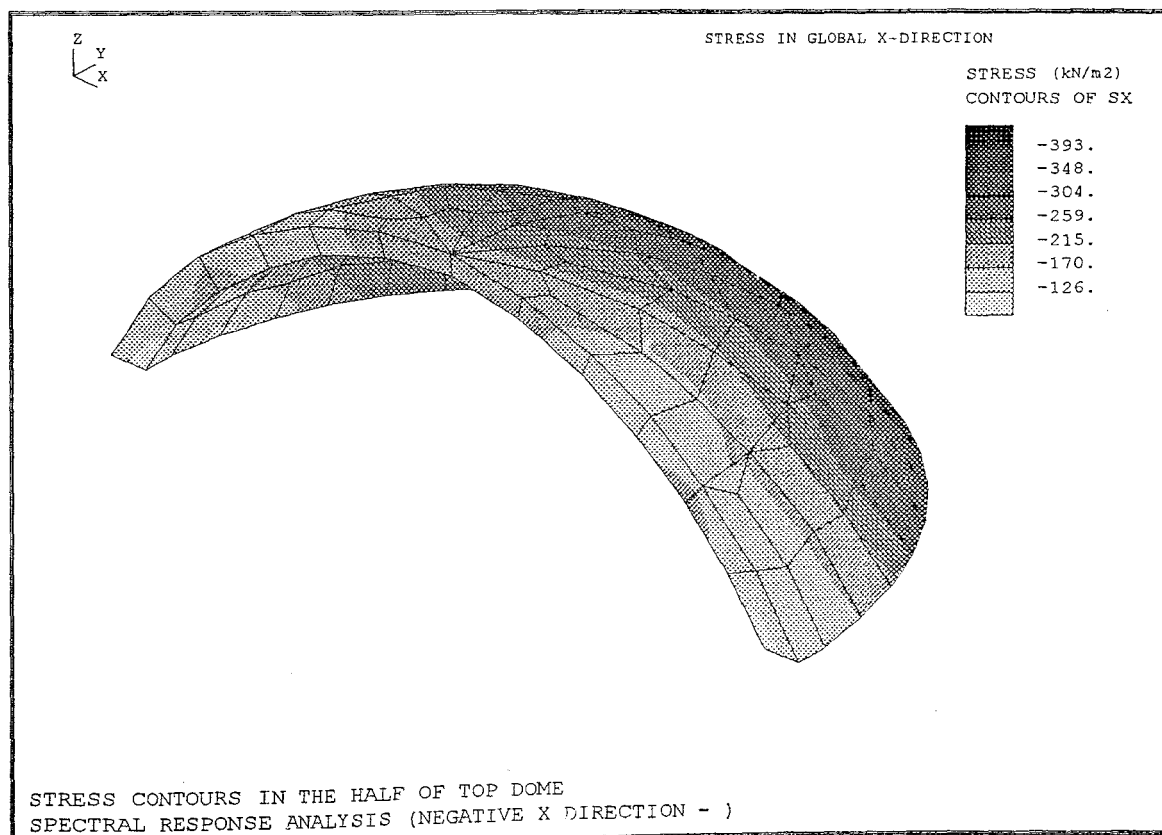


FIGURE 4.58 Stress Contours in the Half of Top Dome.Spectral Response Analysis (Negative X Direction-) Stress in Global X Direction

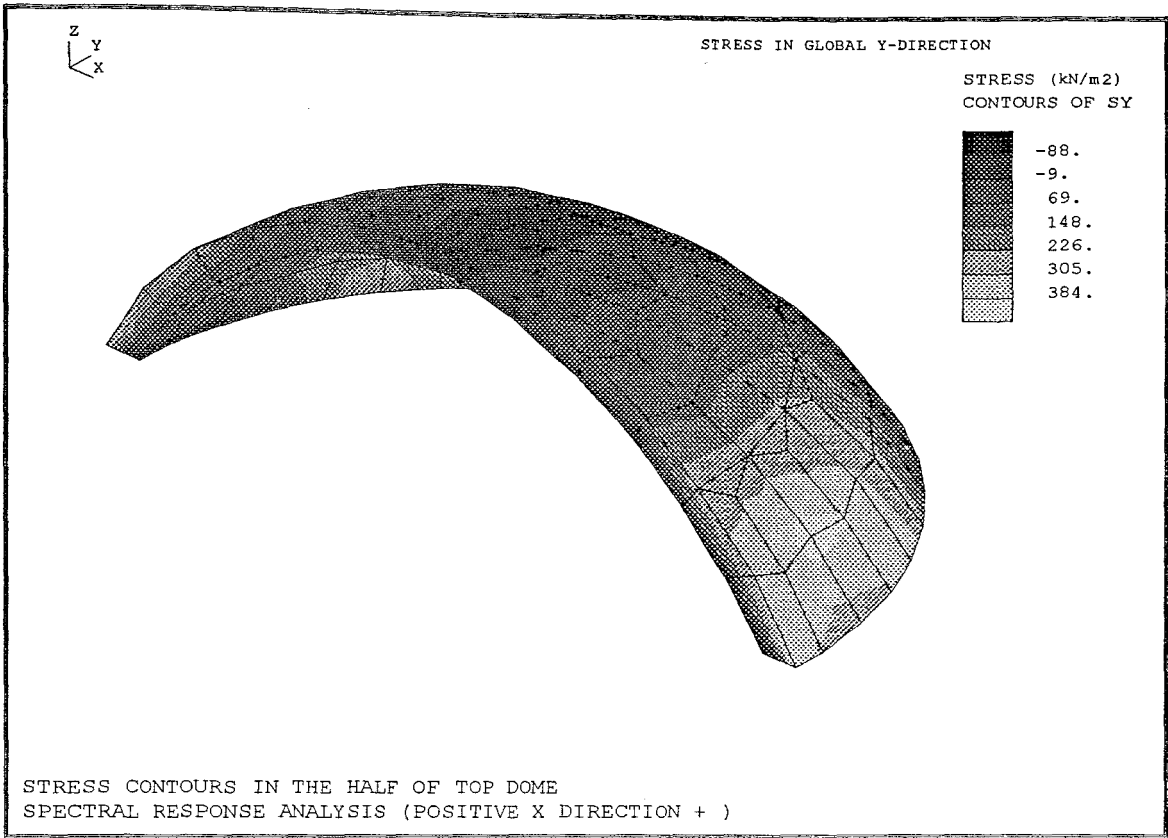


FIGURE 4.59 Stress Contours in the Half of Top Dome.Spectral Response Analysis (Positive X Direction+) Stress in Global X Direction

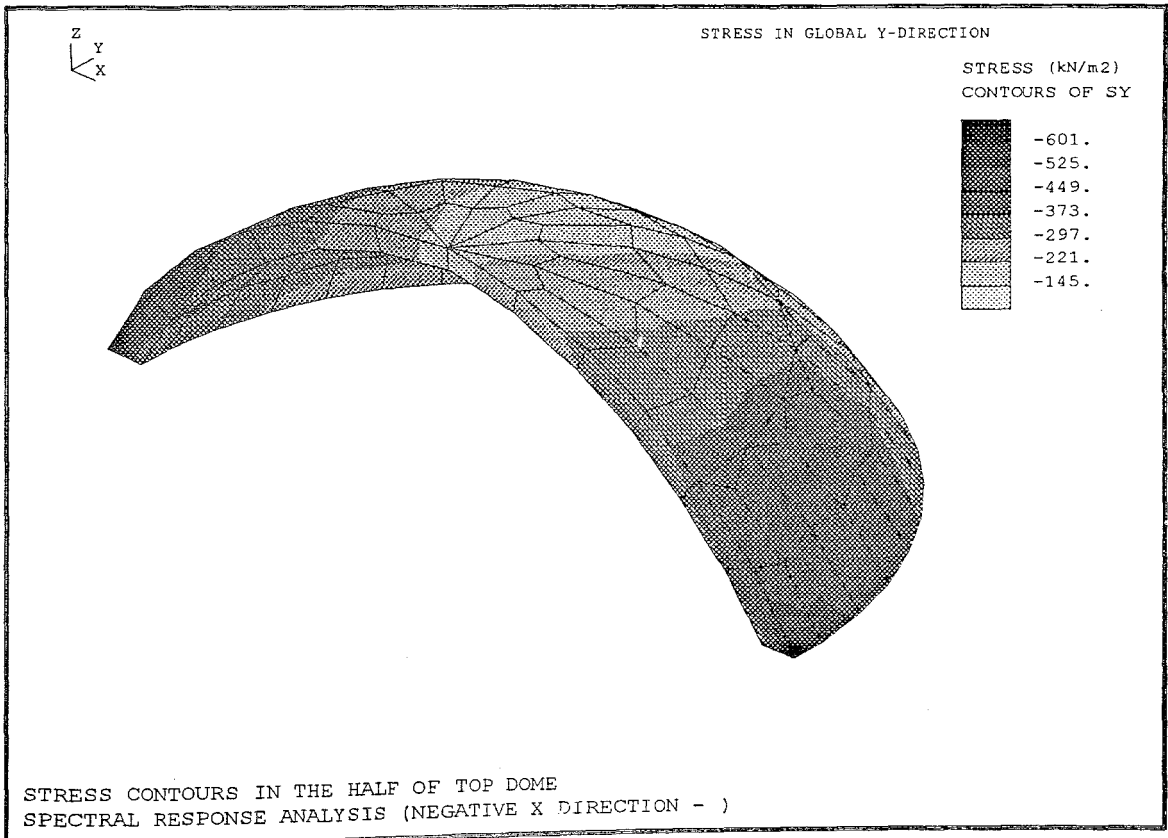


FIGURE 4.60 Stress Contours in the Half of Top Dome.Spectral Response Analysis (Negative X Direction-) Stress in Global Y Direction

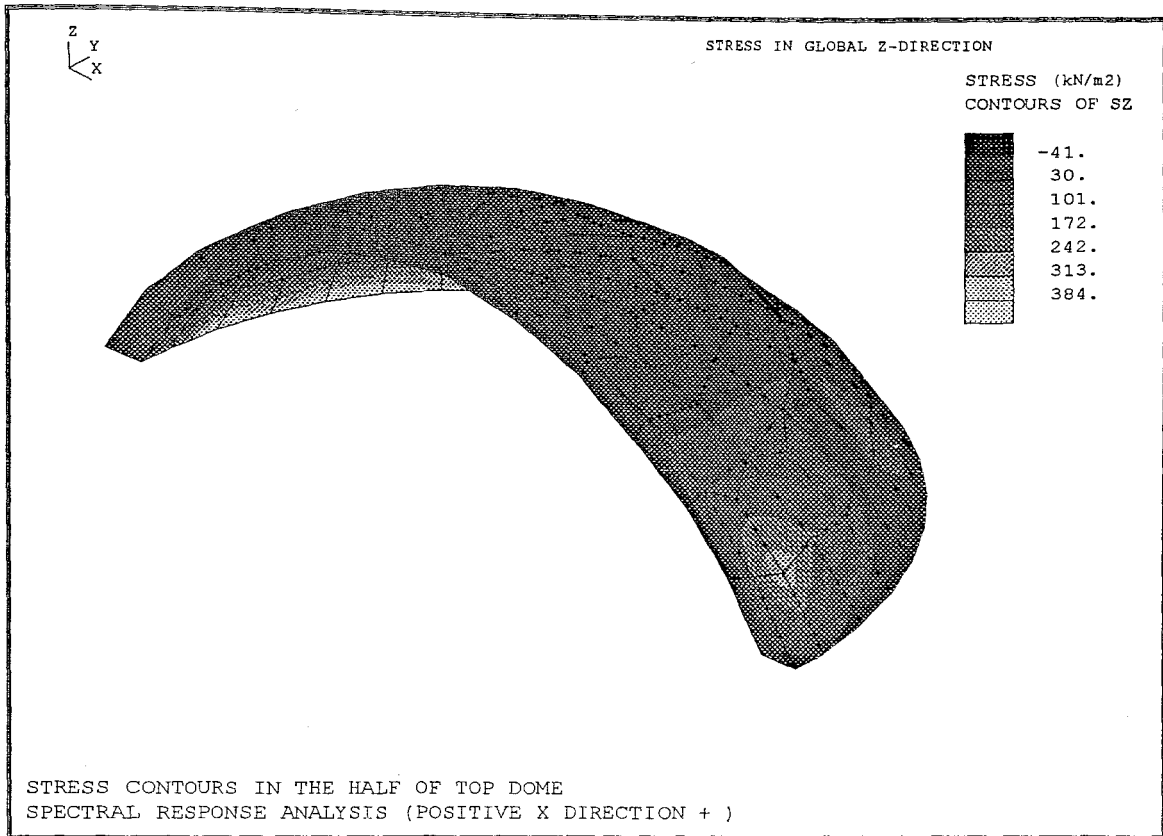


FIGURE 4.61 Stress Contours in the Half of Top Dome.Spectral Response Analysis (Positive X Direction+) Stress in Global Z Direction

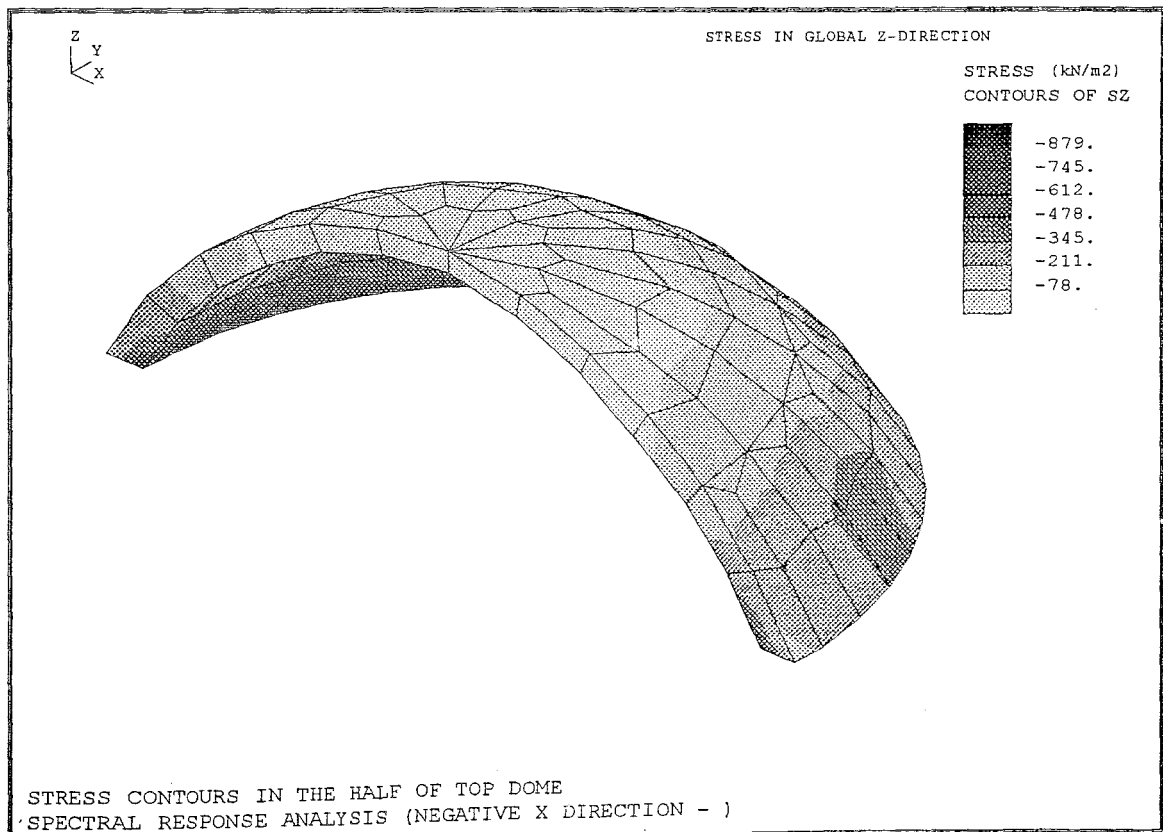


FIGURE 4.62 Stress Contours in the Half of Top Dome.Spectral Response Analysis (Negative X Direction-) Stress in Global Z Direction

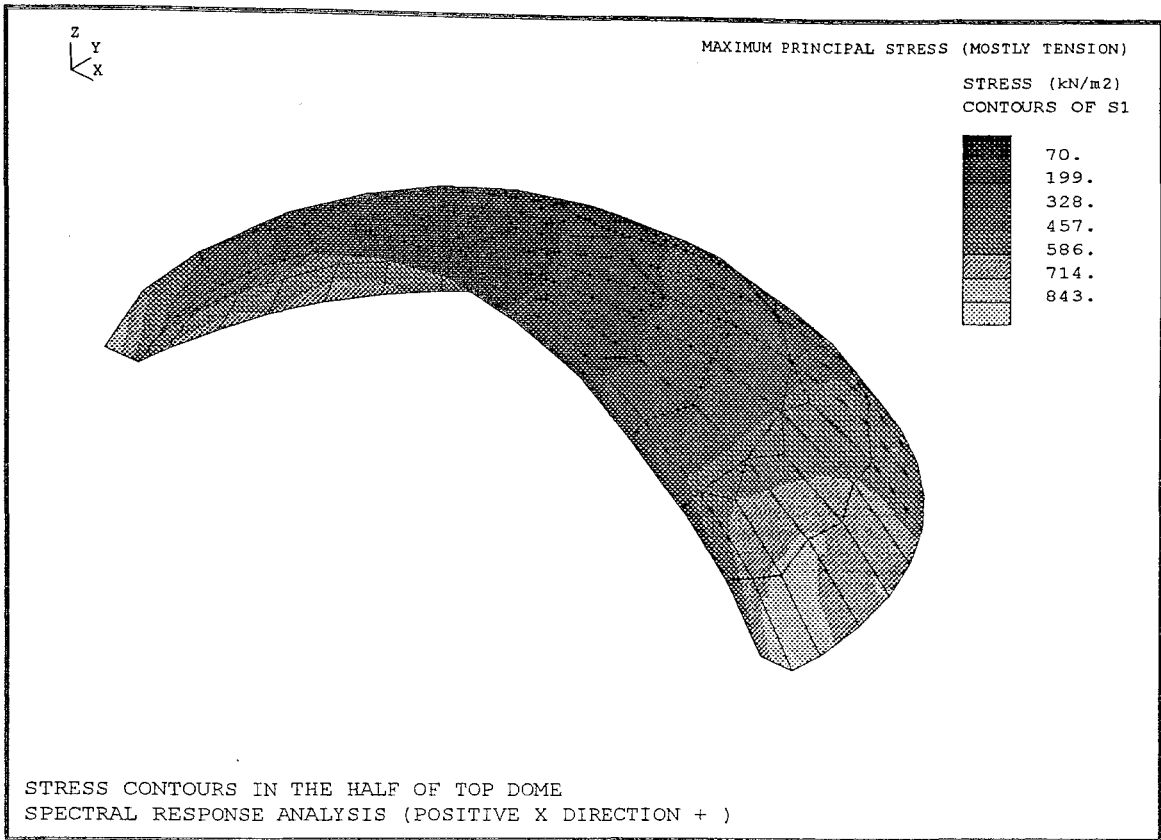


FIGURE 4.63 Stress Contours in the Half of Top Dome.Spectral Response Analysis (Positive X Direction+) Maximum Principal Stress (Mostly Tension)

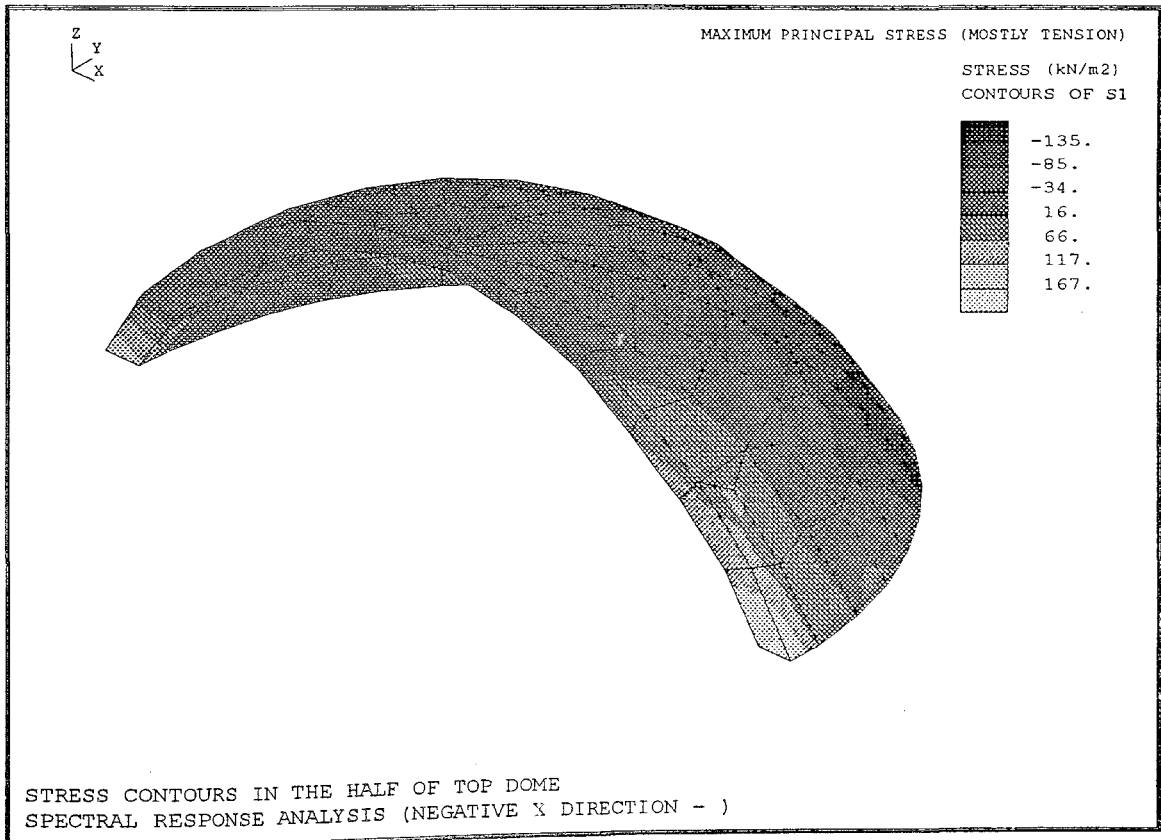


FIGURE 4.64 Stress Contours in the Half of Top Dome.Spectral Response Analysis (Negative X Direction-) Maximum Principal Stress (Mostly Tension)

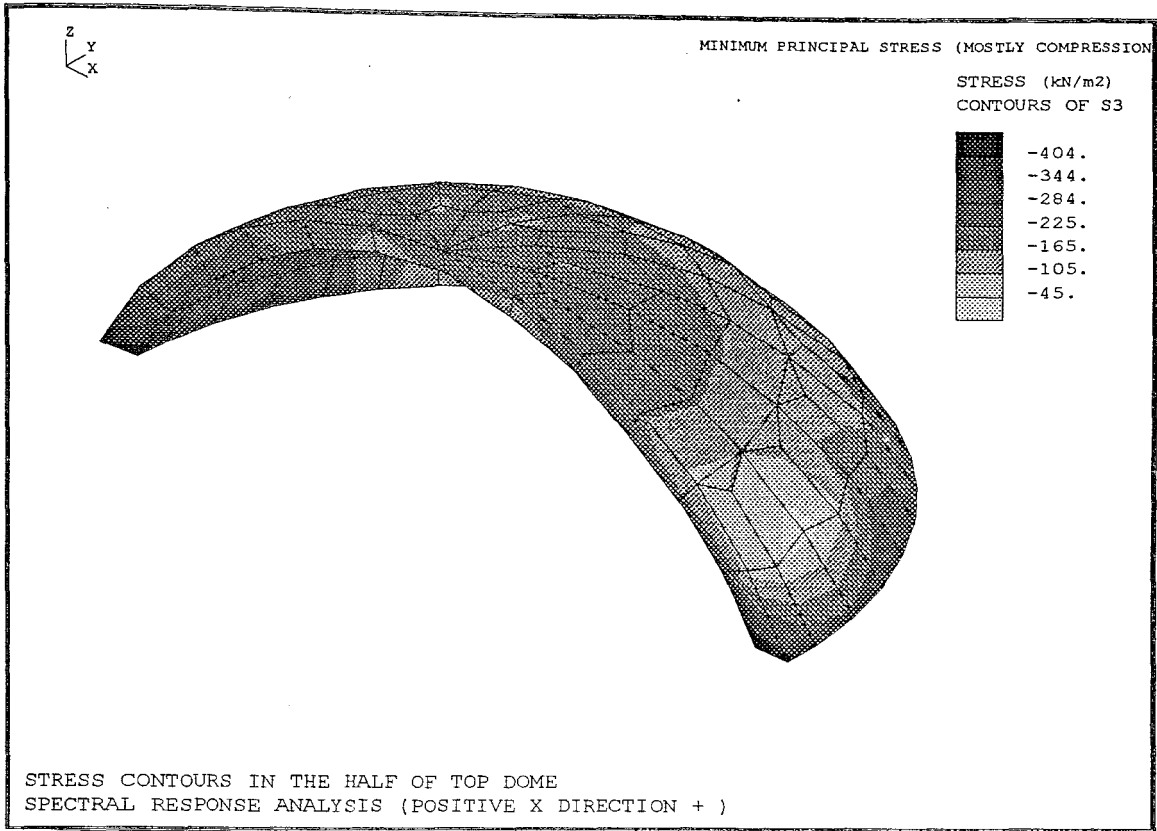


FIGURE 4.65 Stress Contours in the Half of Top Dome.Spectral Response Analysis (Positive X Direction+) Maximum Principal Stress (Mostly Compression)

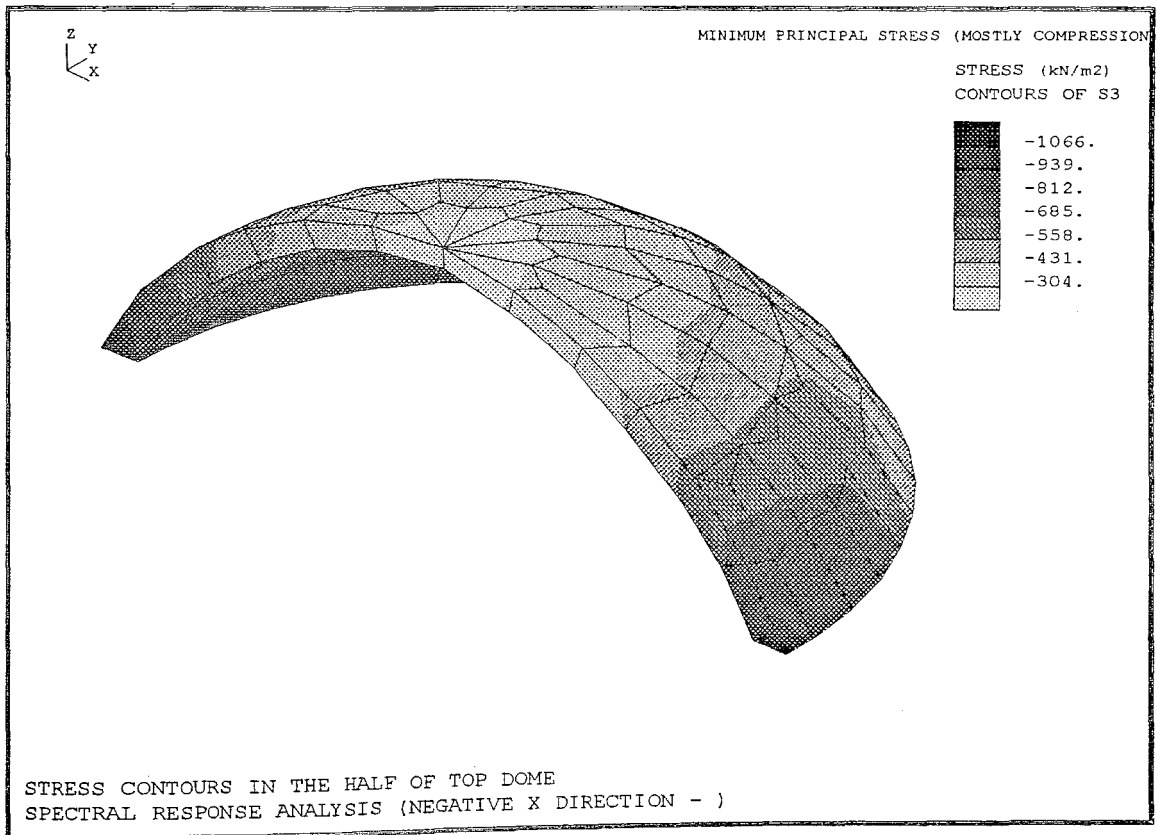


FIGURE 4.66 Stress Contours in the Half of Top Dome.Spectral Response Analysis (Negative X Direction-) Maximum Principal Stress (Mostly Compression)

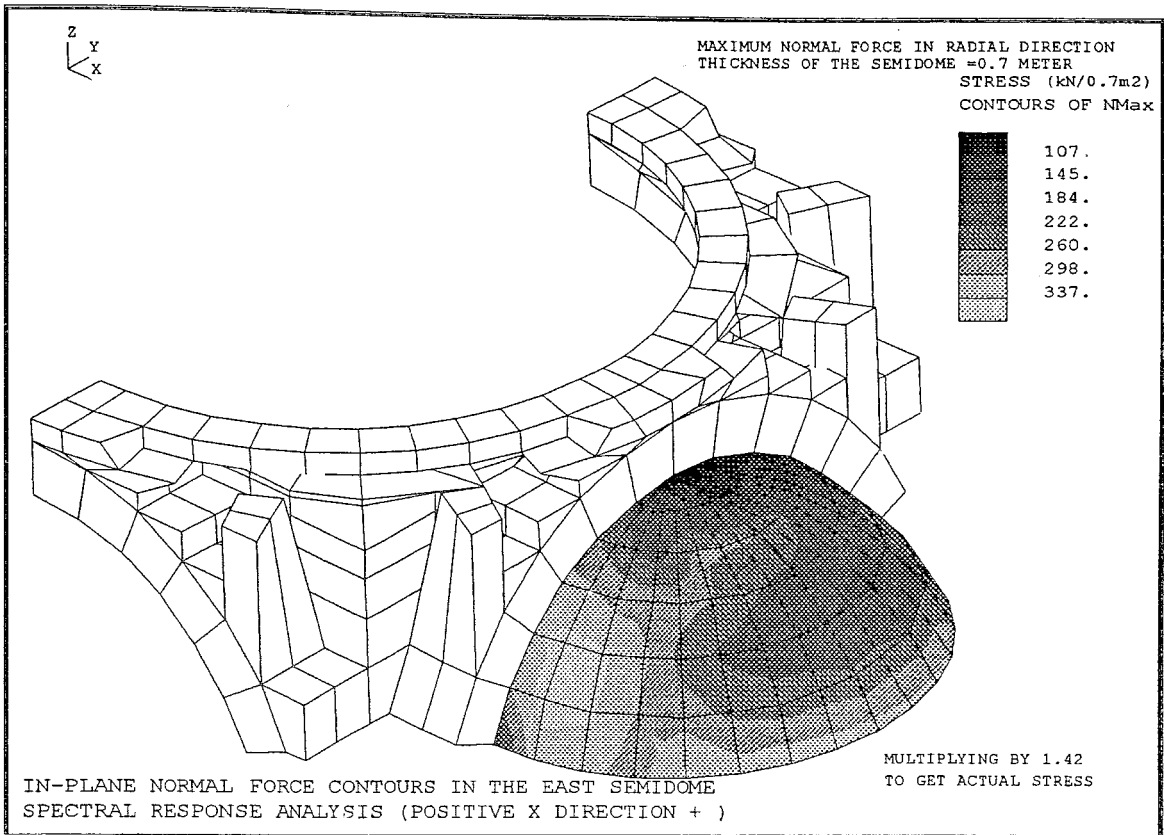


FIGURE 4.67 In-Plane Normal Force Contours in the East Semidome.Spectral Response Analysis (Positive X Direction+) Maximum Normal Force in Radial Direction

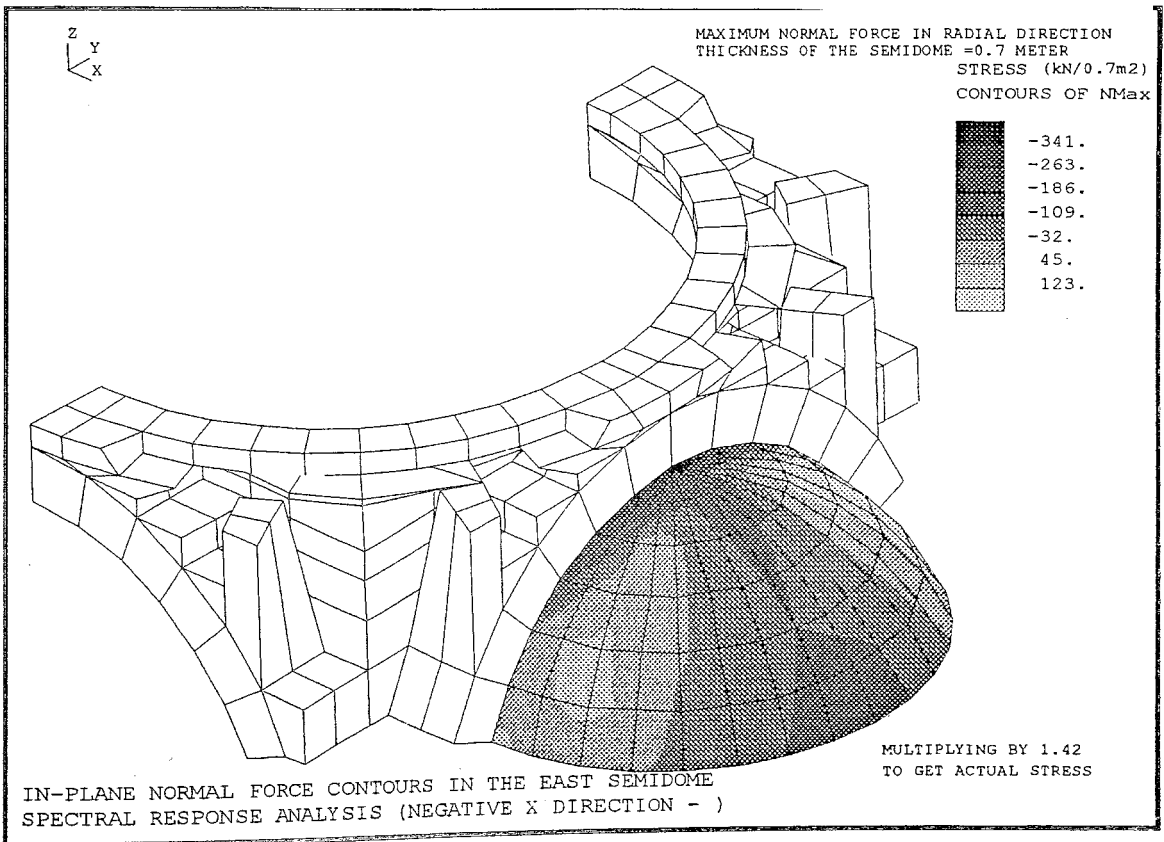


FIGURE 4.68 In-Plane Normal Force Contours in the East Semidome.Spectral Response Analysis (Negative X Direction-) Maximum Normal Force in Radial Direction

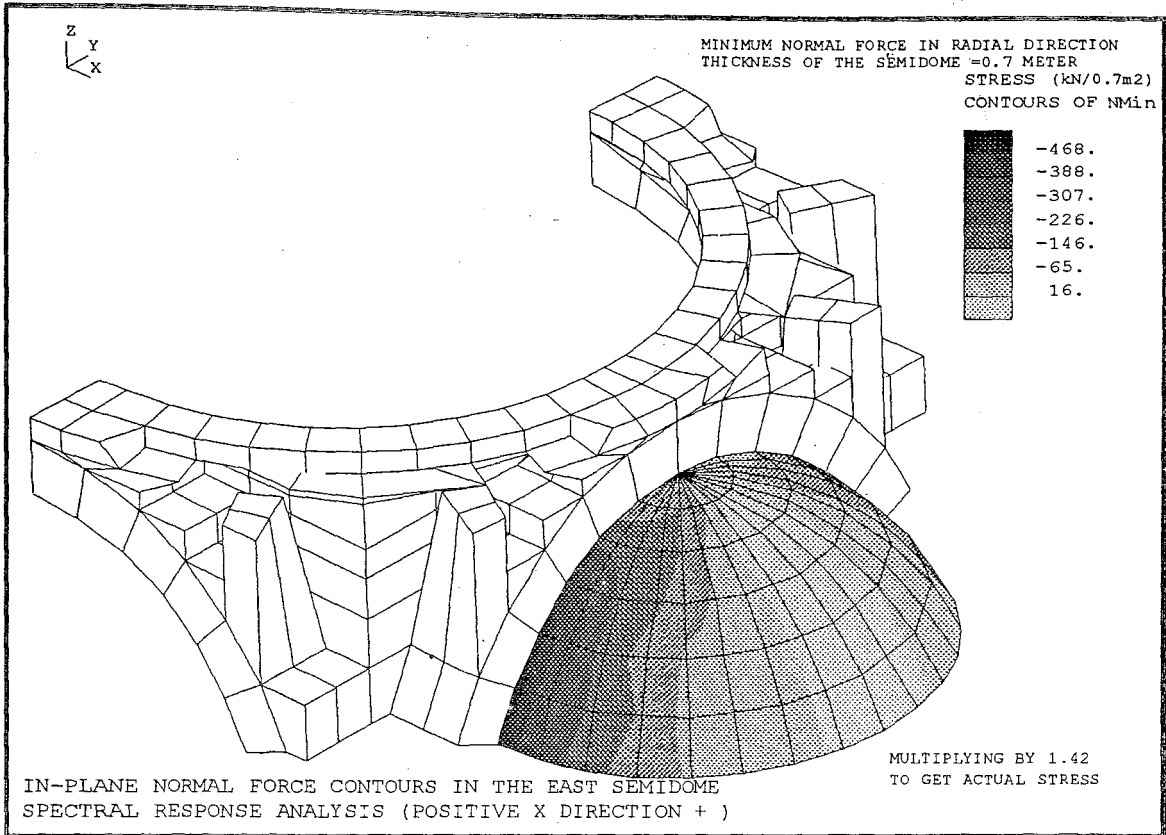


FIGURE 4.69 In-Plane Normal Force Contours in the East Semidome.Spectral Response Analysis (Positive X Direction+) Minimum Normal Force in Radial Direction

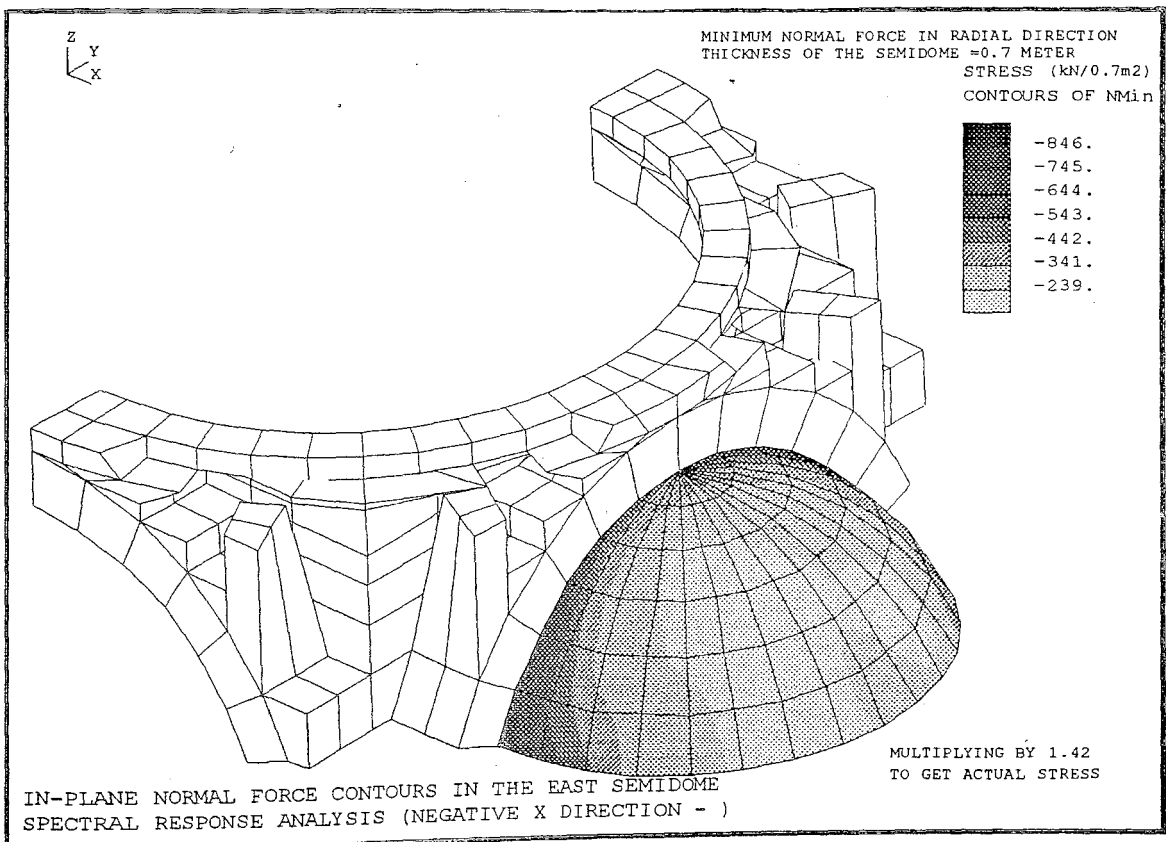


FIGURE 4.70 In-Plane Normal Force Contours in the East Semidome.Spectral Response Analysis (Negative X Direction-) Minimum Normal Force in Radial Direction

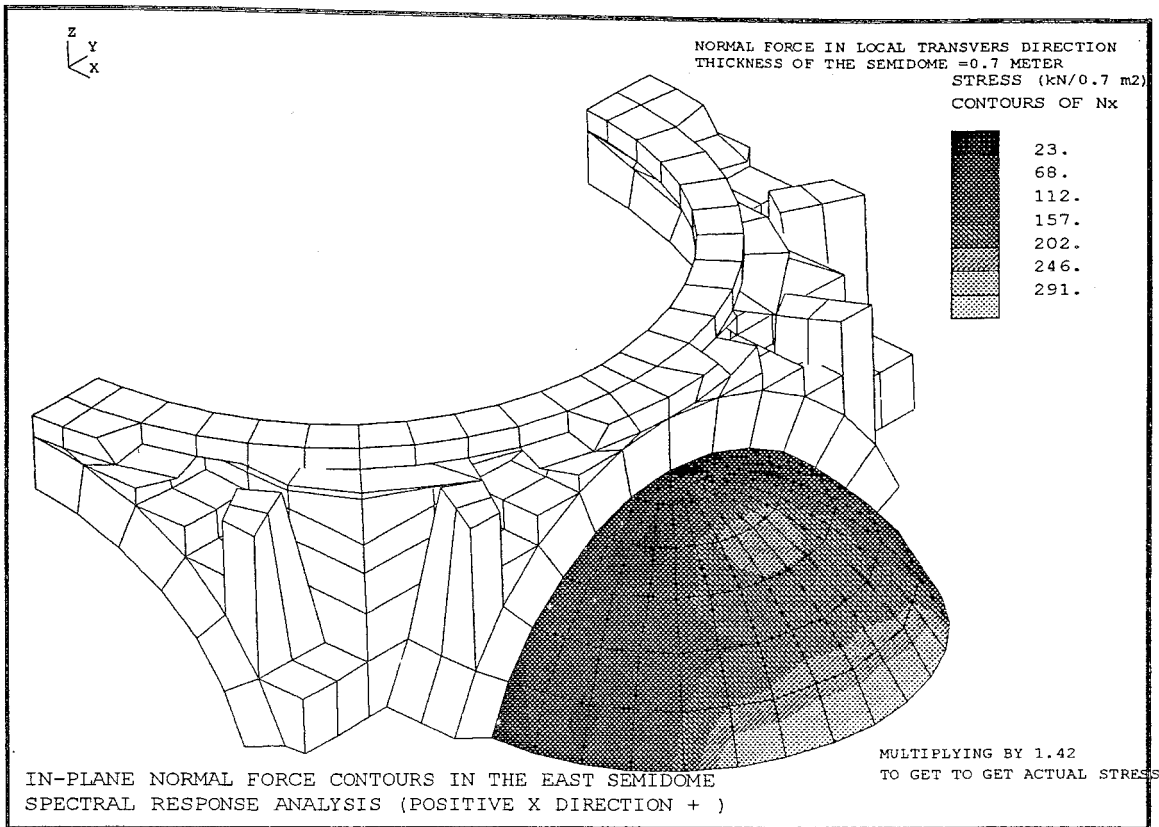


FIGURE 4.71 In-Plane Normal Force Contours in the East Semidome.Spectral Response Analysis (Positive X Direction+) Normal Force in Local Transverse Direction

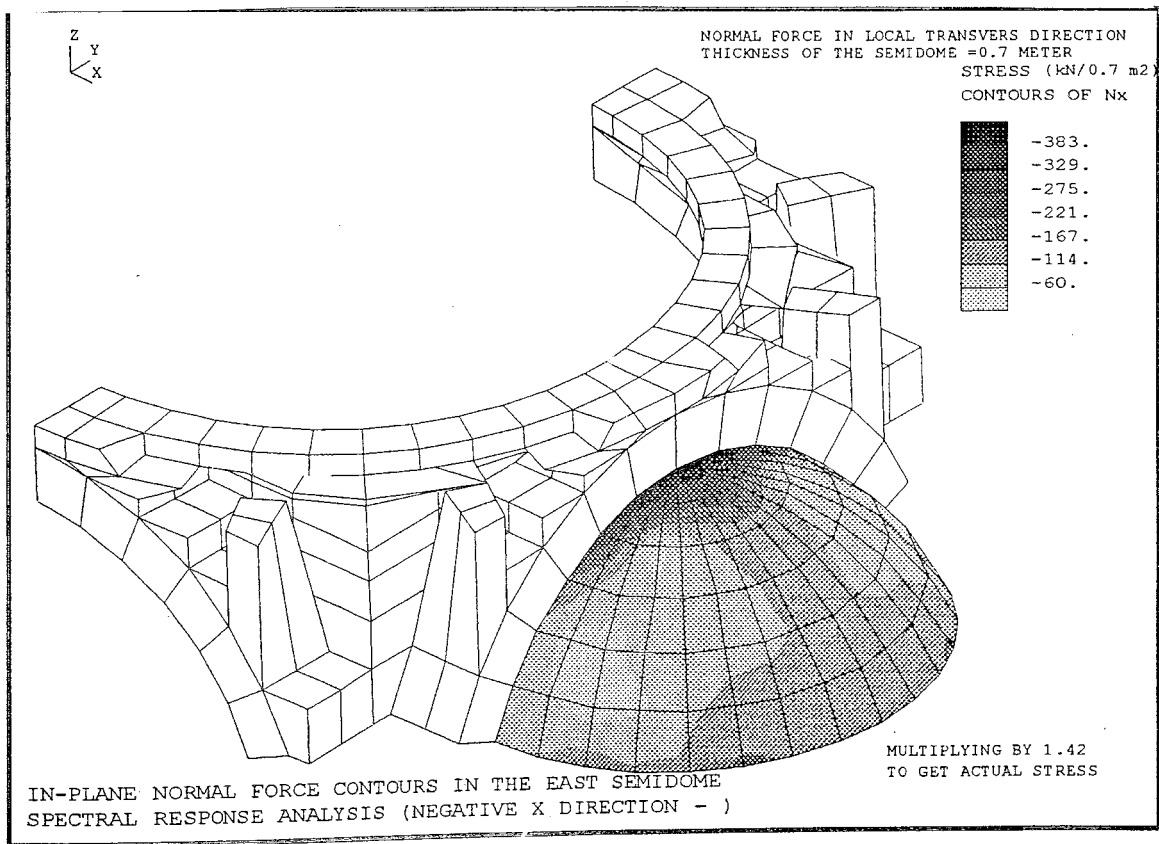


FIGURE 4.72 In-Plane Normal Force Contours in the East Semidome.Spectral Response Analysis (Negative X Direction-) Normal Force in Local Transverse Direction

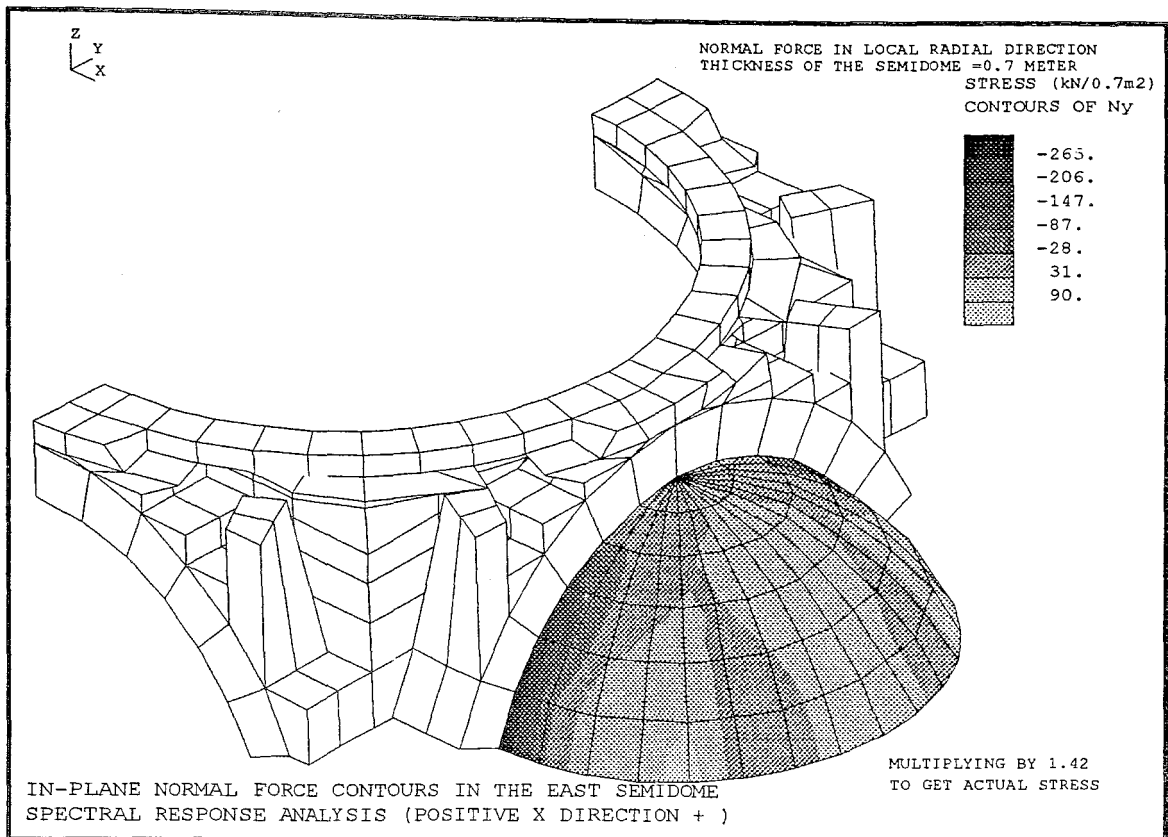


FIGURE 4.73 In-Plane Normal Force Contours in the East Semidome.Spectral Response Analysis (Positive X Direction+) Normal Force in Local Transverse Direction

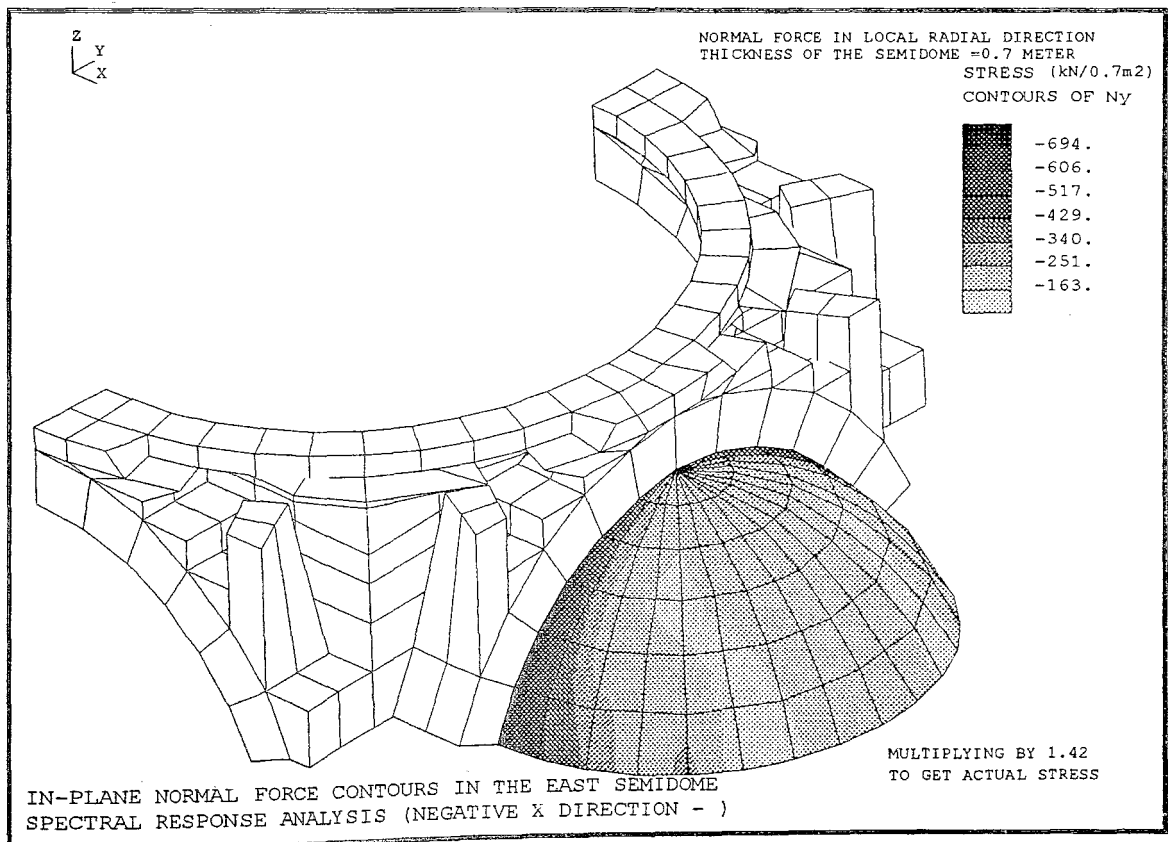


FIGURE 4.74 In-Plane Normal Force Contours in the East Semidome.Spectral Response Analysis (Negative X Direction-) Normal Force in Local Transverse Direction

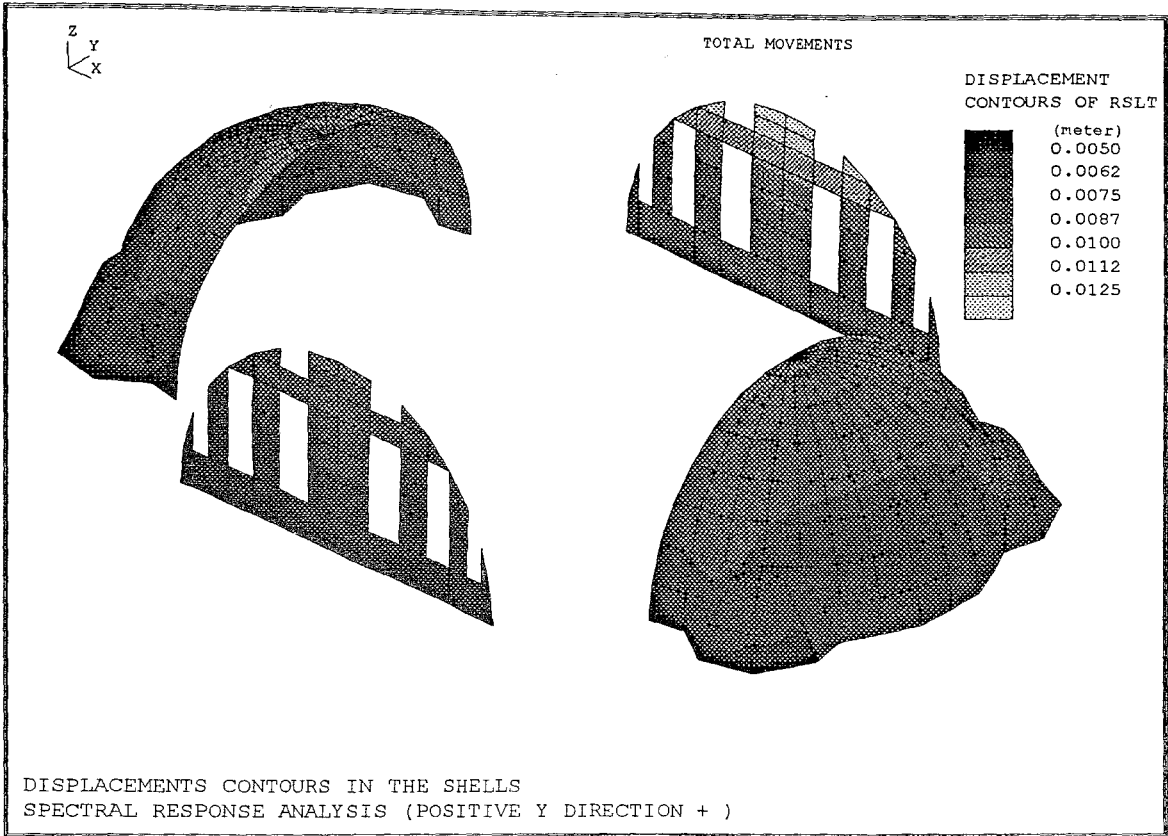


FIGURE 4.75 Displacement Contours in the Shells.Spectral Response Analysis (Positive Y Direction+) Total Movements

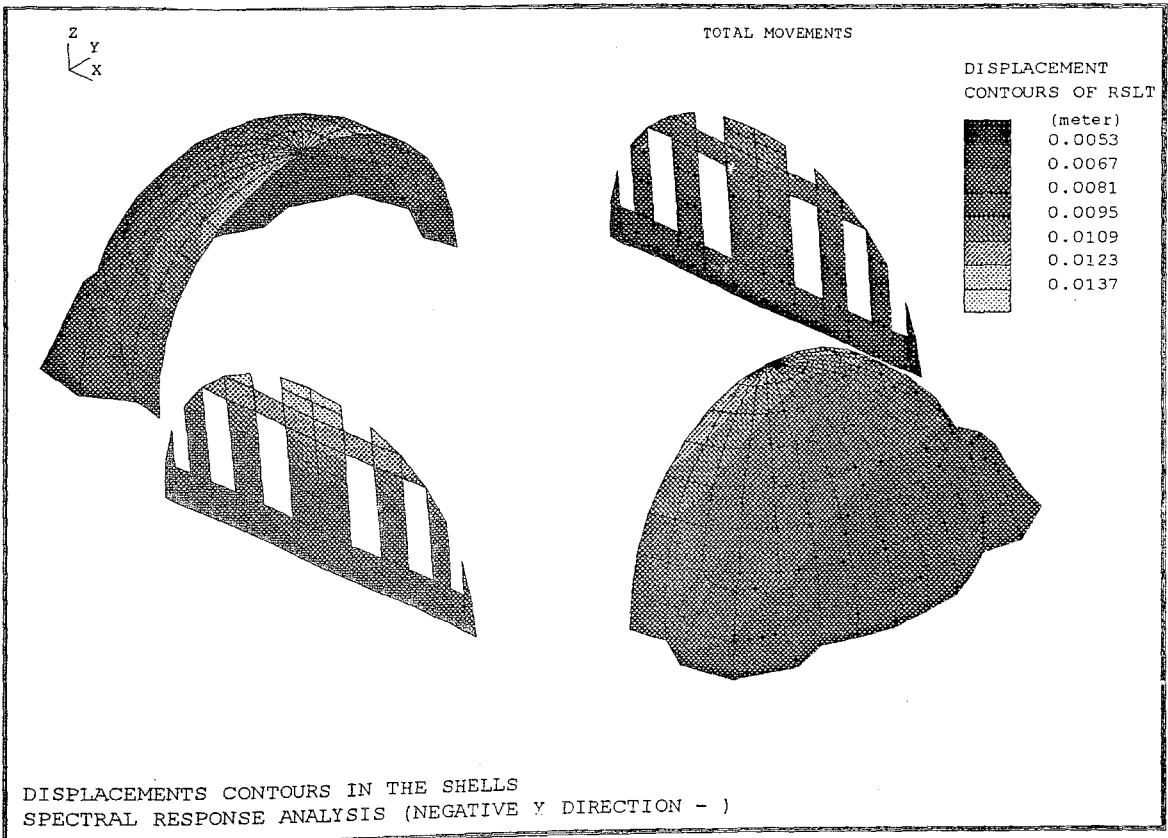


FIGURE 4.76 Displacement Contours in the Shells.Spectral Response Analysis (Negative Y Direction-) Total Movements

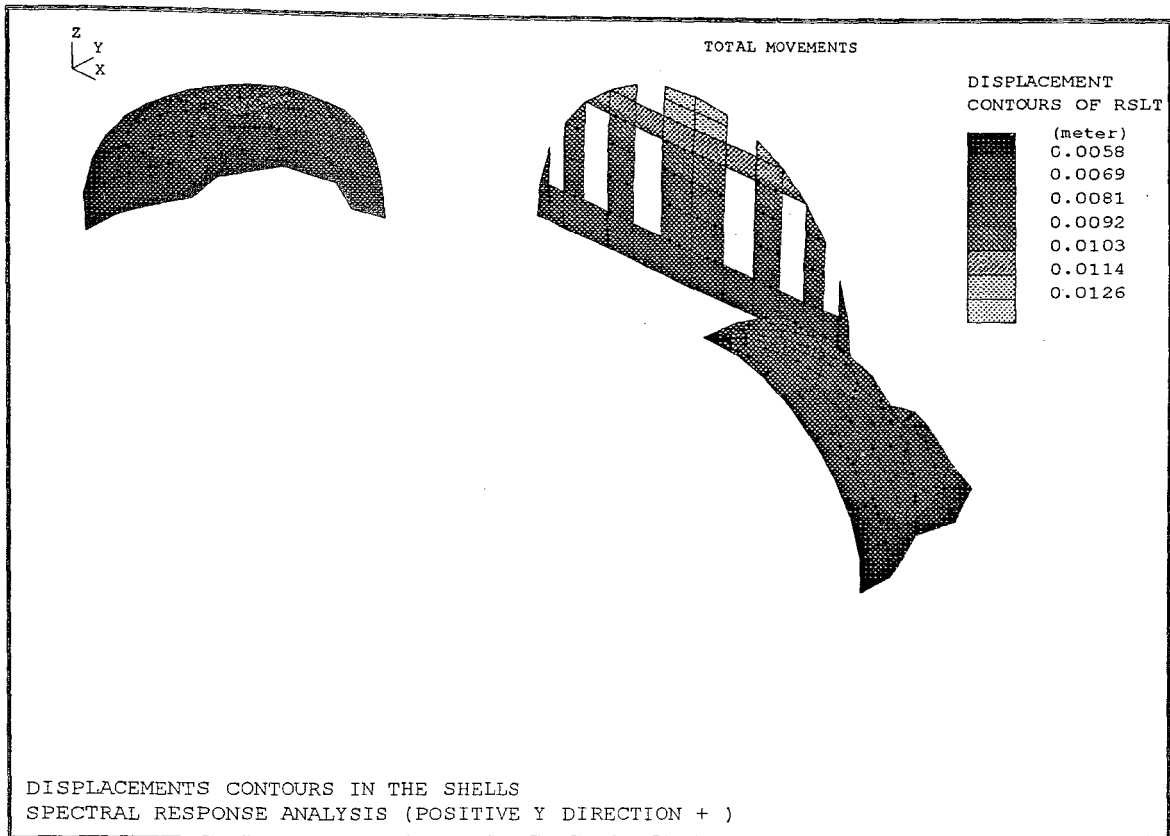


FIGURE 4.77 Displacement Contours in the Shells.Spectral Response Analysis (Positive Y Direction+) Total Movements

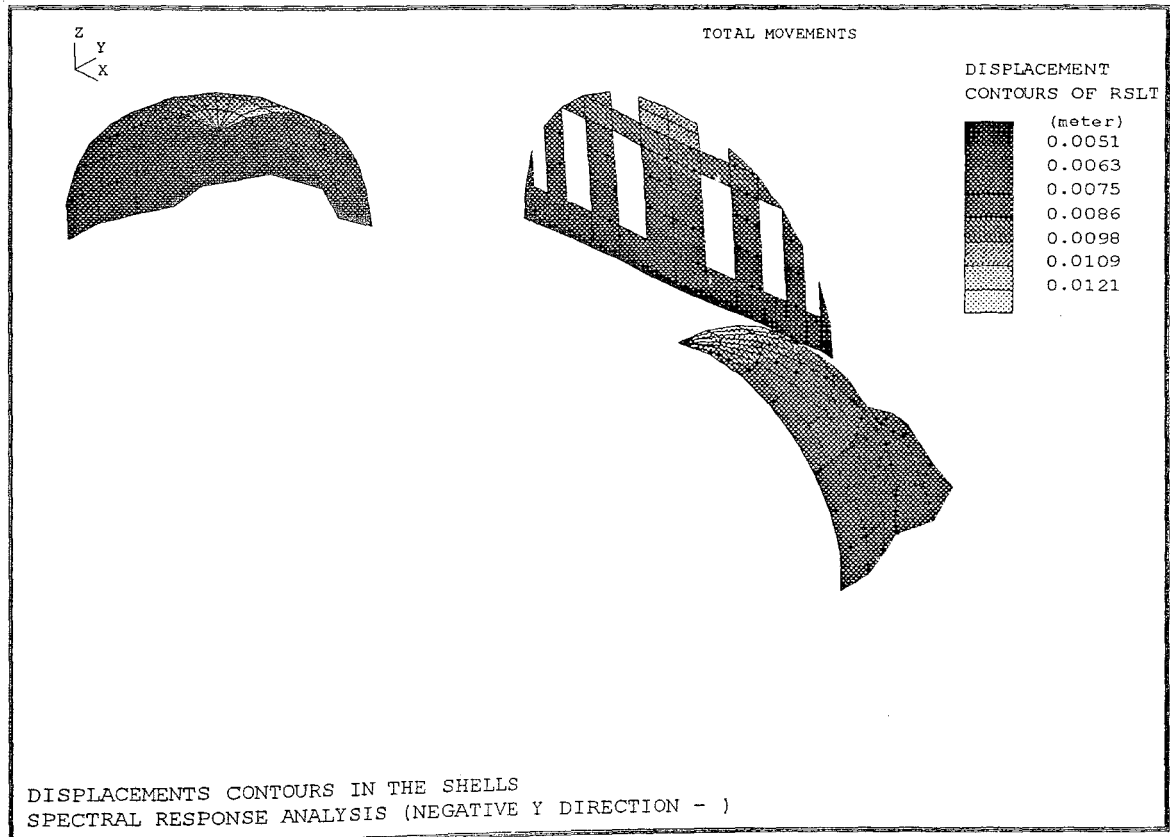


FIGURE 4.78 Displacement Contours in the Shells.Spectral Response Analysis (Negative Y Direction-) Total Movements

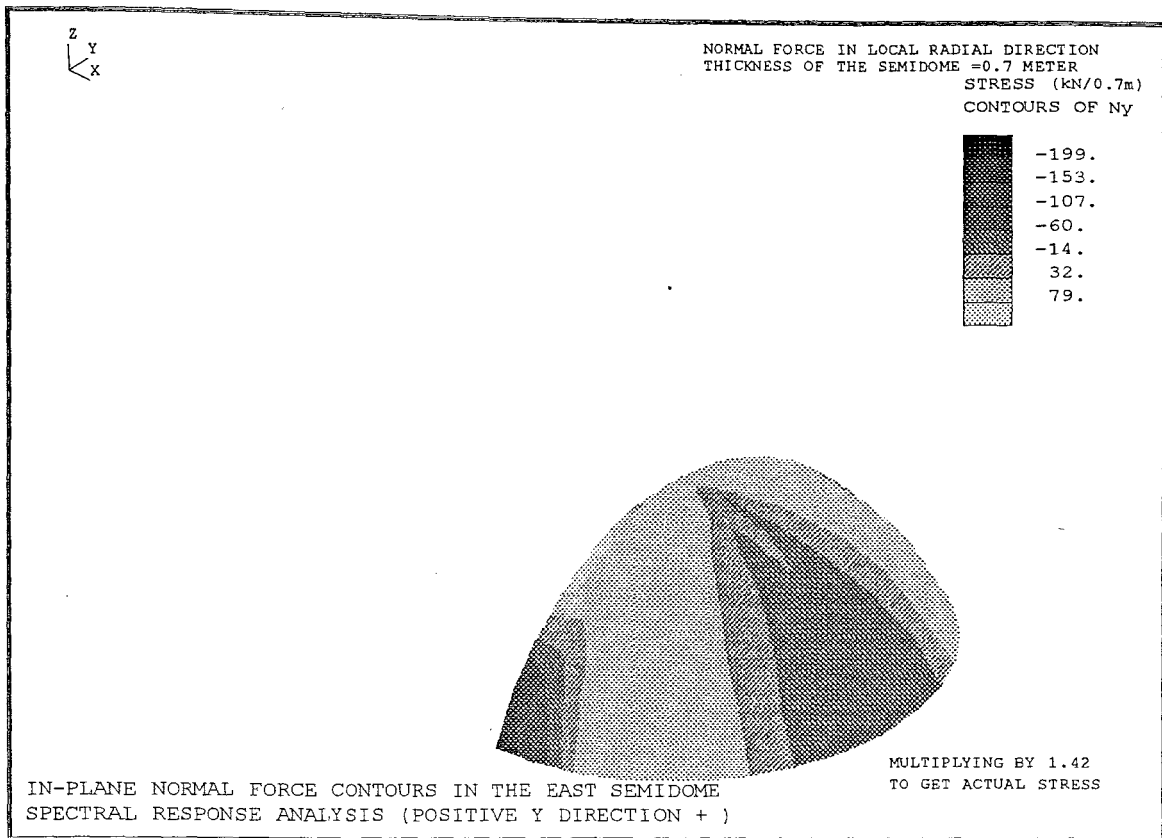


FIGURE 4.79 In-Plane Normal Force Contours in the East Semidome. Spectral Response Analysis (Positive Y Direction+) Normal Force in Local Radial Direction

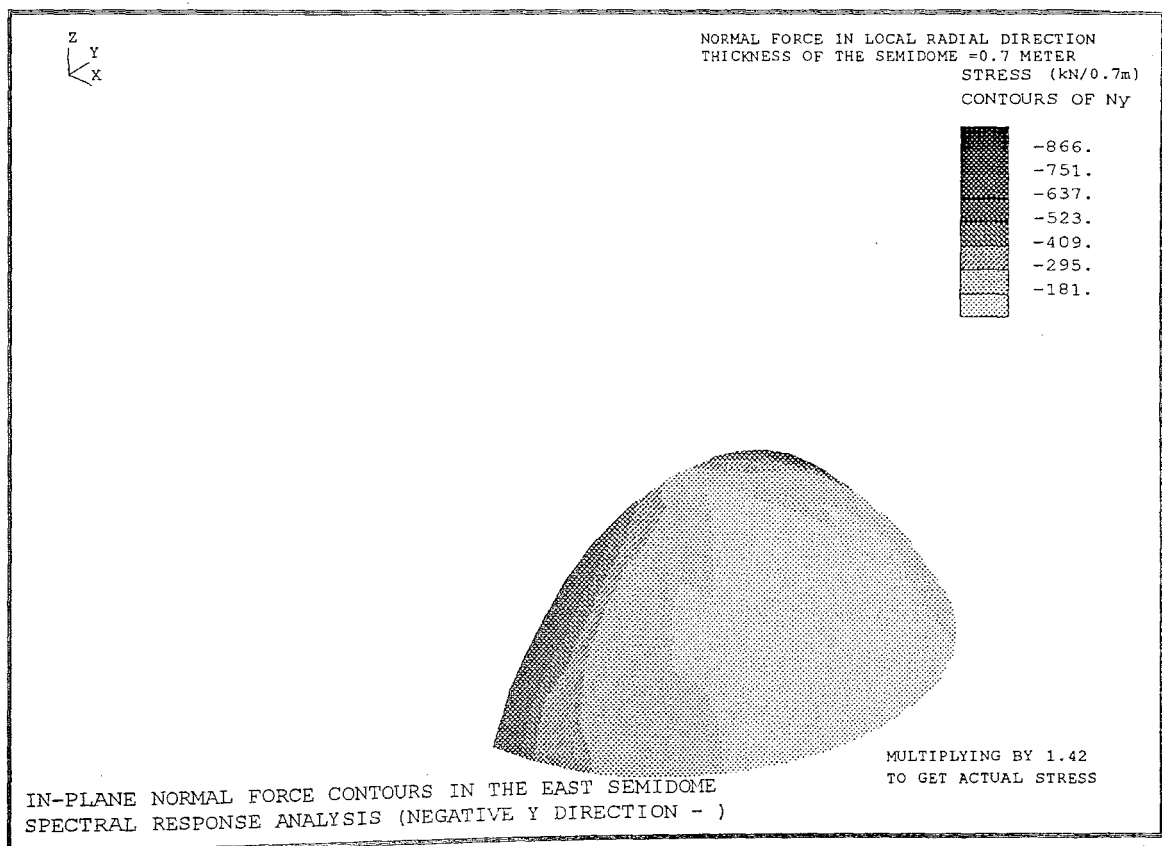


FIGURE 4.80 In-Plane Normal Force Contours in the East Semidome. Spectral Response Analysis (Negative Y Direction-) Normal Force in Local Radial Direction

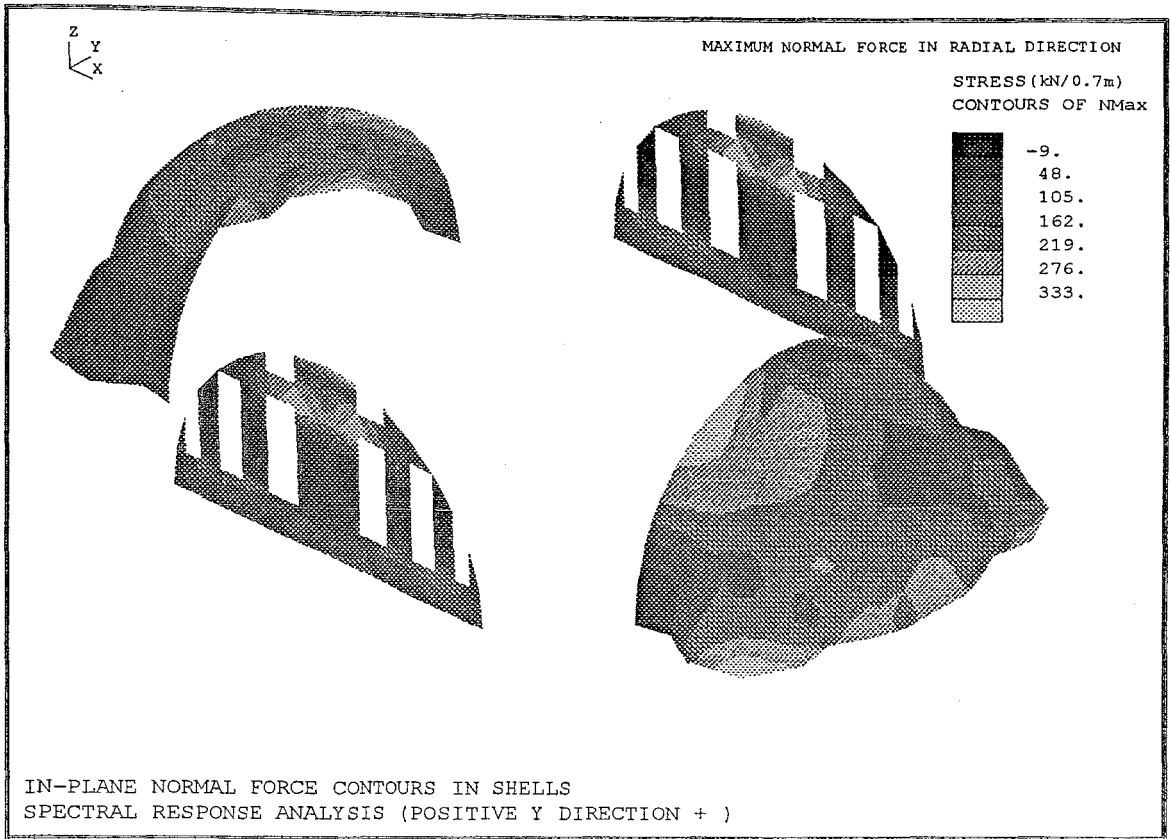


FIGURE 4.81 In-Plane Normal Force Contours in the East Semidome.Spectral Response Analysis (Positive Y Direction+) Normal Force in Local Radial Direction

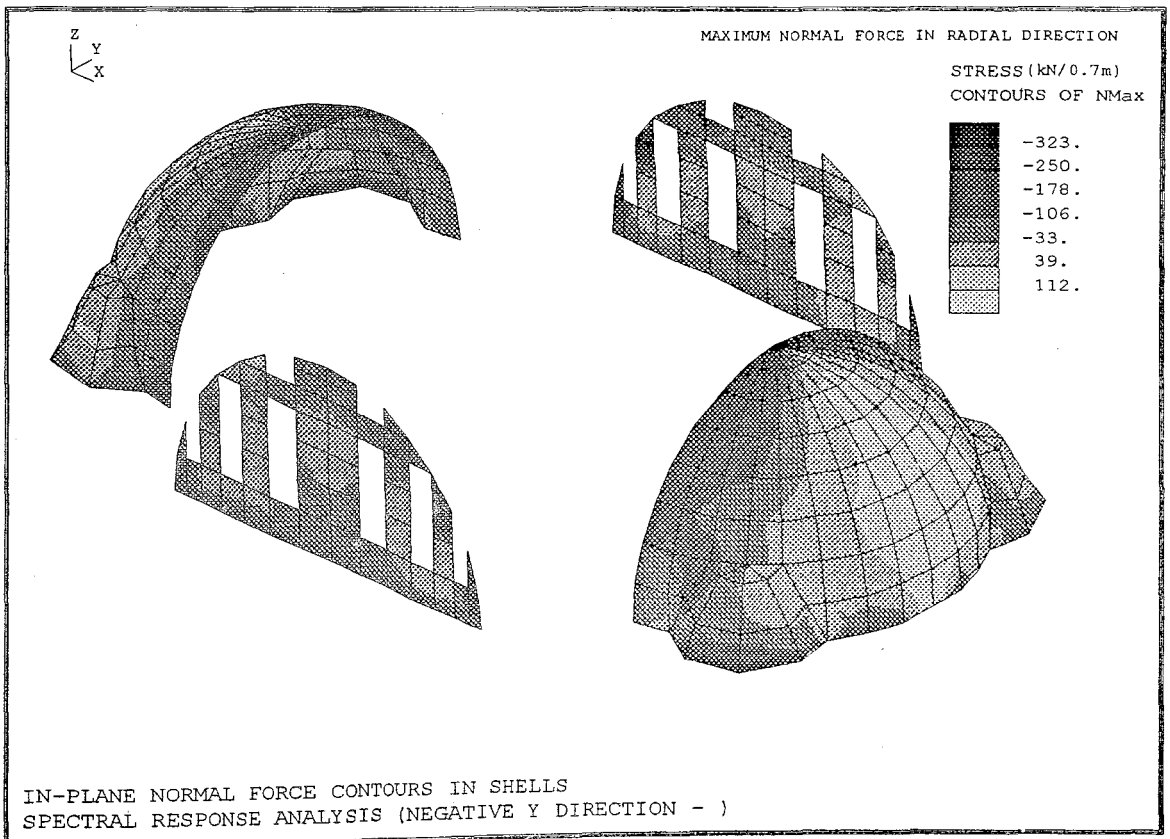


FIGURE 4.82 In-Plane Normal Force Contours in the East Semidome.Spectral Response Analysis (Negative Y Direction-) Normal Force in Local Radial Direction

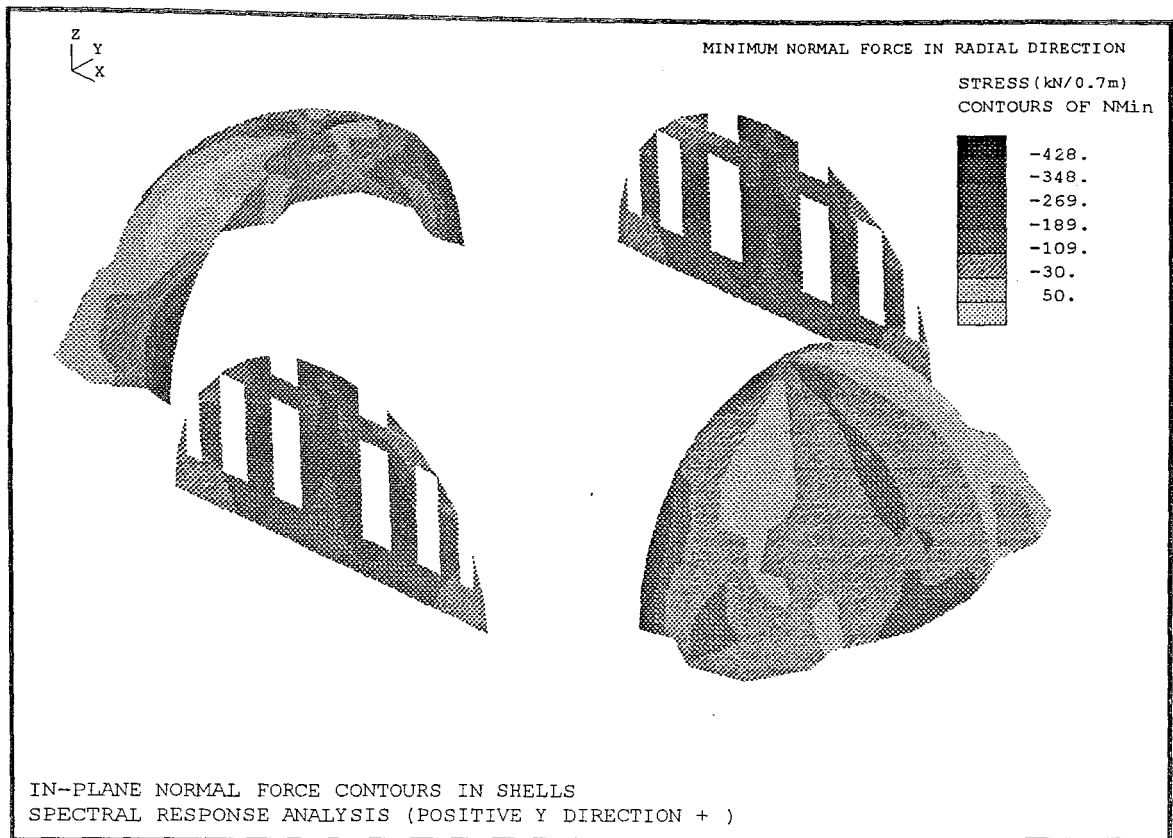


FIGURE 4.83 In-Plane Normal Force Contours in the Shells.Spectral Response Analysis (Positive Y Direction+) Minimum Normal Force in Local Radial Direction

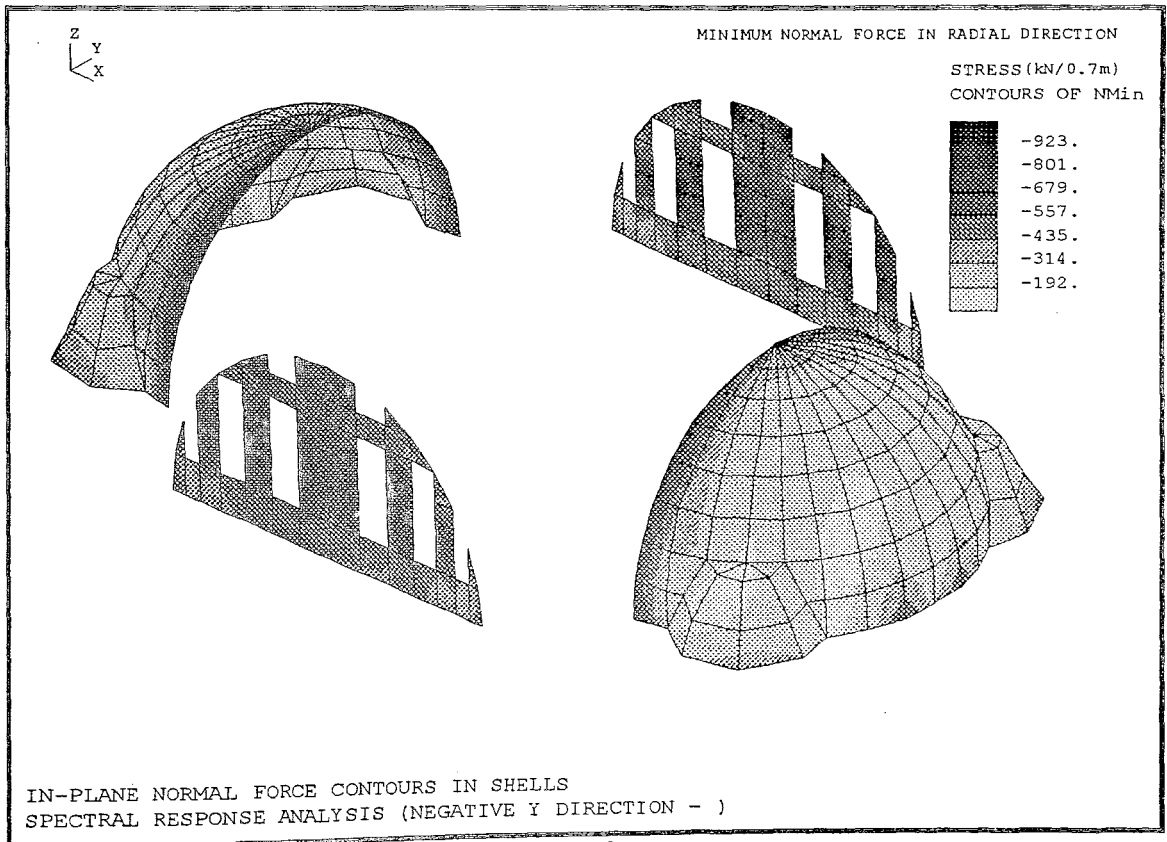


FIGURE 4.84 In-Plane Normal Force Contours in the Shells.Spectral Response Analysis (Negative Y Direction+) Minimum Normal Force in Radial Direction

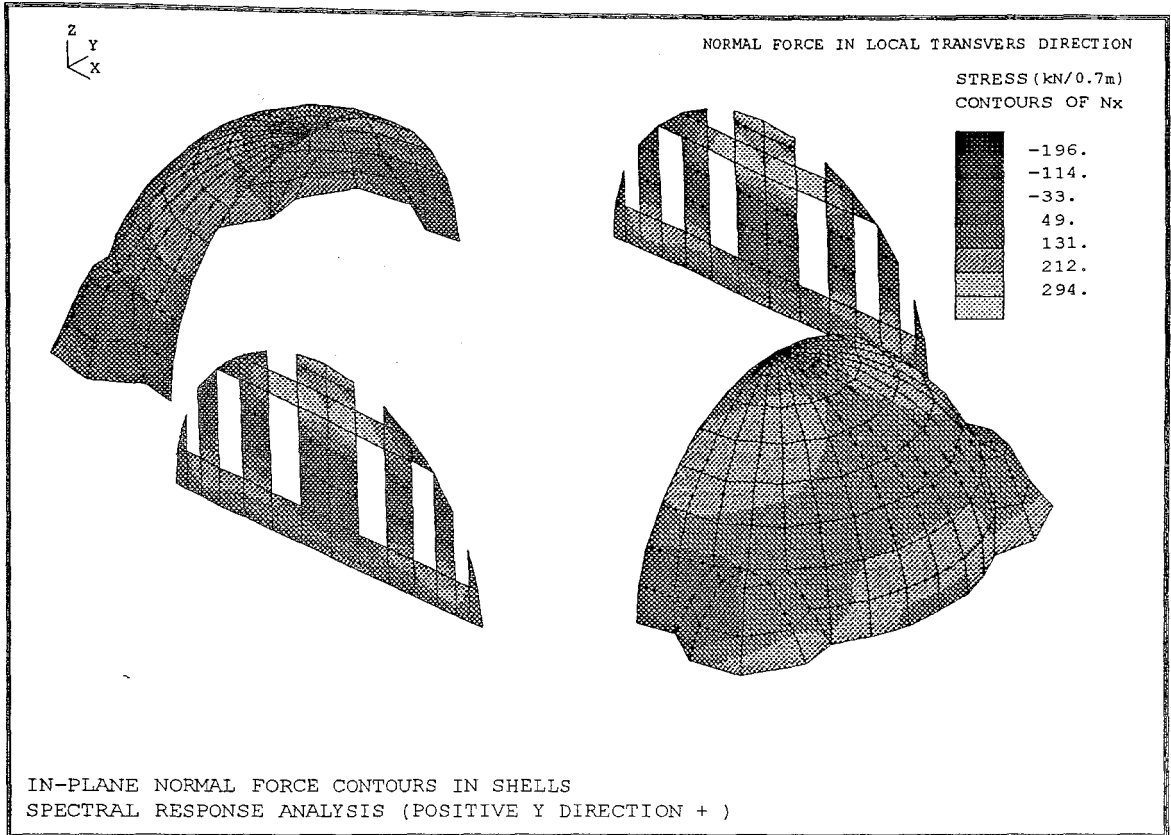


FIGURE 4.85 In-Plane Normal Force Contours in the Shells.Spectral Response Analysis (Positive Y Direction+) Normal Force in Local Transverse Direction

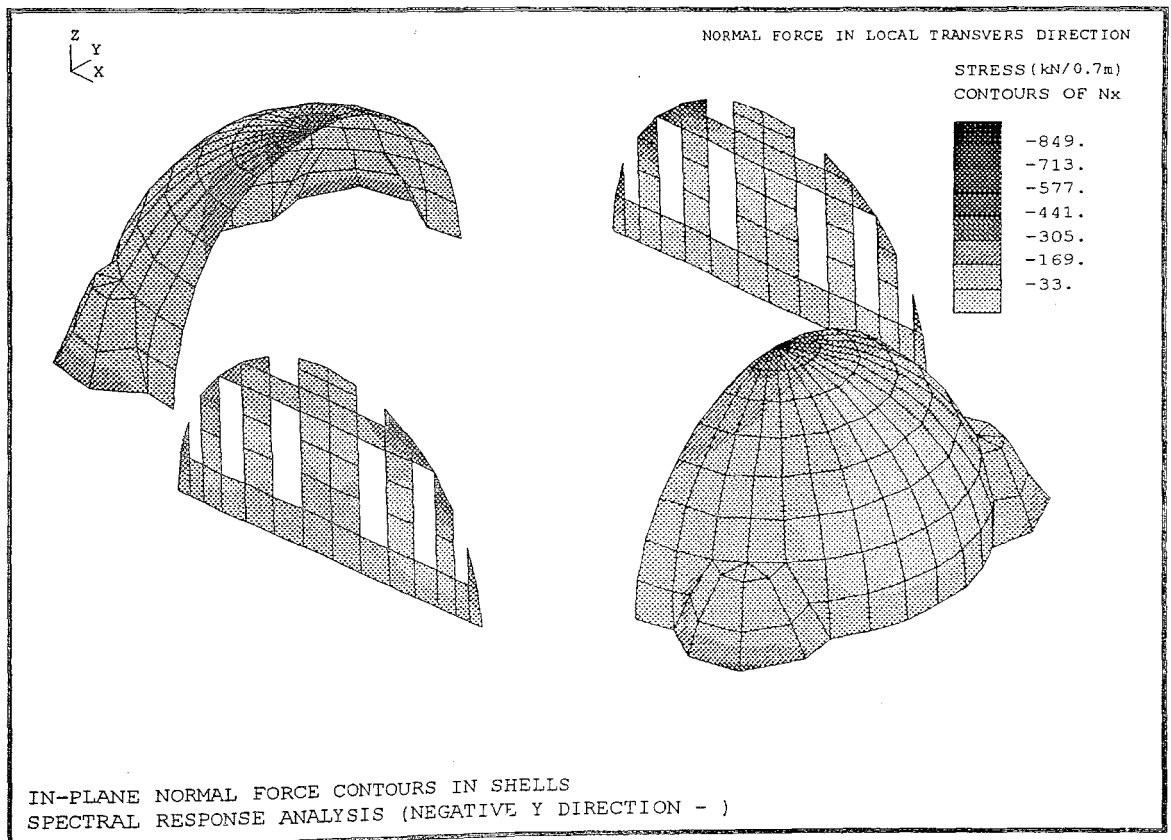


FIGURE 4.86 In-Plane Normal Force Contours in the Shells.Spectral Response Analysis (Negative Y Direction-) Normal Force in Local Transverse Direction

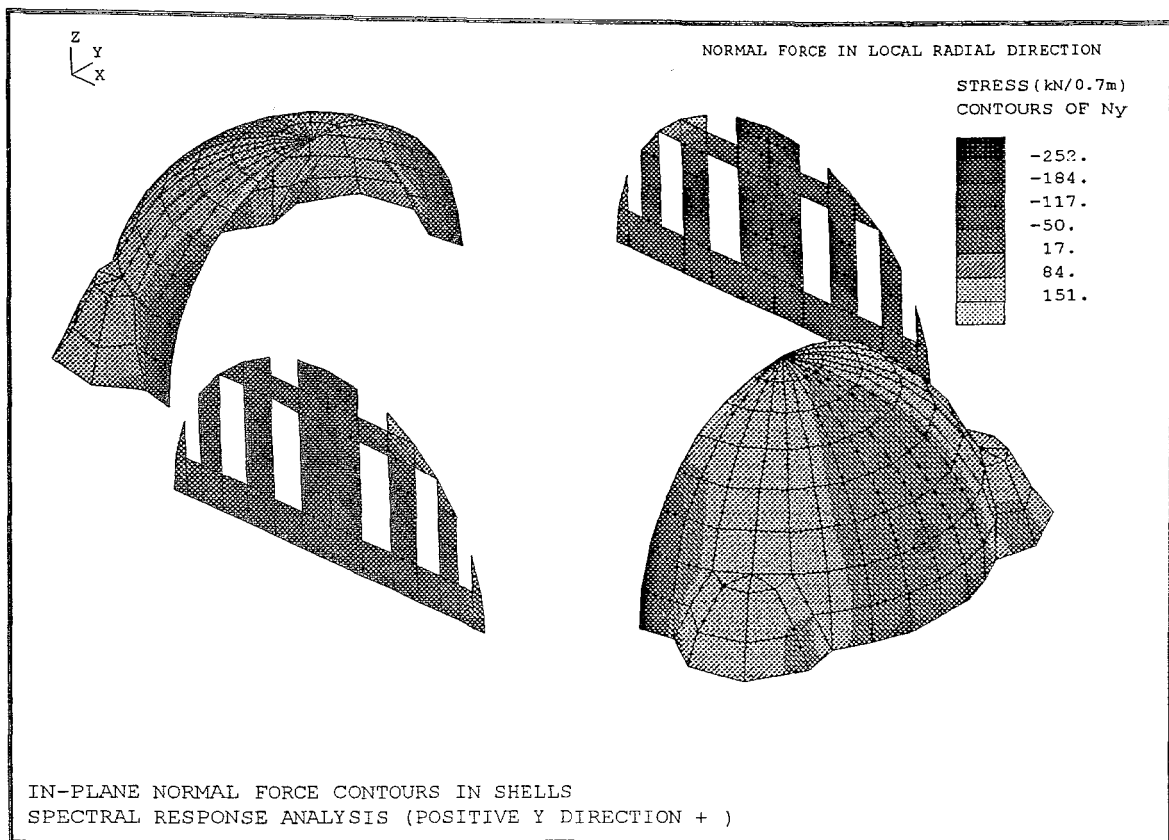


FIGURE 4.87 In-Plane Normal Force Contours in the Shells.Spectral Response Analysis (Positive Y Direction+) Normal Force in Local Radial Direction

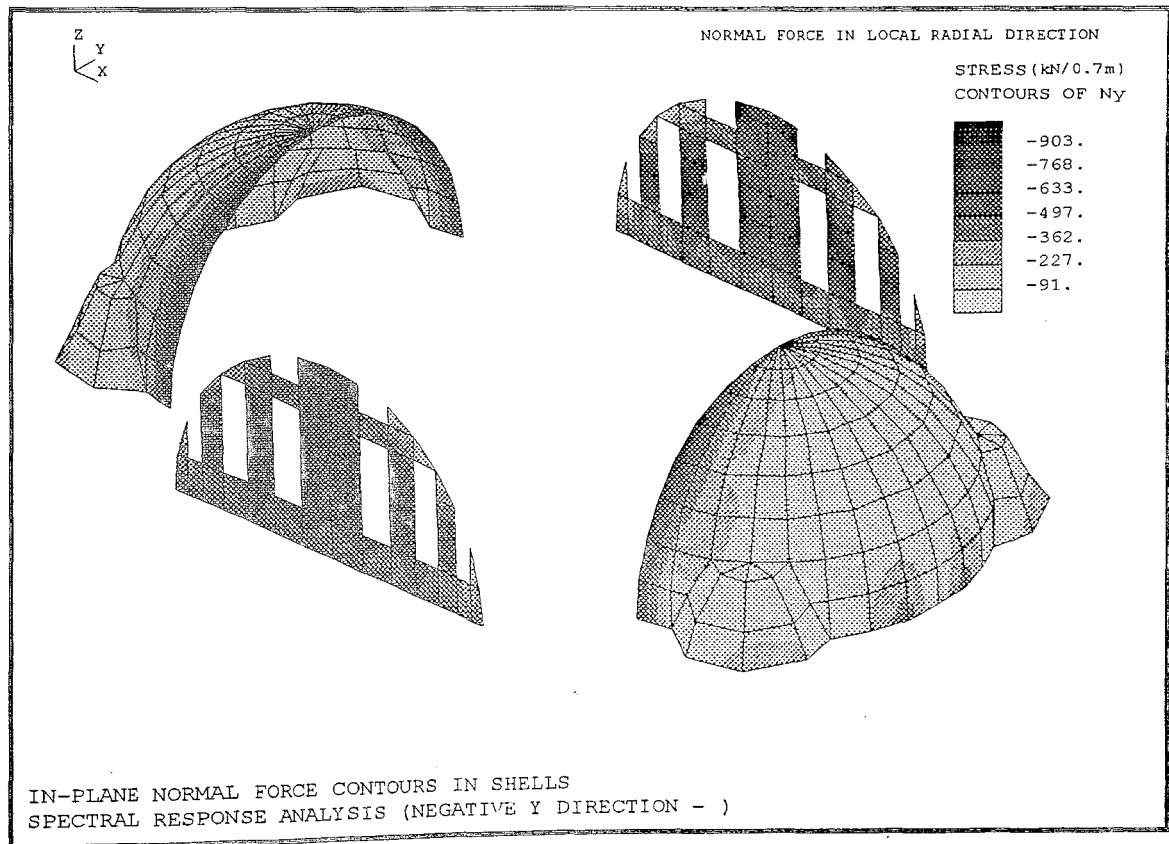


FIGURE 4.88 In-Plane Normal Force Contours in the Shells.Spectral Response Analysis (Negative Y Direction-) Normal Force in Local Radial Direction

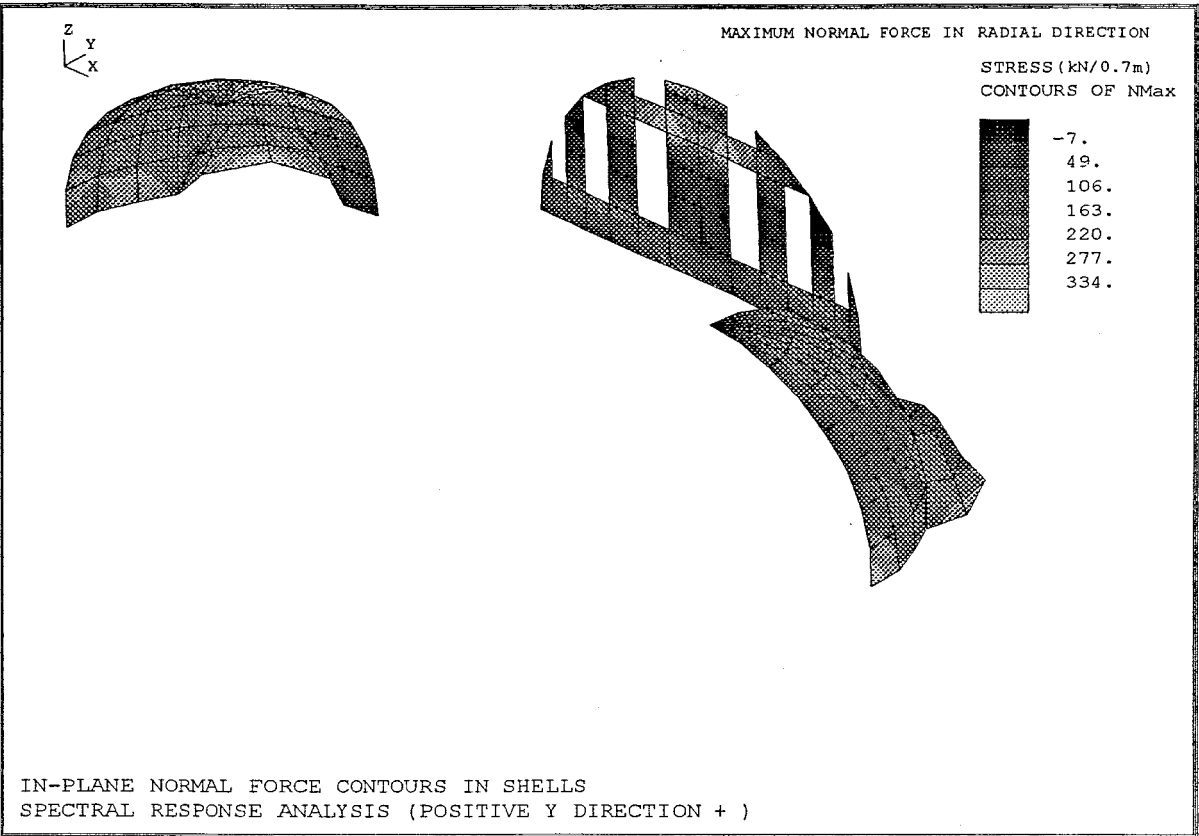


FIGURE 4.89 In-Plane Normal Force Contours in the Shells.Spectral Response Analysis (Positive Y Direction+) Maximum Normal Force in Local Radial Direction

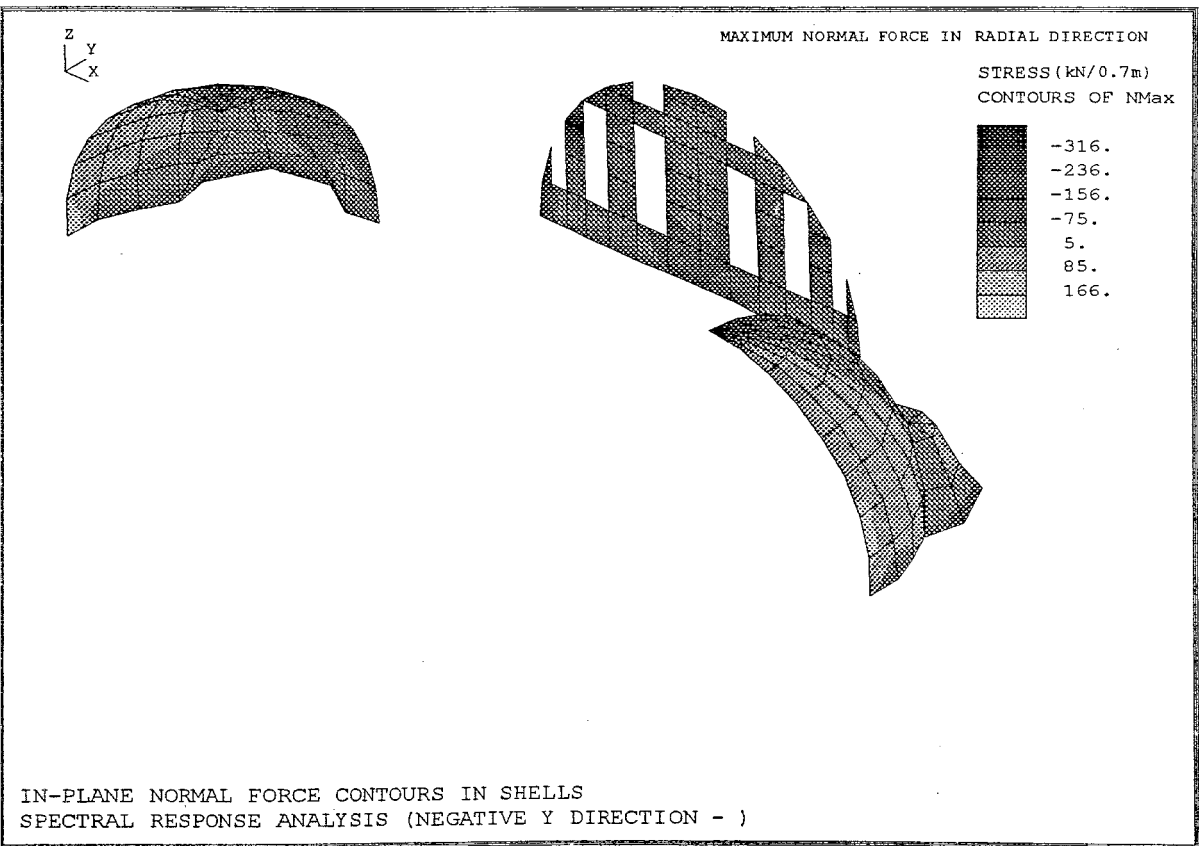


FIGURE 4.90 In-Plane Normal Force Contours in the Shells.Spectral Response Analysis (Neagative Y Direction-) Maximum Normal Force in Local Radial Direction

Table 4.3 Comparison of Model Frequencies

Mode	Ambient Test Results	Earthquake Results 28.05.1994	Results of Previous Model (Ref 9)	Results of Improved Model
1	3,38 cps	3,38 cps	3,26 cps	3,24 cps
2	3,44 cps	3,42 cps	3,65 cps	3,42 cps
3	4,26 cps	4,3 cps	4,58 cps	4,3 cps
4	4,71 cps	*	5,21 cps	4,73 cps
5	5,85 cps	*	5,35 cps	4,74 cps

* Could not be computed

CONCLUSION

Aimed at the exploration of the earthquake performance of the Süleymaniye Mosque, the present study is the extension of the previous study carried out by Ahmet Selahiye.

The three-dimensional finite element model previously prepared was improved by adding the small domes, lowering the foundation level 2.5 m below the previous level and increasing the number of elements to achieve maximum precision. These improvements were realised after the preliminary studies on the structural system and the material properties.

In order to determine the material parameters suitable for the definition of the edifice, diagnostic investigations were conducted using non-destructive testing techniques (Schmidt Hammer tests and ultrasonic pulse velocity measurements). The results obtained were used in the model and the resulting frequencies were compared with those obtained by ambient vibration tests. By using this comparison, different material properties were applied to the model in order to obtain a model of the best conformity with the ambient vibration test results.

Four different boundary conditions were analysed for a number of different combinations of material properties.

Several dynamic runs were carried out and finally a model with the nearest frequency values to those of ambient vibration tests was selected.

The advanced model showed an acceptable compatibility with the test results, the earthquake results of 28.05.1994 and the results of the previous model prepared by Ahmet Selahiye.

As a future work, a thorough investigation should be done in order to compile appropriate information about the structural details.

Unfortunately, precise documents of the works are not found in the archives. The chronicle usually reports the payment of the works, but not their location and technical details which would be very useful for the analysis. It is essential to obtain as-built drawings and full description of the works for the future studies on the edifice.

6-REFERENCES

- 1- *Ö.Lütfü Balkan*
Süleymaniye Camii ve İmaretini İnşaatı, Türk Tarih Kurumu
- 2- *Ergin Arıoğlu, Nihal Arıoğlu*
“Mimar Sinan’ın Taşıyıcı Olarak Kullandığı Küfeki Taşının Müendislik Gizemi”
Mimar Sinan Dönemi Yapı Etkinlikleri Semineri, 1999, İstanbul
- 3- *E. Durukal, Ö. Yüzügüllü, K. Beyen*
“Non-destructive Testing Techniques of Structural Materials in Historical Structures”
INCOMARECH-RAPHAEL 97/E/412 Compatible Materials for the Protection of European Cultural Heritage Pact 55, 1998, Athens
- 4- *Ioanni Papayianni*
“Criteria and Methodology for Manufacturing Compatible Repair Mortars and Bricks”
INCOMARECH-RAPHAEL 97/E/412 Compatible Materials for the Protection of European Cultural Heritage Pact 56, 1998, İstanbul
- 5- *Ahmet Selahiye*
“Determination of Dynamic Properties of Süleymaniye Mosque”
M.Sc. Thesis, Boğaziçi University, Kandilli Earthquake Observatory and Earthquake Research Institute, Department of Earthquake Engineering
- 6- *Evliya Çelebi*
Evliya Çelebi Seyahatnamesi I-X
Üçdal Neşriyat Yayınları & Birleşik Dağıtım, İstanbul, 1996
Prepared by Mümin Çevik
- 7- *N. Çamlıbel*
“Earthquake Risk Analysis on Historical Buildings in İstanbul”
Studies in Ancient Structures, Proceedings of the International Conference
July 14-18, 1997, İstanbul
- 8- *M. Erdik, E. Durukal, A. Çakmak*
“Assesment of the Earthquake Performance of Hagia Sophia”
Studies in Ancient Structures, Proceedings of the International Conference
July 14-18, 1997, İstanbul
- 9- LUSAS Finite Element System
Theory Manuals
FEA Ltd., United Kingdom
- 10- *K. Anadol, Ersin Arıoğlu*
“Earthquake Resistance of Süleymaniye Mosque”
Fifth World Conference on Earthquake Engineering, 1973, Rome

11- *K.Anadol, Ersin Arıođlu*

“Tarihsel Perspektifte Süleymaniye Camii’nin Depremesel Mukavemeti
Deprem Arařtırma Enstitüsü Bülteni No:6,1974

12-*K.Anadol, Ersin Arıođlu*

“Koca Sinan’ın Mühendisliđi ve Tarihsel Perspektifte(1577-1972) Süleymaniye Camii’nin
Depremesel Mukavemeti”
Sinan’ın Osmanlı Türk Şehircilik ve Belediyeciliđi’ne Katkısı- Yuvarlak Masa Toplantısı,5-7
Eylül, 1988, İstanbul

12- *M.Karavezirođlu, J.Papayianni, G.Penelis*

“Mortars and Grouts in Restoration of Roman and Byzantine Monuments “
INCOMARECH-RAPHAEL 07/E/412 Compatible Materials for the Protection of European
Cultural Heritage Pact 56,1998,İstanbul

13- *A.S.Çakmak, A.Mrolopolu, M.Erdik*

“Dynamic Behaviour and Earthquake Response of Hagia Sophia”
INCOMARECH-RAPHAEL 07/E/412 Compatible Materials for the Protection of European
Cultural Heritage Pact 56,1998,İstanbul

14- *I.Papayanni, M.Stefanidou*

“Repair Mortars Suitable for Interventions of Ottoman Monuments”
Studies in Ancient Structures, Proceedings of the International Conference
July 14-18,1997, İstanbul

15- *Dođan Kuban*

Sinan’ın Sanatı ve Selimiye,Tarih Vakfı,1997

16- *Metin Sözen, Sami Güner*

Arts in the Age of Sinan, Ministry of Culture and Tourism of the Turkish Republic.

17- *Ray W.Clough*

Earthquake Resistant Design,John Wiley&Sons,Ltd

18- *S.Mircan Kaya, M.Nuray Aydınođlu, M.Erdik, Ö.Yüzüğüllü*

“Determination of Dynamic Characteristics of Süleymaniye Mosque by Analytical and
Experimental Methods”
INCOMARECH-RAPHAEL 07/E/412 Compatible Materials for the Protection of European
Cultural Heritage Pact 56,1998,İstanbul

APPENDIXES

APPENDIX

HISTORICAL EARTHQUAKES OF ISTANBUL

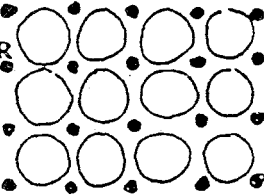
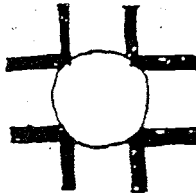
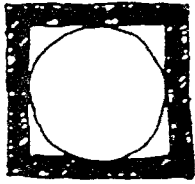
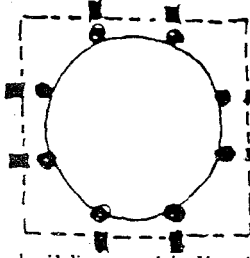
24 August	358	Damage in İstanbul.
2 December	362	Damage in newly finished Hagia Sophia.
	396	Strong earthquake in İstanbul .
June	402	Strong earthquake in İstanbul.
	403	Strong earthquake in İstanbul.
1 April	407	Many houses were damaged in Bakırköy. Tsunami wave observed.
	412	Damage in the city walls.
6 November	447	Many buildings were damaged during the earthquake. An important portion of the city walls and 57 of 96 fortification towers collapsed.
25 September	478	Significant damage in İstanbul. Partial collapse of the inner city walls.
16 August	542	Significant damage in İstanbul. Damage in Constantin and Arcadius churches. Collapse of the statues and obelisks.
6 September	543	Strong earthquake in İstanbul. Damage in Hagia Sophia.
16 August	554	Damage in many buildings and the city walls. Damage in the east main arch of Hagia Sophia.
14 December	557	Many Buildings damaged. Many casualties. Previously damaged east main arch of the Hagia Sophia collapsed with the eastern part of the main dome.
26 October	740	Significant damage in İstanbul. Damage in the city walls and Aya İrini Church.
10 April	861	Many buildings were damaged.
9 January	869	Many buildings were collapsed. Many casualties. Partial collapse in Hagia Sophia.
25 October	989	Damage in many buildings. Partial collapse of the city walls. Damage in Hagia Sophia and Valens Aqueduct (Bozdoğan Kemeri). West main arch of Hagia Sophia collapsed causing Damage in the main dome and in the west semidome.
1 June	1296	Many buildings were damaged.
	1323	Many buildings were damaged.
18 October	1343	Many buildings were damaged. Tsunami wave observed. Hagia Sophia were damaged.
6 November	1344	Strong earthquake in İstanbul. Partial damage in city walls.
19 May	1346	East side of Hagia Sophia collapsed because of the fall of its east main arch.

- 16 January 1489** Many minarets collapsed. One of the strongest earthquakes hit İstanbul. Nearly every building was damaged. Liquefaction observed. About 1000 houses and lots of mosques collapsed. About 5000 (5% of the population) casualties. Damage in Hagia Sophia, Bayazıt, Fatih, Atik Ali Paşa and Davut Paşa mosques, in Topkapı Palace, Galata Tower, Theodosius Obelisk, Anadolu and Rumeli Fortresses and city wall.
- 10 May 1556** Many buildings were damaged. Cracks in the walls of Hagia Sophia. Damage in the Fatih mosque.
- 17 February 1659** Damage in many old buildings. Damage in Süleymaniye mosque.
- 25 April 1689** Slight damage through İstanbul.
- 11 July 1690** 20 casualties. Damage in some buildings, Fatih mosque and Topkapı Palace.
- 25 May 1719** Damage in 40 mosques and 27 towers. Damage in Mehmet Bey, Bayazıt, Sinan Paşa, Bali Paşa and Pertev Paşa mosques.
- 2 September 1754** Damage in many buildings. Intensive Damage in Üsküdar and Balat.
- 22 May 1766** Damage in many buildings. 880 casualties. A dam in upper Kağıthane and a cistern in Sultanahmet collapsed. Damage in Hagia Sophia, Bayazıt, Fatih, Süleymaniye and a number of mosques.
- 10 July 1894** Extensive damage in İstanbul. Severe damage in Fatih, Bayazıt, Eminönü, and in Kapalıçarşı. 276 casualties. Many Buildings were severely damaged. Damage in three dams. The Tsunami wave of 1.5 m created damage in Yeşilköy. Damage in Hagia Sophia, Fatih and a number of mosques and churches And Topkapı Palace.

DESTRUCTIVE EARTHQUAKES IN ISTANBUL

	Date	Epicenter N	Epicenter E	Magnitude	Intensity(MM) (at epicenter)	Distance from Epicenter (km)	Intensity (MM) In İstanbul	Acc %g
1	30-04-1557	41	29	6,4	VIII	0	VIII	12
2	30-07-1633	41	29	5,5	VII	0	VII	-
3	28-06-1648	41	29	7,0	IX	0	IX	18
4	1718	41	29	6,2	VII	0	VII	-
5	25-05-1719	408	29,4	7,3	X	25	IX	18
6	03-09-1763	41	29	5,8	VII	0	VII	-
7	23-04-1766	40,8	28,2	7,6	X	72	IX	17
8	28-02-1855	40,2	29,1	7,7	X	90	VIII	14
9	10-07-1894	40,6	28,7	7,8	X	54	IX	21
10	09-08-1912	40,5	27,0	7,8	X	177	VII	-
11	04-01-1935	40,5	27,5	6,9	IX	137	VI	-
12	18-03-1953	40,0	27,3	8,0	XI	182	VII	-
13	06-10-1964	40,3	28,2	7,0	IX	102	VI	-
14	22-07-1967	40,7	30,8	7,2	IX	150	VI	-

A classification of the Anatolian Mosque According to Support

<u>support system</u>	<u>structural parti</u>	<u>examples</u> <u>before Sinan</u>	<u>dome</u> <u>diam.</u>	<u>Sinan's</u> <u>mosques</u>	<u>dome</u> <u>diam.</u>
COLUMNAR GRID		Great Mosque, Bursa (1399)	10.6 m	Piyale Pasa Mosque, Istanbul (1574)	8.5 m
ABUTTING WALLS		Yildirim Mosque, Bursa (1395) Yesil Mosque, Bursa (1424)	11.5 m 12 m	Haseki Hurrem Sultan Hamami,* Ist. (1557) Nisançi Mosque, Istanbul (1589)	8 m 13 m
PERIMETER WALLS or DOME ON CUBE		Yesil Mosque, Iznik (1378) Yildirim Mosque, Mudurnu (1382) Sultan Bayezid M., Edirne (1488)	11 m 19.5 m 21 m	Coban Mustafa Pasa M., Gebze (1523) Hadim Ibrahim Pasa M., Istanbul (1551) Mihrimah Sultan M., Istanbul (1565 ?)	14 m 12 m 18 m
POLYGONAL PIERS		Uc Serefeli M., Edirne (1447) Fatih Mosque, Istanbul (1470) Atik Ali Pasa M., Istanbul (1497) S. Bayezid M., Istanbul (1506) Fatih Pasa M., Diyarbakir (1520)	24.1 m 25 m 12.5 m 18 m 10 m	Sehzade Mehmed M., Istanbul (1548) Sinan Pasa Mosque, Istanbul (1555) Suleymaniye Mosque, Istanbul (1557) Kara Ahmed Pasa M., Istanbul (1558) Selimiye Mosque, Edirne (1574)	19 m 12.5 m 25 m 12.5 m 31.2 m

* This is the only building on this list that is not a mosque; it is a bath house.